EXPERIMENTAL AND THEORETICAL STUDIES ON STRESSES IN AND DEFORMATION OF WIRE ROPES UNDER AXIAL TENSILE LOADS

by

William Stanley Utting

A thesis submitted in accordance with the requirements
of the University of Liverpool for the
Degree of Doctor in Philosophy

Department of Mechanical Engineering,
The University of Liverpool.

Liverpool March, 1984

SUMMARY

Carefully instrumented tests were performed on strands of seven wire construction and comparison made between experimental results and mathematical modelling of strand response under tensile load. Strand geometries covered a practical range of lay angles between 9.1° and 16.4°, and wire diameters, in all but one strand, were 3.94 mm (core) and 3.73 mm (helicals).

The test rig developed for this programme incorporated a strain gauged load cell for measurement of tensile load and torque generated in the strand in tension under conditions of fixed, free and partial torsional end restraint. An instrument was designed and developed for simultaneous measurement of strand extension and rotation. Other instrumentation included strain gauging of helical wire surfaces.

Test results showed that strand extension in free end tests were up to 70% greater than that in fixed end tests and that extensions were greater for strands with lower helix angles. Torque generated was greater for strands of lower helix angle in fixed end tests as was rotation in free end tests. Surface strains revealed uneven load sharing between helical wires, with strain ranges about the mean being greatest near strand end grips. Repeated loading of the strands did not decrease the unevenness of this loading.

Mathematical modelling of strand response was developed to

take account of the change of helix angle under load, Poisson effects in wires, wire flattening under interwire pressure and the effect of friction between core and helical wires. In fixed end tests, computed predictions underestimated strand extension by between 0.1% and 5.2%, and overestimated generated torque by between 1.1% and 4.5%. In free end tests, computed predictions overestimated extension by between 0.8% and 3.7%. Measured extensions were closer to computed predictions than to predictions which did not take account of Poisson effects, flattening and interwire friction, in tests over the whole range of end conditions, from fixed to torque-free. Computed predictions overestimated strand rotation by between 8.5% and 12.7%. These comparatively large differences can be accounted for, in part, by the rotation of helical wires about their own axes as they roll over the core without slipping; this rotation is in the opposite sense to overall strand rotation. Helical wires were found to take a lower share of total strand load than that predicted. This is consistent with differences noted above between predictions and test results on strand extension and rotation.

High speed photographs taken at strand fracture and immediately afterwards were obtained for one of the strands tested. These revealed transient radial outward displacement of helical wires ('birdcaging') that cannot be detected by other means.

ACKNOWLEDGEMENTS

There are many people to whom the author is greatly indebted:

Professor Norman Jones, my Supervisor, for his enthusiastic yet patient guidance and encouragement;

Mr. Henry Plant of British Ropes for supplying test strands and facilities for wire testing, and for advice and encouragement throughout the project;

Mr. Frank Cummins and his colleagues in the Drawing Office for advice and assistance with the design and supply of test equipment;

Mr. Ted Hobson and his workshop staff for their careful manufacture of test rig and 'extrometer';

Mr. Steve Pennington for assistance with modifications to test equipment and, on occasions, with test procedures;

Mr. Dave Brookfield for advice on instrumentation;

Mr. John Boyes and his colleague, Roy Coates, for advice and assistance with computing and plotting programmes;

Mr. Bob Birch for the time and trouble he took to set up and operate the high speed camera at strand fracture;

The Marine Technology Division of the Science Research Council for the Research Grant which supported this study;

Mrs. Joyce McIntosh for her care and skill in typing from a less than immaculate manuscript;

and finally to my wife, Susan, and to Jane and Hugh; the encouragement and active support of my family has been the major factor which ensured the completion of this thesis;

my sincere thanks to them all.

LIST OF SYMBOLS

I Strand Geometry

α	Strand helix angle
β	Strand lay angle $(\beta = \pi/2 - \alpha)$
d_c	Core wire diameter
d_h	Helical wire diameter
r	Helix radius $(r_o = (d_c + d_h)/2)$
A_h	Helical wire cross sectional area $(A_h = \pi d_h^2/4)$
I_h	Helical wire, second moment of area (diam.) $(I_h = \pi d_h^4/64)$
J_h	Helical wire, second moment of area (polar) $(J_h = \pi d_h^4/32)$
A_c	Core wire cross sectional area $(A_c = \pi d_c^2/4)$
J_c	Core wire, second moment of area (polar) $(J_c = \pi d_c^4/32)$
m	No. of wires in strand

II Material Constants

E	Young's modulus
ν	Poisson's ratio

III Forces and Moments

P	Axial force in strand
M	Torque in strand
T_c	Axial force in core

III Forces and Moments

M_c	Torque in core	
T	Axial force in helical wire	
G	Bending moment component	Helix normal axis
N	Shear force component	Helix normal axis
G'	Bending moment component	Helix binormal axis
N'	Shear force component	Helix binormal axis
X	Contact force component per unit length	Helix binormal axis
K'	Bending moment component per unit length	Helix binormal axis
Y	Contact force component per unit length	Helix normal axis
K	Bending moment component per unit length	Helix normal axis
Z	Contact force per unit length parallel to wire axis	
Θ	Torque due to contact forces per unit length	
F	Frictional force between core wire and each helical wire	
F'	Frictional force per unit length of wire surface	

IV Strains and Displacements

ε	Strand axial strain
ε_c	Core axial strain ($\varepsilon_c = \varepsilon$)
ξ	Axial strain at axis of helical wire
ε_H	Axial strain on helical wire surface
ε_B	Strain on helical wire surface due to bending
ϕ	Strand rotation

IV Strains and Displacements

δ_x Change in strand helix radius due to interwire contact

k Helix wire curvature about normal axis

k' Helix wire curvature about binormal axis

τ Helix twist (tortuosity)

V Relative Motion Between Core and Helical Wires

δ Linear distance between a point on the helical wire and a point on core wire after loading, which were in contact before loading.

δ' Linear motion between wires per unit length of helical wire.

μ Coefficient of friction between core and helical wires.

S_1 Torsional stiffness of core wire

S_2 Axial stiffness of core wire

S_3 Bending stiffness of helical wire

S_4 Torsional stiffness of helical wire

C_S Slip ratio

S_x Flattening stiffness between wires

Suffixes applicable to δ, δ', F and F' above

H Helical wire

C Core wire

A Direction parallel to wire axis

Suffixes applicable to δ, δ', F and F' above

T	Direction tangential to wire axis
N	No friction between wires (100% slip)
F	Friction present but no slip between wires
S	Slip between wires (friction present)
P	Due to axial load

CONTENTS

CHAPTER 1

INTRODUCTION AND LITERATURE SURVEY

1.1 Introduction

Since Albert (1) successfully introduced wire ropes for use as mine winding ropes, their use as load bearing elements has proliferated in a large number of engineering applications. The strength of steel allied to the flexibility of a rope construction, the geometry and wire size of which can be selected to suit the required use, give the engineer an extremely versatile component which can be incorporated into the design of a variety of structures and mechanisms.

Although a wire rope is essentially an element for transmitting a tensile load, the rope construction is such that the individual wires, which go to make up a rope, are subjected to bending, torsional and bearing loads, as well as tension. The magnitude and distribution of the stresses resulting from these loadings determine overall rope response, in terms of extension and, in certain circumstances, rotation. In the case of a rope subjected to cyclic loading, stress levels at the critical positions will also affect rope endurance.

Of particular interest to the rope designer are the stress levels and distribution at the rope ends where the tensile load is transferred to another component. For dynamic applications this is usually effected by winding the rope round a sheave and onto a drum. The bearing and frictional loads thus applied to

the rope, through the wires in the outer layer, further complicate the stress distribution in all the individual wires of the rope. Terminations are applied at the ends of ropes in both static and dynamic applications; the mechanism of transfer from individual wires to the gripping medium of the termination can give rise to stress concentrations.

Friction between wires can affect the complexity of the stress distribution and, hence, the rope response to load as well as rope endurance. Lubricant, used also as a protective against corrosion, can therefore constitute an important element of the rope design and of the recommendations on rope utilisation.

The foregoing paragraphs indicate the wide scope available to workers engaged in research and development on wire ropes. The survey which follows refers to some of the work reported in this field.

Other references, given in later chapters of the text, are concerned mainly with the development of equipment and testing techniques.

1.2 Historical

Albert (1), a mining overseer in the Harz Mountains of Bavaria, appears to be the first successful manufacturer and user of iron in wire rope. Weber (2) records that others theorised about its use before the 1830s, including Leonardo da Vinci in the 15th century, but that Albert deserves the greatest credit for having introduced it as a successful tool in industry. Forestier-Walker (3) tells of the Englishmen, George Smith, an engineer, and George Binkes, a cordage maker, who made wire rope in about 1830. However, their ropes, made of relatively fine wires in conventional cordage machinery, proved largely unsuccessful. Their parallel wire selvage ropes were too stiff and in their 'formed ropes', the soft iron wires broke up rapidly. Only in ships rigging were they used successfully.

Albert's rope consisted of three strands having four wires each, of 0.144 in. diameter. Thirteen men were employed, who produced about 50 ft. in 1 hour. Albert was aware of the problems of wires twisting about their own individual axes and counteracted this by rotating the strand in the opposite direction during the laying process. Since he had available only short lengths of wire from which to produce the ropes required for mine shafts of 1400 ft. or more, frequent splicing was necessary. This he achieved by laying the new wire beside the old for 40 ins. and binding it with a few turns of thin wire; this latter being for easy location of join only, as transfer of load was achieved by interwire friction, the other wires providing

adequate normal forces within the plaited rope. Albert was also aware of corrosion problems and advocated the use of 'artificial grease or oily composition; and in default of those a mixture ... two thirds of oil and one third of colophorium of resin.' This was intended as protection; lubrication of the individual wires of the rope did not appear to concern him. His experience with hemp ropes, chain ropes - which he also tested extensively - and wire ropes convinced him that the last of these proved best in terms of strength, endurance and overall cost.

Weber (2) tells how Albert's ropes were sold to mines all over Europe. From the late 1830s, however, others developed machinery which was capable of faster manufacture and complex constructions, involving 36 wires or more. Weber continues by tracing the major developments in wire rope machinery and ends by comparing the theoretical breaking load of Albert's rope, 6000 kp, with that of a not untypical modern rope (1974) of 383,000 kp.

Forestier-Walker (3) records the history of the Wire Rope Industry in Great Britain from 1830 to 1952. The Industry flourished in the 19th century and no fewer than 46 companies were in business until World War I. The depressed state of the market after the war resulted in takeovers and amalgamations, the most notable of which was the British Ropes Conglomerate, formed in 1924 by 8 companies, which has continued to absorb smaller firms since.

Sayenga (4) traces the development of the Wire Rope

Industry in the United States. The American pioneers in this field were largely influenced by Europeans and many of them spent time in Germany, France and Britain studying bridge design and the use of wire ropes in haulage and ropeway applications. Impressive achievements in the fields of suspension bridges, cable cars, shovels and draglines, among others, followed in the next 150 years. However Sayenga concludes by expressing concern about the future prospects of the Industry in America, where competition from Japan and Korea pose a commercial threat to established home companies.

1.3 Review and Survey Papers

Costello's (5) review paper on the Analytical Investigation of Wire Rope covers some of the theoretical papers up to 1978 on the subject of response to loading. These deal with strand and rope of mainly simple constructions subjected to tensile and torsional loading under conditions of both fixed and torque free ends.

Bahke (6) lists more than 50 variables which affect the strength and endurance of wire rope. These come under the seven major headings of wire material, treatment, construction, geometry tolerance, operating conditions, duty class and stress and stress-ability in both static and dynamic loading. He reports that it has not been possible to obtain longer service from rope with alloy steel wire, under normal conditions in bending fatigue, than with rope from wire of plain carbon steel. His tests are confined to the latter. A wire modulus value of 196 kN/mm^2 is quoted up to stress values of 500 N/mm^2, above which the stress/strain curve becomes non-linear. In considering the bending of wire ropes, Bahke gives interwire friction coefficients of 0.1 and 0.3, when determining stress values at contact points between wires of different layers in the rope.

Gibson's paper (7) describes certain aspects of wire rope behaviour in tension and bending which ultimately determine useful rope life. Of particular interest is the phenomenon he describes in which a hoist rope under tension exhibits changes in rope

geometry (lay length and rotation) along its length, although each end is prevented from rotating. He also summarises the results of a number of bending fatigue tests on ropes of diameter ranging between $\frac{1}{2}$ inch and $3\frac{1}{2}$ inch. Among the more significant conclusions is that continuous application of lubricant improved rope life by more than fifty percent.

A guide to potential users of wire rope in the marine environment is given by Sharp (8). Recommendations are made for specific applications and reasons given for rope discard in each case. Fatigue characteristics are given for a number of typical wire rope constructions. Load/extension characteristics exhibit differences after the rope has been 'bedded down', as compared with the initial curve when the rope is first loaded.

Boyle (9) records the results of a survey conducted on 234 ropes of general engineering type (not including specialist users like lifts, cable belts, conveyors, mine hoists, oil well drilling, etc.) which had been returned after failure in service. Mechanical damage due to either excessive wear or gross overloading accounted for 65% of the total, while failure at terminations accounted for 11%, corrosion or corrosion fatigue for 10%, fatigue for 5% and the remainder failed for a miscellany of reasons.

Babel (10) lists available methods of testing wire rope and outlines the principles involved for each. There is a

tabulated survey of faults, causes, influence on rope strength and visual indications present for each fault.

A useful background to acceptable industrial practice, particularly in the Mining Industry, is given in Ropemans Handbook (11) published by the National Coal Board.

1.4 Mathematical Modelling of Strand and Rope Response

Some of the earlier workers in this field considered only tensile forces in the component wires of a wire rope. Hall (12) attempted to prove that stresses in the outer wires of a rope are greater than stresses in the inner wires. His observation that the outer wires of ropes in service break first was put forward as proof of his theory on their larger stress values. He also wrote that the components at right angles to wire tension which binds and tightens strands to each other and to the centre strand can be readily calculated but are of little interest.

Hruska (13) appears to have been moved to publish his paper on the tensile forces in wire ropes as the result of a strong desire to refute Hall's assumptions (12). Hruska also considered only tensile forces in wires, whether helical wires in outer layers or the straight wire at the centre of a core, and dealt with tensile loading of ropes in which the ends are restrained from rotation. His analysis shows that core strain, which is equal to overall rope strain, must be greater than strains in the initially longer helical wires and developed expressions to determine the load taken by each layer of a spiral wound rope. These layers may be of different material, different lay angle and different diameter from each other. From his experience as a user of wire ropes, he observed that broken wires take their full share of the rope load within 'a few lays' of the break, due to friction with adjacent wires,

and noted further that a wire rope may have all its wires broken (at different positions along the length of the rope) and still carry the load.

In his paper on radial forces in ropes Hruska (14) shows that these forces increase inwards for each layer of rope construction. For certain constructions this means that the outer layers are well supported by the next layer inwards but that for some inner layers, point contact at wire crossovers gives high contact stresses.

Hruska's third paper (15) considers tangential forces in ropes and shows how to determine the torque generated in a multi-layer rope under tensile load, due to tensile forces in the wires. He comments that it would be theoretically possible to make a torque-free rope, but that this would not be of practical use!

The last decade has been marked by a succession of papers from Costello and his fellow workers (16, 17, 18, 19, 20, 21, 22, 23, 24, 25) who have taken a more fundamental approach than their predecessors in modelling the response of wire ropes, usually of simple construction, to tension, torsion and bending. The individual wires of a strand are treated as thin rods subjected to tension, bending, twisting and bearing loads (where they have line contact with each other) after Love (26). A strand consisting of a single layer of helical wire is considered. The assumptions made are as follows; there are no frictional

forces between the wires, the wires just touch in the unloaded state; the core is relatively soft in comparison with the cable (helical) wires so that radial force exerted by the core is neglected. Phillips and Costello (16) regard the strand as a collection of smooth rods whose original unstressed configurations are those of helices and which under the action of axial and/or torsional loading on the strand are strained to the configuration of a different helix showing changed helix radius, curvature and tortuosity from the original. The bending and twisting couples acting on the wires are given by the simple bending and torsion theories applied to a straight bar of circular cross-section, in which original diameter is known, as are the elastic and shear moduli of the material. Equilibrium equations are developed and yield expressions for the line contact loads between adjacent wires, as well as overall axial load and axial torque on the strand. Results from these non-linear expressions are computed for contact loads and final helix angles in the cases of some three-wire and six-wire strands subject to a range of axial/torsional load ratios. A criticism of these results is that for strands of known engineering materials, the load range considered is larger by at least an order of magnitude than that which would fracture the strand. Only small areas, near the origin of the graphs shown are therefore of practical interest.

Costello and Phillips (17) give a more accurate expression for the geometry change of the strand under load and, in another

paper (18), take account of wire extension in the compatibility equations.

The main conclusions from the three papers (16, 17, 18) are that a cable with its ends fixed against rotation is always stiffer than one whose ends are free to rotate and that the exact type of end condition is an important factor in determining cable stiffness. Furthermore, the stiffness of fixed end cables is independent of the axial load being applied but the stiffness of cables whose ends are free to rotate increases sharply with increasing load. In a further paper, Costello and Sinha (19), starting from the same assumptions as before, consider the torsional stiffness of the same single-layer strand. They conclude that the torsional stiffness is not significantly affected by the axial load or twisting moment applied at the ends of the cable.

Turning from single strands to stranded rope, Costello and Sinha (20) and Costello and Miller (21) consider the static behaviour of wire ropes by treating the strands of a rope in the same way as previous papers have treated the individual wires of a strand. Once the extensional and rotational responses of the constituent strands are determined, as in (18, 19), they can be incorporated in equilibrium expressions applied to the rope. The authors state that the treatment presented in (20) can be applied to other types of rope cross-section. The conclusions to paper (21) include the fact that there are important

differences between the response of Lang lay and Regular lay ropes. The former, in which the rotational direction of the wire lay in a strand is the same as the direction of strand lay in the rope, should never be used when the ends of the rope are free to rotate. There is practically no stiffness and the lay just 'runs out' - (unwraps itself). Regular lay, by contrast, tends to stiffen as load increases.

Two other papers consider strands of two concentric layers of opposite lay. Costello and Miller (22) extend previous work on single layer strands to predict the combinations of pitch of an inside left lay rope and outside right lay rope which will produce a non-rotating rope, in which friction is neglected. Results are shown for a rope of 1 x 19 construction, but the theory is general and can be applied to ropes with other cross-sections. Phillips, Miller and Costello (23) consider contact stresses between wires at crossover points in the same rope of 1 x 19 construction. Among their conclusions is the fact that although contact force is small (about 0.0005 times the tensile force applied to the rope) the contact stresses can be significantly larger than the stresses in the wires due to tension.

The case of single layer strands comprising wires of initially elliptical cross-section is considered by Velinsky and Costello (24) in which the treatment is similar to that of Costello et al. (18, 19) for wires of circular cross-section. The axial stiffness of the rope is less for rope having wire of elliptical cross-section than for the case of circular section

wire but this reduction only becomes significant as helix angles become very much less than 90° (down to about 60°) when strand ends are free to rotate. Abrasion resistance of such ropes is claimed to be improved since they present a larger contact surface area, but due to the complex nature of contact problems, stresses due to line contact loads are not discussed.

Costello and Butson (25) extend the treatment of strands in tension (18) to consider the bending of a seven wire strand over a sheave. The effects of bending moments on strand, as well as contact forces and torques between sheave and wires, are superimposed on the tensile effects. Among the authors' conclusions is the fact that the core wire receives the largest axial strain and that for large diameter ropes made up of small wires, the large twisting moment, which is imparted by the sheave to the rope in order to maintain equilibrium, may be the cause of excessive wear in wires and grooves.

Durelli and others (27, 28, 29) and Chi (30, 31) represent the work of another group who extended the original work of Hruska (13, 14, 15). Machida and Durelli (27) consider a seven wire strand comprising a straight core and six helical wires subjected to axial tensile and torsional loading. Interwire contact deformation and Poisson's effect due to the axial strain on individual wires are neglected, as is the friction between wires in contact with each other. Normal contact force between wires is considered but the effect on strand response of shear force on the cross-section of a

wire is neglected. Bending and torsion of the helical wires is taken into account by determining the change in geometry of the original helices under loading which, unlike free helical springs, are constrained by the core wire to maintain a constant helix radius. The elementary theories of bending and torsion are applied to the case of a bar of circular cross section when determining stresses in the helical wires and core. Where there is contact between core and helicals, the core is assumed to act as a simple bar in tension and torsion. The relations between overall external forces on the strand and loadings on the individual wires can readily be obtained from considerations of equilibrium. By assuming that deformations are small enough to neglect the change in helix angle under load, linear expressions are obtained for the response of the strand as a whole, as well as for the stresses and strains at all points on the constituent wires.

Chi (30, 31) whose work was simultaneous with that of Durelli et al. (27, 28, 29) also used the Strength of Materials approach in his analysis of multi wire strands in tension and combined tension and torsion. In (31), Chi considers strands having wires numbering five to twelve and suggests a design procedure for a non-spinning rope of three layers, including core wire. Experimental work on seven wire strand is described by Durelli and his fellow workers in (28) and (29). Both Durelli (27, 28, 29) and Chi (30, 31) compare the results with their own theories and this aspect is further discussed in section 1.5.

Huang (32) also considers the response to axial tensile and torsional loads of a strand with a core wire. This author has published a number of papers, but these are mainly concerned with the mechanics of textile strands. However this particular paper (32) is of interest since it considers the effect on strand geometry of Poisson effects on the individual wires. Contact between adjacent helicals and between helicals and the core is taken into account but contact deformation (flattening) is neglected in the analysis. Friction between wires is considered but even though slip is assumed possible between adjacent helical wires and a coefficient of kinetic friction is introduced into the analysis, rotational slip between core and helicals is assumed not to occur. Results computed from the non-linear expressions set up, to cover a range of engineering and textile lay angles show that helicals, initially in contact with the core and each other, are separated from each other when the strand is loaded. The analysis thereafter considers contact only between core and helicals. Curves are presented of dimensionless quantities in which axial strain, interwire forces, core wire tension, helical wire tension and strand rotation are plotted against the tensile axial load applied to the strand. These curves are for four lay angles from 10° to 40° in both the fixed end case and when ends are free to rotate. The same criticism can be levelled against these graphs as has been in the case of Phillips and Costello (16) in that only small areas near the origin of the axes are relevant for practical wire rope strands

constructed with engineering materials. However, this treatment does explain the fact, noted in conclusion by the author, that tensile strength of strands with a central core is considerably reduced if strand ends are free to rotate.

This section would not be complete without mention of two early workers in this field, Matheson (33) and Hansom (34). In the course of experimental work on locked coil stranded rope, theory was developed to predict rope response to axial tensile and torsional load. A concentric rope can be regarded as a statically indeterminate structure in which the final partition of load between the constituent layers depends on their relative elasticity. Starting with the simplest strand consisting of a core wire (layer one) and single layer of helical wires (layer two) expressions for the rotational and extensional response to load, both tensile and torsional, are developed from which simultaneous equations yield load sharing information as between the layers. A step by step process is then utilised to determine the effect of outer layers. The effect of bending and torsion on helicals is considered, after Love (26), as is the effect of the mean shear stress across the helical wire section.

Two further papers consider the testing that is required to determine rope response under tensile and torsional loading. Glushko (35) describes the stiffness of rope under 'pure tension', 'pure twisting', 'free tension' and 'free twisting' and develops expressions to predict the response of a rope to combined tension and twisting, which can be regarded as a system

with two degrees of freedom. Kollross (36) considers the total torque in a rope as the sum of the torque generated by tension applied to the rope and that due to torsional rigidity. These torsional stiffnesses can be determined analytically, considering one strand or layer at a time, or experimentally by tensile and torsion tests. The torsional rigidity of a rope lies between that of the sum of the individual wires, free from friction, and that of a homogeneous round bar.

Knapp (37, 38, 39) and Nowak (40) represent a specialist area in the general field of wire rope behaviour. The function of helically armoured cables is not exclusively or even primarily to bear tensile and/or torsional load. The spiral strand configuration may consist of a number of layers of different materials having widely different elastic moduli (e.g. steel armour wire, copper conductors, plastic insulation). The analysis of cable response to tension, torsion and bending loads can therefore become vastly more complex than that for a conventional wire rope, especially as the requirement of zero rotation under tensile load is important in this application. Among the assumptions in Knapp's analysis (37) are that the helical wire diameter is small compared with lay length and that the torsional stiffness of these wires is neglected. Moreover, the helical wire diameter is assumed not to reduce due to inter-wire contact and the core element is considered linearly elastic in the direction of the cable axis while remaining either rigid or incompressible in the radial direction. In an earlier paper

Knapp (38) compares experimental results from two cables with stiffnesses predicted from his analysis. Restraining torque predictions in the fixed end condition overestimate by 5.7% in one case and underestimate by 1.5% in the other. Rotations in the free end condition are underestimated by 16% and 11.6%.

Hobbs and Raoof (41) consider large spiral strands and treat each layer as an orthotropic sheet. The stiffness of each sheet in its principle directions are defined by reference to contact stress theory. Slip histories are predictable, from micro-slips in the periphery of contact patches at low loads to gross slip at higher loads. Hysteresis in the strand under cyclic loading is also predictable. Experimental work on wire stress measurement, wire to wire slip and overall hysteresis is in substantial agreement with the theory.

1.5 Experimental Work on Wire Rope and Strands

Durelli et al. (27, 28, 29) report tests on a seven wire strand and compare their results with the theory described in (27), see section 1.4 above. Durelli, Machida and Parks (28) have used brittle lacquer coating and electrical resistance strain gauges mounted on the wire surface in directions parallel to wire axes, to determine strains in the helical wires of steel strands subjected to tensile loads. Strand axial extension between sockets as well as the strains on individual wires, was measured for tests (a) with the strand ends fixed and (b) with strand ends free to rotate, strand rotation also being measured in the latter case. Bending tests were also performed by setting the strand horizontally and applying a vertical load. The authors conclude that the response of the strand is essentially in agreement with the theory developed in reference (27). Strains in some wires, however, are not linearly proportional to load and that at a transverse cross-section of the strand, corresponding points in different wires do not carry the same amount of stress. They state that this behaviour may be due to the following;

(a) local variations in wire geometry;

(b) foreign particles between helical wire and core;

(c) variation in friction between wires and core.

Repetition of the load does not alter appreciably the non-linear behaviour of the wires, nor the uneven distribution of load between wires. The average longitudinal strain of the

core is larger than the average longitudinal strain of the helical wires.

Durelli and Machida (29) also tested some oversize plastic models of strands in tension, torsion and bending. They believed that by going to oversize models the experimental difficulties involved in taking measurements on small steel wires would be overcome and increase in precision of the measurements as well as easy control of the laboratory loading conditions would be possible. In addition to brittle lacquer and the single grid electrical resistance strain gauges which were also used in tests on steel wire strands (28), it was possible to attach Huggenberger gauges and a rosette strain gauge to the surfaces of the oversize models. One difficulty that was not overcome, however, was elastic motion within the end grips. A correction for this 'lost motion' was applied to the theory and experimental results then compared. The authors point out several discrepancies with theory, and the uneven load sharing between nominally identical wires found in the tests on steel wire strand (28) is again in evidence with the plastic strand.

Matheson (33) and Hansom (34) tested locked coil ropes in tensile and torsional loading. The complete rope was tested first and the tests then repeated after each layer was stripped away. The properties of each layer have then been estimated from the difference between the rope response to load with and without that layer. Results from simple seven wire specimens were found to be in fair agreement with values from the analysis developed

by the authors (see section 1.4). Average discrepancies noted include 6.1% underestimate of strand extension and 3.5% overestimate of rotation in the case of tensile load without torsional restraint. There are greater discrepancies in specimens with more than two layers and this is considered consistent with the condition of partial looseness of outer layers on inner layer (or core). Exploratory work using strain gauges on the outer wires showed that outer wires of the test ropes were unequally stressed.

Others (42, 43, 44, 45) have investigated the strains on the wire surfaces of seven wire strands using electrical resistance strain gauges. Martin and Packard (42), who mounted gauges on the core wire as well as on the helicals and Paolini and Bazzaro (43) reported on hysteresis in strand response and wire strain in a loading cycle. Paolini and Bazzaro (43) put this down to friction between the wires which also accounts for the unequal loading of helical wires as revealed by the strain gauge readings. They used gauges of T and Y configuration, some of the former being mounted three alongside each other such that axial and circumferential strains on the wire crown and on each side of it were obtained. The results from these gauges, insofar as they were intended to reveal the bending and torque on individual wires are, however, inconclusive due mainly to the inequality of loading between wires noted above. Mancini and Rossetti (44) used gauges, mounted on wire crowns parallel and perpendicular to wire axes, for the purpose of determining wire stresses in strands

subjected to bending round a pulley. Results indicate that the strand does not behave like a beam of solid section. Molinari (45) used axially mounted strain gauges on the crowns of one wire at half lay intervals and also on the crowns of the other five wires at a cross section at distance half a lay length from a deliberate break made in the first wire. By comparing the load taken at each gauge position before and after the break, he showed that load sharing between the other wires is such as to maintain torsional and bending equilibrium of the strand and that by a distance of $2\frac{1}{2}$ lays from the break, the broken wire takes about 20% of the load it had taken before the break. This can be compared with the observation of Hruska (13) on broken wires in a rope, see section 1.4.

A more comprehensive test programme on the problem of load take up by broken wires is reported by Wiek (46). Using a six strand rope with wire rope core (6 x 26 + i.w.r.c.) he mounted six strain gauges on the crown of a single wire at distances of one wire lay length from each other. Breaks were made in the wire at distances starting with 12 lay lengths in the opposite direction from the first of the gauges. The rope was loaded, strain readings noted, unloaded and the process repeated after each break. In conditions of static loading the wire was found to take up its full load at four wire lays from the break while for dynamic conditions, in which the rope was loaded in bending with a pulley, eight wire lays were required before the broken wire took its full load. A gauge mounted on

an adjacent wire showed a 13% reduction in its share of the load at a distance of one wire lay from the break. There was also a reduction in the load taken by wires in the strand diametrically opposite, which, logically, thus maintains equilibrium in the loaded rope.

Wiek (47, 48, 49, 50) has used strain gauges mounted on wire surfaces to investigate a number of other wire rope phenomena. In comparing wire stresses in Regular lay and Lang lay ropes (48) he found that load sharing between nominally identical wires was more uneven in the case of the latter. This he put down to the manufacturing process in which wire tension differences, introduced while the wires are being stranded, cannot be corrected when strands are made into rope, since the strand lay is in the same direction as wire lay. He doubts, as a consequence, that Lang lay rope has greater endurance than Regular lay rope since the effect of the higher tensile stress levels in the more highly stressed wires, which give greater stress ranges in service, outweigh the effects of lower Herzian stress in Lang lay ropes due to greater surface area bearing on sheaves. In tests on 'non-spinning' ropes (49) he was able to mount strain gauges on some of the inner wires and found that inner layers take more load in the case of tensile tests where rope ends are free to rotate than they do in tests where the ends are fixed. Load sharing between wires was again found to be uneven; the surface of one of the inner wires remained in axial compression throughout the tensile loading of the rope!

For the wires in the outer layer, he reports standard deviations from mean stress of 60% in the fixed end case and 80% in tests with ends free from torsional restraint. Among his conclusions is the statement that such differences (of stress) cannot be neglected in endurance calculations. In another paper, Wiek (50) considers the possibility of statistical analysis from a limited number of tensile and bending tests on ropes of the construction 6 x 26 + i.w.i.c., having fixed ends, which have had strain gauges attached in a few selected locations. He concludes that 2.5% of the wire crowns in a rope under tension can have stresses which exceed the calculated value by 100% and that 2.5% of the crowns at the most highly stressed diametral positions of a rope subjected to bending can have stress values which exceed those calculated by 25%.

Nesterov et al. (51) describe an experimental method of determining the load taken by each layer of a spiral strand rope. The rope is held under load at a predetermined extension. After noting the tensile load and restraining torque acting on the rope, all the wires of the outer layer are cut through, while taking care to maintain the same overall extension and rotational position, and the tensile load and restraining torque again noted. The differences in the load and torque represent the contribution of the layer removed to the overall stiffnesses, axial and rotational.

Hankus (52, 53) reports on tensile tests performed on 35 mine winding ropes of diameters ranging from 22mm to 92 mm and

of a variety of constructions. Considerable permanent elongation was recorded under the first load, even when the magnitude of this load was as low as a seventh of the load required to produce the limit of proportionality in the load/extension characteristic of the rope. Subsequent loading to higher levels did not produce as much permanent elongation as the first loading, Hysteresis was attributed to frictional resistance between wires as well as the permanent elongation.

In another paper, Hankus (54) describes tests to determine the torque generated ('spinning moments') of winding ropes subjected to tensile load. The mean value found from tests on single layer spiral strand ropes differs by 10% from that predicted in a straight line expression which he developed theoretically. For more complex ropes the differences between experimental and predicted values of torque generated under tensile loading were found to be greater than 10%.

Gibson et al. (55) developed an expression to predict the torque generated in ropes subject to tension. Using a sensitive strain gauged load cell they monitored tests on Lang lay rope loaded a number of times to about 60% of breaking strength. Agreement between theory and experiment was reported to be within 2%. Other tests on non-rotating rope of 18 x 7 construction revealed the influence of rotation on torque developed in the rope. In addition, it was found that breaking strength was 34.2% less in the free end tests in tensile loading as compared with fixed end loading.

Torsion tests on three wire and seven wire strand are reported by Slight (56). His work was concerned with the development of multiple strand helical springs. The specimens, in the case of seven wire strands, were therefore of unusual geometry in that core diameter to helical diameter ratios ranged from 1.2 to 2.0, as compared with the more usual 1.0 to 1.1. Torsional stiffness in the direction of 'winding up' (a tendency to increase the number of coils over a given length) was found to be greater than the aggregate stiffness of the individual wires by up to 80% at the largest helix angle and the largest diameter ratio. Stiffness in the unwinding direction was very much lower and response was found to be similar to that of six open coil helical springs in parallel, plus one straight wire.

The relevance of rope behaviour determined in static tests to that experienced under conditions of dynamic loading have been called in question by a number of workers. Among these is Krolovets (57) who tested 19 ropes of different constructions ranging in diameter from 3.5 mm to 25.0 mm. Moduli were determined under conditions of static loading and unloading in which extensions were measured over a gauge length of 830 mm, and compared with those calculated after determining the velocity of propagation of the elastic wave in a stretched rope. Dynamic moduli from experimental work agreed within ±10% of theoretical values. The values of modulus determined experimentally were higher for dynamic conditions than for static

conditions by up to 60%. Among his conclusions is the fact that dynamic modulus is independent of rope tension and is affected by stretch and wear to an insignificant degree. He also suggests that the method used for determining the modulus of elasticity of a piece of rope by stretching a short piece of that rope does not give a true value. Moduli should be determined under working conditions.

Hankus (58) measured the frequency of free damped vibrations of a rope and utilised the Rayleigh approximation method to determine dynamic moduli of mine winding ropes. For rope lengths of 500 m, under simulated conditions of emergency braking, he found differences of 20% to 25% with empty skip and 25% to 35% with full skip between dynamic and static moduli.

Stonesifer and Smith (59) tested a number of stranded ropes of 6 x 19 construction in tensile fatigue. Among their findings was the fact that 'working in' of a new rope at reduced load offers no advantage in subsequent rope endurance under cyclic loading. Maximum life was achieved with periodic overloads just large enough to reach yield since this lowers compliance and gives maximum crack retardation. A single initial overload was more practical, however, and nearly as beneficial. They also concluded that wire break density was not a good quantitative indicator of breaking strength; nor did it give a reliable prediction of impending failure.

Drucker and Tachau (60) analysed the results from tests reported by a number of earlier workers. They first examined the effects of average tensile stress, nominal bending stress and nominal maximum combined stress on rope endurance in bending fatigue tests of a rope round a sheave. However, the most significant factor affecting endurance was found to be bearing pressure between rope and sheave.

Interwire pressure of strands and ropes has been examined by a number of workers who, like Drucker and Tachau (60), realised the importance of bearing pressure and consequent contact stresses in wires. In similar papers, Starkey and Cress (61) and Leissa (62) have analysed stranded rope of construction 6 x 7. Critical stresses occur between wires which suffer point to point contact at strand crossover points. Flattening occurs and stresses reach yield values. Relative motion during wire bending, caused by tensile load on the rope, results in fretting at these contact points, thus inducing fatigue cracks. The propagation of these cracks leads to complete failure of individual wires.

Bert and Stein (63) examined the critical crossed wire contact points of a 6 x 37 stranded rope with i.w.r.c. Photomicrographs of wire rope cross-sections clearly show wire deformations to be localized in two crossed wire contact regions. Analysis of stress levels in all wires is tabulated and the largest contact stress value is calculated as more than five times the yield stress of wire material. Rotation

of the rope by only 3^{o} in the 'tightening' (or winding up) direction results in a contact stress increase of 28%.

Dong and Steidel (64) describe a stress freezing photo-elastic technique which simulates contact loading between wires in wire rope. They show that maximum shear stress occurs at a depth of about $\frac{1}{2}$ width of the contact surface below the surface of cylinders in contact.

Laura et al. (65) describe how maximum load carrying capacity and rope modulus are affected by the type of construction and the nature of the core used. Acoustic emissions were used to detect imminent wire rope failure and use made of the fact that velocity of propagation of a longitudinal pulse in a wire rope and the transverse damping coefficient increase with increased applied tensile load. They regarded the 'Poissons ratio' of a rope as a measure of the looseness of the rope construction. The value of this ratio was found to be greater than unity at 50% of breaking load and reducing from this at higher loads.

Transverse contraction of ropes under load was examined also by Bechtloff (66) in the course of tensile tests on new ropes. There is some scatter in the results so that the effect of lay (Regular or Lang) and galvanising is not conclusive. Values of 'Poissons ratio' for the ropes vary between 0.5 and 1.8.

1.6 Wire Rope Terminations

Efficient and safe load transfer from wire rope to adjacent load bearing element is a design requirement which demands at least as much attention as that of the load bearing capability of the rope itself. A description of most available types of wire rope end attachments is given by Myers (67) together with recommendations for particular applications. He states that swaged fittings are 95 - 100% efficient and are more resistant to fatigue than are poured zinc sockets. Babbitted sockets, which are often fitted in the field, are not to be confused with zinc-poured sockets. Many babbitt metals do not adhere well to wires, whereas zinc does, and babbitted sockets have been shown to pull out at 50% of rope breaking strength.

Hilgers (68) gives a detailed account of approved procedures for end fixing with zinc and other alloy sockets. He recommends that wires should not be bent to more than 90° prior to pouring socket alloy since the tensile strength of wire is reduced by 4% to 6% if bent only once. 'Filling capacity' of various alloys is investigated: this is the ability of the alloy to penetrate between the wires of the rope where they have been separated from each other in the conical end grip. Casting temperature has an effect on the mechanical strength of the wires and there is a reduction of 4 to 5% even after half a minute of the tempering effect at 400 - 500°C. He records that there is no difference in the

effect of different taper angles in the conical end grips, ranging between 1:5 and 1:13.3. Adhesion strength reduces with increasing wire diameter since breaking strength of wire increases with the square of the diameter, whereas surface area increases only linearly.

Christen (69) has a different approach to Hilgers (68) on the question of bent over wires in socketed end grips. In a programme of tests on locked coil ropes and stranded ropes he reported that an effective increase in rope strength was achieved by hooking over the round wires. Lack of adhesion between wire and zinc is less important since the hooked wires interfere with each other in the throat of the conical grip; this could be critical in the case of a lift rope when a fire causes metal in the core to melt but the rope would remain capable of sustaining load. However, Christen reports that hooked over ends that were annealed, for the purpose of the test programme, broke under load in the majority of cases.

Dodd (70) describes development work on resin as a socketing medium. It was originally thought that bonding forces were important but experience has shown that the major restraining force is the wedging action within the socket. Choice of resin lay between the epoxide and polyester based variety, the decision going to the latter since its longer cure times and higher temperature dependence give better control. Silica was chosen as the best filler since it is not coarse enough to cause sedimentation yet not fine enough to

cause respiratory problems during mixing. The gel time for the polyester resin with silica is 10-15 minutes and the termination is capable of taking the full breaking load of the rope after one hour. Tests comparing resin with zinc socketing material, using ropes having one zinc socket termination and one of resin tested under proof load, had to be discontinued when the zinc extruded. Other claims for resin are that there is no annealing of the wire as in zinc socketing, as reported also by Christen and no melting away of the protective lubrication.

Gathman (71) reports on the results of over 800 laboratory tests on ropes ranging in diameter from $\frac{1}{4}$inch to $3\frac{1}{2}$inch without any failure of resin attachments. Tests on $\frac{7}{8}$inch diameter ropes showed that resin-poured sockets outlasted zinc-poured sockets in axial fatigue at moderate loads. Penetration was found to be better with resin than zinc.

A comprehensive test programme to determine the efficiency of nine different types of wire rope termination is reported by Matanzo and Metcalf (72). Static tension tests were performed with each type of fitting on ropes of five diameters between 13 mm and 51 mm, four at each diameter of which two were of regular lay having different constructions and two of Lang lay having the same two constructions as the Regular lay ropes. Statistical analysis of the results shows that resin-poured sockets were better than zinc-poured sockets, but they were only third and fourth best overall. Swaged sockets were most efficient, followed by flemish loop with steel sleeve and thimble.

Chaplin and Sharman (73) show that the process by which wire is gripped in a resin socket depends initially on adhesion between wire surface and resin. This initiates an extrusion or wire drawing effect of the resin in the conical socket. Increasing radial force between cone and resin is then transmitted through the resin and imposes a tighter grip on the wire as tensile load on the rope increases.

1.7 Other Considerations

Some of the references in the literature survey covered in sections 1.1 to 1.6 are of direct interest to users of wire rope and many are written by users. However, the subjects of in service inspection, testing, discard criteria and recommendations on rope usage are outside the scope of this study.

CHAPTER 2

THE DEFINITION OF OBJECTIVES

2.1 Lessons from the Literature

Uncritical perusal of the work done in this field, as revealed by the subject titles of the references given in the literature survey, might lead one to believe that the behaviour of wire ropes under load was now well understood. Activity has ranged from that of the rope user, on one hand, who attempts to establish discard criteria from his own observations, to the mathematical modeller, on the other hand, who analyses the response to load of elegant helical constructions. The studies appear, therefore, to adequately cover the whole field of wire rope stiffnesses and endurance, as well as the stress distribution in individual wires. However, closer examination of the literature does give some pointers to areas in which further useful work could be done.

It is certain that there is a large amount of published work on the mathematical modelling of the response of simple strands to various loadings. This includes Costello et al. (18, 19), Huang (32), Machida and Durelli (27), Chi (30, 31), Matheson (33) and Hansom (34). Costello et al. (20, 21, 22)also extend their analysis to some more complex spiral and stranded ropes and among some less rigorous analyses of complex rope structures are those given by Glushko (35), Kollross (36) and, for armoured cables, Knapp (37, 38,

(39). The contribution of Hobbs and Raoof (41) to the understanding of interwire slip in large spiral strands should also be noted here. The modelling of response to load in more complex constructions and larger ropes would, therefore, also appear to be well covered. However, all those workers who have compared their predictions with experimental results have reported discrepancies. If, therefore, one now seeks to bridge any remaining gaps between idealised models and the behaviour of real strands or ropes, it seems advisable to turn to the assumptions made at the start of each analysis that has been presented. Costello et al. (18, 19) neglect frictional forces between the wires and radial force between core and helical wires. Machida and Durelli (27) and Chi (30, 31) also neglect frictional forces and, like Costello, do not consider either the Poisson effect on individual wires in tension or the flattening effect on wires due to interwire contact pressures. Huang (32) does consider friction and Poisson effects but assumes no rotational slip between core and helicals and omits flattening effects from his analysis. All these models also neglect end effects due to the influence on strand geometry of the transfer of load from strand to grip.

The references to experimental work on wire rope and strand are not quite as numerous as those on mathematical modelling of response to load although the testing of full scale ropes has been reported by a number of workers. Among these are Drucker and Tachau (58), Hankus (52, 53), Gibson et al. (55),

Wiek (48, 49), Nesterov et al. (51) and Krolovets (57). Although some of their findings have general application, they were usually seeking information on response and/or endurance of a particular type of rope or rope construction and were not as concerned with the general principles of rope behaviour. The more fundamental experimental studies have been performed on simple strands. Among those reported, only Matheson (33) and Hansom (34) appear to have tested more than one wire strand, and this was only in the course of a comprehensive programme investigating the load bearing capacity of each constituent layer of a more complex spiral locked coil rope. Durelli et al. (28, 29) tested oversize plastic strands as well as a wire strand, but the lay angles of both wire and plastic strands were less than 10^{o}, thus representing only one end of the range of strand geometries found in practical use. Others testing simple strands appeared to be interested in only limited aspects of strand response to load. Among these Martin and Packard (42) and Paolini and Bazzaro (43) examined hysteresis in strand response and wire strain, Mancini and Rossetti (44) were interested in wire strains during strand bending and Molinari (45) was concerned with load take up by a broken wire. One essential element present in accurate tensile and torsional testing of conventional solid testpieces that is absent from the literature on wire ropes concerns the response over a known gauge length. With the exception of Hankus (52) who mounted a dial indicator between straps around large ropes under tensile test, workers in this field appear to

have been content with measurements of extensions and rotations that were taken between end grips.

The foregoing paragraphs show that despite the volume and apparently comprehensive coverage of the field by the available literature, there were a number of aspects of wire rope response that merited further study. The following section examines some of these aspects and indicates how the objectives of the current study were formulated.

2.2 Decisions on the Form of this Study

A prerequisite to this examination of objectives was that the results of the study should be capable of contributing to the understanding of wire rope behaviour in such a way as to give practical benefit to designer and/or user. From this starting point, it was a short step to the decision that there should be a major experimental content. In looking at the literature (see particularly section 2.1 above) it is evident that the testing of basic strands was potentially the most fruitful area of work.

The seven wire strand consisting of a straight core wire round which are wrapped six helical wires, is the simplest of practical strand constructions. It provides the basic element from which either spiral strand ropes, or more complex stranded ropes are built up. Experimental results obtained can be compared with existing theoretical predictions of Machida and Durelli (27) and Costello et al. (18, 19), after the latter has been modified to take account of the contribution of the core. The decision was taken, therefore, at this stage, to test seven wire strands.

It was decided next to confine strand testing to axial loading in tension. In order to ensure that test conditions corresponded as nearly as possible with those that occur in practice, the testing was to have the facility that torsional restraint on strand ends should be variable, as required, from free to completely fixed.

For the range of tensile loading conditions planned, it was decided that strand behaviour which required measuring and recording are, load, torque generated, strand extension, strand rotation and strain on wire surfaces in selected locations. End effects were considered of great importance. Insofar as uncontrolled movement of strand, extensional and rotational, both elastic and irreversible, must be expected within strand end grips, however efficient, it was considered necessary to incorporate a facility for measuring strand extension and rotation under load, over a known gauge length in a region where end effects are minimised. However, since the influence of end grips have an effect on the stress distribution in individual wires, strain measurement on wire surfaces should be effected at points along the whole length of the strand, and particular attention paid to obtaining strain readings as close to the end grip as possible.

Previous workers in this field have not studied experimentally the effect of differences in initial strand geometry on strand response to load. (See section 2.1 above). In order to extend this work, therefore, it was decided that a number of strands having different initial geometry should be tested. The variables in strand geometry are lay length (which affects helix angle), core diameter and helical wire diameter. In practical strands, the ratio of core diameter to helical diameter ranges from 1.0 to about 1.1. Since it is rather more difficult to produce a range of strands having the same helix

angle but different diameter ratios than to produce strands from the same wires, with a range of lay lengths, it was decided to use the latter in the test programme. These were, in fact readily available, courtesy of British Ropes Ltd., over a range of practical lay angles, from 9.1^{o} to 16.4^{o} and wire diameters 3.94 mm (core) and 3.73 mm (helicals).

The availability of the strands from British Ropes dictated the decision which would otherwise have had to be made on strand size. The range within which the choice of strand size would have had to be made are load capacity of the test rig to be developed, at the upper limit, and wire size to which a strain gauge could be effectively attached, at the lower limit. Fortunately, the available strands fell comfortably within this tolerance.

2.3 Objectives

The decisions made concerning the form of this study and described in the previous section can now be formalised as the objectives.

(a) Experimental Work

(i) Axial loading in tension of 7-wire steel strands.

(ii) Torsional restraint of ends ranging from fixed to free.

(iii) Instrumentation: measurement required of the following; axial load; restraining torque; wire surface strain in selected locations; strand extension and rotation over known initial gauge length.

(b) Comparison of Results with Existing Theory

Experimental results are to be compared with strand response and wire stresses as predicted by Machida and Durelli (27) and Costello et al. (18, 19) as modified to take account of load taken by the core. Particular attention to be paid to stress concentration effects near end grips.

(c) Further Theoretical Work and Comparisons

An attempt is to be made to incorporate interwire friction and slip, Poisson effects due to tension in wires and the effect of flattening due to interwire pressure. The accuracy of these predictions is to be compared with those of Machida and Durelli (27) and Costello et al. (18, 19).

CHAPTER 3

TEST EQUIPMENT

3.1 Introduction

In order to fulfil the objectives of this study, as determined in the previous chapter, the development of certain items of test equipment was an essential first step. This chapter describes details of the design and, where appropriate, calibration of the equipment.

3.2 Test Rig

Two circular section columns of 95 mm diameter which had been part of an old press became available and were incorporated in the design of a test rig for tensile tests on wire rope and strands having their axes horizontal. See Figures 3.1 and 3.2. The availability of a suitable hydraulic ram and hand pump also influenced the form and orientation of the loading system. Specifications are given below:

I Load: up to 600 kN (60 tonf) ... ram capacity.

II Extension: up to 76 mm (3 in) ... max. ram travel.

III Test specimen length: up to 1500 mm (including grips).

IV Strand grips: conical shaped resin socketed terminations. Further details are given in chapter 4, section 4.

V Adaptor incorporating a large thrust ball race permits tensile tests with torsional end restraints ranging from zero ('free end' tests) to fixed end, zero rotation. This adaptor is locked in position for fixed end tests.

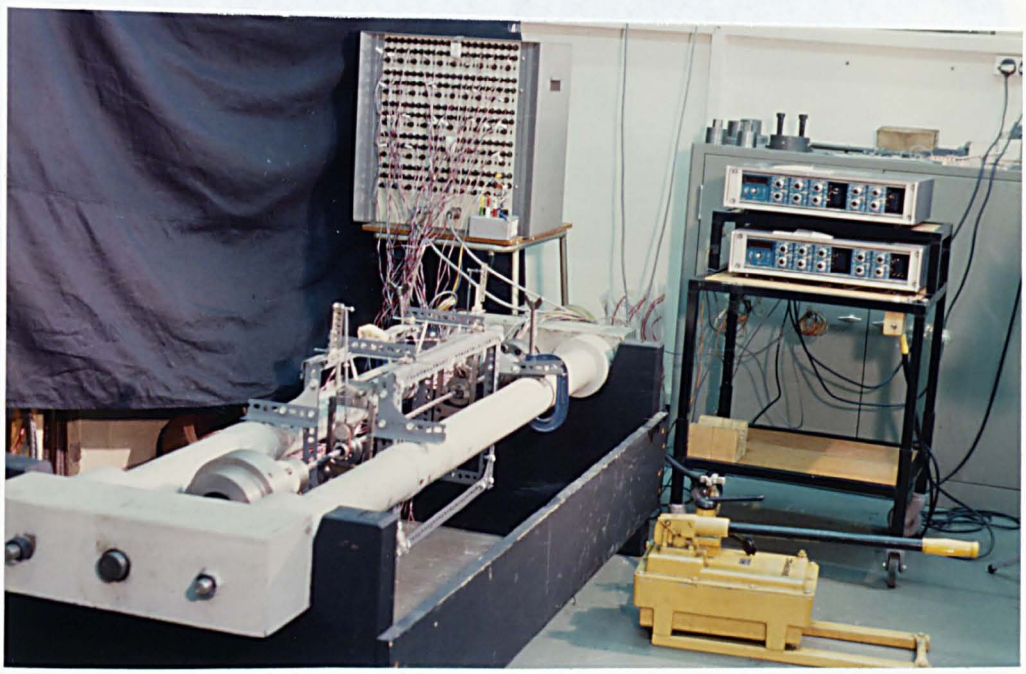

Figure 3.1. Strand Testing Equipment:General View.

Plan View.

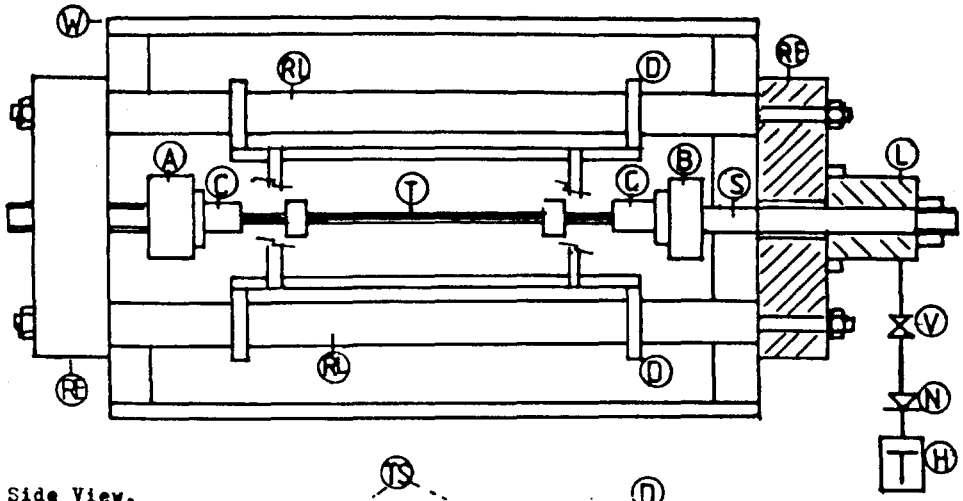

Side View.

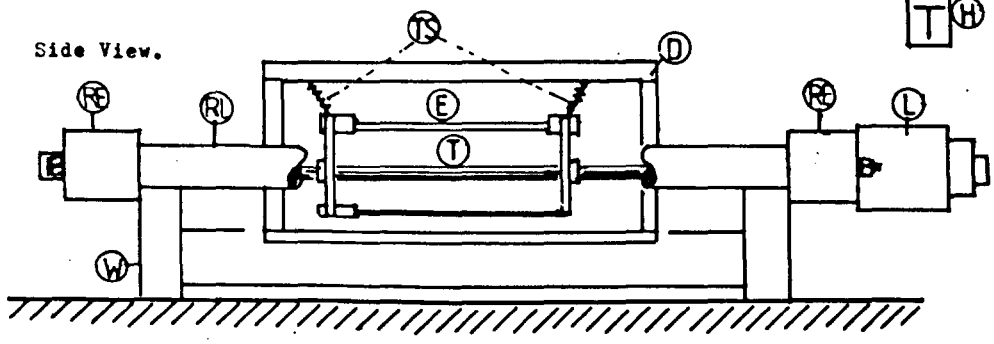

Figure 3.2. Test Rig for Wire Strand.

A	Adaptor.
B	Boss.
C	Conical Strand Grip.
D	Dexion Support.
E	Extrometer. (See Figure 3.5.)
RL	Rig Longitudinal Bar.
RE	Rig End Member.
H	Hand Pump.
N	Non return valve.
V	Valve.
L	Load Ram.
S	Strain Gauged Load Cell.
T	Test Strand.
TS	Tension Springs.
W	Wooden Support.

3.3 Load Cell

3.3.1 Design

This comprises the 50.8 mm (2 in) dia. loading rod (S) which is located in the centre bore of the loading ram (L). See Fig. 3.2. Strain gauges are mounted on the surface of the rod where it emerges from the rig end member (RE). Four circuits were used in the course of the testing; two were designed to give output from tensile load and two from torque generated in the strand. The duplication of circuits was considered necessary when the data logger was commissioned (see section 3.5) so that one output could be fed to the data logger and the other could be used as a monitor on a digital display at the site of the rig. In fact, the gauges of one of the tension circuits were dislodged in the shock impact between load cell and rig end member, following the fracture of a strand under test. In analysing results, only those from the remaining tension circuit and from the torsion circuit giving least output due to tension were used. (See section 3.3.2).

The configuration and overall dimensions of the load cell were largely dictated by the rig layout, in particular the loading ram bore of just over 2 inch diameter. Nevertheless, it was possible to follow the recommendations of Pople (74), who stated that stress in commercial transducers is limited to 30% of the yield value, in order to minimize hysteresis. The recommendations of Virgoe (75), mainly concerned with ensuring reasonable life for the transducer, included a limitation

of 6% side load on rated capacity, which is acceptable in tensile testing of strand and the fact that loading should not be transmitted through threads, which had to be disregarded for reasons of space and rig configuration. This last feature (threaded connections on each end of the loading rod) may have contributed to crosstalk in the torsion circuits of the load cell, when in tension but the calibration procedures (see section 3.3.2) take full account of this. See Appendix A.1., sections A.1.1 and A.1.2 for details of the circuitry used in the load cell, and Appendix A.6, section A.6.1, for strain gauges types and application techniques.

3.3.2 Calibration

(i) Tensile Loading

Screwed and flanged adaptors for tension calibration were attached to the ends of the load cell rod so that it could be located in the grips of a 50 tonf Denison testing machine. Calibration up to 200 kN gave linear output from the tension circuit, with no detectable hysteresis or deviation other than that due to difficulty in reading the Denison scale. See Appendix A.1 and Fig. 3.3.a. From Table A.1.1.& Fig. 3.3.a., the slope of the tension/output plot is

$$\frac{dP}{dV_P} = 20 \text{ kN/mv} \qquad 3.1$$

There was also some output from the torsion circuits when the load cell was subject to tension. In order to obtain an

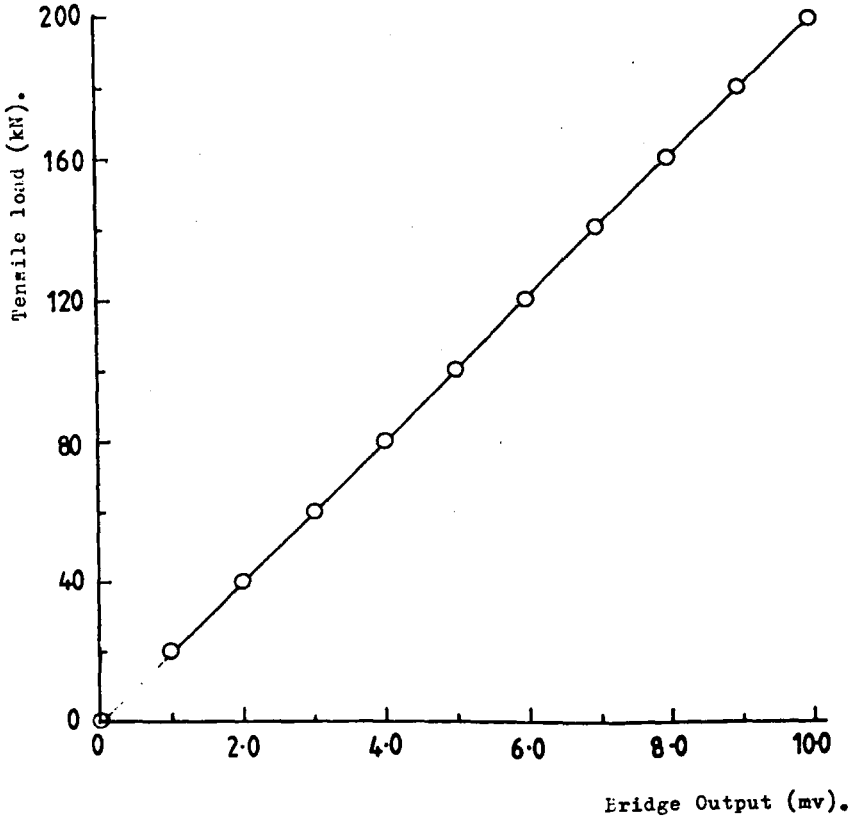

Figure 3.3.a.Load Cell Tension Circuit.Tensile load/Bridge output.

Points from Table A.1.1.(Appendix A.1.)

accurate assessment of this output, it was necessary to load the load cell in the rig itself, using a $\frac{5}{8}$ in. dia. rod in the normal place of the strand, since end effects from the Denison test machine, used at the limit of its clearance between grips, were not constant as load increased. The problem associated with the lack of precision in manufacture of screwed ends, as suggested by Virgoe (75), is a likely reason, since the loading axis may change, and is not likely to coincide with the geometric axis. It can be seen that even in the test rig, at low loads, the effect is not linear, but this is probably due to self weight effect of the loaded rod and the load cell itself. (See Appendix A.1, Table A.1.2 and Fig. 3.3.b). However, it would appear that the slope of the linear part of the graph of output from the torsion circuit against tension in the strand (Fig. 3.3.b) constitutes a valid correction factor for use in the determination of torque generated during strand tests. From Table A.1.2 and Fig. 3.3.b, the slope of the tension/output plot can be taken as

$$\frac{dP}{dV_M} = -0.188 \text{ kN}/\mu v \qquad 3.2$$

except at low loads.

The output from the torque circuits under tensile load is obviously an undesirable feature in a load cell designed to measure torque. The problem may be due to screwed ends, as discussed above, but also due to slight misalignment of strain gauge axes when they are being attached to the load cell surface.

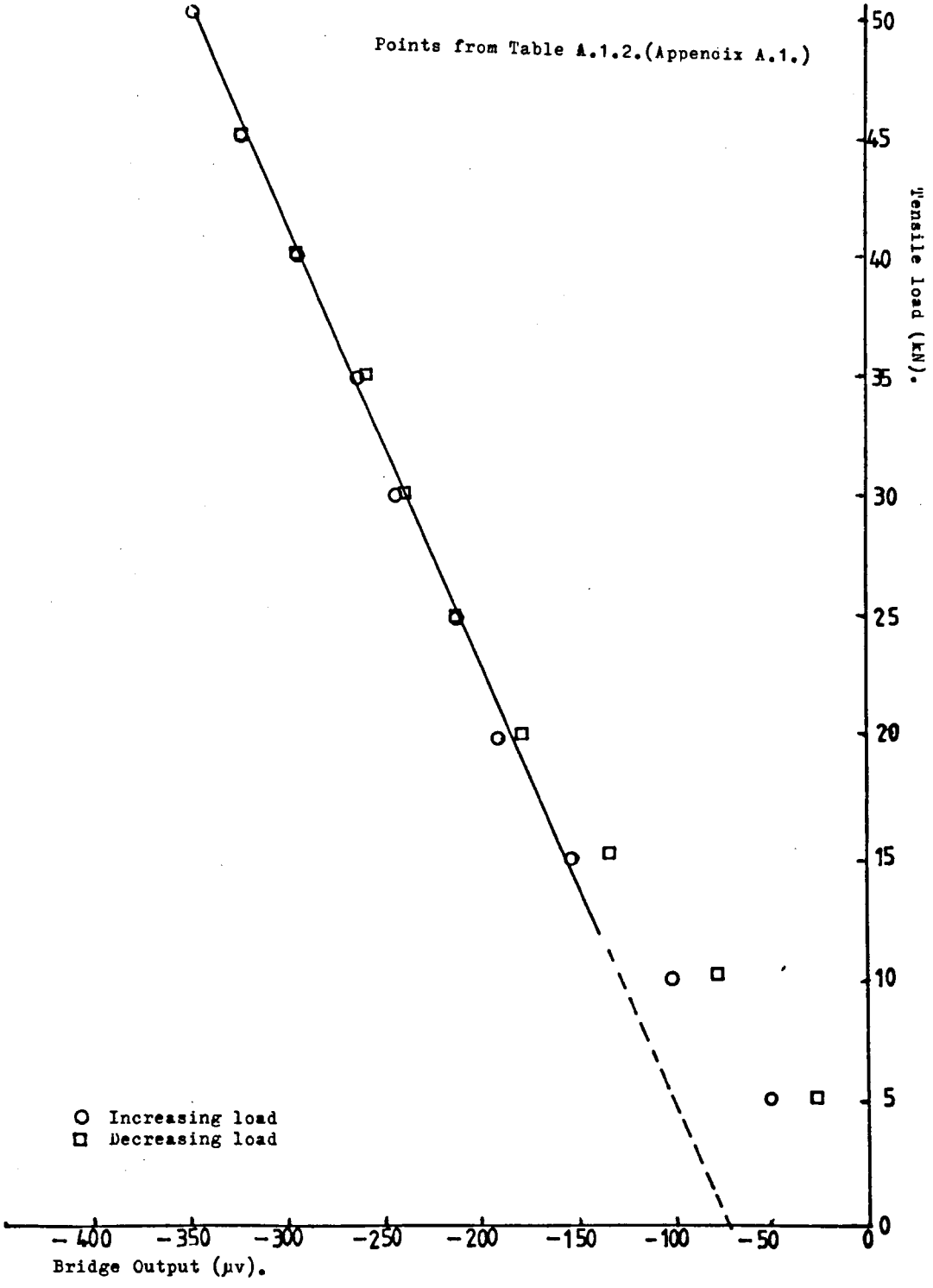

Figure 3.3.b. Load Cell Torsion Circuit. Tensile load/Bridge output.

The nett effect is to give an equivalent overall gauge misalignment. This effect is greatly increased in a situation, as here, where maximum strains from the torsion range are very much less than maximum strains from the tension range of tests. See Appendix A.1, section A.1.3 for an explanation of this phenomenon.

(ii) Torsion

Screwed adaptors having squared ends were attached to the ends of the load cell rod so that it could be located in the grips of an Avery torsion testing machine. Calibration up to 100 Nm gave linear output from the torsion circuit with no detectable hysteresis or deviation other than that due to difficulty in reading the Avery scale. See Appendix A.1 and Fig. 3.3.c.

From Table A.3 and Fig. 3.3.c, the slope of the torque/output plot can be taken as

$$\frac{dM}{dV_M} = 9.9 \times 10^{-3} \text{ Nm}/\mu v \qquad 3.3$$

There was no detectable output from the tension circuits of the load cell when it was subjected to torque.

However, from expressions 3.2 and 3.3 above, it is now possible to express the generated torque in a strand as

$$M = M' + 0.053P \qquad 3.4$$

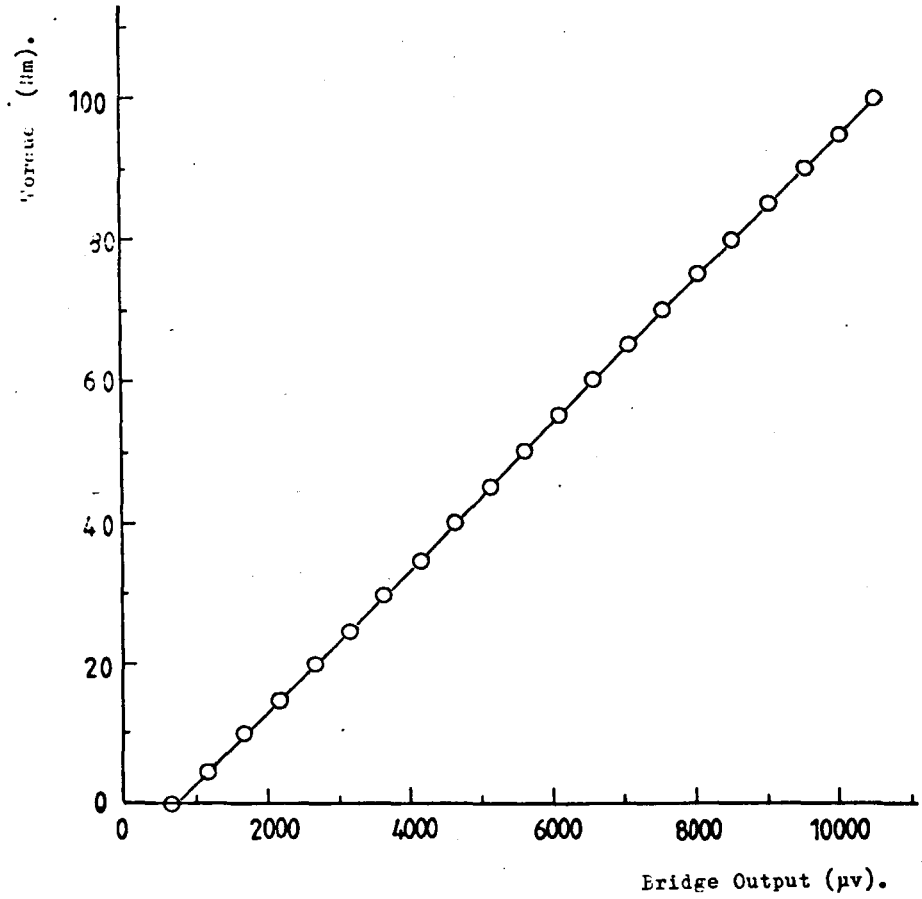

Figure 3.3.c.Load Cell Torsion Circuit. Torque/Bridge output.

Points from Table A.1.3.(Appendix A.1.)

where M is the actual torque generated in Nm,

M' is the apparent torque as indicated by the amplifier output,

and P is the tension in the strand in kN.

3.4 "Extrometer"

3.4.1 Design

This device is used for simultaneous measurement of strand rotation and extension. See Figures 3.4, 3.5 and 3.6. Specifications are given below:

I Gauge lengths: 225mm to 600 mm in steps of 95 mm (but this can be adjusted to suit the application).

II Extension: 50 mm (equal to half range of displacement transducer).

III Rotation: linear up to 320°.

IV Strand diameter: 11.5 mm (with changed grip plates this can be in the range 0 - 15 mm).

Grips are screwed tight over a rubber sheet of 1 mm thickness fitted all the way round the strand (see Figure 3.4 and 5). The grip plate housing is mounted in the inner race of a ball bearing (B) the outer race of which fits into a boss (BS) which is itself pivoted about a horizontal axis X_2X_2, perpendicular to the test strand axis. The vertical members of the extrometer are pivoted about axis X_1X_1 at the top, which gives a 2:1 displacement ratio to the displacement transducer mounted at the bottom of the vertical members on the axis X_3X_3. The axes $X'_1X'_1$, $X'_2X'_2$ and $X'_3X'_3$ are horizontal axes for the left hand vertical member corresponding to axes X_1X_1, X_2X_2 and X_3X_3 for the right hand member. (See Figure 3.5).
The rotation of the strand at each of the gauge lengths is

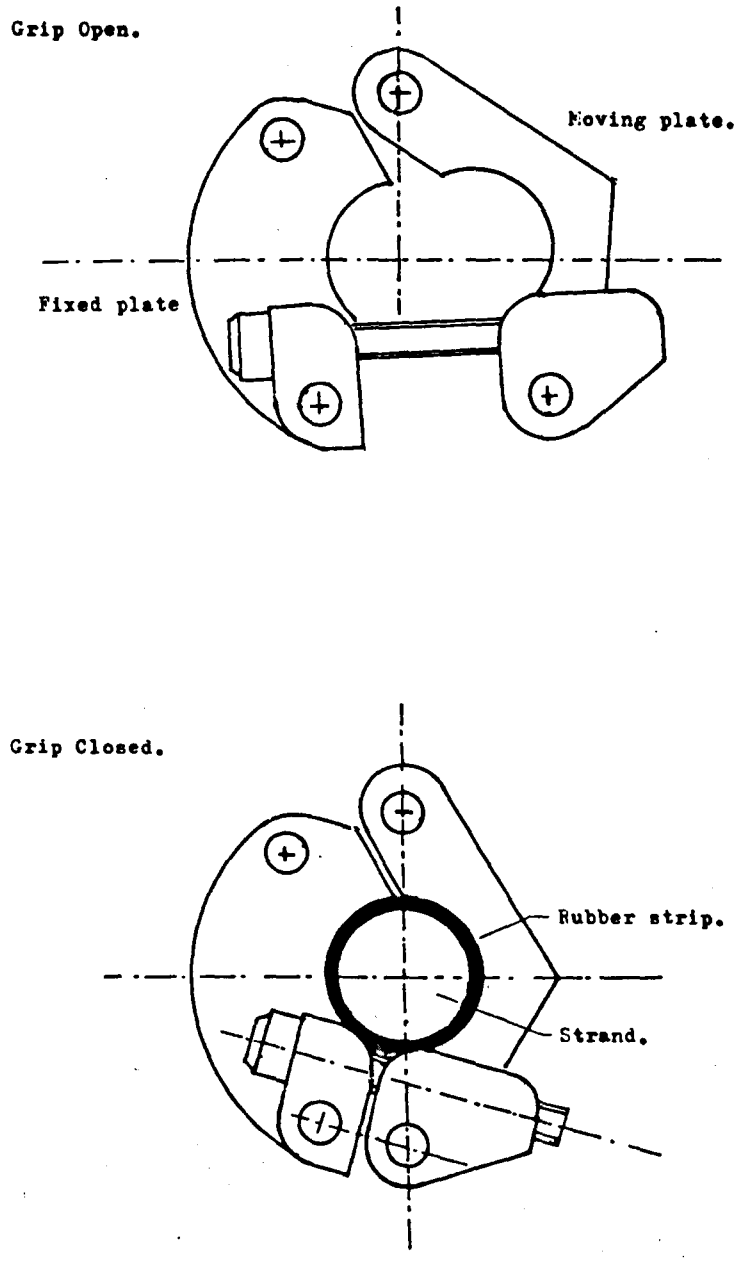

Figure 3.4. Extrometer Grips.

FIGURE 3.5. EXTROMETER.

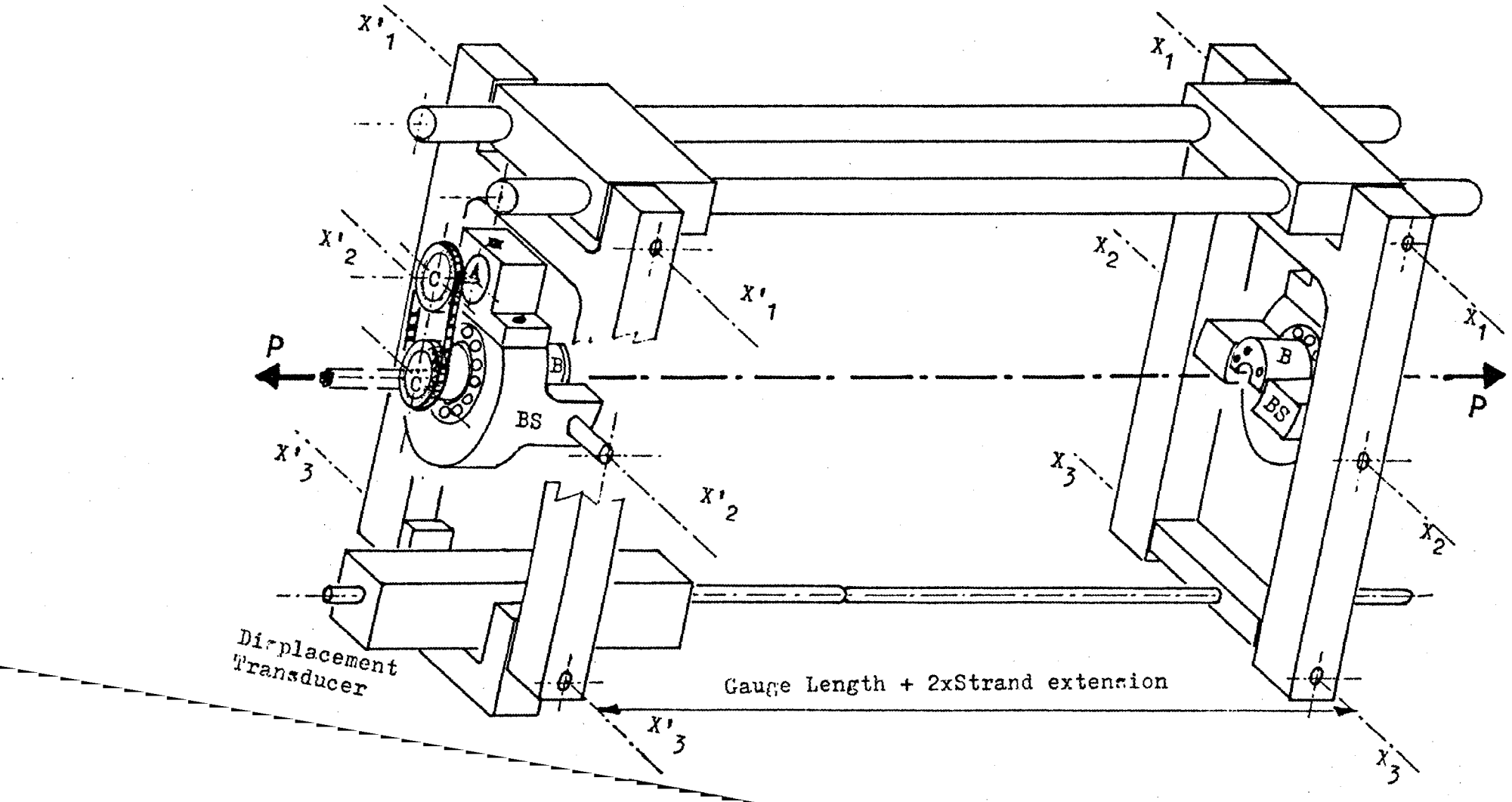

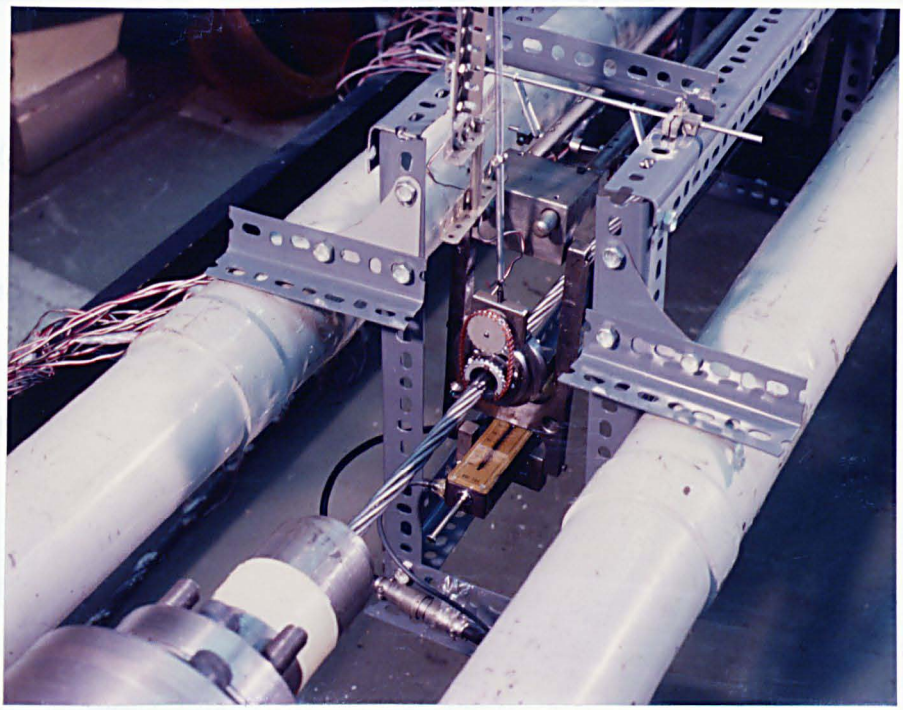

Figure 3.6.Extrometer in position showing sprockets and displacement transducer.

transmitted through a sprocket (C) (mounted axially on the grip housing) and a chain of plastic covered wire to another sprocket (C) mounted on the spindle of a rotary potentiometer (A), gripped in the boss BS. The potentiometers are connected electrically such that the voltage output is proportional to strand rotation over the gauge length $(\phi_2 - \phi_1)$.

The whole weight of the extrometer is taken on 4 tension springs (TS) (see Figure 3.2) suspended from a Dexion support (D) (see Figure 3.2) resting on the rig's longitudinal bars (RL) (see Figure 3.2). The extrometer is thus designed to transmit virtually no loading to the strand during the course of a test.

See Appendix A.2 for details of circuitry used in the extrometer.

3.4.2 Calibration

(i) Extension

Relative movement of the grips was achieved by use of a screwed rod of 1 mm pitch, held in one grip while a tapped boss, attached to a second rod, having suitable collars, was rotated through a sleeve held in the second grip. Increments of 10° of rotation of the screw in the boss gave linear displacements of $\frac{1}{36}$ mm and this was calibrated against the output of the displacement transducer, which was led to one channel of the bridge/amplifier unit. Although the design and manufacture of the extrometer were such as to minimize slop and play in

bearings, it had to be expected that a comparatively large instrument involving two grips, twelve bearings in six pivot axes and a linear displacement transducer would have some backlash. In addition to the determination of the relation between extension and bridge output it was therefore important to establish the magnitude of this backlash in the system.

Table A.2.1., Appendix 2, gives the calibration over 5.25 mm ($5\frac{1}{4}$ revolutions of the screw; pitch 1 mm). The slope of the extension/output relation was determined by least squares calculation. The backlash is determined by the difference between the intercepts of the straight line expressions from each direction (clockwise and anti-clockwise screw rotation).

From Appendix A.2, A.2,3 and A.2.4 extension in mm is given by

$$\delta_{INC} = 2.498 \times 10^{-3} \; L_F + 2.612 \qquad 3.5$$

$$\delta_{DEC} = 2.505 \times 10^{-3} \; L_F + 2.499 \qquad 3.6$$

where L_F is the output from the displacement transducer circuit in volts.

By difference in intercepts, backlash is 0.11mm.

From 3.5 and 3.6, the slope of the extension/output plot can be taken as

$$\frac{d\delta}{dL_F} = 2.5 \times 10^{-3} \quad mm/v \qquad 3.7$$

(ii) Rotation

Relative rotation was achieved by use of the same screwed rod described in the extension calibration, but with the screwed boss locked on the rod. Increments of 5° over 320° were calibrated against output from the rotary potentiometer circuit. The slope of the rotation/output relation was determined by least squares calculation. The backlash is determined by the difference between the intercepts of the straight line expressions from each direction.

From Appendix A.2, A.2.5 and A.2.6, rotation in degrees is given by

$$\emptyset_{INC} = -199.6\ R_F + 161.29 \qquad 3.8$$

$$\emptyset_{DEC} = -199.6\ R_F + 160.83 \qquad 3.9$$

Where R_F is the output from the rotary potentiometer circuit in volts.

By difference in intercepts, backlash is 0.46°.

From 3.8 and 3.9, the slope of the rotation/output plot can be taken as

$$\frac{d\emptyset}{dR_F} = -200^{\circ}/v \qquad 3.10$$

Note that the backlash of the extrometer is discussed further in Chapter 5, sub-section 5.5.4, and it is concluded that results on load/extension and load/rotation relations are not affected.

3.5 Data Processing

3.5.1 Data Logger

One of the objectives in the later preliminary tests on strands (see section 4.5.3) was to adapt an existing data logging system for use with up to 35 channels of output from strain gauges and load cell. The bulky control box and digital indicator, together with the punch paper tape and printer tape units permanently connected to this system (and used regularly by other workers), was situated some 30 metres from the strand test rig. It was necessary therefore to develop a switch for remote triggering of the control box and to calibrate strain gauge outputs in order to take account of line losses. Details of this calibration are given in Appendix A.3.

3.5.2 Computation and Graph Plotting

The punched tapes obtained from the data logger for each load cycle performed in tests on strands were fed into the Systime PDP11 computer belonging to the Department of Mechanical Engineering. Suitable programming enabled conversion of raw data from strain gauges to values of wire surface strain, using the calibration figures obtained in Appendix A.3, and output from load cell circuits was converted to tensile load values and torque generated in the strand. Extrometer readings of strand extension and rotation were entered manually via the keyboard. After programming in the relevant calibration figures and suitable scaling of parameters required, the graph plotting facility attached to the computer was used to obtain plots of strand response under load (see figures in Chapter 4 and 5).

CHAPTER 4

PRELIMINARY TESTS

4.1 Summary of Objectives

Before embarking on a comprehensive programme of tests in furtherance of the main objectives of the study, as laid down in Chapter 2, section 2.3, a number of preliminary tests were performed. These served the purpose of commissioning the test rig and proving all the elements of the test system under actual loading conditions. The aims of these tests can be itemised as follows.

4.1.1 Strand Terminations

Although strand extension and rotation is designed to be measured over a pre-determined gauge length intended to be at such a distance from end terminations that end effects are minimal, the efficiency with which the strand wires are gripped is still an important element in the success or otherwise of strand testing. The study of end effects on stress distribution in and load sharing between individual wires is facilitated if strain gauges are attached as close as possible to the end grips. Wire slip in the socketing medium of the grip under load effectively increases strain gauge distance from the location of the gripping action. Uncontrolled rotation of the strand in the grip resulting from excessive elastic distortion in or disintegration of the socketing medium in the grip can effectively reduce the degree of torsional restraint intended for a particular test. The experience of

Durelli and Machida (29), who had to correct their theory to allow for 'lost motion' in the grips, is salutary in this regard. Cone size and wire end preparation required modification during the course of these preliminary tests. See Appendix A.4.

4.1.2 Strain Gauges

The reliability with which the strain gauges could be attached to the surface of the strand wires and the validity of the outputs from these gauges throughout the tests had to be established and, in the case of reliability, improved. In addition it was necessary to determine the number of gauges which would be required in the main test programme, in order that strand preparation time be minimized while ensuring that essential features of stress distribution in and load sharing between wires were all examined. Strain gauge types and application technique are described in Appendix A.6.

4.1.3 Other Instrumentation and Data Processing

Changes in some items of equipment used and development work on others was required as the tests progressed. A description and calibration details were given in Chapter 3, section 3.3, of the data logging system. Other developments are described in the course of the rest of this chapter.

4.1.4 Elastic Modulus of Wires

The validity of any comparison between experimental

results and the mathematical modelling of strand response depends, among other things, on the accuracy of the wire elastic modulus used in the calculations of the modelling. It was therefore necessary to determine this modulus within reasonable confidence limits. Tests on core wire revealed a modulus value that was lower than that expected for steel wire. A fuller investigation was required and this is reported in Appendix A.5.

4.2 Strand I

The first strand to be tested had been made available by courtesy of British Ropes, before the completion of the test rig described in Chapter 3, section 3.2. It was therefore necessary to use a 50 tonf capacity Denison tensile testing machine, which limited the strand test length to 527 mm and dictated the outside dimensions of the end grips. The 'extrometer', for simultaneous measurement of extension and rotation over a pre-determined gauge length was also not yet available and in any case, it was designed for use on a strand subjected to tensile loading on a horizontal axis. The current design cannot be used in a vertical load axis machine of the Denison type. The instrumentation possible for this test was therefore confined to strain gauges, three of which were attached at about the middle of the strand, two on one wire at a distance of about half a lay length from each other and the other on the wire diametrically opposite the first gauge (See inset of Figs 4.1 and 2). The design of end grip had been decided in the light of the experience gained by British Ropes Ltd. at Doncaster and the Health and Safety Executive Research Departments at Sheffield and Buxton. The termination consists of a steel body with conical hole and the socketing medium used is the polyester based resin with silica filling from the Wirelock Co. See Dodd's paper on this subject (70). The progress in the development of strand terminations through the course of this study is given in Appendix A.4.

Strand details were as follows: core wire diameter 3.94 mm, helical wire diameter 3.73 mm, lay length 115 mm.

The strand was loaded and strain readings recorded in each of 30 loading cycles, with increasing maximum load each cycle. As the load reached 92 kN, on the 27th load cycle, loud 'cracks' were heard from inside one of the end grips. The noise was heard again at about the same load during the 28th load cycle. More cracks were heard on the next two cycles, taken to 100 kN and the loading then increased until strand fracture occurred at 130.5 kN. All wires broke at about $\frac{1}{3}$ distance from one end and a birdcage effect in the helical wires occurred at the other end, adjacent to the grip. Inspection of the end grips revealed that a disc of resin had broken away from the back of each grip across a plane perpendicular to the strand axis, at the extremity of the bends in the wires. The resin between hooked ends was broken in small pieces and the hooks appear to have locked with each other, effectively jamming the throat of the conical hole.

Strains measured in first and last loading cycles are shown in Figs 4.1 and 4.2 respectively.

4.3 Strands II and III

The test on strand I showed that two diametrically opposite wires did not take an equal share of the load and in an attempt to eliminate the possibility that the unsymmetrical distribution of hooked over wires within the socketing medium contributed to this inequality of loading, it was decided to try unbent wire ends in strand II. The avoidance of resin breakup and the jamming of hooks in a random manner at the throat of the conical hole was another objective. The strand test rig was available at this time and was used for the termination test on strand II. The terminations sustained load as it was increased up to 40.5 kN, but all wires then started slipping through the resin at one end and load fluctuated about 8.1 kN until the wires pulled out completely. Fig. 4.3 shows the wires at the end of the strand after they have pulled out of the resin socketing medium. Remnants of the resin (orange coloured flakes) and plasticine (used to seal the end during pouring of the resin mixture) are seen on the wires of the strand. (See Appendix A.4, section A.4.2 on socketing procedure). Fig. 4.4 shows part of the truncated cone of resin which was knocked out of the steel grip body after the test. The holes through which the wires were pulled can be clearly seen.

Strand III, tested next, consisted of that part of strand II which includes the end which did not pull out of the termination and a length of strand short enough to fit in the Denison

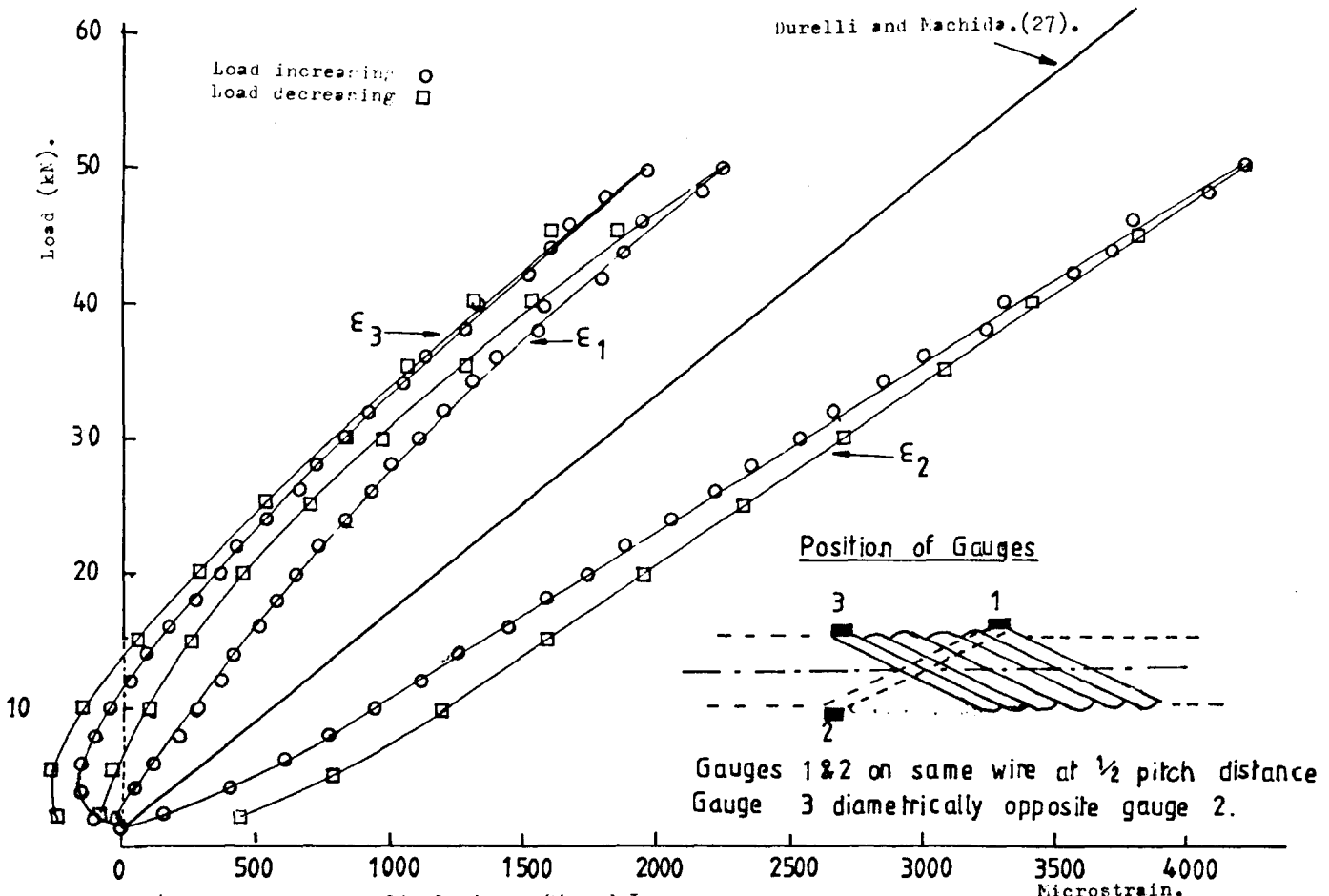

Figure 4.1. Load/Axial strain on helical wires. Strand I.
(First loading.)

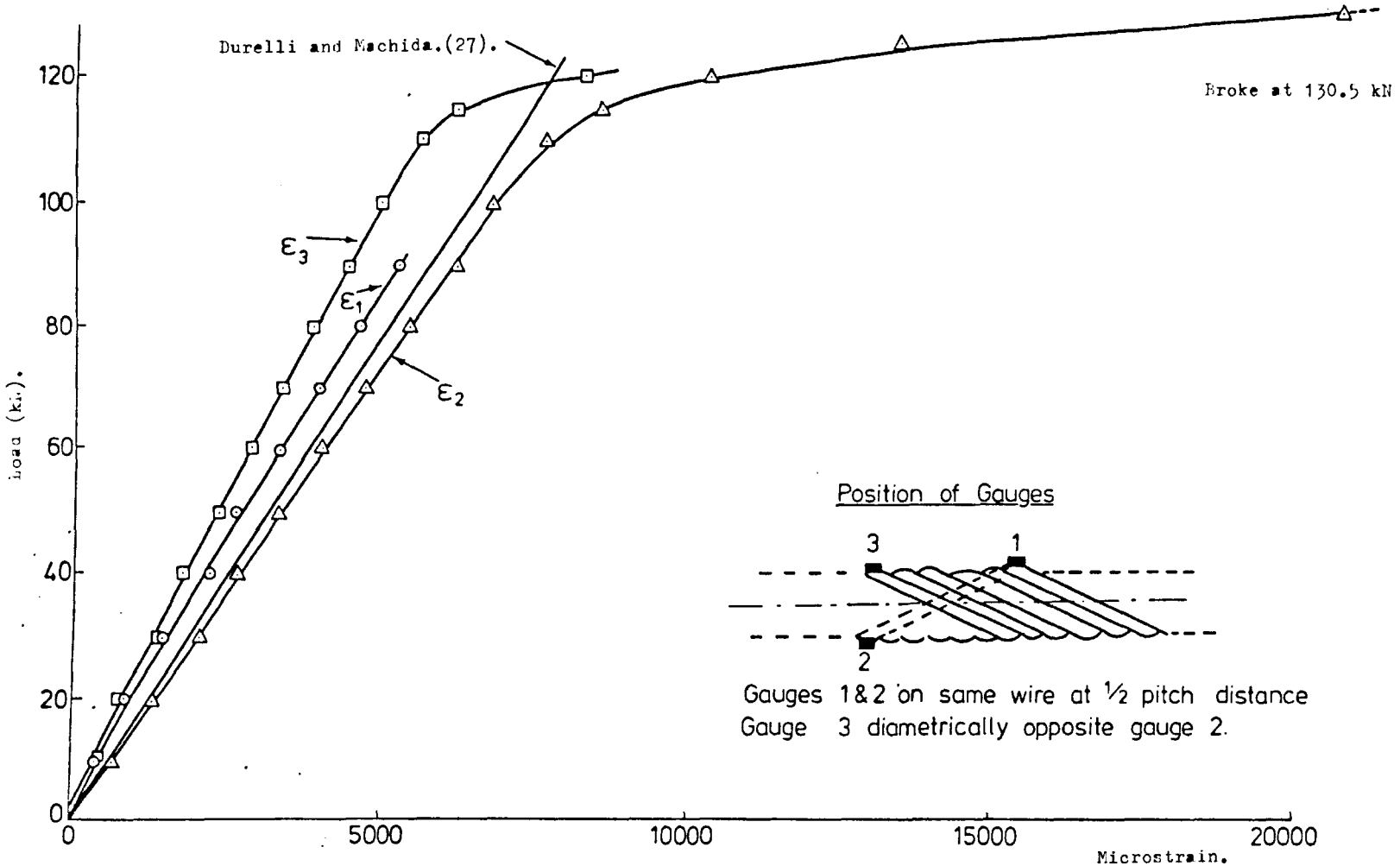

Figure 4.2. Load/Axial strain on helical wires. Strand I.
(Final loading to fracture.)

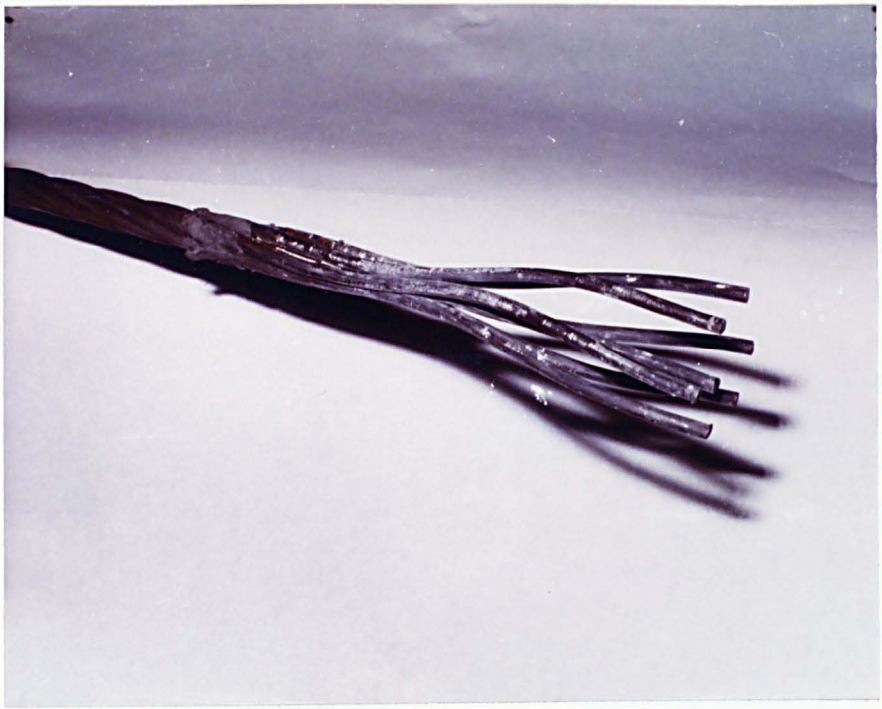

Figure 4.3.Strand II.Wires pulled out of resin.

Figure 4.4.Strand II.Resin cone after wires pulled out.

50 tonf testing machine, when the opposite end was socketed. The new socket included a steel disc with seven holes (See Appendix A.4, Fig. A.4.1.C). The disc made no improvement on gripping efficiency and the wires pulled out again at a load which fluctuated within two or three kN of about 80 kN.

4.4 Strand IV

4.4.1 Strand Preparation

The extrometer, for simultaneous measurement of strand extension and rotation, was now available. It was therefore possible to proceed with the objectives of commissioning equipment and proving test techniques, as described in section 4.1 of this chapter. The strand tested had a marked initial curvature and was from another length having the same specification as strands I, II and III. Extrometer bosses and grip bodies were threaded onto the strand before the end termination procedure was instituted, as described in Appendix A.4. For this strand, wires were bent through 180° to form single hooks within the resin.

Strain gauges were attached to wire surfaces with grids parallel to wire axes over five lay lengths (pitches) of the strand, the third of these pitches located at the middle of the strand; see Fig. 4.5 .(For gauge types and application techniques see Appendix A.6).

4.4.2 Loading Programme

Table 4.1 gives the maximum load and end condition for each of the 67 loading cycles to which the strand was subjected. For fixed end tests, the adaptor was locked in position. (See Fig. 3.2). For free end tests, the adaptor was left free to rotate. Due to small frictional resistance torque within the thrust bearing of the adaptor, it was necessary to turn the adaptor carefully until output from the torsion circuit showed zero

Figure 4.5. Strand IV: Position of Strain Gauges.

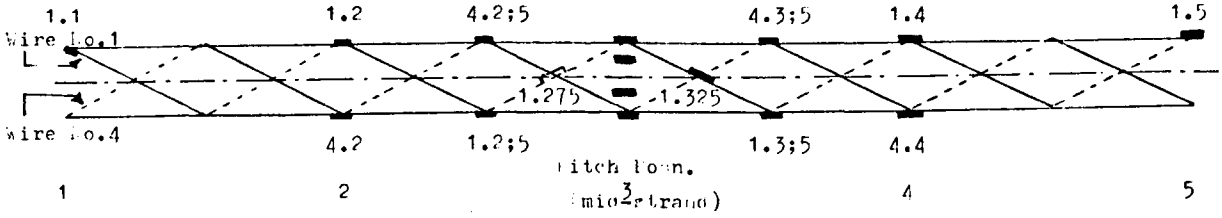

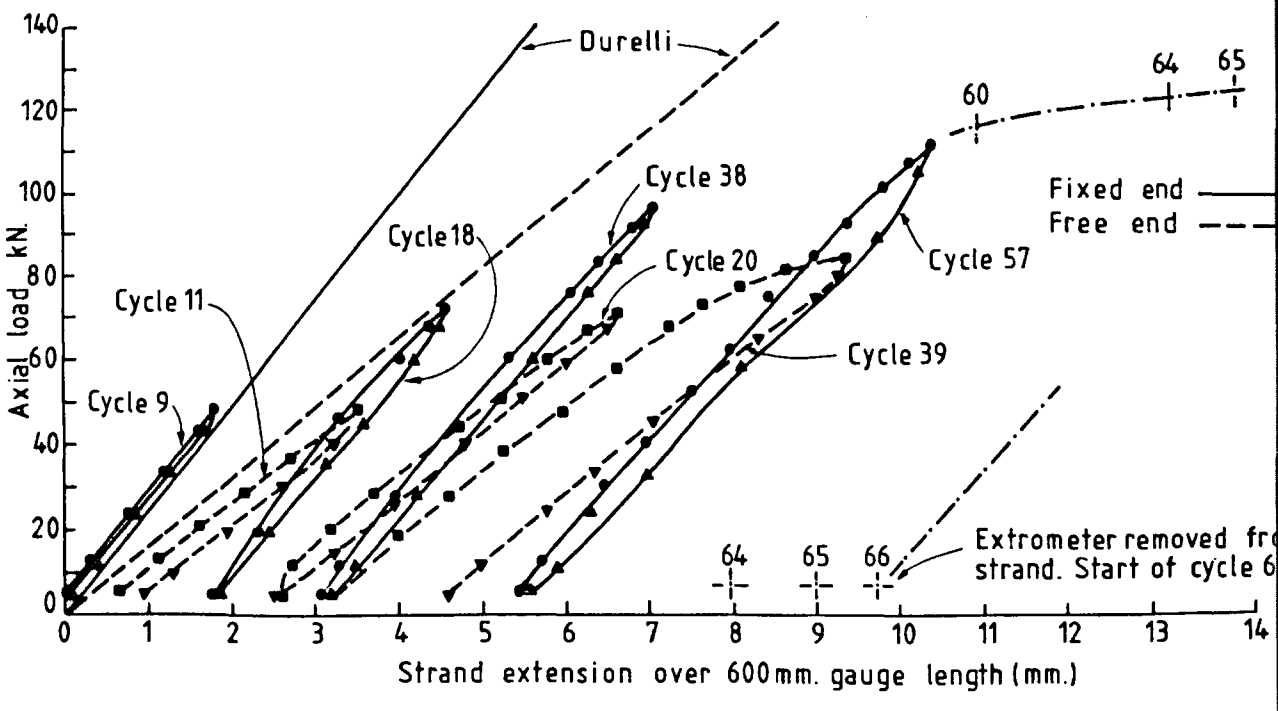

Figure 4.6. Load/Extension. Strand IV.

Strand IV Loading Programme

Table 4.1

Cycle Nos	Max. Load kN	Fixed or Free	Comments
1	20.0	Fixed	18 strain gauges, tension, torque, extension and rotation, recorded on pro-forma, by hand.
2 & 3	24.0	"	
4	28.0	"	
5	32.0	"	Strain gauges outputs on WSM P350A and 2 WSM 10-channel bridge and switching units.
6	36.0	"	
7	40.0	"	
8	44.0	"	Other outputs on FYLDE bridge/amp. units.
9	48.0	"	
10 & 11	48.0	Free	
12	52.0	"	
13	52.0	Fixed	
14	56.0	"	
15	60.0	"	
16	64.0	"	
17	68.0	"	
18	72.0	"	
19	65.8	Free	
20	71.4	"	
21	71.4	"	
22	71.6	Fixed	
23	70.0	Partially	
24	60.0	Restrained	
25,26,27,28	72.0	Fixed	Extrometer disconnected and reconnected. Load up to previous maximum only, to check extrometer reliability and reproducibility of results.
29,30,31	72.0	Free	
32	72.0	Fixed	
33	76.0	Fixed	16 strain gauges only from here on.
34	80.0	"	
35	84.0	"	
36	88.0	"	
37	92.0	"	
38	96.0	"	
39	83.8	Free	
40	96.0	Fixed	
41 & 42	59.8	"	
43 & 44	60.0	"	Tension, torque, extension, rotation and 6 gauges outputs put on FYLDE & U.V. Recorder.
45	70.0	"	

Strand IV Loading Programme

Table 4.1 (Continued)

Cycle Nos	Max. Load kN	Fixed or Free	Comments
46	80.0	Fixed	
47	90.0	"	
48,49,50,51,52	96.0	"	Cycle 52. 'Crack' heard in grip.
53	96.70	"	
54	100.7	"	
55	106.6	"	
56	107.8	"	
57	109.9	"	
58	59.8	"	
59	111.9	"	
60	115.8	"	
61	107.1	"	'Crack' heard in grip. Big drop in tension.
62	104.9	"	
63	115.4	"	
64	119.9	"	
65	122.3	"	
66	124.0	"	Extrometer disconnected.
67	127.4	"	Break. Wire No. 1 inside grip. (Core also? Unconfirmed)
68	105.1	"	Max. load on remaining wires. Pulled out from grip.

restraining torque. This output reading for each tension increment was determined from expression 3.4 before each test under free end (zero torque) condition. The outputs from the 18 strain gauges were read on a Welwyn Strain Measurement P350A bridge unit connected to two ten-channel switch and balance units, up to load cycle 24. Two gauges went down at this stage and from cycles 33 to 42 only 16 gauges were monitored, reduced to 6 from cycle 43 when the outputs from the six gauges at mid-strand (1.3 to 6.3 at pitch position 3) were connected to the FYLDE bridge amplifier unit, the outputs of which were connected to six channels of a U.V. Recorder. Strain gauge readings from the test on strand I (see Fig. 4.2) had shown that at 96 kN (max. load in cycle 40) the elastic range was now likely to be exceeded and it was not reasonable to expect that the recording by hand would be possible from up to 22 circuits while a particular load was maintained, since creep would almost certainly occur. The use of a U.V. recorder would, it was hoped, overcome this problem since a continuous record giving simultaneous output from all channels would be obtained from the traces as load was steadily increased. The output from FYLDE circuits already connected to tension and torque circuits (load cell) and the extension and rotation circuits (extrometer) were also connected to four channels of the U.V. recorder at this stage. The extrometer was disconnected after the 66th cycle and the load then increased until the strand fractured. Fracture load was 127.4 kN, only one helical wire breaking inside one of the end grips. This wire 'birdcaged' individually to the other

grip. The strand was still able to sustain load and generate torque until two wires (core and one other helical) pulled out from the resin, having straightened out their hooked ends in the process. Note that the extrometer was attached to the strand at the start of the loading programme at a holding tension in the strand of 5 kN, and load was not reduced below this between load cycles.

4.4.3 Results and Discussion

(i) Strand Extensions

Fig. 4.6 shows plots of tensile load against strand extension for certain selected fixed and free end loading cycles. The predictions of Durelli et al. (27) are also shown for comparison. The strand stiffness is seen to be significantly less in the free end condition than the fixed end condition. The onset of yield, or detectable non-linearity in the load/extension plot, occurs at a lower load in the free end case than in the fixed end case. Hysteresis in the strand, greater in the free end tests, was evident in all cycles. (This is over and above the hysteresis due to backlash in the extrometer, as determined when it was calibrated. See Appendix A.2).

(ii) Strand Rotation

Fig. 4.7 shows plots of tensile load against strand rotation for selected load cycles with free ends. The predictions of Durelli et al. (27) are seen to be in reasonable agreement. Strand hysteresis is again in evidence.

Figure 4.7. Load/Strand Rotation.(Free End Tests.) Strand IV.

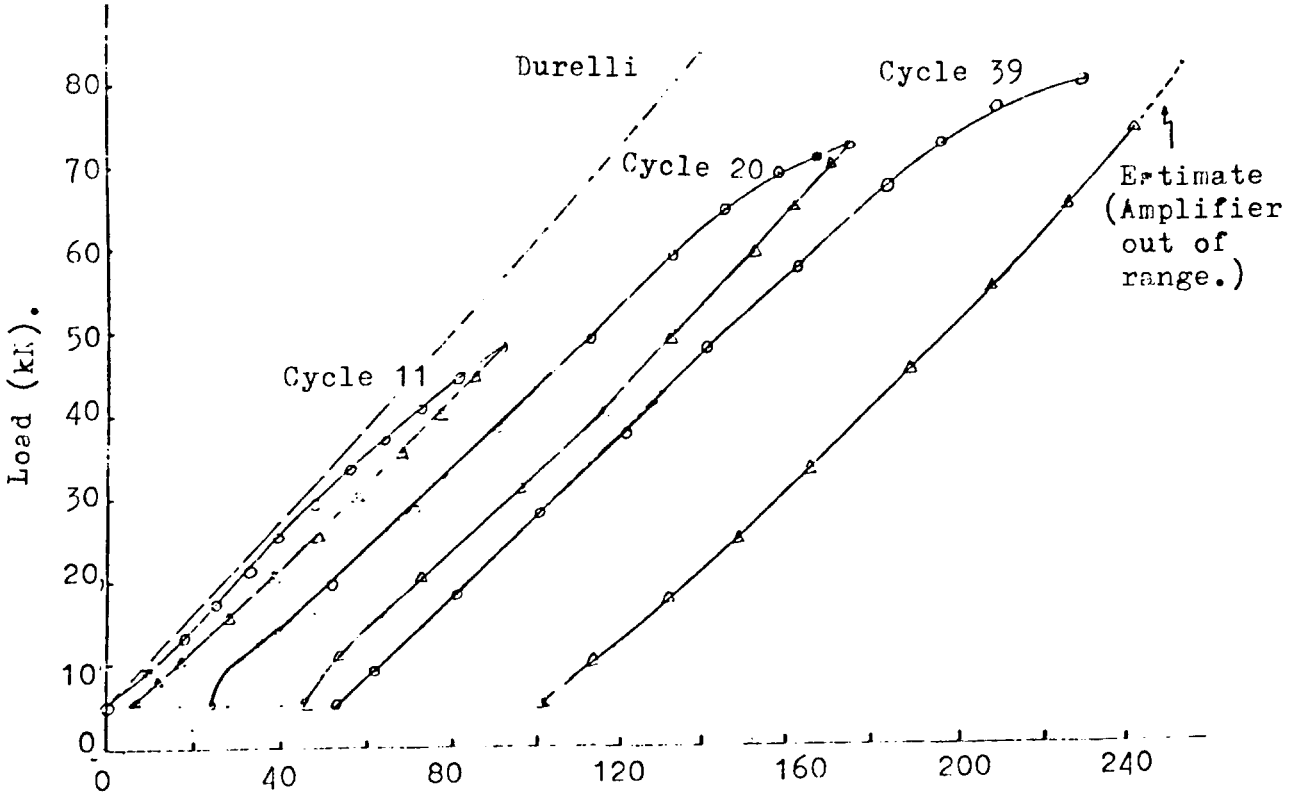

(iii) Torque Generated

The first torsion circuit was used for this test. A second circuit was attached after this test. The results from this second circuit were used in all subsequent tests. The results from the first circuit are therefore not shown here, although results from the first did show a linear tension/torque relation in all load cycles in the fixed end condition, slightly steeper than that of the prediction by Durelli et al. (27).

(iv) Surface Strains on Helical Wires

Strain differences along the strand are shown in Fig. 4.8 for the fixed end case and Fig. 4.9 for the free end case. There are lower mean strains in the free end case than the fixed end case. Deviations from the mean (and from the Durelli prediction) are greater in the free end case than the fixed end case, but these deviations reduce with increased load. The strain variation along the length of each wire cannot be fully analysed without gauges on them all. It cannot be determined, therefore, whether these strain variations are due to redistribution of load sharing between wires as the initially curved strand straightened under load.

Fig. 4.10 and Fig. 4.11 show that there is unequal load sharing between wires at strand mid-section, the deviations from the mean being greater in the free end case than the fixed end case.

Figure 4.8.Wire Strains along Strand;Fixed End Tests Strand IV.

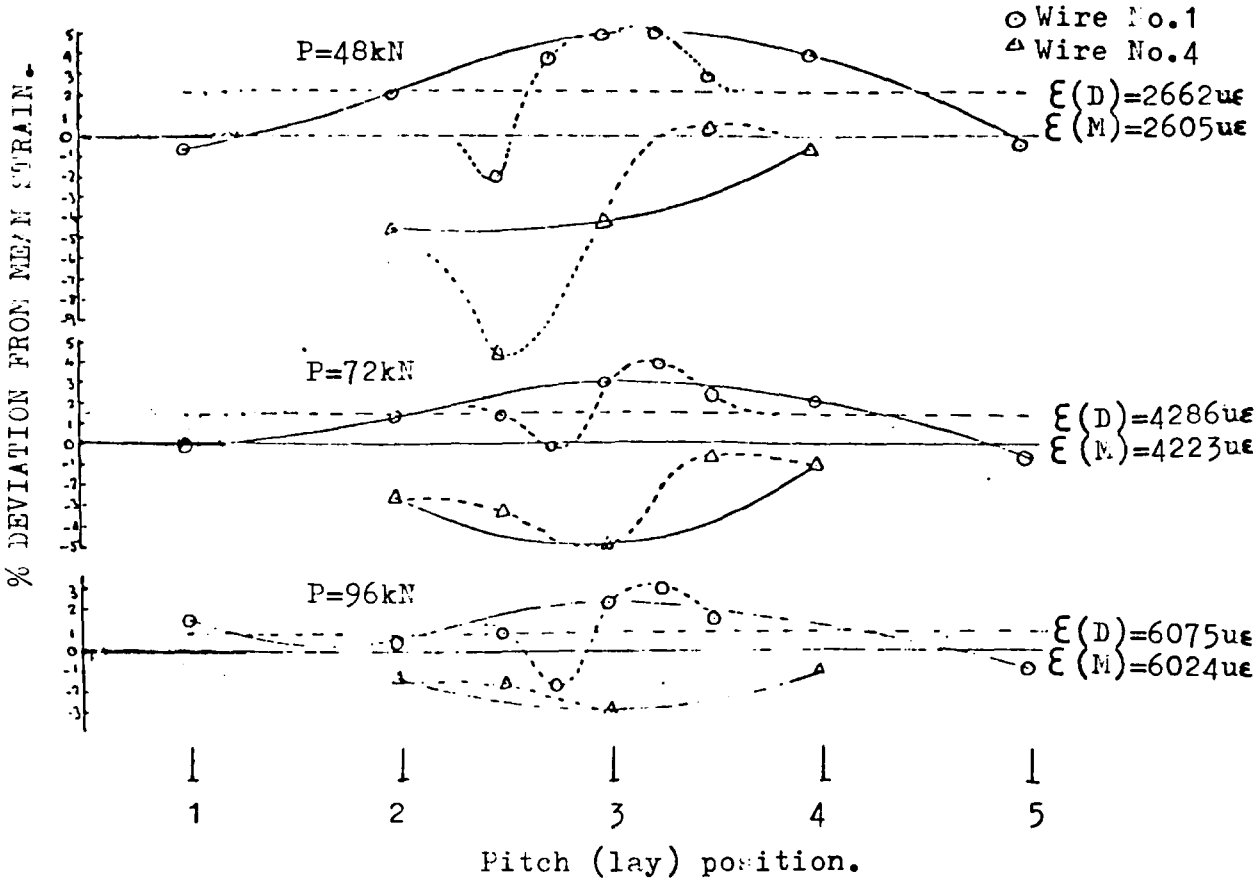

KEY:(Figures4.8 & 4.9)
ε(D)=Durelli prediction of wire strain.
ε(M)=Mean of strains on six helical wires.

Figure 4.9.Wire Strains along Strand;Free End Tests Strand IV.

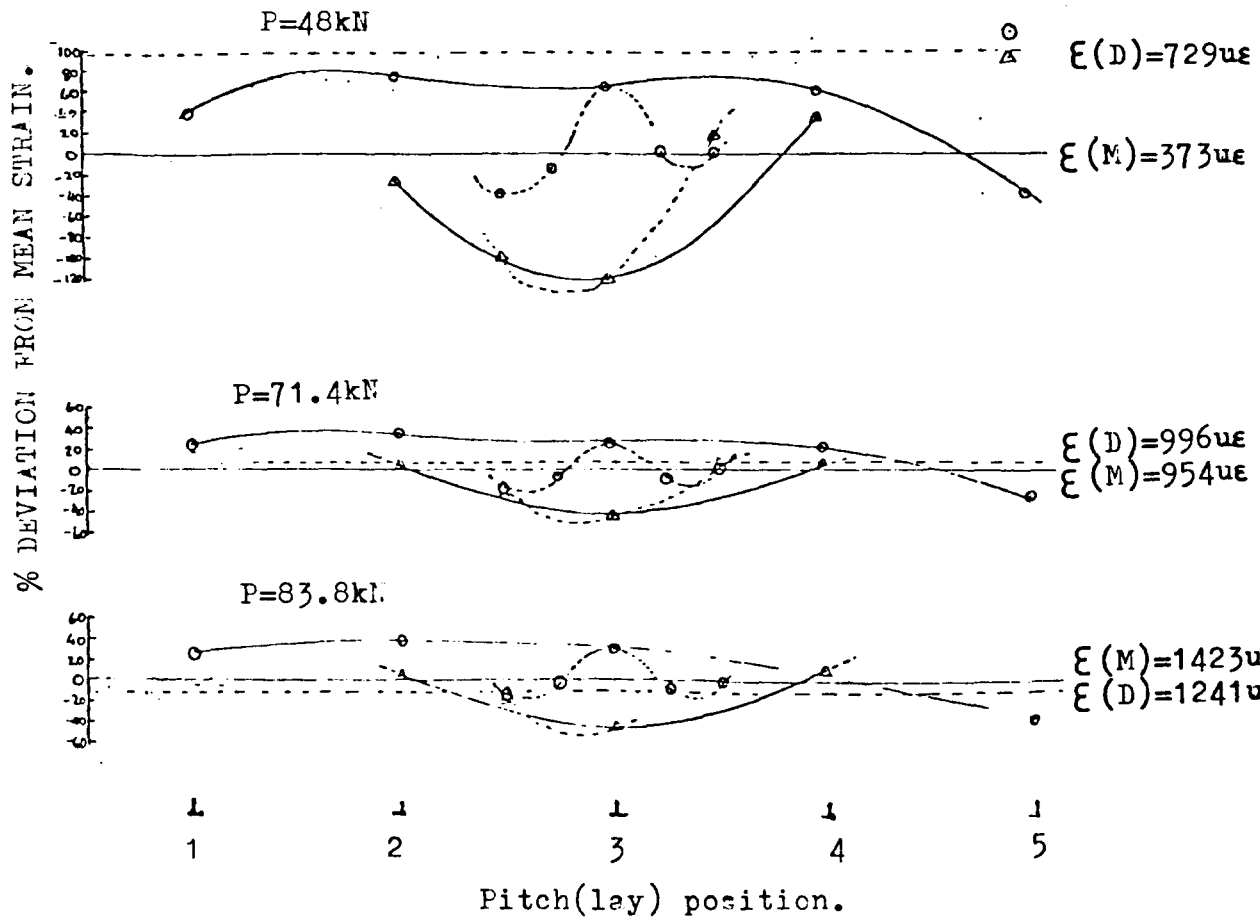

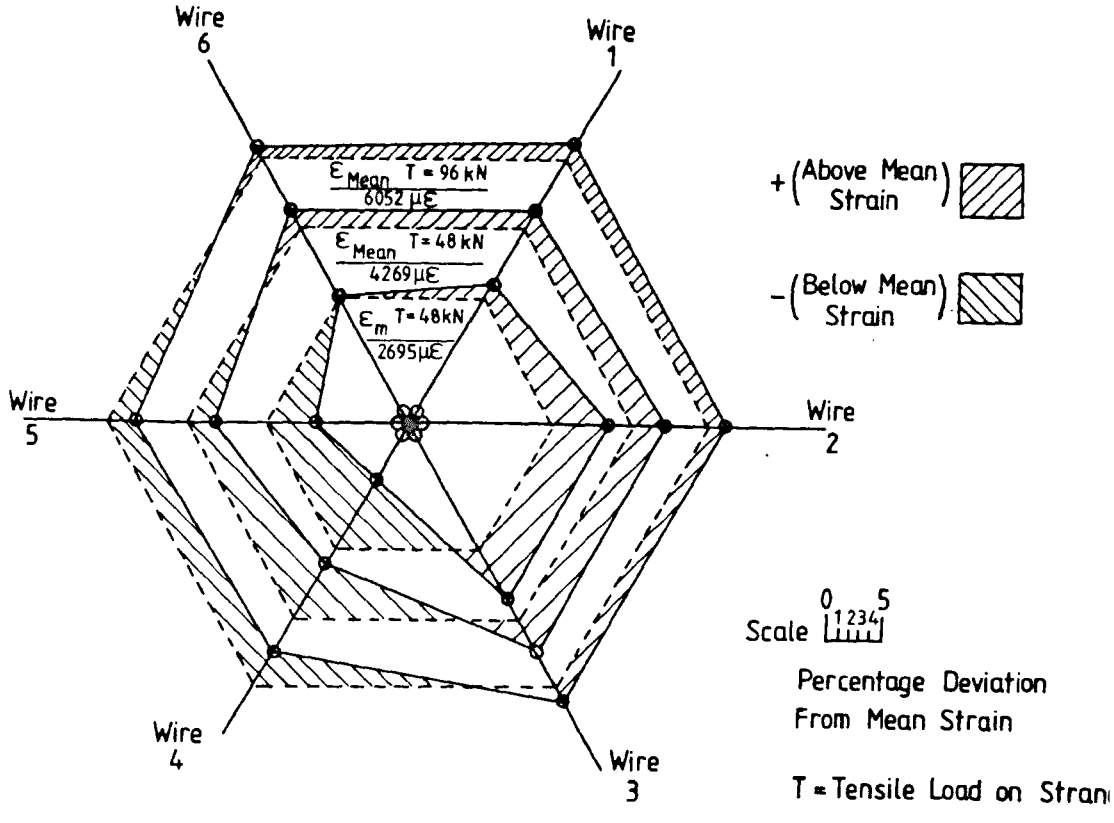

Figure 4.10. Wire strains; cross section of strand. Strand IV.
(Fixed end tests.)

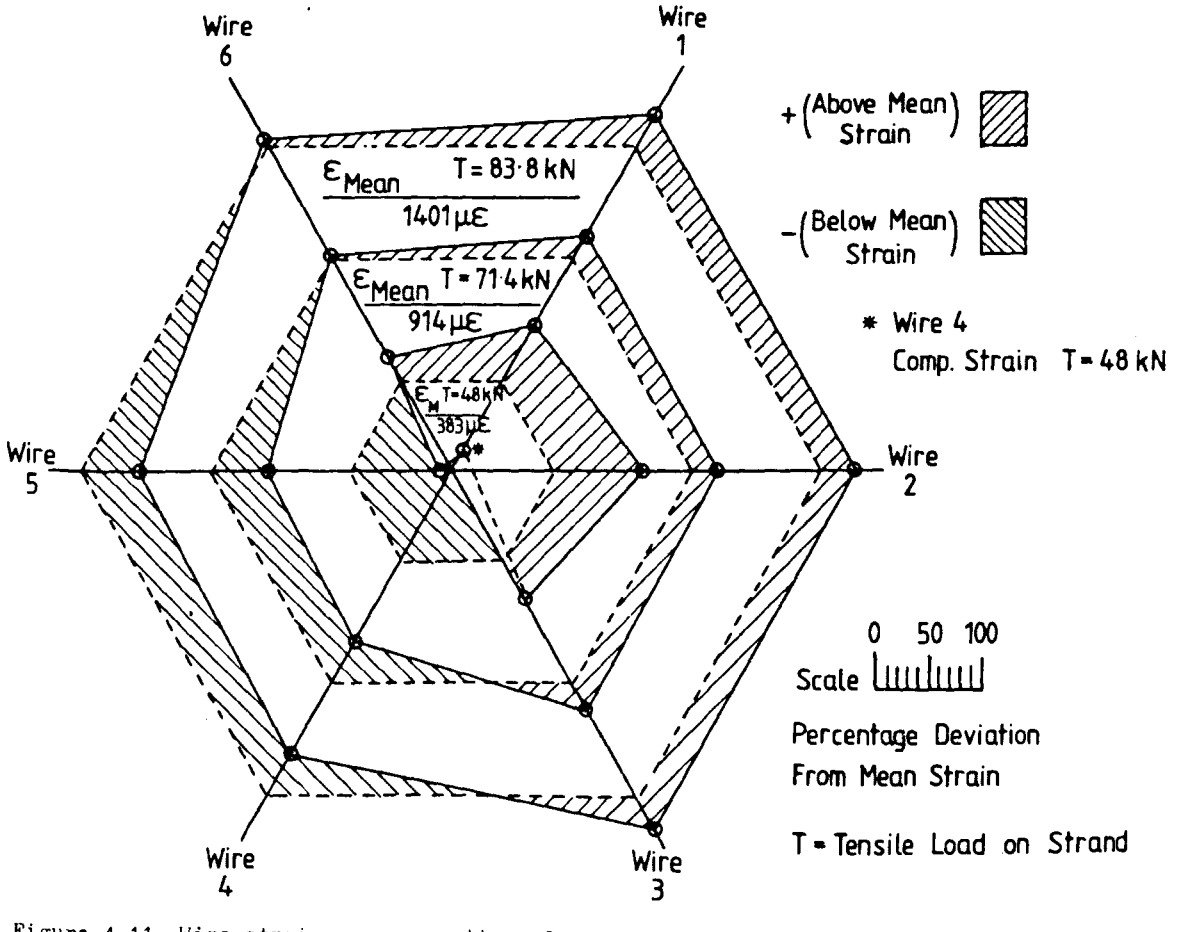

Figure 4.11. Wire strains; cross section of strand. Strand IV.
(Free end tests.)

4.4.4 Conclusions from Strand IV Test

(i) Equipment Performance and Requirements for the Next Test

The extrometer appeared to perform satisfactorily. The need for a larger number of strain gauges highlighted the problems of recording, by hand, the results from a large number of output channels. The ultra violet recorder did not solve the problems since only 10 channels could be accommodated and laborious processing of the trace is necessary in such non-digital outputs. The availability of an existing data logger with punch tape and printed tape outputs for up to 50 channels prompted the decision to use this for the next test. Duplicate tensile and torque circuits on the load cell were thought to be required for monitoring of strand tests at the side of the rig. (See also Chapter 3, section 3.1 and Appendix A.1).

It was clear that more strain gauges were required if stress distribution along the whole length of strand were to be investigated. To reduce labour in strand preparation and increase gauge reliability, it was decided to use strain gauges with leads already attached. (See Appendix A.6, section A.6.2).

(ii) Results on Strand Response to Load

The predictions of Durelli et al. (27) on extension, torque and rotation appeared to agree reasonably closely with the experimental results. There was uncertainty, however, about the influence of the initial curvature of the strand, particularly on strain values along the strand. The need in future tests for very much straighter test strands was evident.

4.5 Strand V

4.5.1 Strand Preparation

This strand possessed no initial curvature and was different from all other strands in this study in that it was galvanised and lubricated. For the length used in this test, mean diameters were 3.73 mm (helical) and 3.91 mm (core), while the mean lay length of 91.92 mm, gave a helix angle of 75.4°. Hooked over wires were used in the end grips as described in Appendix A.4.

4.5.2 Strain Gauges

In order to obtain more information about surface strains, 39 strain gauges were attached as shown in Fig. 4.12. The type shown in Fig. A.6.2(i) (with leads attached) were used, including 3 sets of 3 gauges mounted parallel to each other as shown in Fig. A.6.2(ii). (For application details see Appendix A.6).

4.5.3 Instrumentation

The data logger system incorporated into the testing system has the control and indicator unit some 30 metres from the test rig. Signal loss over this length of lead was calibrated and details are given in Appendix A.3. A trigger for the control unit was developed for remote operation by switch from the side of the rig. The data logger is connected to punch tape and printed paper tape outputs, and when both are operational the switch speed is two circuits per second. For loading beyond yield, the printed paper tape was disconnected, and switching

Figure 4.12.Strand V: Position of Strain Gauges.

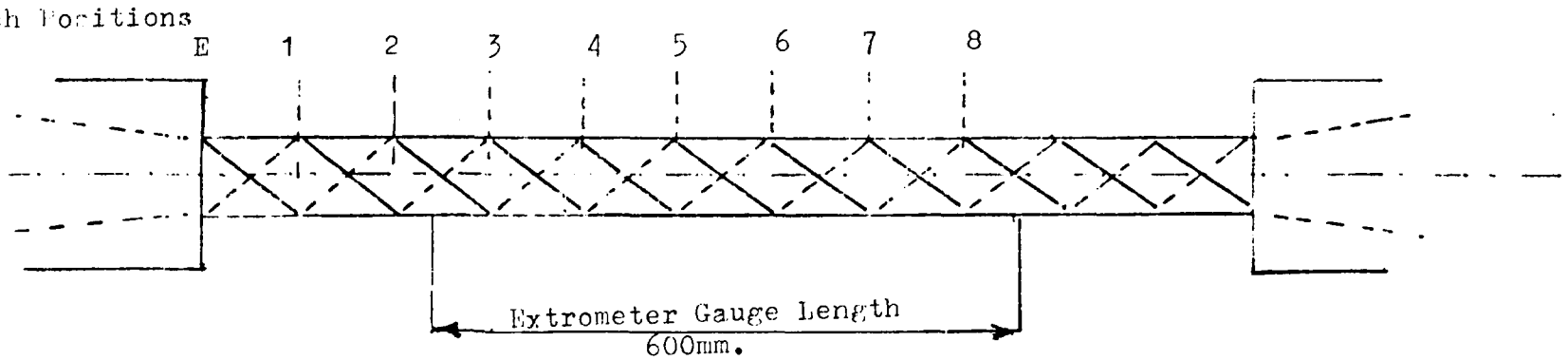

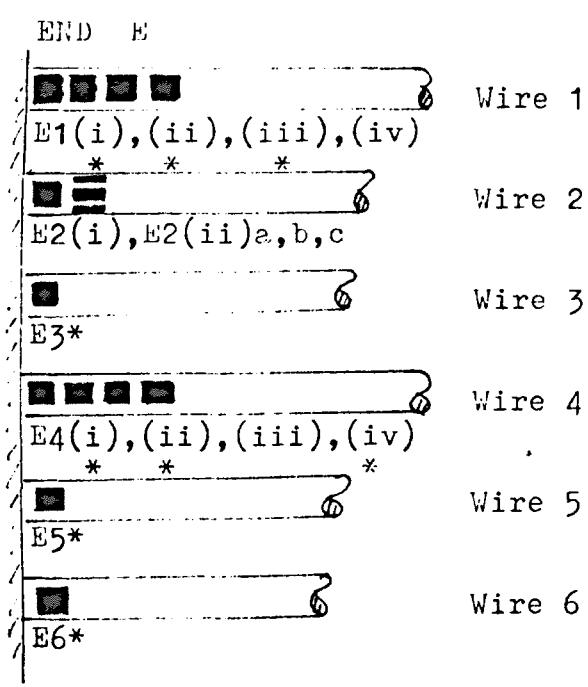

Pitch Position 6.

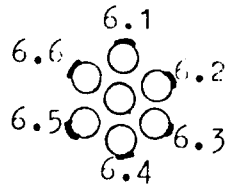

Pitch Positions.7&5.

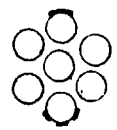

Pitch Positions.8,4,3,2&1.

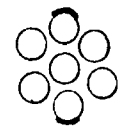

*Indicates strain gauges lost when refitting end grip.

speed is thereby increased to about 10 circuits per second. Strain gauges for duplicate torque and tension circuits were attached to the load cell rod for the purpose of monitoring loading during tests. (See Chapter 3, section 3.3.1). The second of the tension circuits was subsequently accidentally destroyed and the results from the second torsion circuit only were used in the main test programme (Chapter 5) and in comparison with computed predictions (Chapter 7).

Punched tape output from the data logger has been fed into the departmental computer and the graph plotting accessory used to produce load/extension, load/torque, load/rotation and load/strain plots.

4.5.4 Loading Programme

Table 4.2 gives the maximum load and end condition for each of the 25 loading cycles to which the strand was subjected. The strand began to pull out of the end grip at that end where strain gauges were adjacent to the grip in the 17th cycle. In the next cycle, a 'crack' was heard within this grip and the load dropped suddenly. The strand pulled out completely after this and it was necessary to fit the end grip again. During this process, which involved the bending into hooks of the individual wires for a second time, nine strain gauges became unserviceable. After the 25th load cycle, taken to a maximum load of 95.3 kN, the extrometer was disconnected. Load was then increased until the strand broke at a load of 99.4 kN.

Strand V Loading Programme

Table 4.2

Cycle Nos	Max. Load kN	Fixed or Free	Comments
1 & 2	20	Fixed	39 strain gauges, duplicate torque and tension circuits to data logger.
3	52.4	"	
4	52.8	"	Tension and torque circuits (original), extension and rotation to FYLDE bridge/amp. unit.
5 & 6	52.9	"	
7 & 8	44.0	Free	
9 & 10	52.8	Fixed	
11 & 12	44.0	Free	
13 & 14	55.0	Fixed	
15 & 16	44.0	Free	
17	63.8	Fixed	Slipping of strand in end grip. Strain gauged end.
18	63.0	Fixed	'Crack' heard in end. Load dropped to 47.4 kN.
Strand pulled out of end at fluctuating load ≯ 24 kN. Hooks straightened out and wires pulled through holes in resin. Wires hooked again and end grip refitted with new resin.			
19	20.0	Fixed	9 strain gauges lost in refitting of grip.
20	65.0	"	'Crack' heard in grip but load maintained.
21	84.0	"	
22	50.3	Free	
23	90.0	Fixed	
24	92.8	"	
25	95.3	"	Extrometer disconnected after this load cycle.
26	99.4	"	Break in 5 helicals at this load.

Five helical wires were severed at a position just inside the resin of the end grip adjacent to the strain gauges. 'Bird-caging' of the broken wires occurred along the strand and ended some 150 mm from the grip at the other end.

4.5.5 Results and Discussion

(i) Strand Extensions

Fig. 4.13 shows load/extension plots of the three last loading cycles before the extrometer was removed. Progressive increase in permanent non-elastic extension is evident, as well as hysteresis in the strand loading cycle.

(ii) Strand Rotation

Fig. 4.14 shows the load/rotation plot for the cycle No. 22, free end case. The irregularity of the plot may be due to variations in interwire slip as the presence and/or effectiveness of lubricant over the gauge length also varied. (Compare with Fig. 4.7 - no lubricant).

(iii) Torque Generated

The torque generated was found to increase linearly with tensile load on the strand. The load/torque slope was found to be greater by 6.5% than that predicted by Durelli et al. (27).

(iv) Surface Strains on Helical Wires (See Table 4.3)

Figs 4.15 and 16 show load/strain plots for load cycle No. 5 (fixed end) up to a max. load of 52.9 kN. Strain differences

Figure 4.13. Load/Strand Extension. Strand V.
Fixed End;Load Cycles 23,24 & 25.

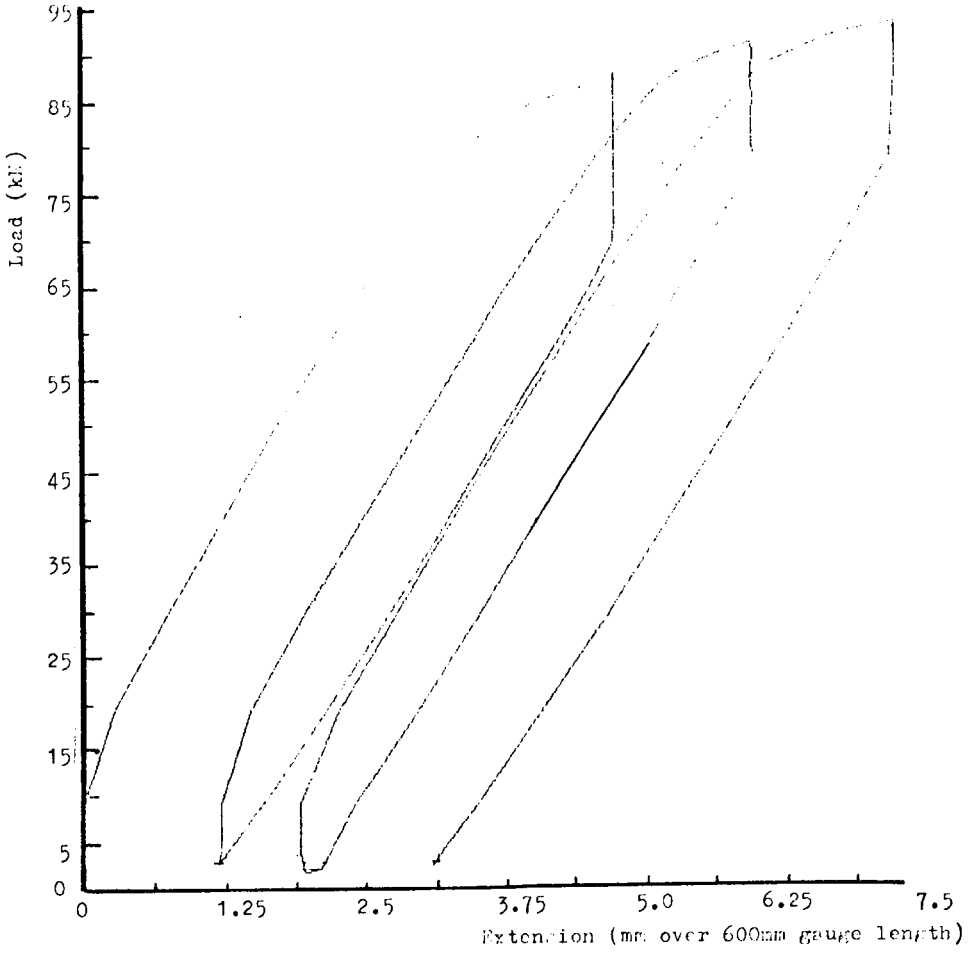

Figure 4.14. Load/Strand Rotation. Strand V.
Free End;Load Cycle 22.

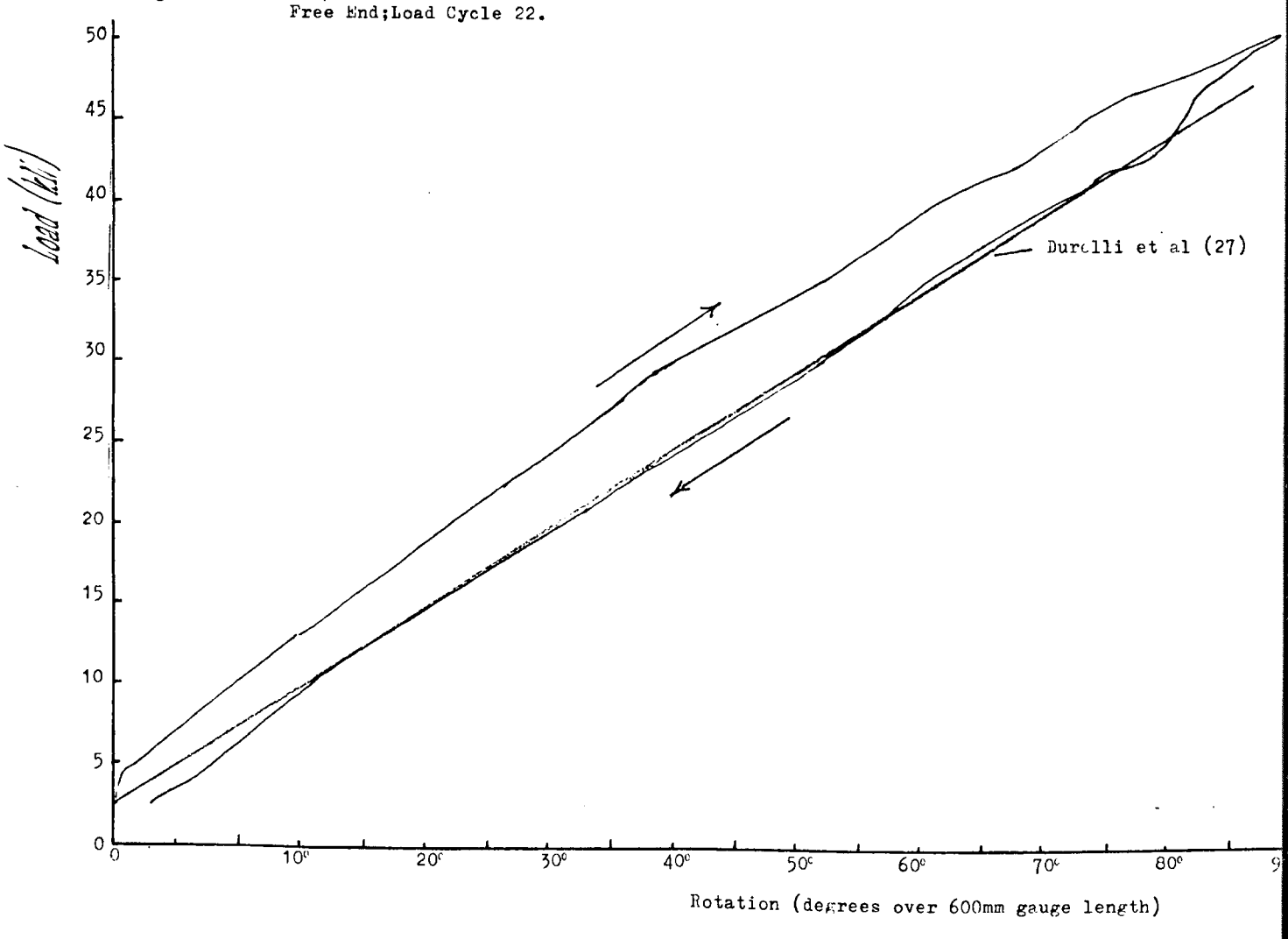

Figure 4.15. Load/Wire Surface Strain.Strand V.
Pitch Position 6:all helical wires.
Fixed End;Load Cycle 5.

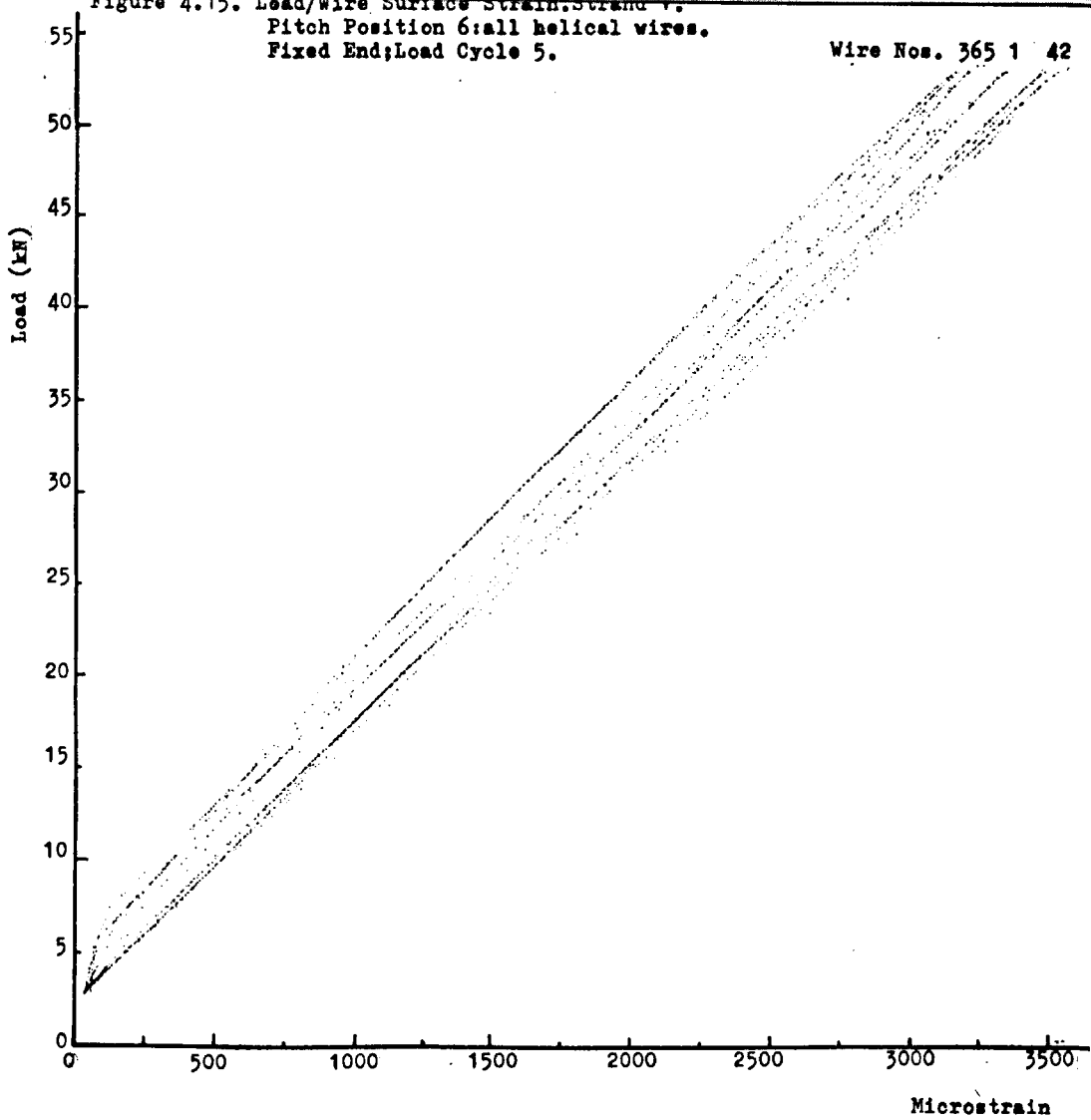

See also Table 4.3.

Figure 4.16. Load/Wire Surface Strain.Strand V.
All pitch positions:Wire No.4.
Fixed End;Load Cycle 5.

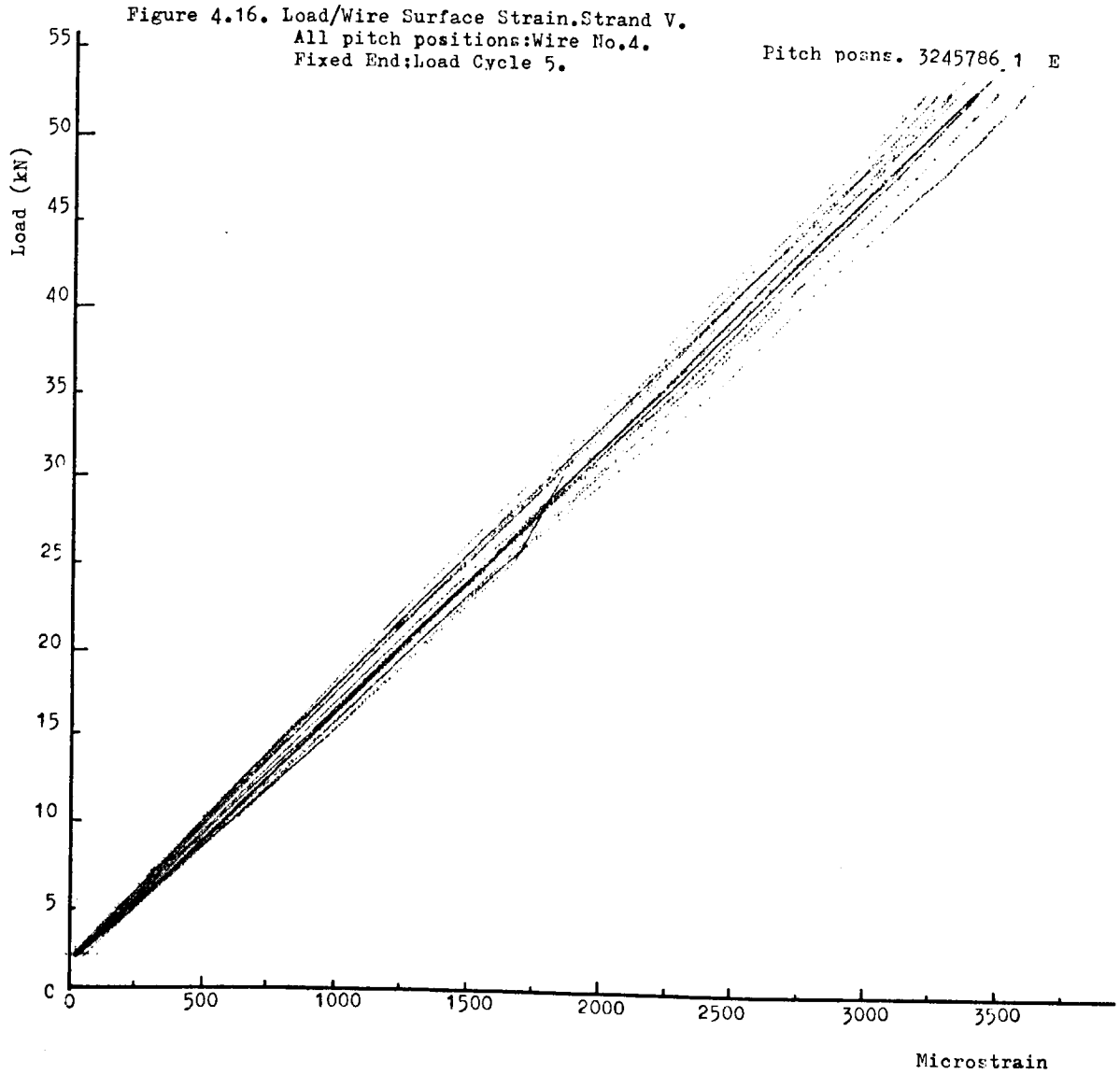

See also Table 4.3.

between wires (Fig. 4.15) and strain differences along a single wire (Fig. 4.16) are evident. These differences reduce at higher loads (see Table 4.3 for Cycle 25) in the fixed end condition. Differences in the free end condition are larger and percentage differences are often of little significance as strain values are negative for some wires and pitch positions. In Fig. 4.17, the plot from load cycle 25, the penultimate loading, becomes non-linear at higher loads. The highest strain is again at a point nearest the end grip. Some redistribution of load sharing along the strand is evident from the fact that the order, maximum to minimum, of the strains of pitch positions were different at the higher loading (Fig. 4.17) from the lower loading (Fig. 4.16). Fig. 4.18 shows surface strain on two diametrically opposite helical wires at strand mid-position. Whereas strain ranges for individual load cycles do not vary greatly, the cumulative effect of load cycling is clearly seen. (There is a strain difference of about 500$\mu\varepsilon$ at the start of the last cycle, assuming a common datum only 3 cycles previously). Fig. 4.19 shows that a much greater variation in strains between wires is present under loading with free ends. The strain plot at pitch position E (near end grip) is not shown. At maximum load, this strain is negative. (See Table 4.3).

4.5.6 Conclusions from Strand V Test

(i) Equipment Performance

The extrometer and load cell performed satisfactorily. The data logger and graph plotting facility also proved themselves

Surface Strain Variations - Strand V

Table 4.3

Load Cycle No.	Max. Load kN	End Conditions	Wire No.(s)	Pitch Position(s)	Mean Strain (≠)	Max. Variation from Mean Strain %
5 (See Figures 4.15 and 4.16)	52.9	Fixed	6,5,4,3,2,1	6	3314	+ 6.2, - 5.7
	52.9	Fixed	6,5,4,3,2,1	E	3289	+13, -25.3
	52.9	Fixed	1 1	8,7,6,5,4,3,2,1 E	3488 3376	+ 4.6, - 4.7 - 3 *
	52.9	Fixed	4 4	8,7,6,5,4,3,2,1 E	3419 2656	+ 4.4, - 3.7 + 6.9 *
22 (See Figure 4.19)	50.3	Free	6,5,4,3,2,1	6	430	+53, -57
	50.3	Free	1 1	8,7,6,5,4,3,2,1 E	452 -427	+43, -55 95 (comp.)*
	50.3	Free	4 4	8,7,6,5,4,3,2,1 E	544 -266	+124, -114 49 (comp)*
25 (penultimate) (See Figure 4.17)	95.3	Fixed	6,5,4,3,2,1	6	8440	+ 8.4, - 6
	95.3	Fixed	1 1	8,7,6,5,4,3,2,1 E	8289	+ 1.8, - 2.4 -33.7, *
	95.3	Fixed	4 4	8,7,6,5,4,3,2,1 E	8249	+ 1.4, - 2.5 + 6.3, *

Continued on next page

Surface Strain Variations - Strand V

Table 4.3 (Continued)

* This figure is variation from mean of strain in all other eight pitch positions on the same wire.

($\neq$) This is the mean of the strain increments above the initial holding load of 3 kN (approx.).

Figure 4.17. Load/Wire Surface Strain.Strand V.
All pitch positions:Wire No.4.
Fixed End;Load Cycle 25.

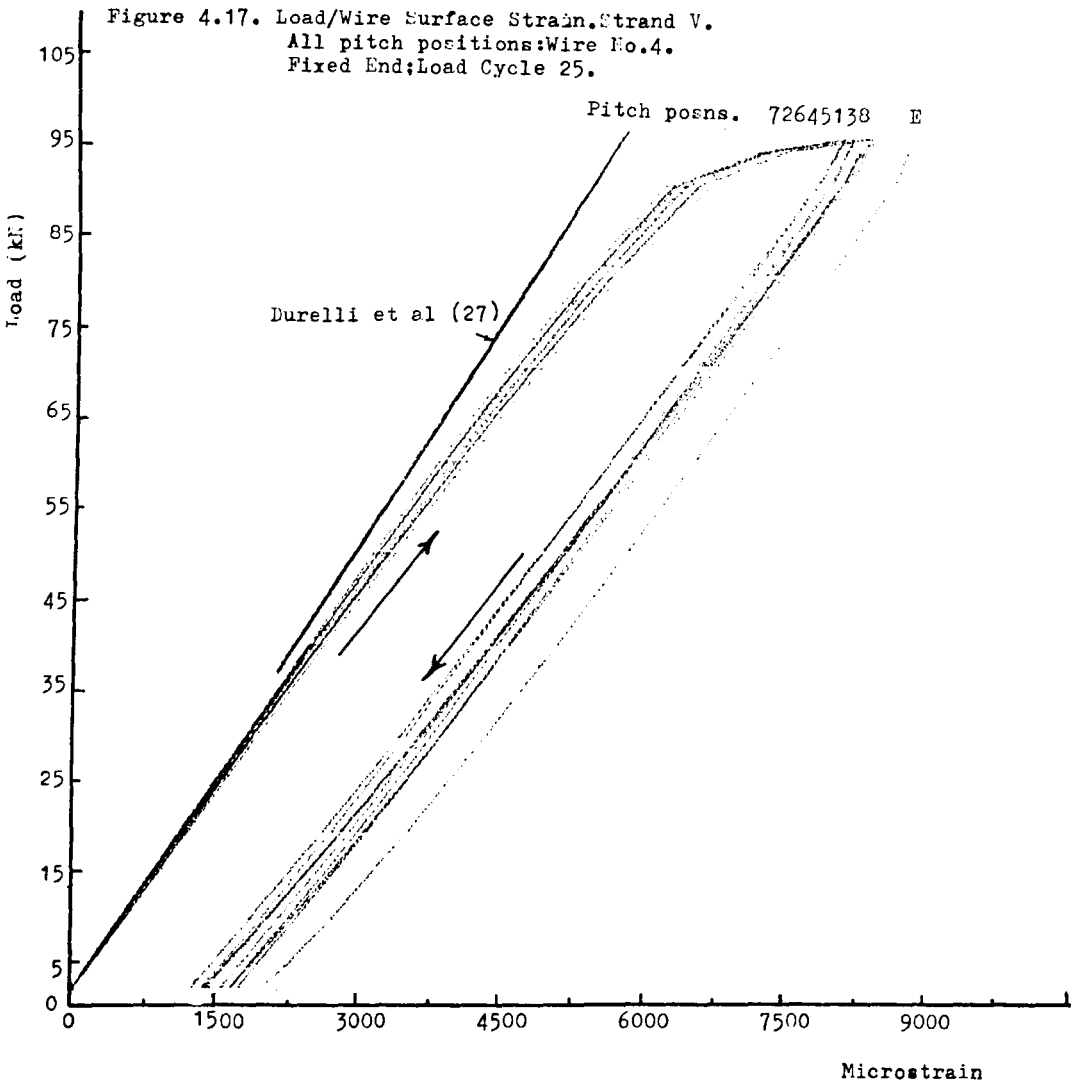

See also Table 4.3.

Figure 4.18. Load/Wire Surface Strain. Strand V.
Mid length; wire No. 1 & 4.
Fixed End; Load Cycles 23, 24 & 25.

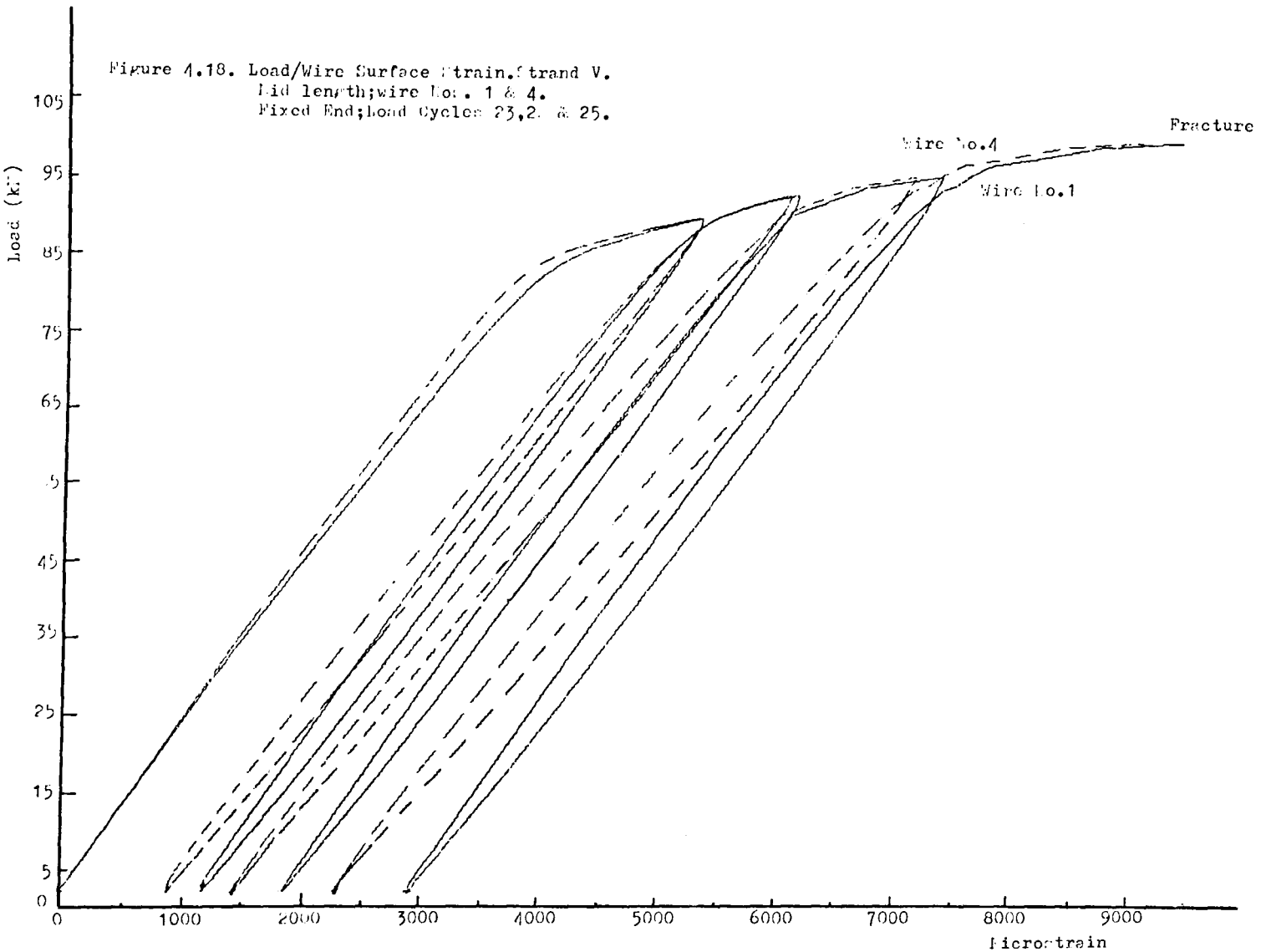

Figure 4.19. Load/Wire Surface Strain.Strand V.
Pitch Position 6:all helical wires.
Free End;Load Cycle 22.

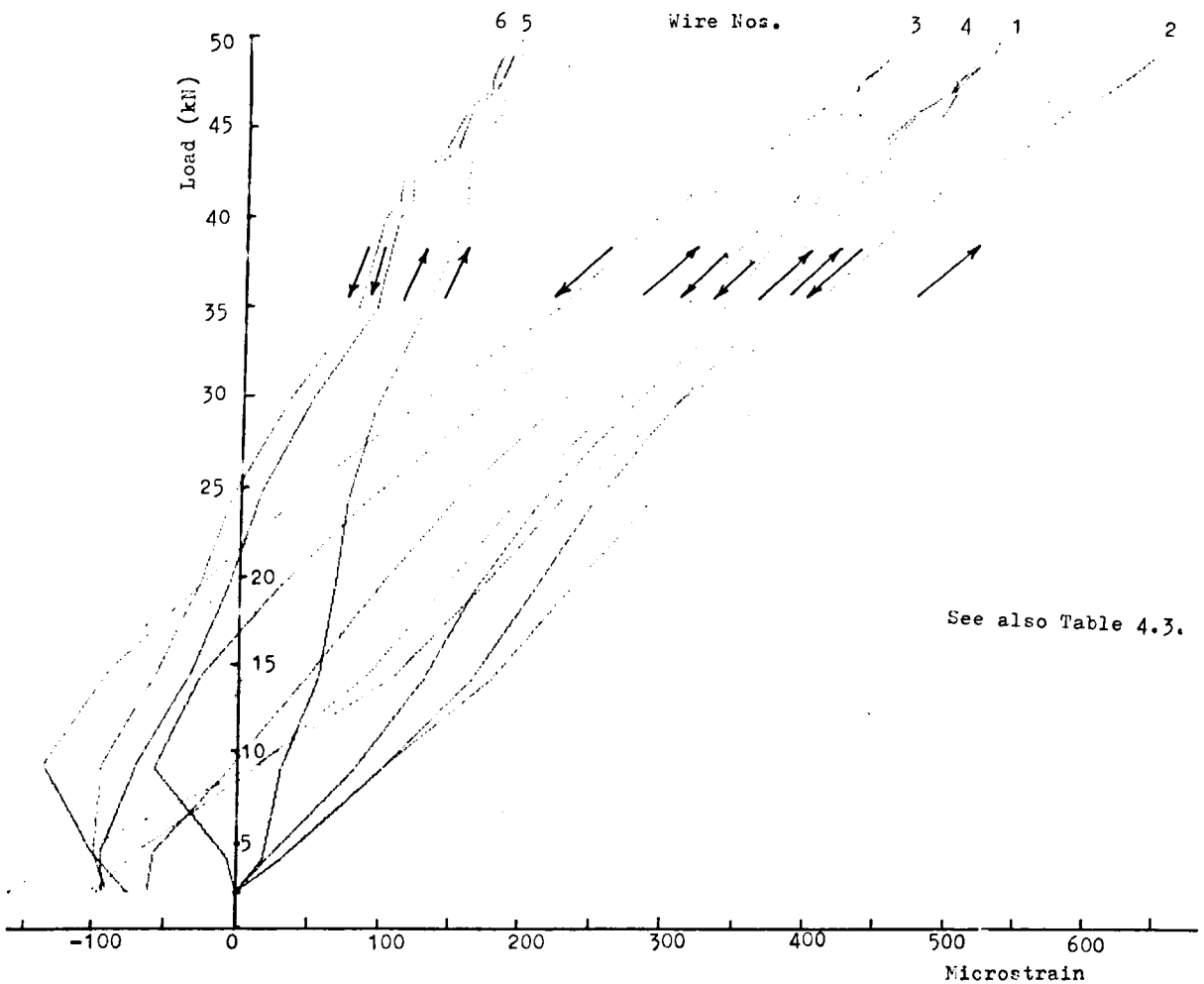

See also Table 4.3.

suitable for use in a comprehensive test programme.

The fact that end grips again proved unsatisfactory prompted the design modification resulting in complete 360° bending of each wire within the resin. (See Appendix A.4). A 'bollard' mechanism is thus employed to complement the initial adhesion between resin and wires.

Strain gauges appeared to have been reliably attached to wire surfaces. The output from the gauges mounted in threes, with axes parallel, though not analysed in detail, appeared consistent and this configuration was considered satisfactory for use in the main test programme.

(ii) Results on Strand Response to Load

Strand extension, rotation and torque generated appeared to agree reasonably with Durelli et al. (27), though departure from a linear load/extension relation at higher loads was evident.

Conclusions from strain measurements are probably the most significant. Variations in load sharing between wires is very much greater in the case of free end tests than fixed end tests, as in strand IV. Variations are greatest adjacent to end grips. Strain differences, in the fixed end condition, between wires at a particular strand cross-section are greater than the differences along the strand in a particular wire, if the end position (E) is not considered.

CHAPTER 5

STRAND TESTS: MAIN PROGRAMME

5.1 Strand Details

The preliminary tests described in Chapter 4 served to prove some of the test equipment, notably the 'extrometer', and test techniques as well as providing an opportunity to develop other equipment. It was now possible to proceed with the major objectives of this study, as defined in Chapter 2, sections 2.2 and 2.3. A number of seven wire strands having core and helical wires of the same diameter as strands I, II, III and IV in the preliminary tests, and a range of helix angles, were made available by courtesy of British Ropes. The strands were all formed in the same stranding machine from seven reels of wire that were unchanged throughout. In order to eliminate strand curvature, each 2 metre length was cut between strander capstan and the take-up reel, as soon as it was produced. Traction to the take-up reel was maintained by a smaller strand wound round the take-up reel which was clamped to the end of the new strand as soon as the previous strand was cut free and unclamped from it. Four lengths of 2 metres were stranded for each of 10 nominal lay lengths, as determined by the fitting of a gear wheel which governed relative rotation of capstan and the helical wire supply reels about their axes. After each gear (strand lay) change, a length of about $1\frac{1}{2}$ metres was stranded and discarded, in order to ensure that test lengths consisted of strand the geometry of which was free from any irregularities due to the

transition.

Five of these strands were selected for carefully instrumented tests. Details are given in Table 5.1. The strand lays were measured over lengths of about 1900 mm and were found to be within 1.1% of the nominal figures, except for strand V1 which was 4.1% less than the nominal lay. Only in the case of strand V1 was the difference considered large enough to warrant comparison of experimental results with theory of both nominal and measured strand geometries.

Nominal and Measured Strand Geometry

Table 5.1

Strand No.	Nominal		Measured		Core dia. mm	Helical dia. mm	*Wire Modulus kN/mm^2
	Lay mm	Angle	Lay mm	Angle			
VI	82.04	73.63°	78.66	72.97°			
VIII	97.79	76.16°	96.69	76.01			
X	110.49	77.70°	111.41	77.80	3.94	3.73	197.9
IX	123.19	78.93°	123.58	78.97			
VII	149.86	80.87°	148.27	80.77°			

* See Appendix A.5 for determination of Wire Modulus.
The grade of wire in these strands is 180 kgf/mm^2 minimum breaking load, to BS2763.

5.2 Strand Preparation

5.2.1 Terminations

In the light of experience gained during the preliminary tests, it was decided that efficient gripping of the individual wires would be best achieved if each were bent through a complete 360° circular arc. This was done by using hand wrenches and the loops, of about 25 mm to 40 mm diameter, orientated in such a way as to minimize interference between wires when confined in the hollow conical grip. The wires were trimmed off at the end of each loop so that they would not emerge beyond the end of the grip, or above resin level when poured. The 'wirelock' polyester resin based socketing medium was poured into the socket of each end in turn, care being taken, by use of a spirit level, that the flange of the grip was horizontal and the free surface of the resin was therefore flush with the flange after pouring. The loops ensured that a bollard type of mechanism was involved in the gripping of the wires, as well as the adhesive and, when developed, the radial gripping forces similar to those present in the extrusion process. (See also Appendix A.4).

5.2.2 Strain Gauges

Tests on strands IV and V showed that differences in strain between wires at the end, near a grip, and for comparison, at mid-strand, are of particular interest. The strain differences along a particular wire are not as great as the differences between wires (with the exception of the extreme end position

near the grip) and it therefore seemed unnecessary to affix gauges at more than the one mid-strand pitch position. Table 5.2 shows the strain gauge distribution and type for each strand. Note that gauges having grid axes perpendicular to wire axis were used in this test programme, in addition to the gauges mounted with grid axes parallel to wire axis. Strain gauge types and application techniques are described in Appendix A.6.

Strain Gauges: Type and Distribution

Table 5.2

Data Logger Channel No.	Strand VI α_o=73.6°	Strand VIII α_o=76.2°	Strand X α_o=77.7°	Strand IX α_o=78.9°	Strand VII α_o=80.9°
1	E11P	E11P	E11P	E11P	E11P
2	E12Aa*	E12A	E12A	E12A	E12Aa
3	E12Ab	E13X	E13π/4	E13π/4	E12Ab
4	E12Ac*	E21P	E21P	E21P	E12Ac
5	E13P	E22A	E22A	E22A	E13P
6	E14Aa	E31P	E31P	E31P	E14Aa
7	E14Ab	E32A	E32A	E32A	E14Ab
8	E14Ac	E41P	E41P	E41P	E14Ac
9	E21P	E42A	E42A	E42A	E21P
10	E22A	E43X	E43π/4	E43π/4	E22A
11	E31P	E51P	E51P*	E51P	E31P
12	E32A	E52A	E52A	E51A	E32A
13	E41P	E61P	E61P	E61P	E41P
14	E42A	E62A	E62A	E62A	E42A
15	E51P	M11X	M11P	M11P	E51P
16	E52A	M12Aa	M12Aa	M12Aa	E52A
17	E61P	M12Ab	M12Ab	M12Ab	E61P
18	E62A	M12Ac	M12Ac	M12Ac	E62A
19	M11A	M13P	M13π/4	M13X	M11A
20	M13P	M2A	M2A	M2A	M12P
21	M2A	M3A	M3A	M3A	M2A
22	M3A	M4A	M4A	M4A	M3A
23	M41A	M5A	M5A	M5A	M4A
24	M42A	M6A	M6A	M6A	M5A
25	M5A	-	-	-	M6A
26	M6A	-	-	-	-

Code: Type and Location.

E: End (near grip).
M: Mid-strand.

1st number (1→6): Wire Number.
2nd number (1→4): Position - order from end (1 nearest end).
1,2,3,4 at distances 5,10,16 23 mm from end.

P: Perpendicular to wire axis. See A.6.2 (i)
A: Axial (parallel) to wire axis. See A.6.2 (iii)
X: Parallel to strand axis.
π/4: 45° to wire axis.
a,b,c: Axial gauges, 3 parallel on same wire. See A.6.2 (ii)
* This strain gauge unserviceable throughout.

5.3 Instrumentation

5.3.1 Load Cell

Tension circuit No. 1, torsion circuit No. 2 and torsion circuit No. 1 (results not used) were connected to three channels of the FYLDE bridge/amplifier unit and output read from the digital display at each load increment. See Chapter 3, section 3.3.2 and Appendix A.1 for circuits and calibration. (Tension circuit No. 2 was connected to the data logger until this circuit became unserviceable following the fracture of strand VI).

5.3.2 Extrometer

Extension and rotation outputs over the 600 mm gauge length were connected to two channels of the FYLDE bridge/ amplifier unit and output read from the digital display at each load increment. See Chapter 3, section 3.4.2. and Appendix A.2 for circuits and calibration.

5.3.3 Strain Gauge Outputs

Strain gauges were connected to the data logger. See Chapter 3, section 3.5.1 and Appendix A.3 for output corrections due to line loss between bridge units and switching control/ indicator unit.

5.4 Loading Programme

The preliminary tests showed that there were significant differences in strand response to load, particularly the slope of the load/extension plots, between tests having fixed and free (zero torque) end conditions. In addition, they showed that non-linearity in the load/extension plot starts occurring at lower loads in the free end case. (See Fig. 4.6). This may be due to the earlier attainment of yield stress levels, particularly at interwire surfaces, and/or the effect of the greater rate of change in helix angle. In any event, the design of a programme of loading cycles in which both fixed and free end tests had to appear, required some consideration being given to the effect of a test with one end condition on strand performance in a test with a different end condition performed afterwards. It was therefore decided to confine tests with the free end condition to loading below 45 kN.

It seemed at this stage that further examination of the effect of end condition on strand response would be of interest, particularly if tests could be performed in which there was quantifiable partial torsional restraint of the ends. This proved possible since the relation between strand tension and torque generated can be determined from fixed end tests, if they are performed first, and by using calibration expression 3.4, the required output from the torsion circuit at a particular tension and fractional torsional restraint can be determined.

Loading programmes for each strand are shown in Table 5.3.

Strand Loading Programme

Table 5.3

Max. Load kN	End Condition	Load Cycle: Strand Number and Helix Angle				
		VI 73.6°	VIII 76.2°	X 77.7°	IX 78.9°	VII 80.9°
20	Fixed	101, 102	201, 202	301, 302	401, 402	511, 512, 513
50	Fixed	103, 104	203, 204	303, 304	403, 404	504, 505
44	Free	*(105,6,7,8):109	205, 206	305, 306	405, 406	‡(506),507,508
44	¼ Fixed	112	207	307	407	511
44	½ Fixed	110	208	308	408	509
44	¾ Fixed	111	209	309	409	510
50	Fixed	113, 114	210, 211	310, 311	410, 411	512
60	Fixed	-	-	-		513
70	Fixed	-	-	-		514
80	Fixed	115, 116	212	312	412	515
85	Fixed	117	-	-		516
90	Fixed	118	213	313	413	517
95	Fixed	119	-	-	-	518
100	Fixed	-	214	314	414	519
102	Fixed	120	-	-	-	-
105	Fixed	-	-	-	-	520
106	Fixed	-	215	315	415	-
110	Fixed	121	216	316	416	521
EXTROMETER DISCONNECTED						
To Fracture Load	"	122,123,124	217	317,318,319	417, 418	522
in kN	"	137.0 kN	139.6 kN	145.4 kN	136.7 kN	137.9 kN

Table 5.3 - Strand Loading Programme (Continued)

* For strand VI, four tests performed in error at unknown torsional restraint.

‡ For strand VII, one test performed " " " " "

Minimum holding load of 3 kN at start of each load cycle, for strand VI; 4kN for strands VII, VIII, IX & X.

Note that loading cycles are numbered 101, 102 ..... for helix angle of 73.6°, 201 ... for helix angle 76.2°, ... and 501 ... 522 for helix angle 80.9°.

The fact that these programmes are not identical indicates that there was a degree of development work necessary, even in this main test programme. The technique for tests under fractional torsional restraint (strands VI and VII) needed perfecting. In addition, caution was exercised in the way that maximum load was increased cycle by cycle, in strands numbers VI and VII, since the 360° wire loops in end grips were being tried for the first time. However, by the time that strands VIII, IX and X were tested, identical programmes were possible. Differences in the number of cycles required to fracture the strand, after disconnecting the extrometer, arose because of attempts to photograph strand fracture with a high speed camera, and the inherent triggering problems involved. (See section 5.5.2).

5.5 Results

5.5.1 Breaking Loads and Types of Fracture

The breaking load of wire rope or strand is of major interest to manufacturer and user. Test procedures to determine this value are well developed and it is always quoted in catalogues and specifications. For this reason, the determination of breaking load for these particular strands was not considered a top priority for this study. However, the values are given here, in Table 5.4, together with details of type of fracture.

The main features of the fracture are also shown in Fig. 5.1, 5.2 and 5.3. Ductile 'cup and cone' fractures are evident in all wires (see Fig. 5.1.a and Fig. 5.3.a). In the longer of the lengths of strand remaining after the fracture, the core wire can be seen to protrude from the helicals (Figs 5.1.a and 5.3.a) and 'birdcaging' is evident adjacent to the grip (Fig. 5.1.b). Except for strand VII, in which only a single wire broke, the nature of the break is as shown in Fig. 5.1. The 'birdcaging' at the grip end of the longer remaining length of strand is shown in Fig. 5.2 for the other four strands. The Fig. 5.3 shows details of strand X, which also is the subject of the high speed photographs described in the next section. Fig. 5.3.a shows the 'cup and cone' wire breaks while Fig. 5.3.b shows details of the end grips. On the left, resin still embedded in the hollow conical grip body exhibits slight crazing. On the right, resin has been pushed out of the grip

Breaking Loads and Types of Fracture

Table 5.4

Strand No.	Helix Angle	Breaking Load (kN)	% Dev. from Mean	Fracture Description (See also Figs 4.1 to 4.5)
VI	73.6°	137.0	-1.6	All wires severed about $\frac{1}{3}$ of strand length from grip. 'Birdcaging' about 70 mm from both ends. Largest 'birdcage' (50 mm dia.) in longer length of broken strand.
VIII	76.2°	139.6	+0.2	All wires severed about 220 mm from end opposite load cell. Double 'birdcage' covering full wire lay length at load cell end.
X	77.7°	145.4	+4.4	All wires severed about 190 mm from load cell end. Double 'birdcage' at opposite end.
IX	78.9°	136.7	-1.9	All wires severed about 160 mm from load cell end. Double 'birdcage' at opposite end.
VII	80.9°	137.9	-1.0	One helical wire broken at end grip. Snaked loose from remaining wires over whole length. Formed a 'single wire birdcage'.

Mean breaking load: 139.3 kN

Figure 5.1. Strand VI after break.

(a) At break.

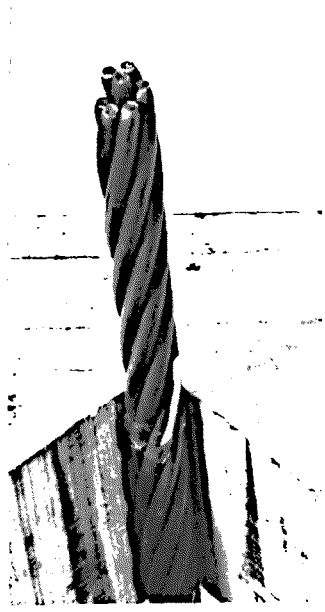

Short end.

Long end.

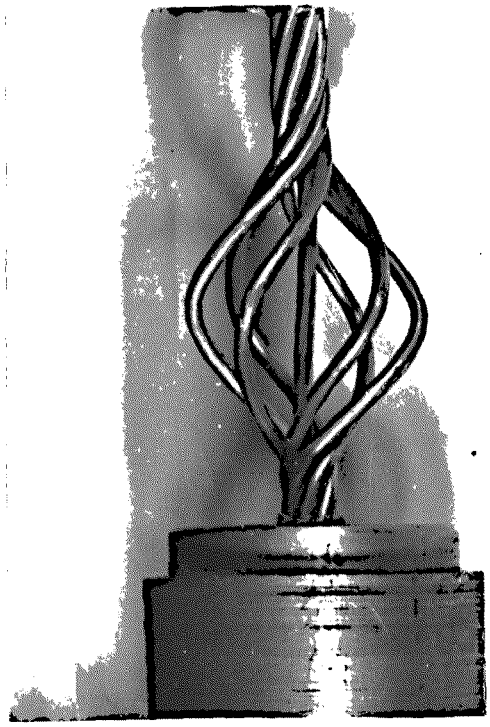

(b) At grips.

Figure 5.2. "Birdcaging" at strand end after break.

Strand VIII
(α =76.2%)

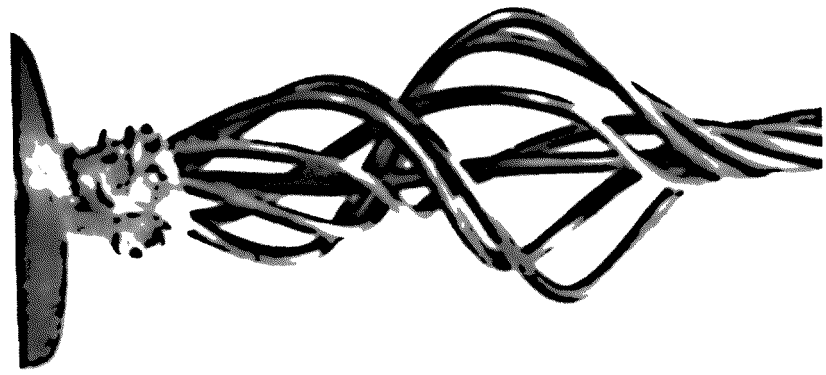

Strand X
(α =77.7%)

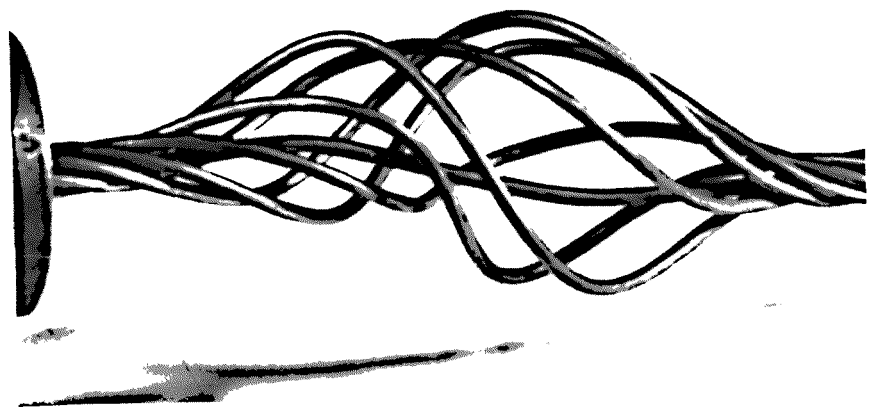

Strand IX
(α =78.9%)

Strand VII
(α =80.9%)

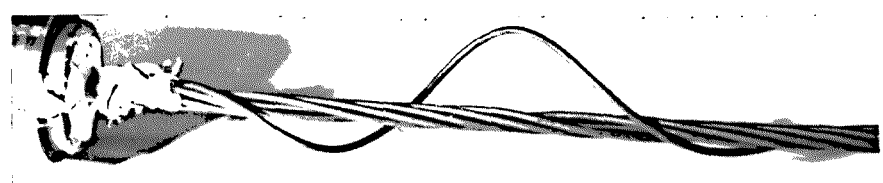

Figure 5.3. Strand X after break.

(a)Strand Ends.

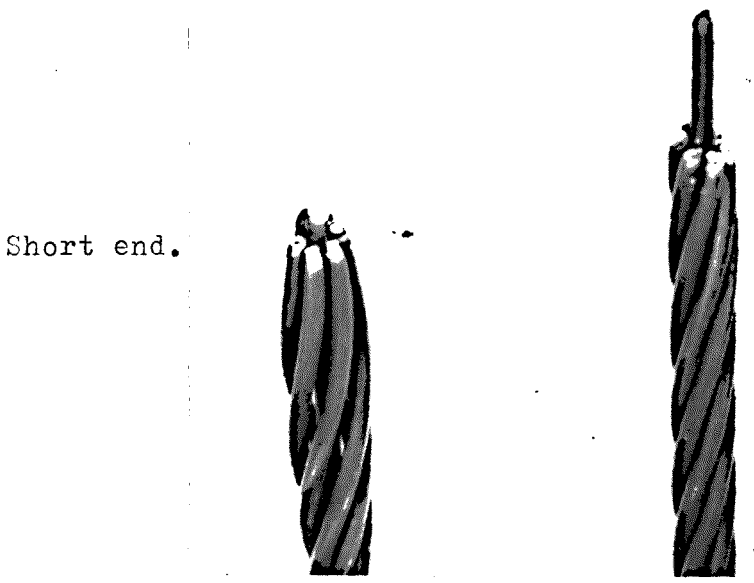

(b)Resin Cones.

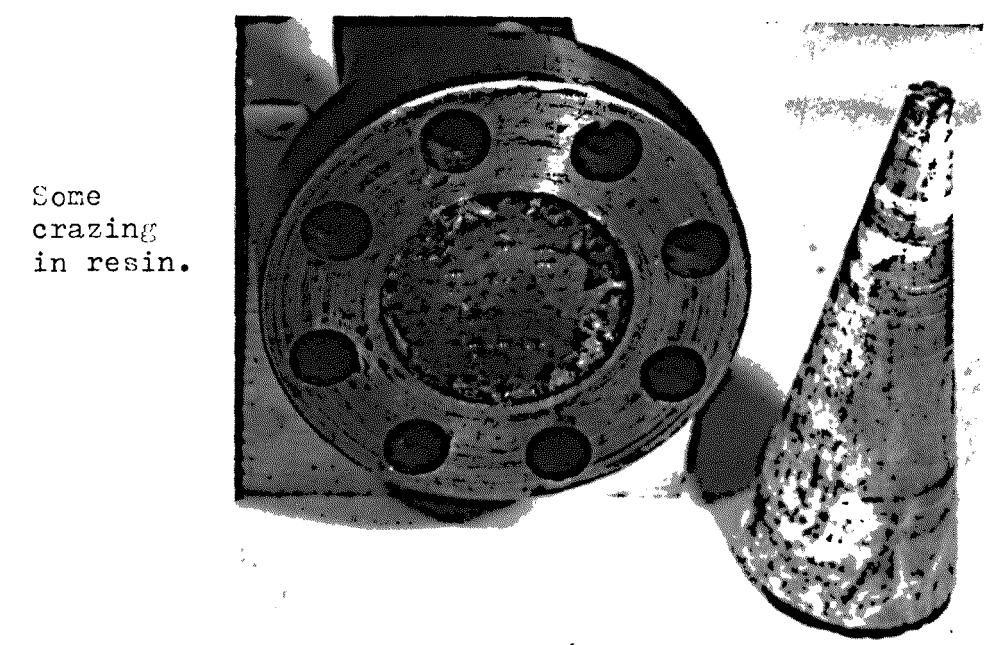

body, after sawing off the strand where it emerged. This cone is seen to be essentially intact. Cones from the other test strands appeared similar to Figs 5.3.a and b except where the resin at the throat of cones from strand VI had considerably more damage where the strand emerges from the grip body. The more complex stress pattern in this region, due to the greater torque generated in this strand may account for this damage. See also Chapter 7, section 7.2.

5.5.2 High Speed Photography at Strand Break

The acquisition of a Hadland high speed camera for use in research on dynamic plasticity, within this Department, prompted an attempt to photograph a strand at the instant of fracture and just afterwards. It was hoped that information might emerge on the propagation of 'birdcages' evidenced in the Figs 5.1 and 5.2, which are photographs taken after the tests were completed.

The major problem encountered was the fact that the instant of strand fracture cannot be predetermined, nor the position where this fracture will occur. The decision on when to start filming becomes a matter of judgment, since there is no warning either acoustic, from 'cracks' in the resin, or visual, of any sort, that can be used to trigger the camera. Some trial and error type development work was done during the fracture of strands VIII and IX, in which a complete film was wasted and some pictures eventually obtained at the very end of another film. Camera speed proved to have been too slow on that occasion and the complete event occurred in the space of 3

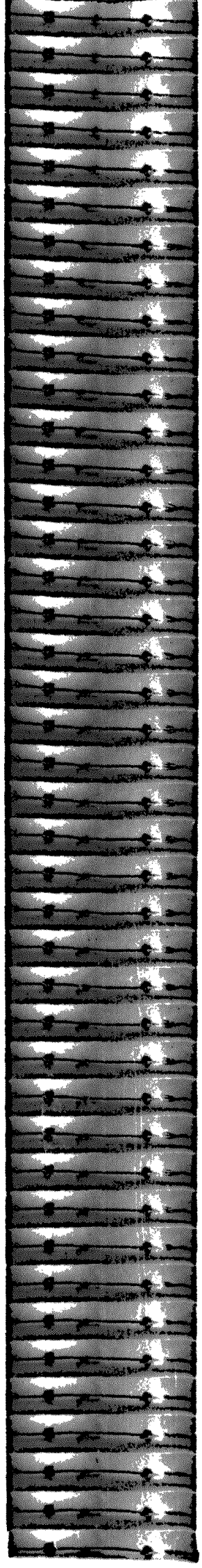

Figure 5.4. Strand Break and "Birdcaging".
Strand X.
147 frames/sec at $\frac{1}{4}$ frame.
(δt=1.7msec.)

frames.

The Figs 5.4 are obtained from the fracture of strand No. X. The extrometer was disconnected from the strand after load cycle No. 16, max. load 110 kN, and loading cycles to maxima of 120 kN and then 126 kN were performed. The rig loading rod at the end opposite to the load cell was then screwed tight in order to allow maximum loading ram travel, if required, and the load taken up to 125 kN, at which point the camera was prepared. Loading was then restarted at maximum pumping speed possible and the camera was triggered as the load passed 130 kN. Fracture occurred shortly afterwards at 145.4 kN. Camera speed was 147 frames/second at $\frac{1}{4}$ frame exposures, giving a print at intervals of about 1.7 msec. Strand fracture is detected in one print, numbered one, and the other prints are numbered sequentially from there.

5.5.3 Data Processing

Raw data from strain gauges, as recorded from the data logger on punched tape, together with strand tension, torque generated, extension and rotation, as recorded from the digital indicator on the FYLDE bridge/amplifier units, were fed to the input of the Systime PDP11 computer. Programming required to produce strain values and other results in suitable units for presentation in convenient tabular form, or for output to data files for use in subsequent graph plotting, is shown in the flowchart Fig. 5.5.

In order to obtain information about the nature of the load/extension, load/rotation, load/strain and load/torque relationships without having to plot out graphs for every load cycle, a programme was devised to look at the data obtained from the programming described in flowchart Fig. 5.5 and determine best straight lines over selected ranges of these loading cycles, by the method of least squares. See flowchart Fig. 5.6. For increasing load, starting at 10 kN, the best straight line for this and the next two points is determined. The deviation from this best straight line of the experimental value at 10 kN is determined next and then the deviations from the third point and every point between this and the maximum load point for the loading cycle. The process is then repeated for the curve consisting of the 10 kN point and the next three points and repeated again until the line considered takes in all points from 10 kN up to and including the point before the maximum load point. The tabular printout from this programme shows up change of slope as load increases and by examining deviation magnitudes and distributions, the presence of 'rogue' points (from typing or punching errors) can be detected, as well as the way that the experimental results depart from linearity. The shape of the plot for the period of decreasing load is also examined. The first points considered are the middle point and the two below it for which slope and deviations at lowest point and others from highest of the three up to the maximum load point for the load cycle. The process is then repeated for the 5 points, consisting of an increase of one point up and one point down over the curve

Figure 5.5. FLOWCHART:DATA PROCESSING.

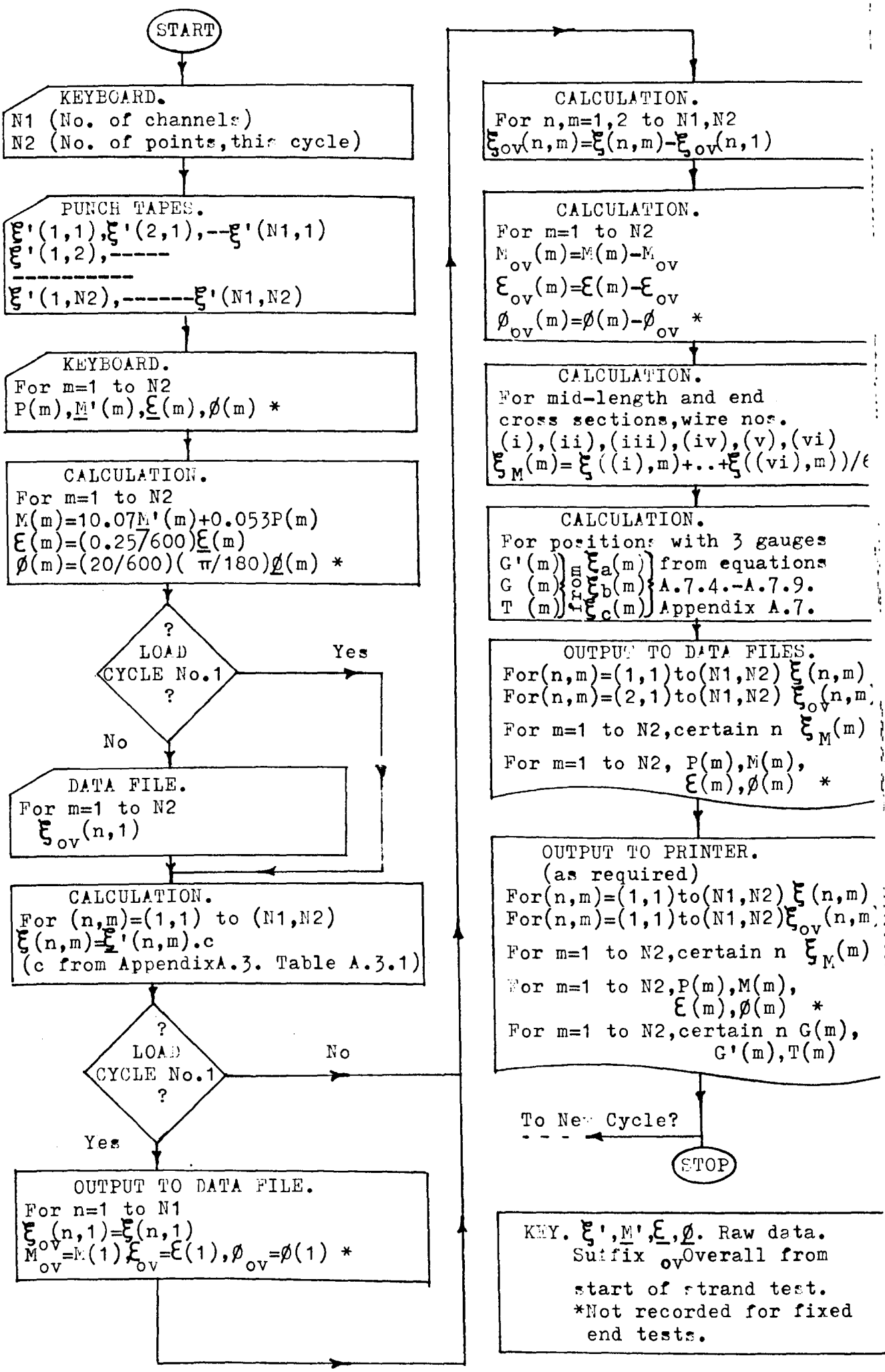

Figure 5.6. FLOWCHART:BEST STRAIGHT LINES.

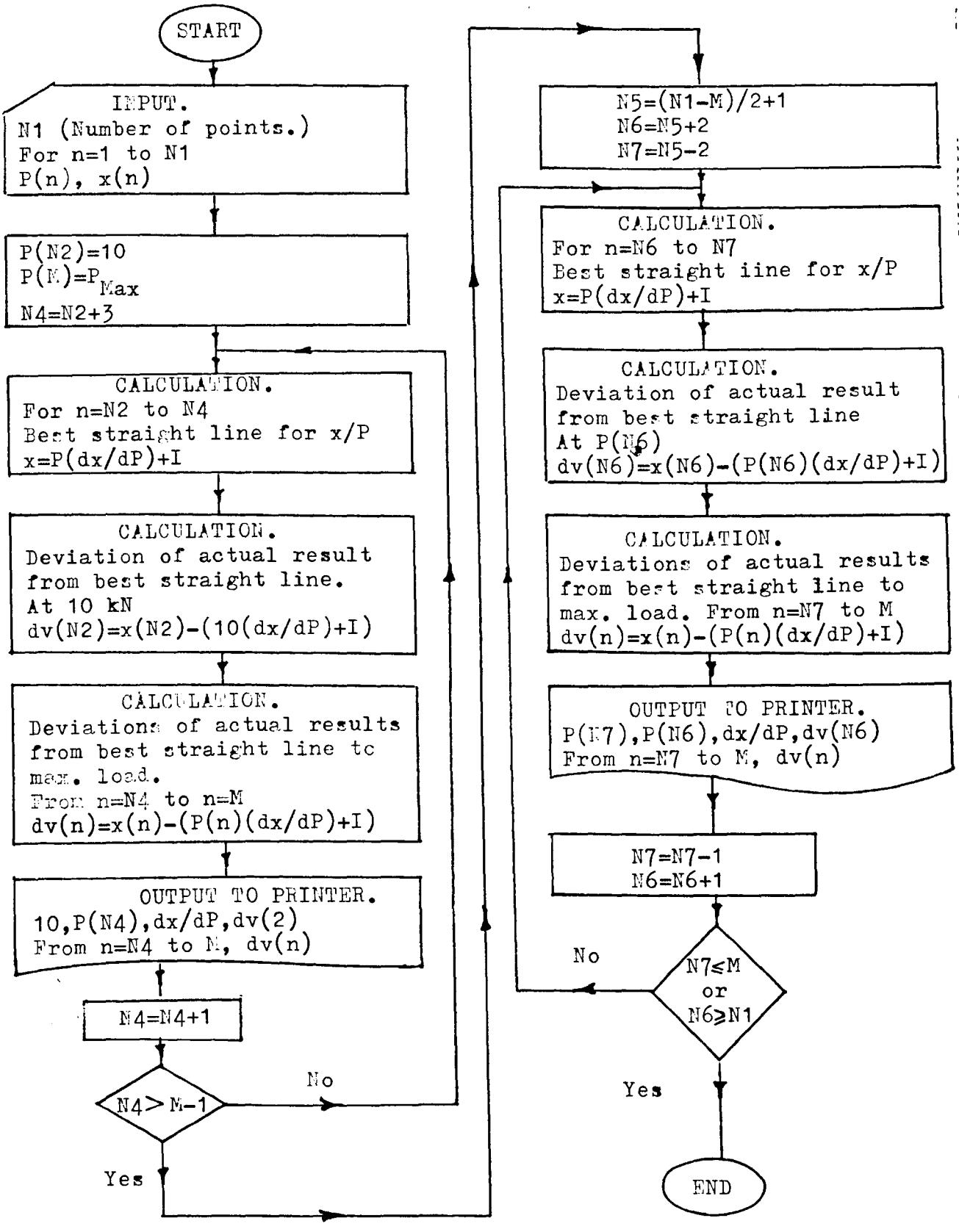

previously analysed. Thereafter, curves covering two points more than the previous curve are considered until the lowest load point, which is the final point in the load cycle, is included.

The graph plotting accessory to the computer has been utilised to obtain plots of load against other parameters. These plots are another way of presenting the information already obtained in the tabulated digital form from the programming outlined in the flowchart Fig. 5.5 and analysis on slope and deviation from linearity given in the programming outlined in the flowchart Fig. 5.6.

5.5.4 Hysteresis Effects from the Extrometer

It should be noted that the extension and rotation data obtained from the extrometer has not been corrected to take account of the hysteresis inherent in the extrometer mechanism, calibration of which is described in Chapter 3 (section 3.2) and Appendix A.2. This hysteresis affects the results only after load reversal in each cycle. When the extrometer mechanism is fully reversed, extension values should be reduced by 0.11 mm (183 microstrain) and rotation by 0.46° (1.31 microradians/mm) over the 600 mm gauge length. The calibration tests showed that reversal of the mechanism was completed within 0.1 mm (166 microstrain) of load reversal (extension). See Table A.2.1.a. There is therefore one short length of the load/extension plot immediately after load reversal, within a load cycle, and another,

at the end of one cycle and the beginning of the next cycle, over which the shape of the plot is uncertain. (See Fig. 5.7). However, it can be seen that over most of the unloading section of the load cycle, the slopes of the corrected and uncorrected curves are idential. The corresponding areas of slope uncertainty for the load/rotation plots cannot be determined from the calibration tests. The magnitude of the error can be gauged, however, when it is seen that with a hysteresis of 0.46^{o}, this constitutes only 3.2% of the 14.37^{o}, which is the smallest overall rotation for any of the cycles in the test programme, excluding those subjected to the fully fixed end condition. (Cycle No. 10, $\frac{3}{4}$ fixed for strand VII).

In fact, none of the slopes from the unloading sections of the load/extension or load/rotation plots are used in the comparison with mathematical modelling of strand response. (See Chapter 7, sections 7.4 and 5). The fact that the corrections have not been applied in either tabulated or plotted results does not therefore detract from the validity of the results presented. Moreover, determination of energy absorption by the strand, as exhibited by the areas of hysteresis loops in plots of strand response, has not been an objective of this study. (Since the areas of these loops affected by uncertainty about the slope of the plot constitute a very small fraction of the total area of the hysteresis plot, an accurate determination of these plots could be obtained if required).

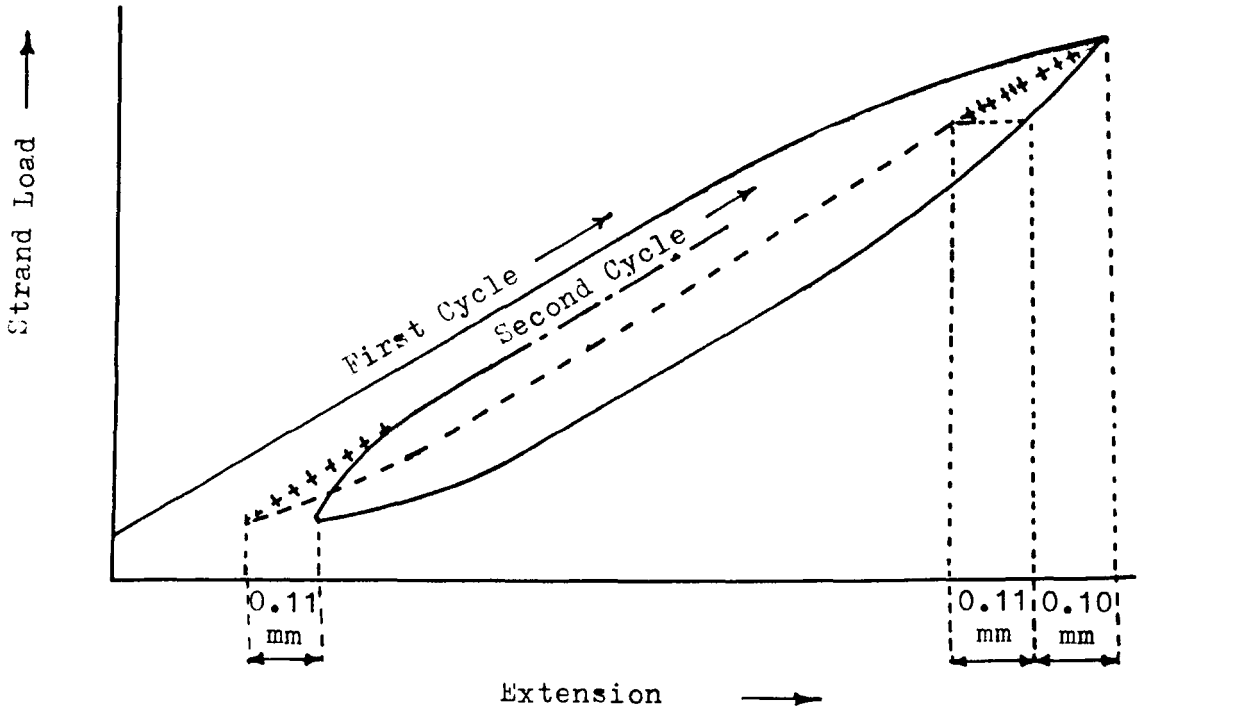

Output from Data Logge

Corrected

Uncertain Slope

Next cycle continued

Figure 5.7.Effect of Extrometer Hysteresis.

5.5.5 Tabulated Results

Samples of the tabulated results obtained from the programming described in flowchart Fig. 5.5 are shown in Tables 5.5 to 5.11.

Extension is tabulated with strand load in Table 5.5. After the strand load (first column) extension is given, for the current cycle (second and third columns) and overall, since the start of the test on the strand (fourth and fifth columns), in units of mm (over the 600 mm gauge length in the second and fourth columns) and microstrain (in the third and fifth columns). Similarly, rotation is tabulated in Table 5.6, the units being degrees (over the 600 mm gauge length in the second and fourth columns) and microradians per mm length of strand (in the third and fifth columns).

Surface strains are given in Tables 5.7 to 5.10. The strain in each of the six wires at the particular strand section is shown in columns two to seven against load in column one. The eighth column gives mean strain. Tables 5.7 and 5.8 give surface strains parallel to wire axis at mid-length and at strand end, (near grip) respectively, while Table 5.9 gives surface strain perpendicular to wire axis at the end (near grip). The gauges mounted perpendicular to the wire axis are nearer the grip than the axially mounted gauges. (See Table 5.2). Table 5.10 is a sample of the tabulation of overall strains in a particular cycle. Note that in this case the surface strains at the holding load of 4 kN are less, in five of the wires, than they

Table 5.5. Load/Extension. Strand IX.

CYCLE403.DAT

LOAD (AXIAL) kN.	EXTENSION (THIS CYCLE) mm.	AXIAL microstrain (this cycle)	EXTENSION (OVERALL) mm.	AXIAL microstrain (overall)
4	0	0	.025	41.6667
5	5.00000E-03	8.33333	.03	50
7	.1225	204.167	.1475	245.833
10	.265	441.667	.29	483.333
15	.485	808.333	.51	850
20	.71	1183.33	.735	1225
25	.895	1491.67	.92	1533.33
30	1.105	1841.67	1.13	1883.33
35	1.315	2191.67	1.34	2233.33
40	1.525	2541.67	1.55	2583.33
42	1.615	2691.67	1.64	2733.33
44	1.6975	2829.17	1.7225	2870.83
46	1.79	2983.33	1.815	3025
48	1.8875	3145.83	1.9125	3187.5
50	1.975	3291.67	2	3333.33
48.8	1.9775	3295.83	2.0025	3337.5
48	1.98	3300	2.005	3341.67
47	1.9825	3304.17	2.0075	3345.83
46	1.95	3250	1.975	3291.67
45	1.905	3175	1.93	3216.67
44	1.86	3100	1.885	3141.67
42	1.775	2958.33	1.8	3000
40	1.69	2816.67	1.715	2858.33
35	1.4775	2462.5	1.5025	2504.17
30	1.265	2108.33	1.29	2150
25	1.075	1791.67	1.1	1833.33
20	.8575	1429.17	.8825	1470.83
15	.6575	1095.83	.6825	1137.5
10	.4275	712.5	.4525	754.167
7	.2775	462.5	.3025	504.167
5	.1525	254.167	.1775	295.833
4	.0825	137.5	.1075	179.167

Table 5.6. Load/Rotation. Strand X.

CYCLE306

LOAD (AXIAL) kN	ROTATION (THIS CYCLE) Degrees.	ROTATION (THIS CYCLE) MicroRads./mm.	ROTATION (OVERALL) Degrees	ROTATION (OVERALL) MicroRads./mm.
4	0	0	2.9942	87.0978
5	1.7964	52.2552	4.7906	139.353
7	5.3892	156.765	8.3834	243.863
10	11.1776	325.143	14.1718	412.241
15	20.7584	603.837	23.7526	690.935
20	29.7404	865.113	32.7346	952.211
25	38.922	1132.2	41.9162	1219.29
30	48.7024	1416.7	51.6966	1503.79
35	58.2832	1695.39	61.2774	1782.49
38	64.0716	1863.77	67.0658	1950.87
40	68.2632	1985.7	71.2574	2072.79
42	72.0556	2096.01	75.0498	2183.11
44	76.4468	2223.75	79.441	2310.85
43	74.85	2177.3	77.8442	2264.4
42	72.6544	2113.43	75.6486	2200.53
41	71.2572	2072.79	74.2514	2159.89
40	69.2612	2014.73	72.2554	2101.82
38	65.4688	1904.41	68.463	1991.51
35	60.4788	1759.26	63.473	1846.36
30	50.4988	1468.95	53.493	1556.05
25	40.7184	1184.45	43.7126	1271.55
20	31.1376	905.756	34.1318	992.854
15	21.5568	627.062	24.551	714.16
10	13.1736	383.205	16.1678	470.302
7	7.78441	226.439	10.7786	313.537
5	4.1916	121.929	7.18581	209.027
4	2.5948	75.4797	5.589	162.578

Table 5.7. Load/Strain. Strand VIII.

CYCLE210.DAT

AXIAL STRAINS ON HELICALS AT STRAND MID-LENGTH.

LOAD kN	WIRE 1 microstrain	WIRE 2 microstrain	WIRE 3 microstrain	WIRE 4 microstrain	WIRE 5 microstrain	WIRE 6 microstrain	MEAN microstrai
4	0	0	0	0	0	0	0
5	50.5767	55.5352	42.6431	45.6182	45.6182	86.2779	54.3782
7	161.647	180.489	150.738	166.606	145.78	270.734	179.332
10	322.302	367.921	332.22	356.02	299.493	513.701	365.276
15	597.003	677.331	641.63	672.373	560.31	884.596	672.207
20	906.414	982.775	959.966	998.642	828.07	1240.62	986.08
25	1212.85	1284.25	1277.31	1323.92	1099.8	1583.74	1296.98
30	1524.24	1600.6	1608.54	1659.11	1389.37	1931.83	1618.95
35	1825.72	1911.01	1928.86	1980.42	1679.94	2260.08	1931.01
40	2130.17	2227.36	2251.16	2305.7	1979.43	2587.35	2246.86
42	2254.13	2357.27	2384.05	2437.6	2102.4	2722.22	2376.28
44	2374.13	2482.23	2510.98	2565.53	2220.42	2849.15	2500.41
46	2499.08	2611.15	2641.89	2695.44	2343.39	2982.04	2628.83
48	2619.08	2737.09	2768.83	2824.36	2463.38	3108.98	2753.62
50	2743.04	2867	2900.72	2955.27	2588.34	3241.87	2882.71
49	2679.57	2801.55	2834.28	2890.81	2522.88	3175.44	2817.09
48	2614.12	2734.12	2766.84	2822.38	2456.44	3105.01	2749.82
47	2552.64	2669.66	2700.4	2758.91	2392.97	3038.57	2685.52
46	2490.16	2604.2	2634.95	2693.46	2329.5	2974.11	2621.06
45	2422.72	2535.78	2565.53	2626.05	2263.06	2904.69	2552.47
44	2361.24	2472.31	2502.06	2558.59	2201.57	2841.22	2489.5
42	2230.33	2338.43	2368.18	2421.73	2073.64	2708.33	2356.78
40	2103.4	2210.5	2239.26	2288.84	1949.68	2579.41	2228.52
35	1789.03	1890.18	1917.95	1960.59	1640.27	2256.12	1909.02
30	1475.65	1571.84	1597.63	1633.33	1335.82	1930.84	1590.85
25	1173.18	1263.43	1284.25	1315.99	1045.25	1608.54	1281.77
20	869.721	956.99	967.899	996.659	762.617	1277.31	971.866
15	570.227	655.514	649.563	671.381	491.883	931.286	661.629
10	265.776	345.112	324.286	331.228	266.025	557.335	343.293
7	117.021	170.572	151.73	154.705	103.137	329.244	171.068
5	15.8672	45.6182	31.7344	34.7095	10.9087	124.954	43.9654
4	-24.2759	-28.2594	-27.7676	-21.8174	-29.751	-30.7427	-27.6023

Table 5.8. Load/Strain. Strand VIII.

CYCLL210.DAT

AXIAL STRAINS ON HELICALS AT STRAND END--NEAR GRIP.

LOAD kN	WIRE 1 microstrain	WIRE 2 microstrain	WIRE 3 microstrain	WIRE 4 microstrain	WIRE 5 microstrain	WIRE 6 microstrain	MEAN microstrain
4	0	0	0	0	0	0	0
5	44.6265	28.7593	18.8423	42.6431	64.4605	70.4107	44.9571
7	212.224	190.406	64.4605	75.3692	156.689	251.892	158.507
10	363.954	368.912	187.431	219.166	329.244	477.999	324.451
15	629.729	665.431	424.448	460.149	605.929	823.111	601.466
20	910.381	967.899	681.298	706.09	886.58	1163.26	885.919
25	1194.01	1267.39	935.173	958.974	1176.16	1484.58	1169.38
30	1491.52	1575.83	1195	1225.74	1483.58	1821.75	1465.24
35	1780.1	1869.35	1445.9	1489.53	1787.04	2149.01	1753.49
40	2074.64	2163.89	1692.83	1764.23	2090.5	2475.28	2043.56
42	2192.65	2287.85	1794.98	1874.31	2217.44	2607.18	2162.4
44	2307.69	2405.86	1892.16	1981.42	2337.44	2732.13	2276.12
46	2426.69	2527.84	1992.33	2093.48	2464.37	2858.08	2393.8
48	2543.71	2646.85	2089.51	2201.57	2587.35	2988.98	2509.66
50	2662.71	2771.8	2189.67	2316.61	2715.27	3123.86	2629.99
49	2595.28	2710.32	2133.15	2257.11	2641.89	3061.38	2566.52
48	2529.83	2647.84	2075.63	2199.59	2569.49	2996.92	2503.22
47	2467.35	2586.35	2023.07	2142.07	2500.08	2930.47	2441.57
46	2405.86	2525.86	1971.5	2086.54	2432.64	2863.04	2380.91
45	2339.42	2461.4	1916.96	2024.06	2360.25	2794.61	2316.12
44	2277.93	2401.9	1866.38	1966.54	2293.8	2727.18	2255.62
42	2150.01	2278.93	1762.25	1846.55	2155.96	2591.31	2130.83
40	2027.03	2157.94	1662.09	1729.52	2023.07	2453.47	2008.85
35	1721.59	1855.47	1407.22	1444.91	1695.81	2117.28	1707.05
30	1419.12	1550.03	1148.39	1173.18	1375.49	1783.08	1408.21
25	1128.55	1249.54	897.488	913.356	1070.04	1461.77	1120.13
20	835.011	945.09	642.622	656.505	773.526	1136.47	831.54
15	547.418	639.646	385.771	407.589	494.868	802.285	546.261
10	272.718	330.236	125.946	156.689	235.833	454.199	262.47
7	141.813	166.63	.9917	37.6846	110.079	254.867	118.178
5	14.8755	22.8091	-39.668	23.8008	47.6016	76.3609	24.2967
4	-27.7676	-20.8257	-43.6348	-4.9585	-9.917	-26.7759	-22.3133

Table 5.9. Load/Strain. Strand VIII.

CYCLE210.DAT

PERPENDICULAR STRAINS ON HELICALS AT STRAND END--NEAR GRIP.

LOAD kN	WIRE 1 microstrain	WIRE 2 microstrain	WIRE 3 microstrain	WIRE 4 microstrain	WIRE 5 microstrain	WIRE 6 microstrain	MEAN microstrain
4	0	0	0	0	0	0	0
5	-10.5523	-7.6744	-6.7151	-15.3488	-16.3081	-16.3081	-12.1511
7	-54.6801	-43.1685	-11.5116	-22.0637	-41.2497	-64.2731	-39.4912
10	-96.8093	-87.2963	-43.1685	-62.3545	-78.6626	-115.116	-80.5812
15	-167.878	-162.122	-95.93	-126.628	-140.058	-196.657	-148.212
20	-240.784	-239.825	-157.325	-191.06	-201.453	-274.36	-217.601
25	-316.569	-316.569	-221.598	-259.011	-260.93	-349.185	-287.31
30	-376.191	-393.313	-288.749	-329.999	-323.284	-427.848	-359.897
35	-473.894	-464.301	-354.941	-400.987	-384.679	-504.592	-430.566
40	-552.557	-536.249	-419.214	-476.772	-445.115	-582.295	-502.034
42	-585.173	-568.907	-446.074	-506.51	-470.057	-614.952	-531.292
44	-616.83	-594.766	-471.976	-536.249	-494.039	-643.69	-559.592
46	-648.487	-624.504	-498.836	-567.906	-518.981	-675.347	-589.01
48	-680.144	-653.283	-523.778	-597.644	-543.923	-706.045	-617.469
50	-712.76	-684.94	-549.679	-629.301	-569.824	-737.702	-647.368
49	-674.533	-668.632	-534.33	-612.033	-553.516	-720.434	-630.58
48	-671.266	-652.324	-518.981	-596.685	-537.208	-703.167	-614.272
47	-659.998	-636.975	-505.551	-580.376	-521.859	-685.899	-598.443
46	-642.731	-621.626	-491.162	-565.028	-507.47	-669.591	-582.935
45	-625.464	-606.278	-476.772	-548.72	-492.121	-652.324	-566.946
44	-608.196	-591.888	-466.342	-532.412	-477.731	-636.016	-551.597
42	-573.661	-562.15	-434.563	-499.795	-447.993	-602.44	-520.101
40	-541.045	-535.289	-407.702	-467.179	-420.173	-569.824	-490.202
35	-456.545	-464.301	-338.633	-389.476	-352.063	-488.284	-415.217
30	-376.046	-391.394	-268.604	-316.539	-284.912	-407.702	-340.871
25	-296.424	-319.447	-201.453	-246.54	-220.639	-330.959	-269.244
20	-214.886	-245.581	-134.302	-177.47	-158.288	-254.214	-197.456
15	-135.201	-170.755	-70.0289	-111.279	-98.8079	-177.47	-127.267
10	-61.3952	-96.0521	-9.593	-46.0464	-42.2092	-98.8079	-58.5173
7	-26.8604	-47.965	16.3081	-14.3895	-15.3488	-54.6801	-23.8226
5	4.7965	-6.7151	14.3895	-14.3895	-3.8372	-12.4709	-3.03778
4	15.3488	7.6744	15.3488	-4.7965	6.7151	[illegible]	[illegible]

Table 5.10. Load/Strain. Strand VIII.

OVERALL STRAINS.

CYCLE210.DAT

AXIAL STRAINS ON HELICALS AT STRAND MID-LENGTH.

LOAD kN	WIRE 1 microstrain	WIRE 2 microstrain	WIRE 3 microstrain	WIRE 4 microstrain	WIRE 5 microstrain	WIRE 6 microstrain	MEAN microstrain
4	-114.046	-22.8079	-15.8713	-58.5093	-49.5852	166.61	-15.7015
5	-63.469	32.7273	26.7717	-12.8911	-3.96699	252.888	38.6767
7	47.6014	157.682	134.867	108.096	96.1947	437.344	163.631
10	208.257	345.113	316.348	297.511	249.908	680.311	349.575
15	482.958	654.523	625.759	613.863	510.725	1051.21	656.506
20	792.368	959.967	944.094	940.133	778.484	1407.23	970.379
25	1098.8	1261.44	1261.44	1265.41	1050.21	1750.36	1281.28
30	1410.2	1577.8	1592.67	1600.6	1339.79	2098.44	1603.25
35	1711.67	1888.2	1912.99	1921.92	1630.35	2426.69	1915.3
40	2016.13	2204.55	2235.29	2247.19	1929.85	2753.96	2231.16
42	2140.09	2334.46	2368.18	2379.09	2052.82	2888.83	2360.58
44	2260.08	2459.42	2495.11	2507.02	2170.83	3015.76	2484.7
46	2385.04	2588.34	2626.02	2636.93	2293.8	3148.65	2613.13
48	2505.03	2714.28	2752.96	2765.85	2413.8	3275.59	2737.92
50	2629	2844.2	2884.85	2896.76	2538.75	3408.48	2867.01
49	2565.53	2778.74	2818.41	2832.3	2473.3	3340.05	2801.39
48	2500.08	2711.31	2750.97	2763.87	2406.86	3271.62	2734.12
47	2438.59	2646.85	2684.53	2700.4	2343.39	3205.18	2669.82
46	2376.11	2581.4	2619.08	2634.95	2279.92	3140.72	2605.36
45	2308.68	2512.97	2549.66	2564.54	2213.47	3071.3	2536.77
44	2247.19	2449.5	2486.19	2500.08	2151.99	3007.83	2473.8
42	2116.29	2315.62	2352.31	2363.22	2024.06	2874.94	2341.07
40	1989.35	2187.69	2223.39	2230.33	1900.1	2746.02	2212.81
35	1674.98	1867.37	1902.08	1902.08	1590.69	2422.73	1893.32
30	1361.6	1549.04	1581.76	1574.82	1286.23	2097.45	1575.15
25	1059.14	1240.62	1268.38	1257.48	995.667	1775.15	1266.07
20	755.675	934.183	952.028	938.149	713.032	1443.92	956.164
15	456.182	632.706	633.692	612.872	442.298	1097.82	645.928
10	151.73	322.304	308.415	272.719	186.439	723.946	327.592
7	2.97488	147.765	135.859	96.1958	53.5516	495.855	155.367
5	-98.1785	22.8103	15.863	-23.7998	-38.6765	291.564	28.2638
4	-140.922	-51.5471	[illegible]	[illegible]	[illegible]	[illegible]	[illegible]

were when loading began.

Bending moments and wire tension, computed from the outputs of three gauges mounted parallel on the same wire, are given in Table 5.11. The analysis for this computation is given in Appendix A.7, together with an assessment of the errors.

A sample of the tabulated results from best straight line and deviations computation, as outlined in flowchart Fig. 5.6, is given in Table 5.12.

5.5.6 Computer Plotting of Results

A selected number of the results obtained for all loading cycles, which were obtained in the tabular form described above, have been plotted, using the graph plotting facility connected to the departmental computer. (See Figs. 5.8 to 5.24). Extension for fixed, free and partially restrained end conditions in tests on strand VIII are shown in Fig. 5.8. The extensions in fixed end tests to higher maximum loads are shown in Fig. 5.9. The extrometer was disconnected after the load cycle to 110 kN maximum.

Rotations for free and partially restrained tests on strand IX are shown in Fig. 5.10. (As explained in section 5.5.4, corrections due to hysteresis effects from the extrometer have not been applied to the tabulated results or the plots in Figs. 5.8 to 5.10).

The mean of the strains recorded on the six helical wires

Table 5.11. Load/Wire Tension and Bending. Strand VII.

CYCLE514

STRAINS FROM 3 PARALLEL GAUGES ON WIRE No.1;
COMPUTED BENDING INFORMATION.

LOAD ON STRAND kN	STRAIN a in microstrain	STRAIN b in microstrain	STRAIN c in microstrain	BDG. MOM. G Nm	BDG. MOM. G! Nm	TENSION T kN
4	0	0	0	0	0	0
5	-15.8672	-2.9751	32.7261	-.0314931	.0340281	.0687489
10	-50.5767	-6.9419	207.265	-.167106	.260454	.544731
20	311.394	339.161	693.198	-.247446	.498194	1.74672
30	872.696	866.746	1262.43	-.252587	.613278	3.04834
40	1476.64	1430.03	1848.53	-.241018	.710191	4.38278
50	2121.25	2033.98	2467.35	-.224308	.79499	5.77235
56	2516.93	2405.86	2850.15	-.215952	.847989	6.62967
60	2735.11	2639.91	3118.9	-.248731	.876761	7.15938
62	2877.91	2769.82	3251.78	-.242304	.900989	7.47113
64	3040.55	2916.59	3401.53	-.233949	.92976	7.82633
66	3200.22	3063.36	3550.29	-.226879	.952474	8.16854
68	3368.8	3219.06	3709.95	-.221094	.978217	8.5351
70	3535.41	3370.79	3864.65	-.213382	1.00547	8.89697
69	3494.75	3328.15	3821.02	-.211453	1.00699	8.81494
68	3438.22	3268.64	3759.53	-.20824	1.0085	8.69921
67	3364.84	3195.26	3684.17	-.206954	1.00547	8.54596
66	3304.34	3133.77	3622.68	-.206312	1.00699	8.42626
65	3239.88	3070.3	3556.24	-.205026	1.00093	8.28635
64	3174.43	3005.84	3490.78	-.205026	.997902	8.15096
63	3111.95	2943.37	3428.31	-.205026	.997902	8.02602
62	3042.54	2875.93	3358.89	-.205026	.991845	7.87818
60	2910.64	2747.01	3229.97	-.206954	.987302	7.61064
55	2583.38	2434.62	2913.61	-.214024	.958531	6.92426
50	2252.15	2121.25	2599.25	-.224951	.92976	6.23591
40	1592.67	1507.38	1989.35	-.257086	.866161	4.87198
30	939.14	920.298	1412.18	-.306575	.779848	3.51288
20	299.493	361.97	855.837	-.360564	.658706	2.13659
10	-168.589	-58.5103	352.054	-.337426	.458823	.867065
5	-111.07	-28.7593	178.506	-.187673	.190798	.351707
4	-34.7095	18.8423	147.763	-.11826	.115084	.284507

Table 5.12. Load/Extension Slopes--Best Straight Lines.

CCYCLE103

EXTENSION SLOPES.

MIN. LOAD. kN.	MAX. LOAD. kN.	NUMBER OF POINTS ---	SLOPE ms/kN.	DEVIATION. (min load) ms.	DEVIATION. (max load) ms.	DEVIATIONS ABOVE MAX. LOAD. ms.					
10	20	3	79.5833	-2.08344	-2.08325	-12.4999	-10.4164	20.8335	11.2502	22.917	17.9167
10	25	4	78.8333	-4.58328	-3.75012	2.08325	37.0833	29.75	42.9165	39.4165	52.5833
10	30	5	78.9167	-4.16647	.83313	35.4165	27.833	40.833	37.166	50.1663	58.9993
10	35	6	79.9286	2.57925	16.865	6.24609	17.2222	11.5315	22.5078	29.3174	27.7935
10	38	7	80.0576	3.58487	3.63989	14.3582	8.40942	19.1279	25.6792	23.8975	17.949
10	40	8	80.284	5.55493	9.53467	3.13306	13.3984	19.4971	17.2622	10.8608	
10	42	9	80.3245	5.94818	2.23193	12.4165	18.4341	16.1184	9.63623		
10	44	10	80.4614	7.43152	9.24438	14.9883	12.3987	5.64258			
10	46	11	80.6062	9.16193	11.5063	8.6272	1.58179				
10	48	12	80.6806	10.1367	6.77295	-.421387					
30	40	3	77.0834	-6.1106	-6.11157	-1.94531	-18.6121	-47.7791	-91.5288	-172.779	-258.196
25	42	5	77.7963	-6.13184	-3.66821	-21.7607	-52.3533	-96.8159	-178.779	-264.909	-342.705
20	44	7	77.7035	-9.29272	-15.843	-46.2498	-90.6199	-172.49	-258.527	-336.23	-334.99
15	46	9	77.4739	-17.4601	-35.8184	-79.9587	-161.6	-247.407	-324.881	-324.1	-327.485
10	47	11	77.171	-26.8058	-65.4653	-146.803	-232.307	-309.479	-309.303	-313.294	
5	48	13	76.9455	-59.364	-126.353	-211.632	-288.577	-288.853	-293.295		

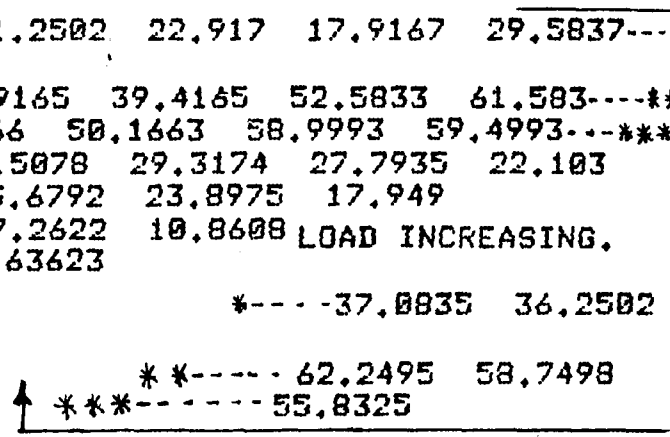

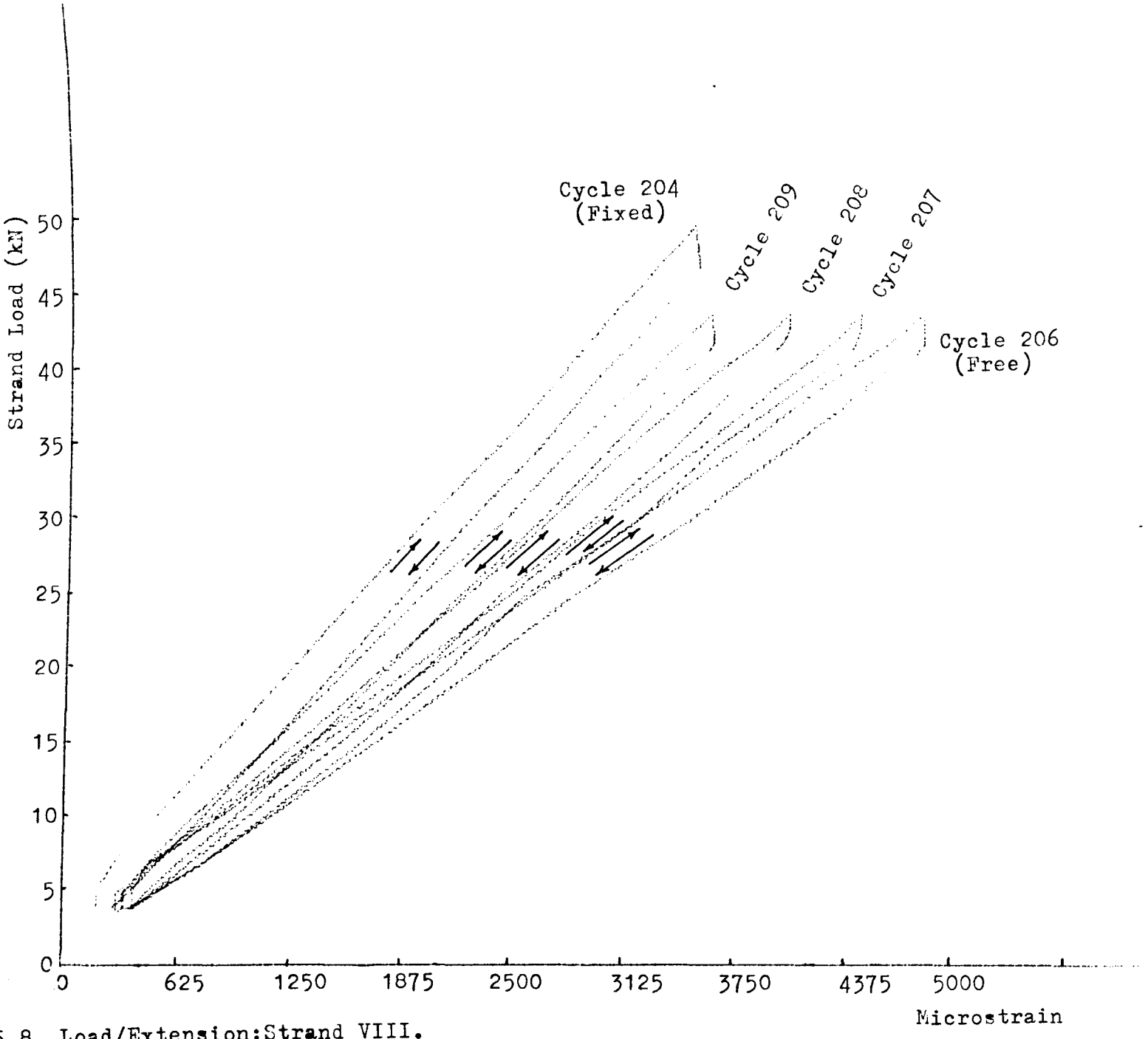

Figure 5.8. Load/Extension:Strand VIII.
Fixed,Partially Restrained and Free Ends.

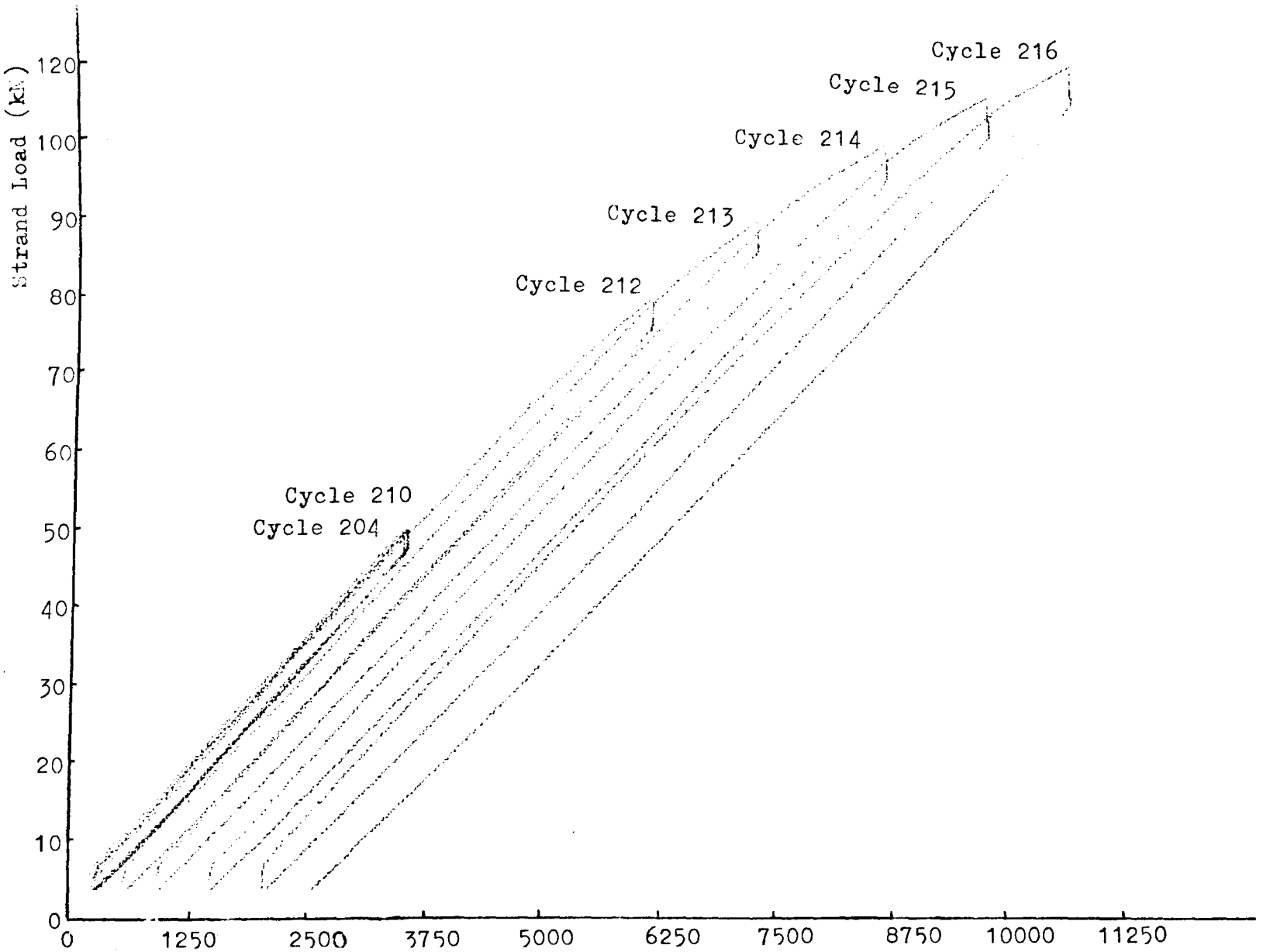

Figure 5.9. Load/Extension:Strand VIII.
Fixed Ends-Increasing Maximum Loads.

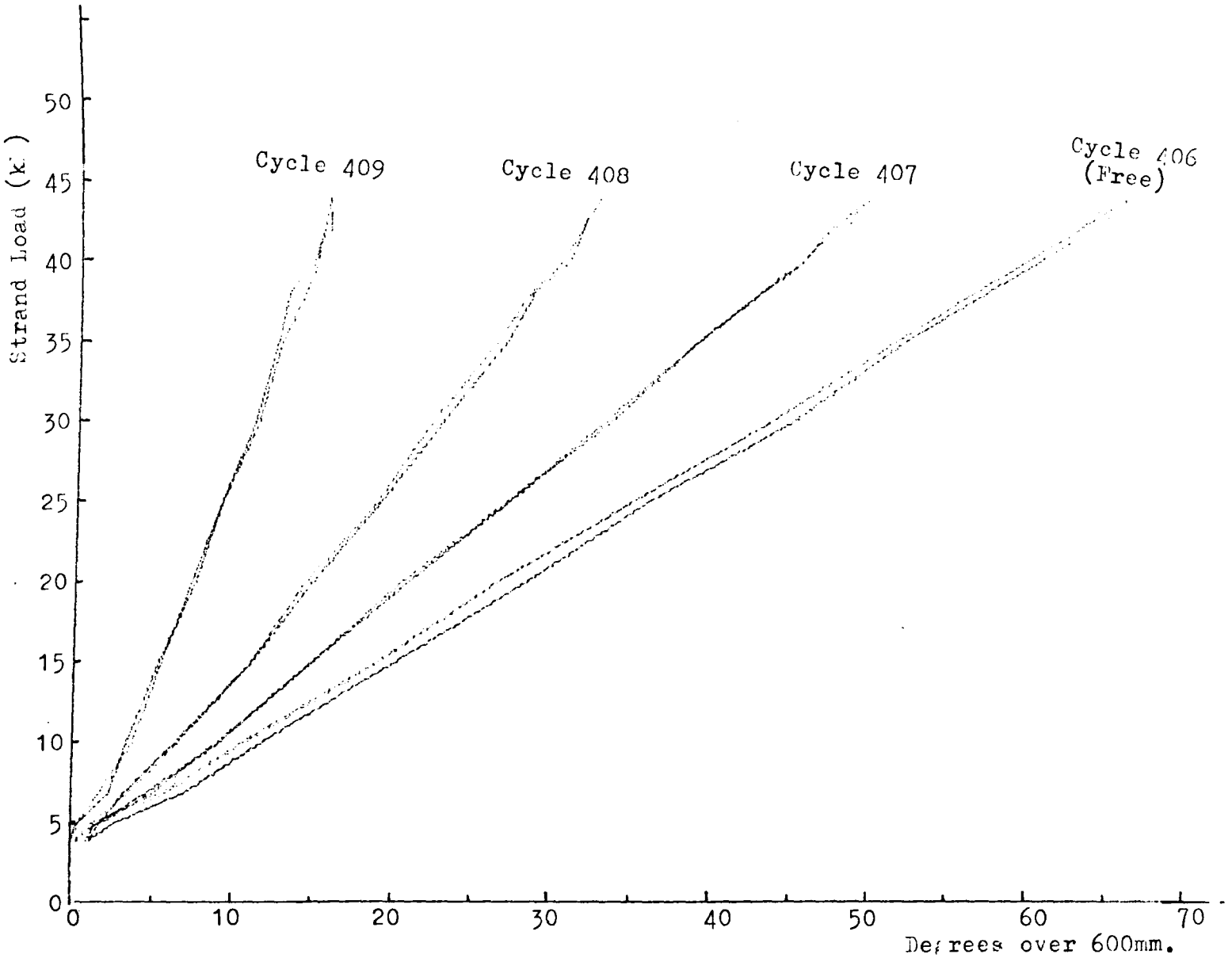

Figure 5.10. Load/Rotation:Strand IX.
Free and Partially Restrained Ends.

are shown for fixed end free end and partially restrained end tests on strand X at mid-length (Fig. 5.11) and near the grip (Fig. 5.12) up to maximum loading of 50 kN. For fixed end tests at both positions, up to strand fracture, see Fig. 5.13. The strains on all wires are plotted for loading up to 50 kN in Figs. 5.14 (mid-length) and 5.15 (near end) and up to 110 kN in Figs. 5.16 (mid-length) and 5.17 (near end). Mean strain for fixed end, free end and partially restrained end tests on strand VI are shown, at mid-length (Fig. 5.18 - axial strains), near end grip (Fig. 5.19 - axial strains) and near end grip (Fig. 5.20 - perpendicular strains). The strains on all wires in a free end test are shown in Fig. 5.21 (mid-length, axial strain), Fig. 5.22 (near end grip, axial strain) and Fig. 5.23 (near end grip, perpendicular strain). For comparison, the strains on all wires in a fixed end test are shown in Fig. 5.24 (mid-length, axial strains).

5.5.7 Torque Generated (Manual Plotting)

It was found that the most convenient way of presenting the results of torque generated was in manually plotted load/torque graphs. For each test strand, graphs were plotted for torque generated against tensile load on the strand, under test conditions of free and partially restrained ends, as well as for the fixed end condition, results for the last of these conditions being taken from the load cycle which followed the free and partially restrained cycles. As described in section 5.4, the output from the torsion circuit expected at a particular strand

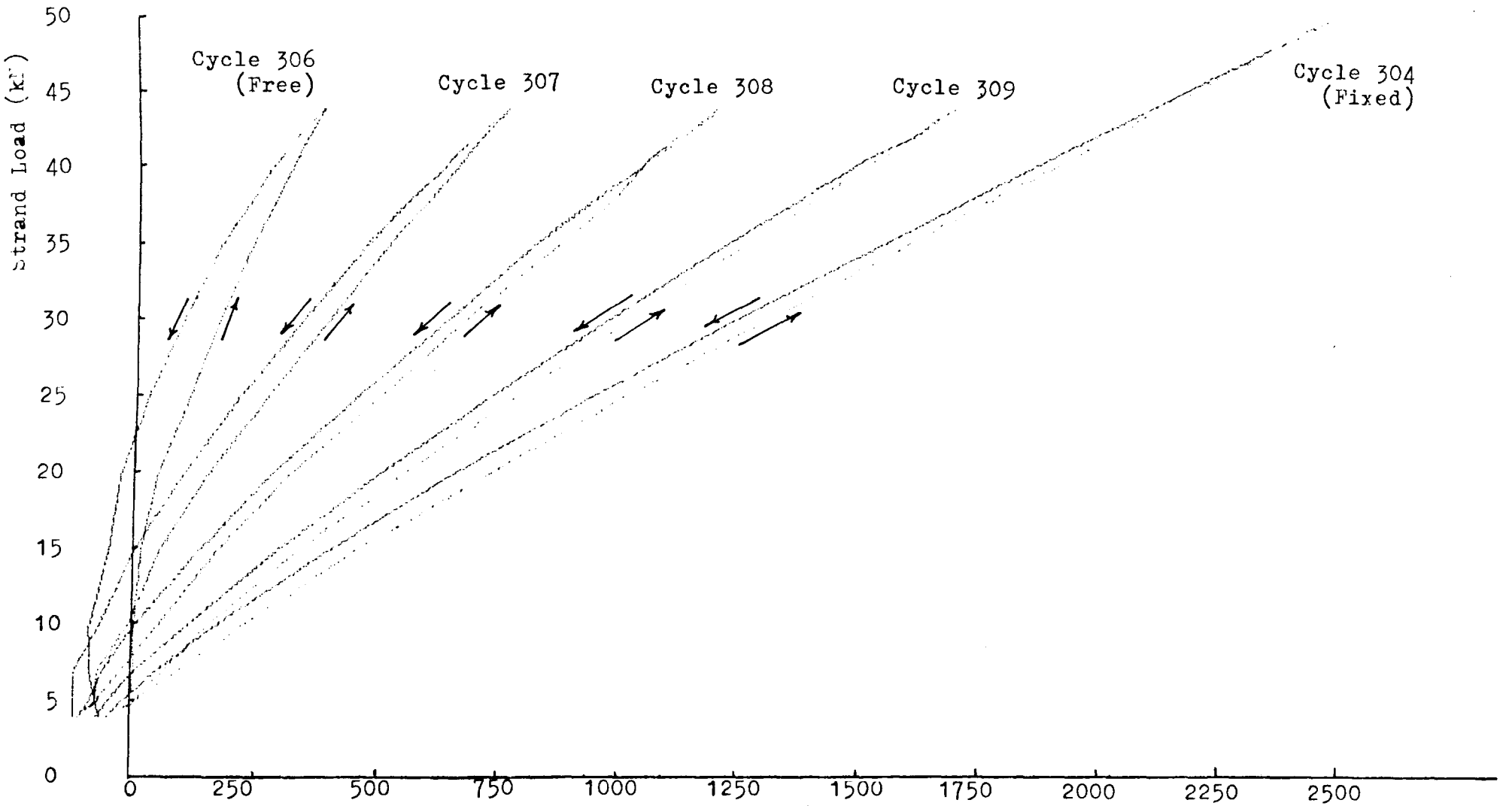

Figure 5.11. Load/Mean of Helical Wire Surface Strains at Mid Strand.
(Direction of Wire Axis):Strand X.
Fixed,Partially Restrained and Free Ends.

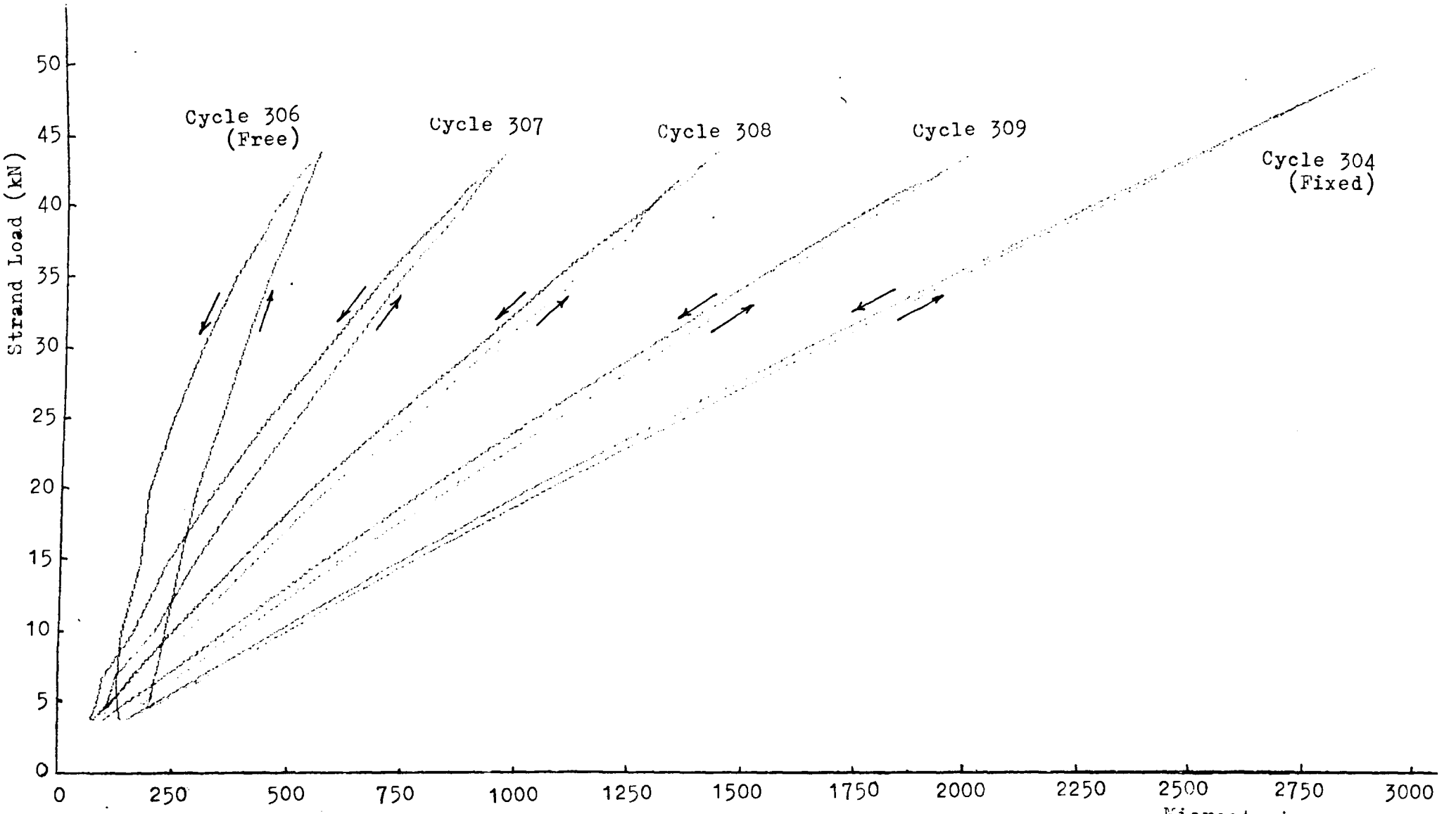

Figure 5.12. Load/Mean of Helical Wire Surface Strains at Strand End.
(Direction of Wire Axis):Strand X.
Fixed,Partially Restrained and Free Ends.

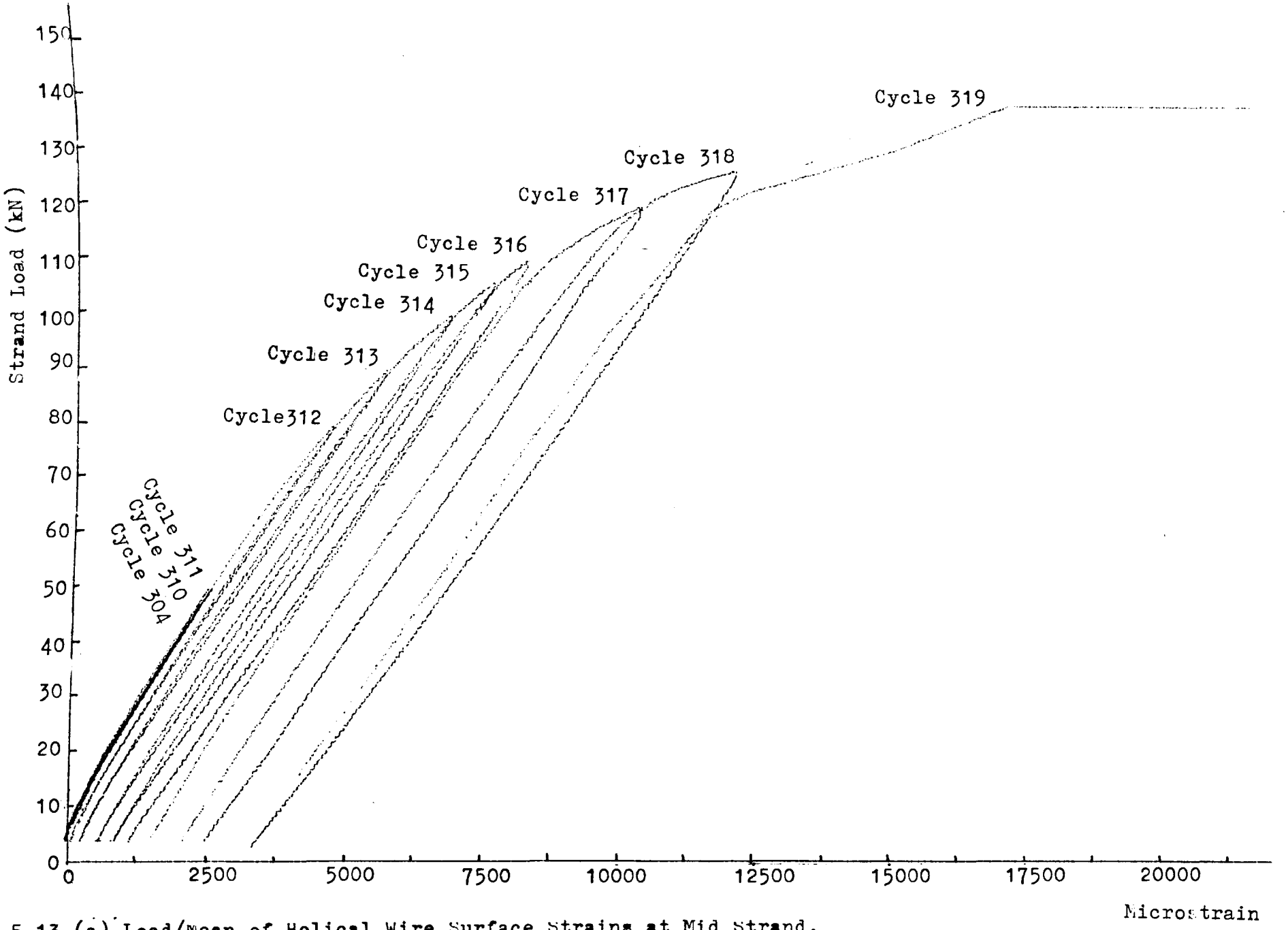

Figure 5.13.(a).Load/Mean of Helical Wire Surface Strains at Mid Strand.
(Direction of Wire Axis):Strand X.
Fixed Ends-Increasing Maximum Loads.

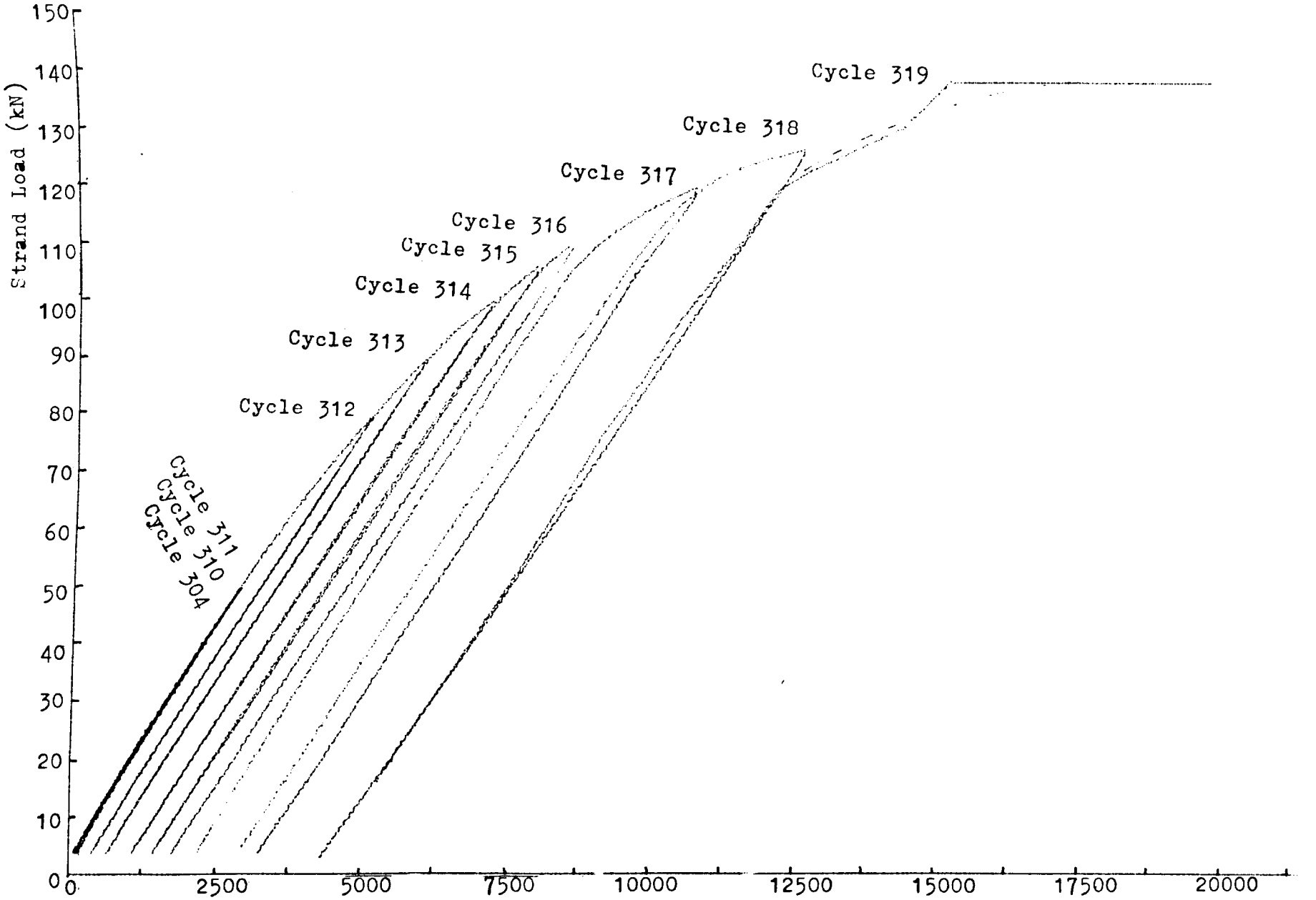

Figure 5.13.(b).Load/Mean of Helical Wire Surface Strains at Strand End.
(Direction of Wire Axis):Strand A.
Fixed Ends-Increasing Maximum Loads.

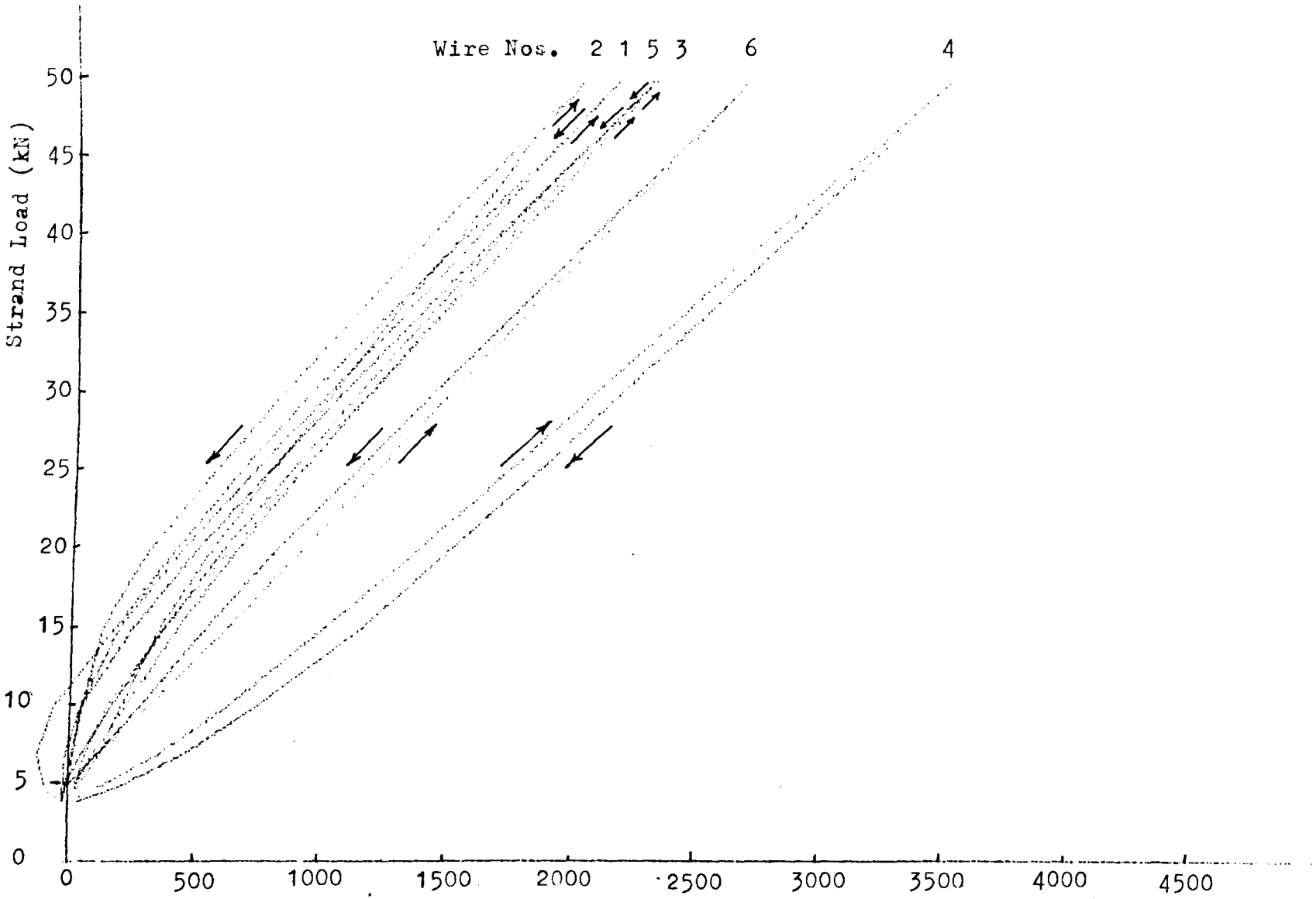

Figure 5.14. Load/Strains on All Helical Wires at Mid Strand.
(Direction of Wire Axis):Strand X.
Fixed End Loading to 50kN.

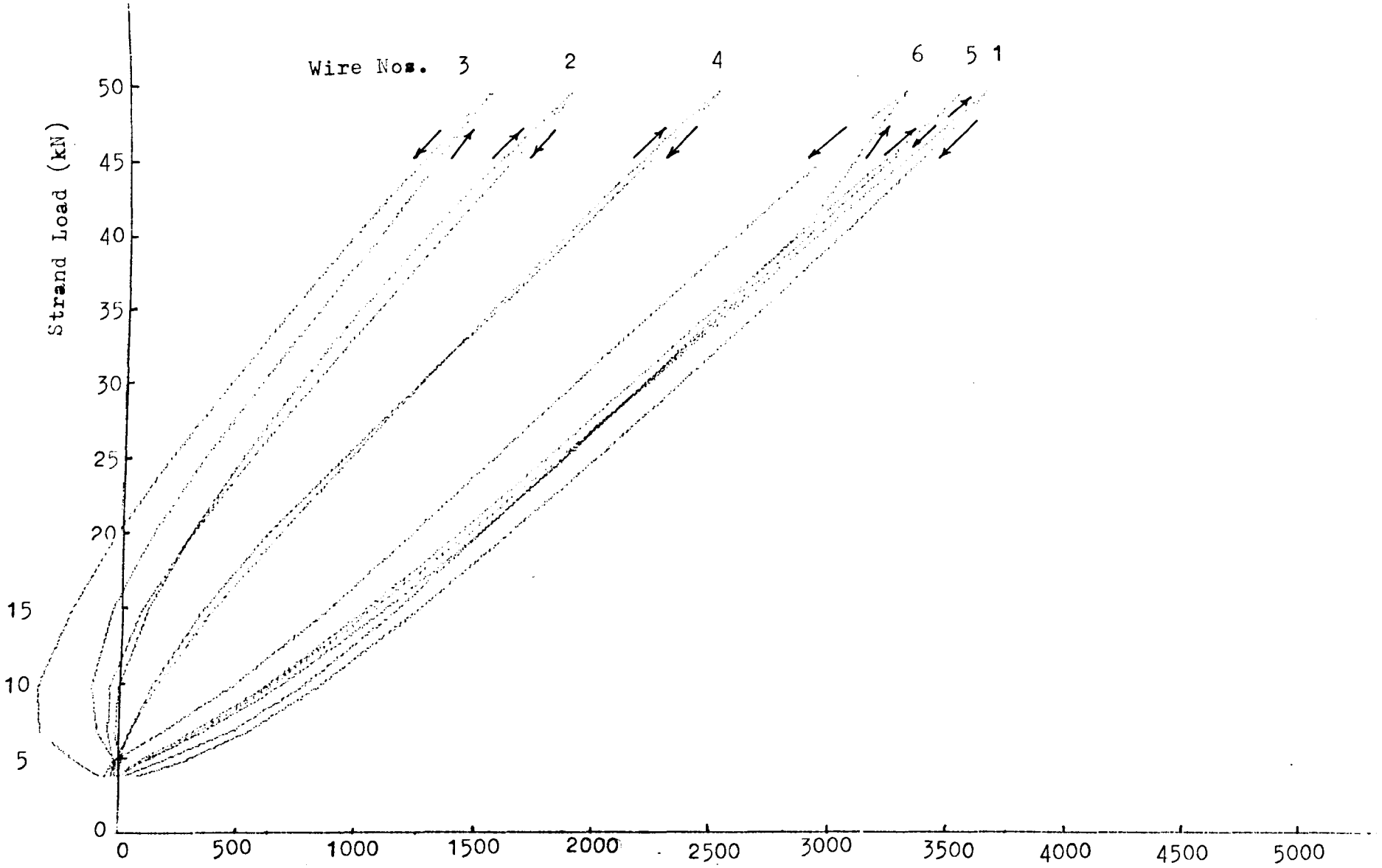

Figure 5.15. Load/Strains on All Helical Wires at Strand End.
(Direction of Wire Axis):Strand X.
Fixed End Loading to 50 kN.

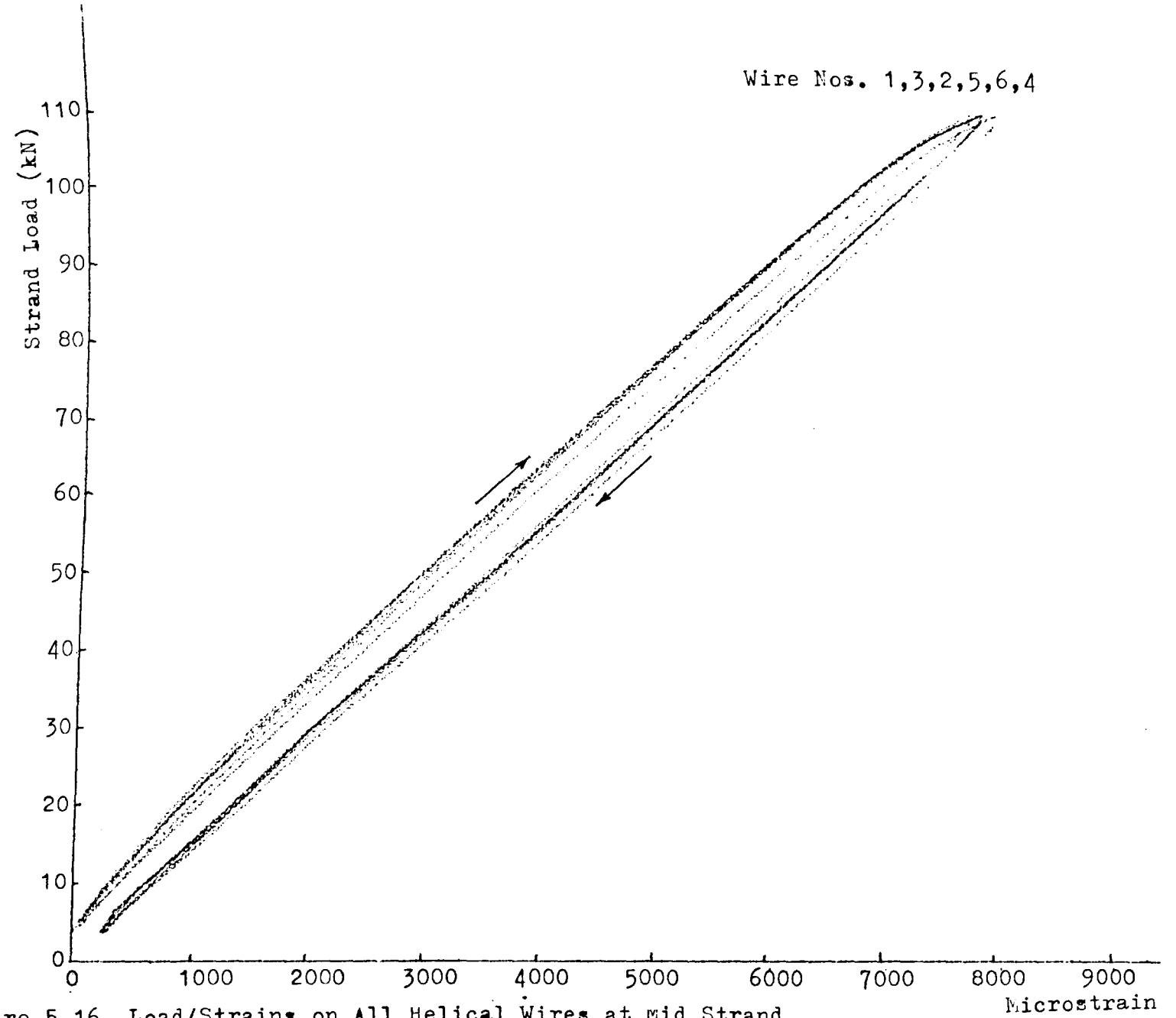

Figure 5.16. Load/Strains on All Helical Wires at Mid Strand.
(Direction of wire Axis):Strand X.
Fixed End Loading to 110kN.

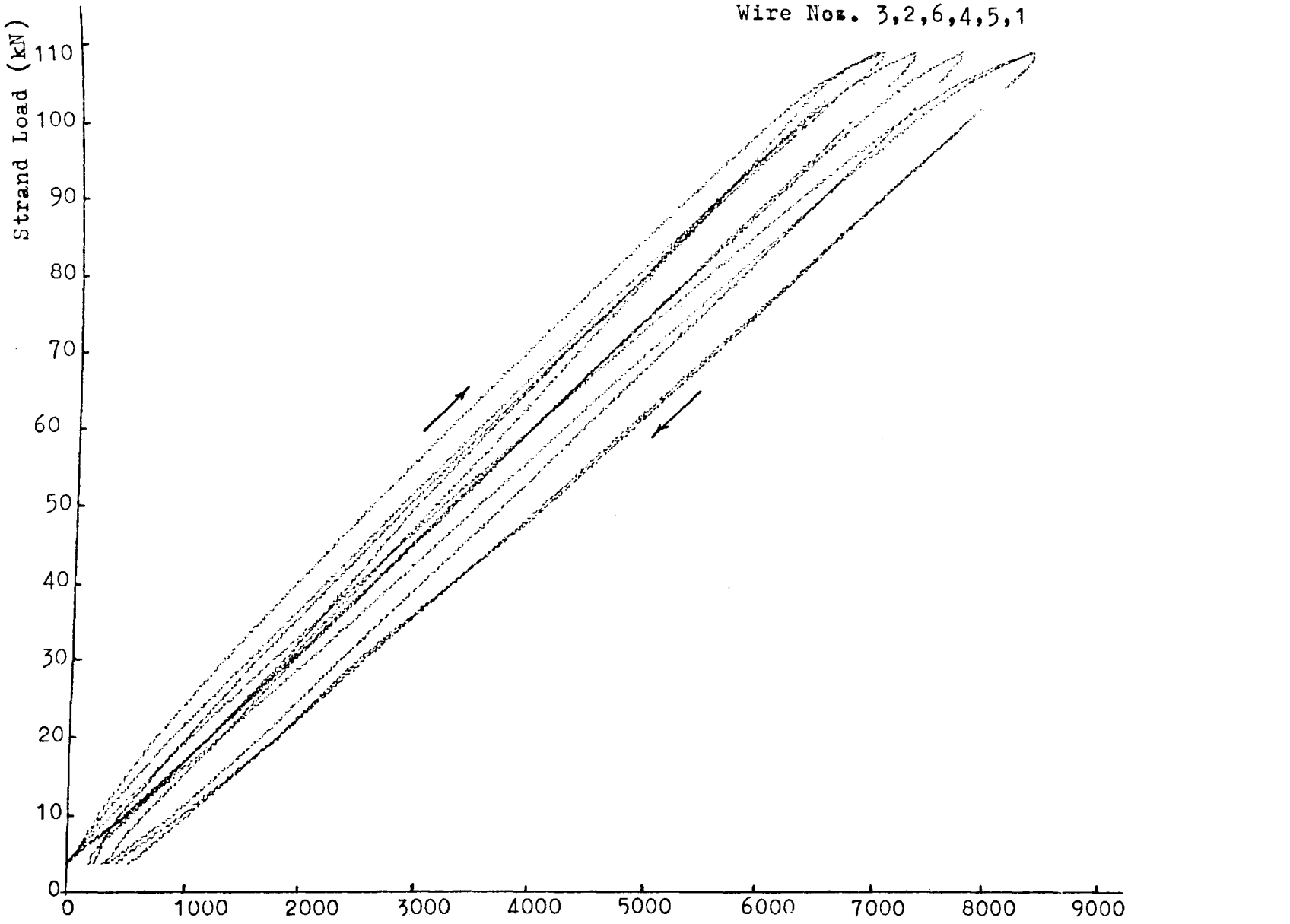

Figure 5.17. Load/Strains on All Helical Wires at Strand End.
(Direction of Wire Axis):Strand X.
Fixed End Loading to 110kN.

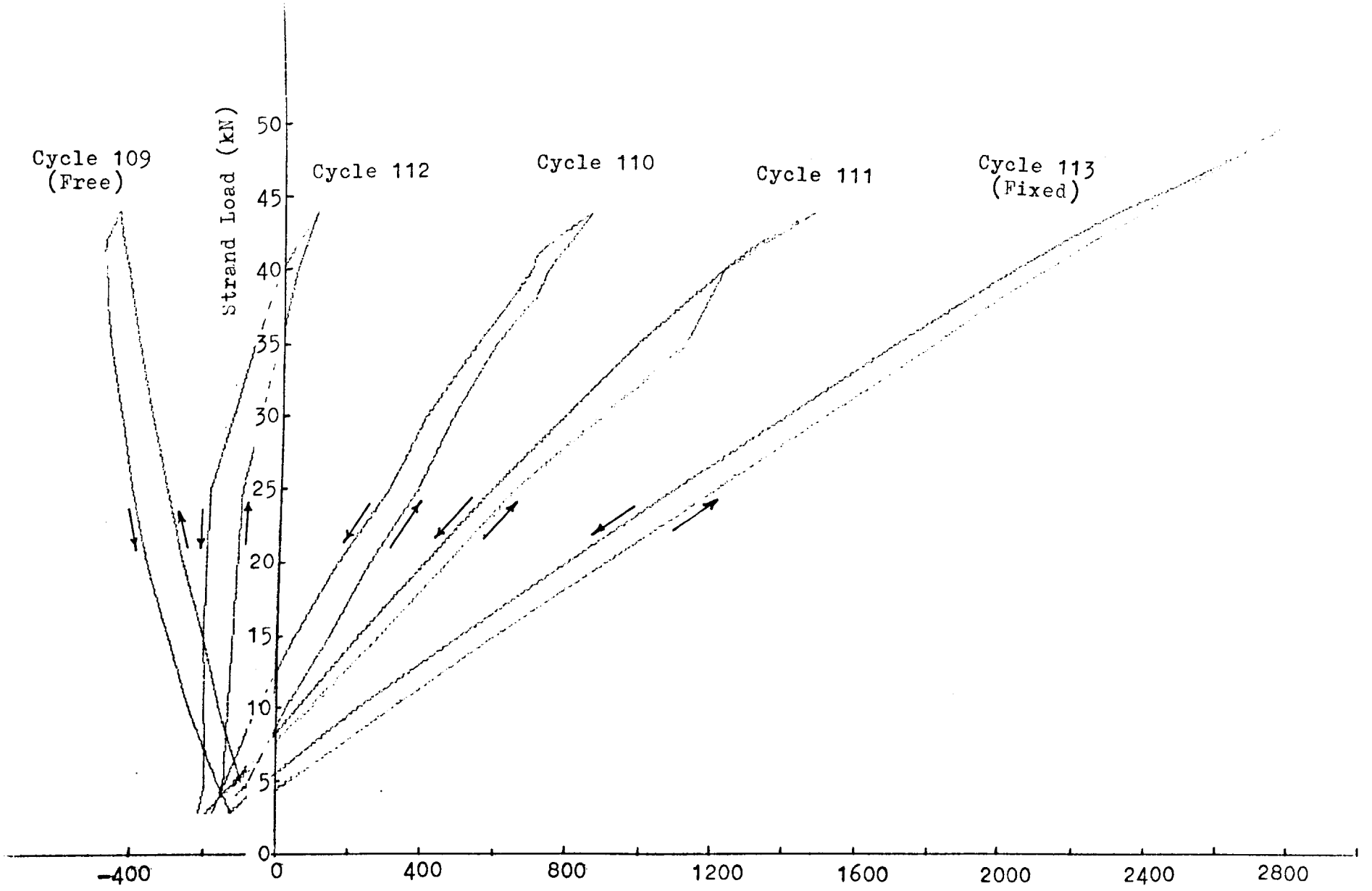

Figure 5.18. Load/Mean of Helical wire Surface Strains at Mid Strand. (Direction of wire Axis):Strand VI.
Fixed.Partially Restrained and Free ends

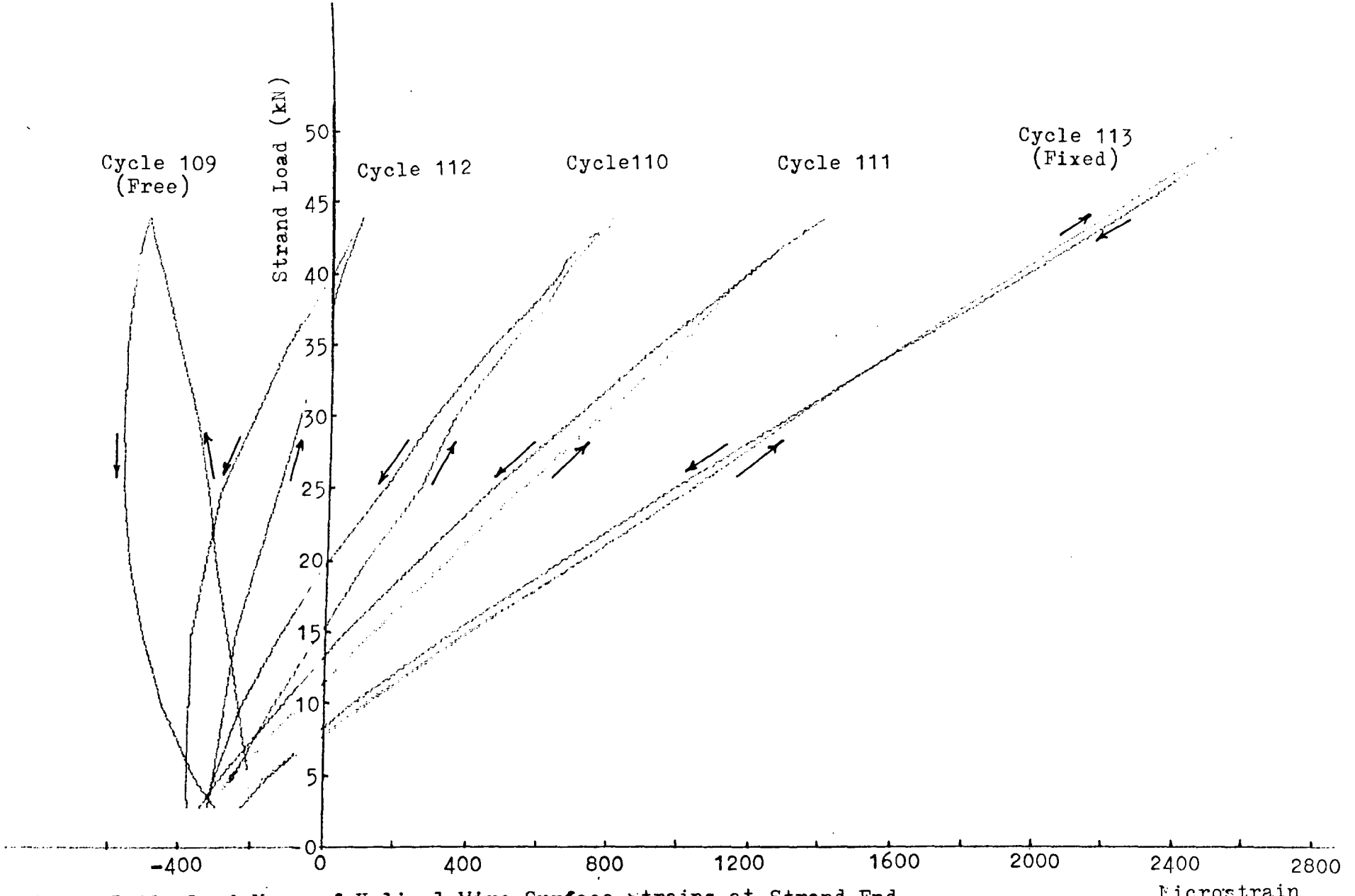

Figure 5.19. Load/Mean of Helical Wire Surface Strains at Strand End.
(Direction of Wire Axis):Strand VI.
Fixed.Partially Restrained and Free Ends.

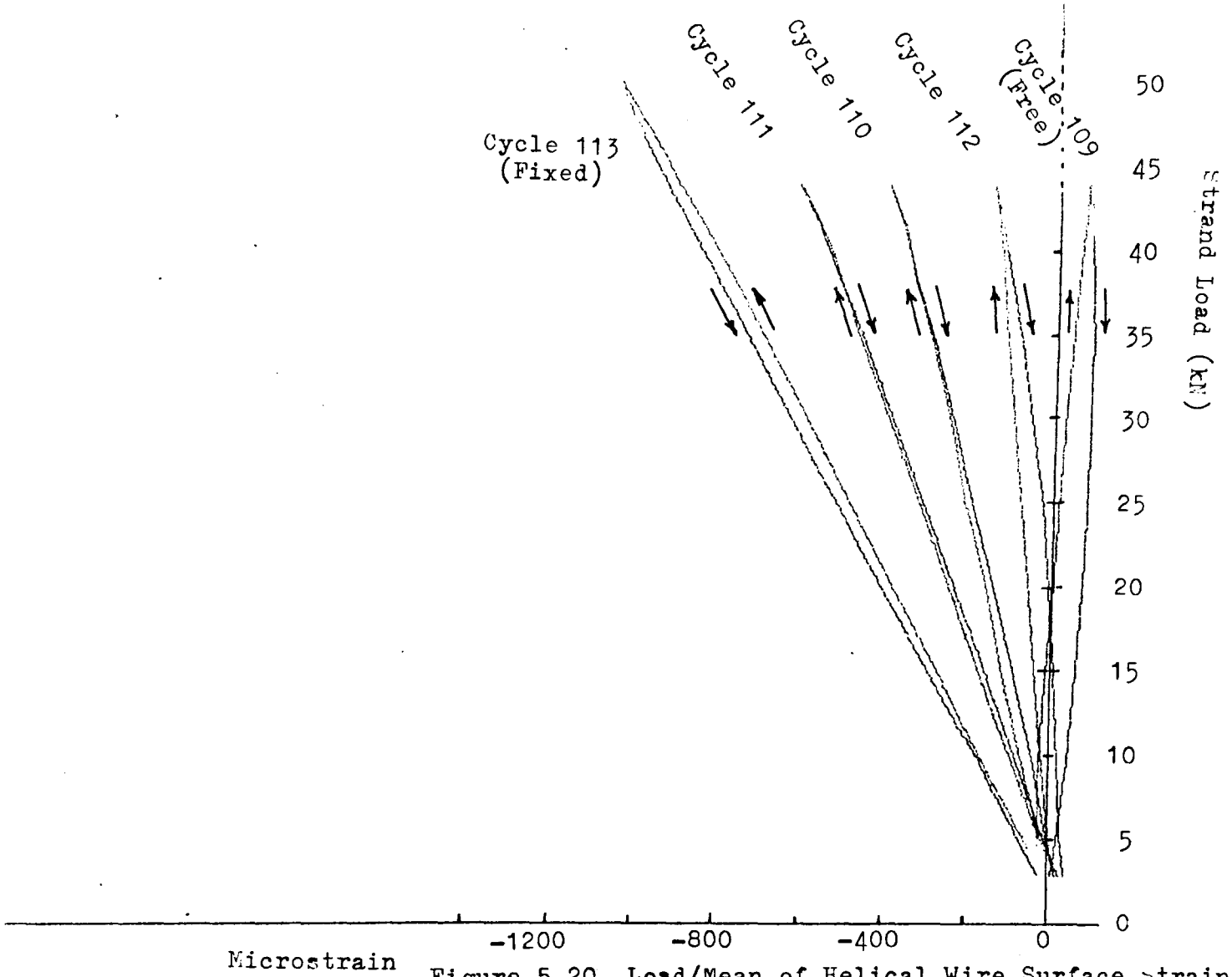

Figure 5.20. Load/Mean of Helical Wire Surface Strains at Strand End. (Direction Perpendicular to wire Axis):Strand VI. Fixed,Partially Restrained and Free Ends.

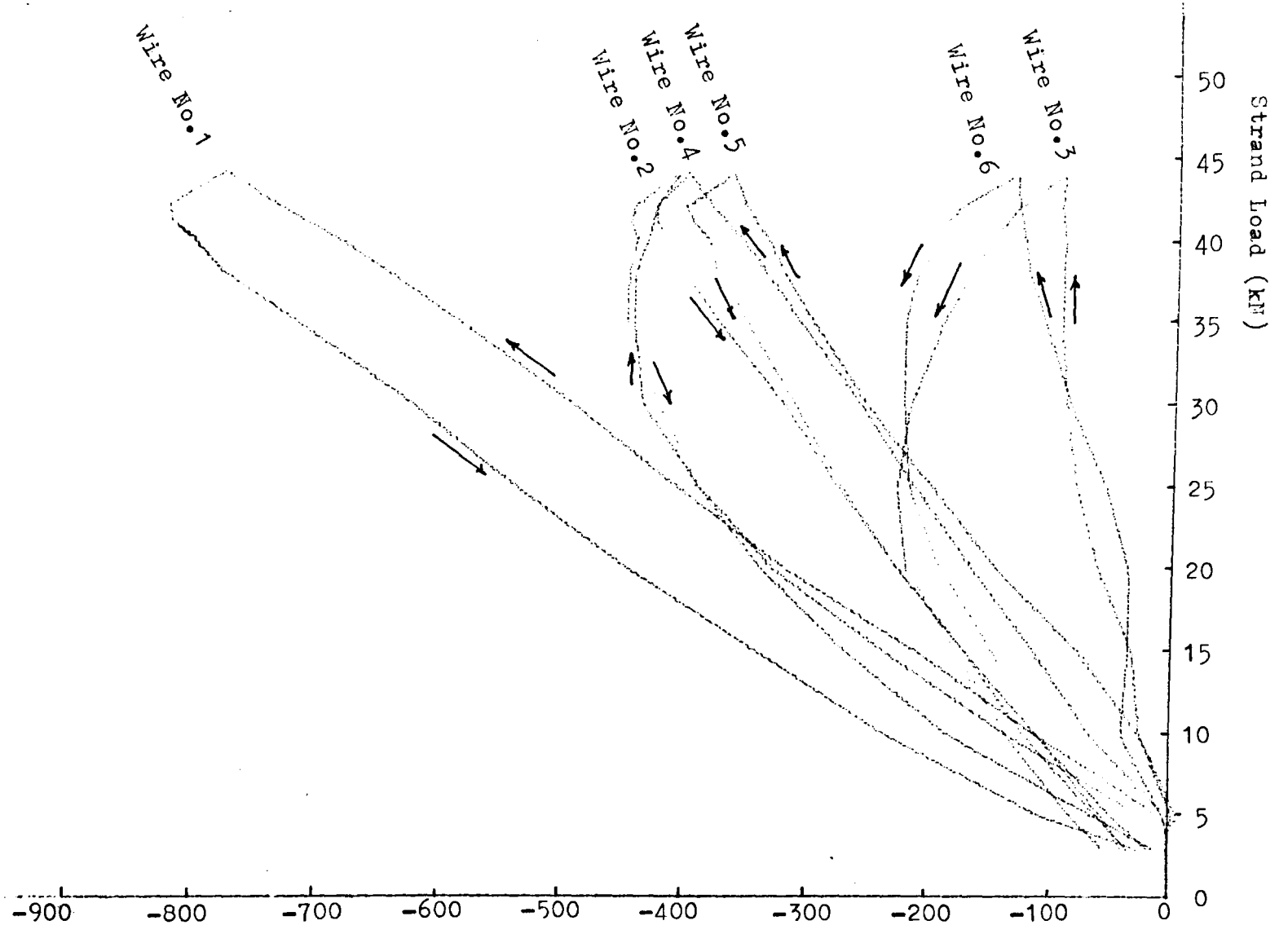

Figure 5.21. Load/Strains on All Helical Wires at Mid Strand. (Direction of wire Axis):Strand VI. Free End Loading to 44kN.

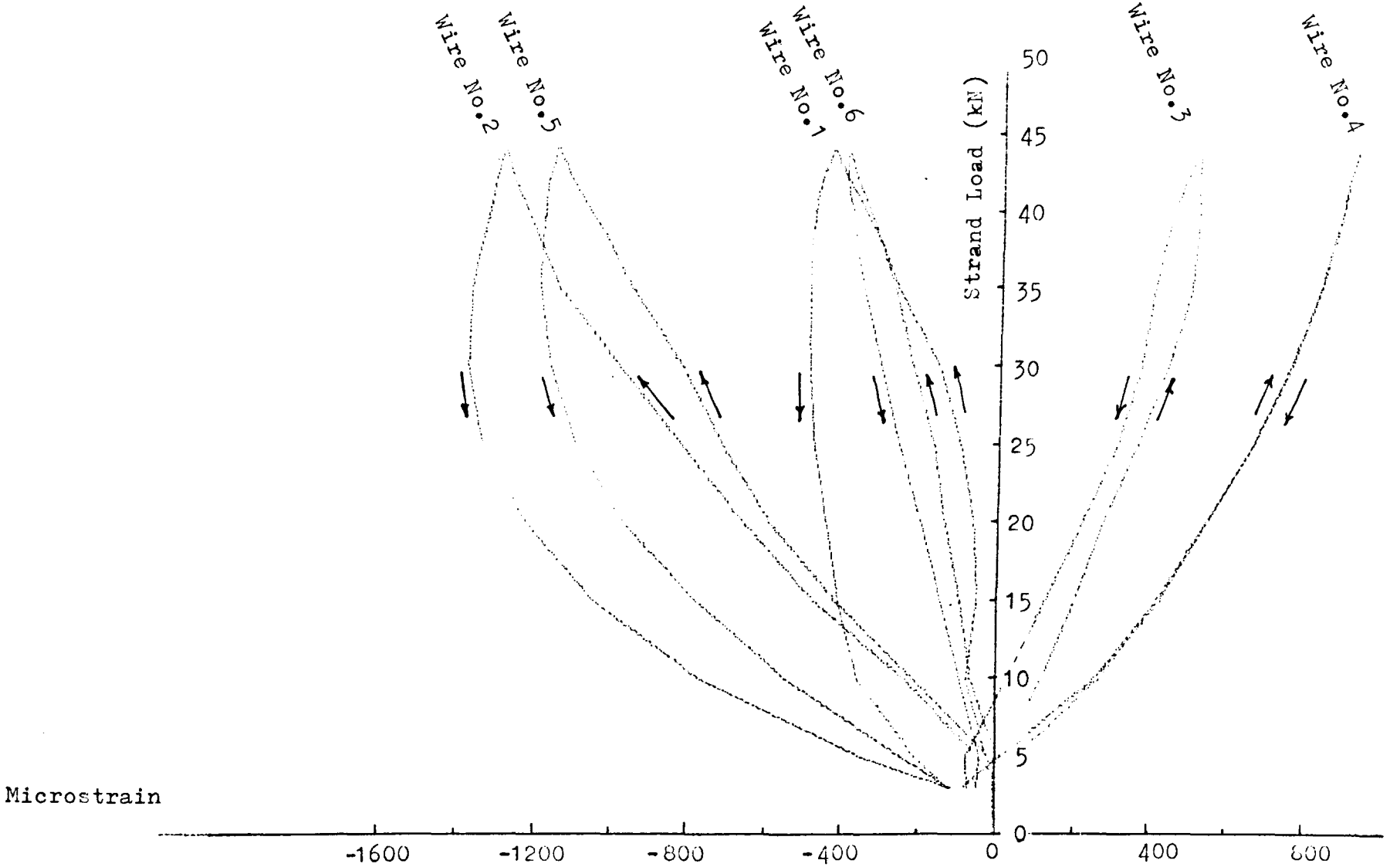

Figure 5.22. Load/Strains on All Helical Wires at Strand End. (Direction of Wire Axis):Strand V1.
Free End Loading to 44kN.

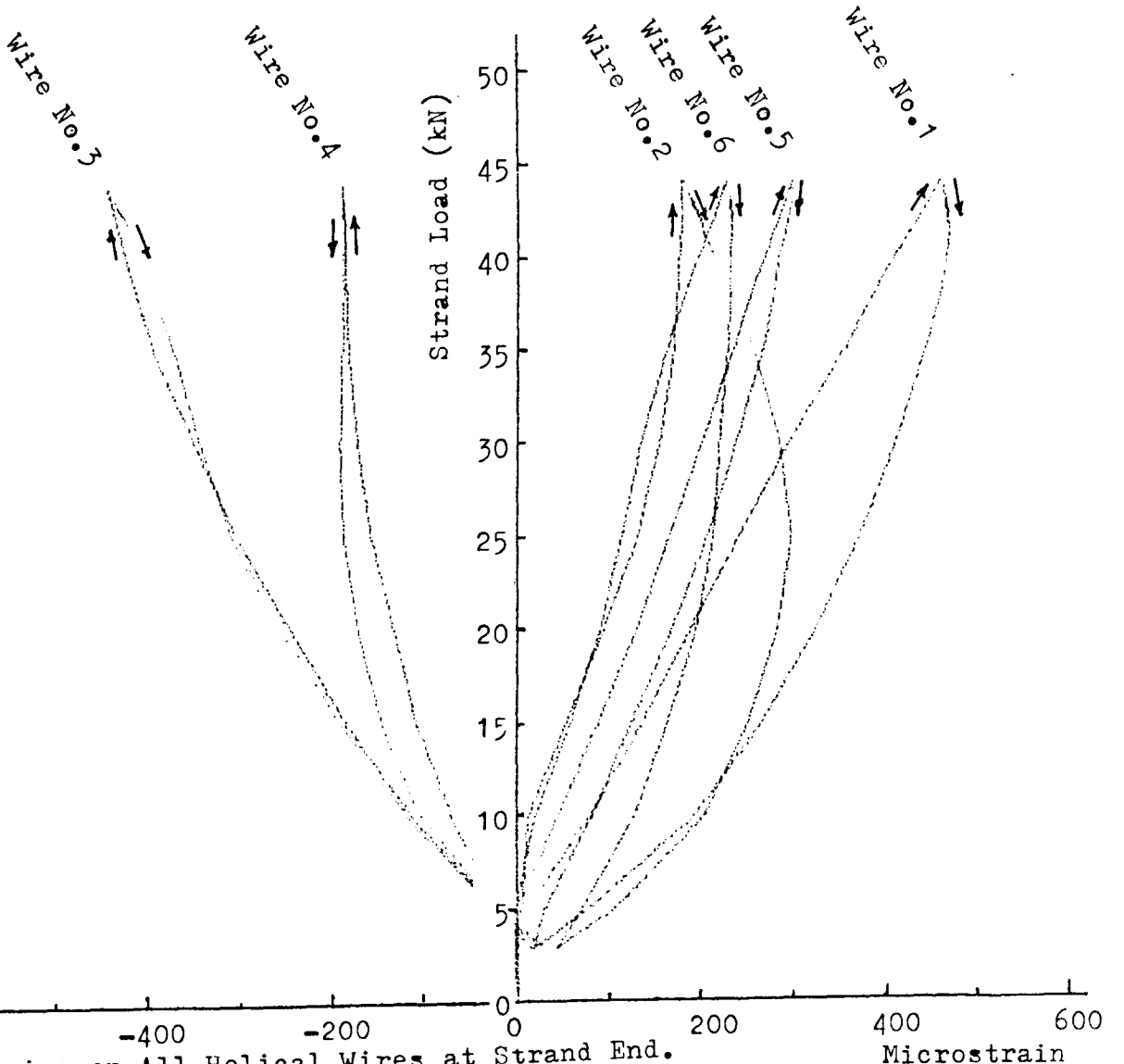

Figure 5.23. Load/Strains on All Helical Wires at Strand End. (Direction Perpendicular to Wire Axis):Strand VI. Free End Loading to 44kN.

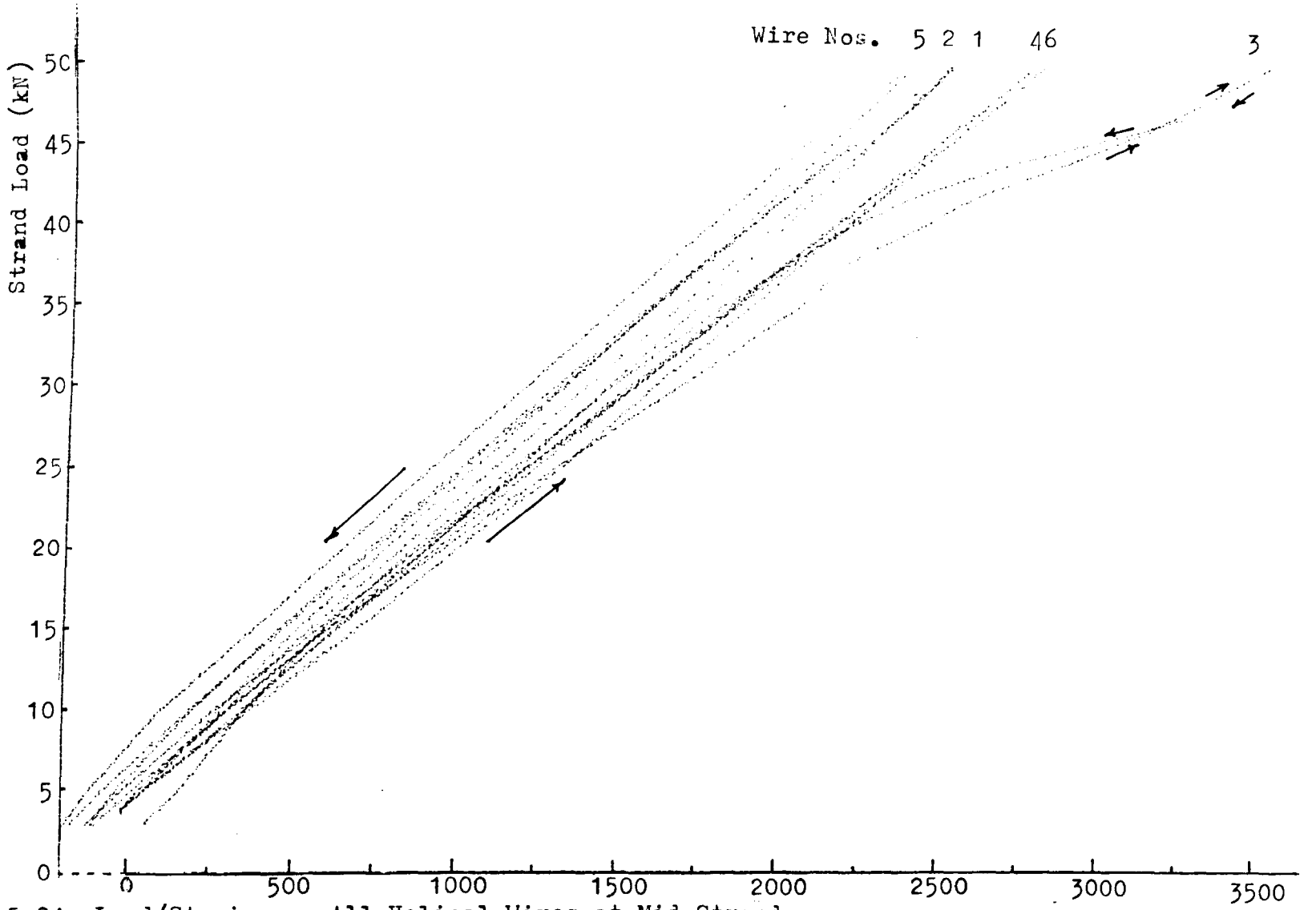

Figure 5.24. Load/Strains on All Helical Wires at Mid Strand. (Direction of Wire Axis):Strand VI.

tension and a predetermined fraction of torsional restraint, can be calculated using expression 3.4. To correspond with procedure used in slope determinations for load against other parameters, (see Fig. 5.6), 10 kN is again used as the starting point for load/torque plots. (See Figs 5.25 to 5.29). The torque/load ratios (reciprocal slopes) from these plots are given in Table 5.13. Note that there is a small reverse torsion (tending to unwind the strand) applied in the case of cycle 206 (Fig. 5.26) and cycle 306 (Fig. 5.27). This is because, when calculating predetermined output from the load cell, for zero torsional restraint, output from torsion circuit No. 1, during the preceding fixed end test, was used in error. (Torsion circuit No. 2, which has the lower output under tension loading, should have been used. (See sub-section 3.3.1 and Appendix A.1)).

Rotation of the strand over the 600 mm gauge length was recorded for the nominally fixed end tests, as well as for the tests with free and partially restrained ends. Elasticity in the resin and partial breakup at the throat of the strand termination permits some relative rotation of the strand ends under the action of the torque generated in strand under tensile load. See sub-sections 5.5.1 and Fig. 5.3.b. This effect is discussed in Chapter 7, section 7.2 and the generated torque compared with theoretical predictions.

Whereas fixed end plots are taken up to only 50 kN Figs. 5.25 to 5.29, for comparison with free and partially restrained

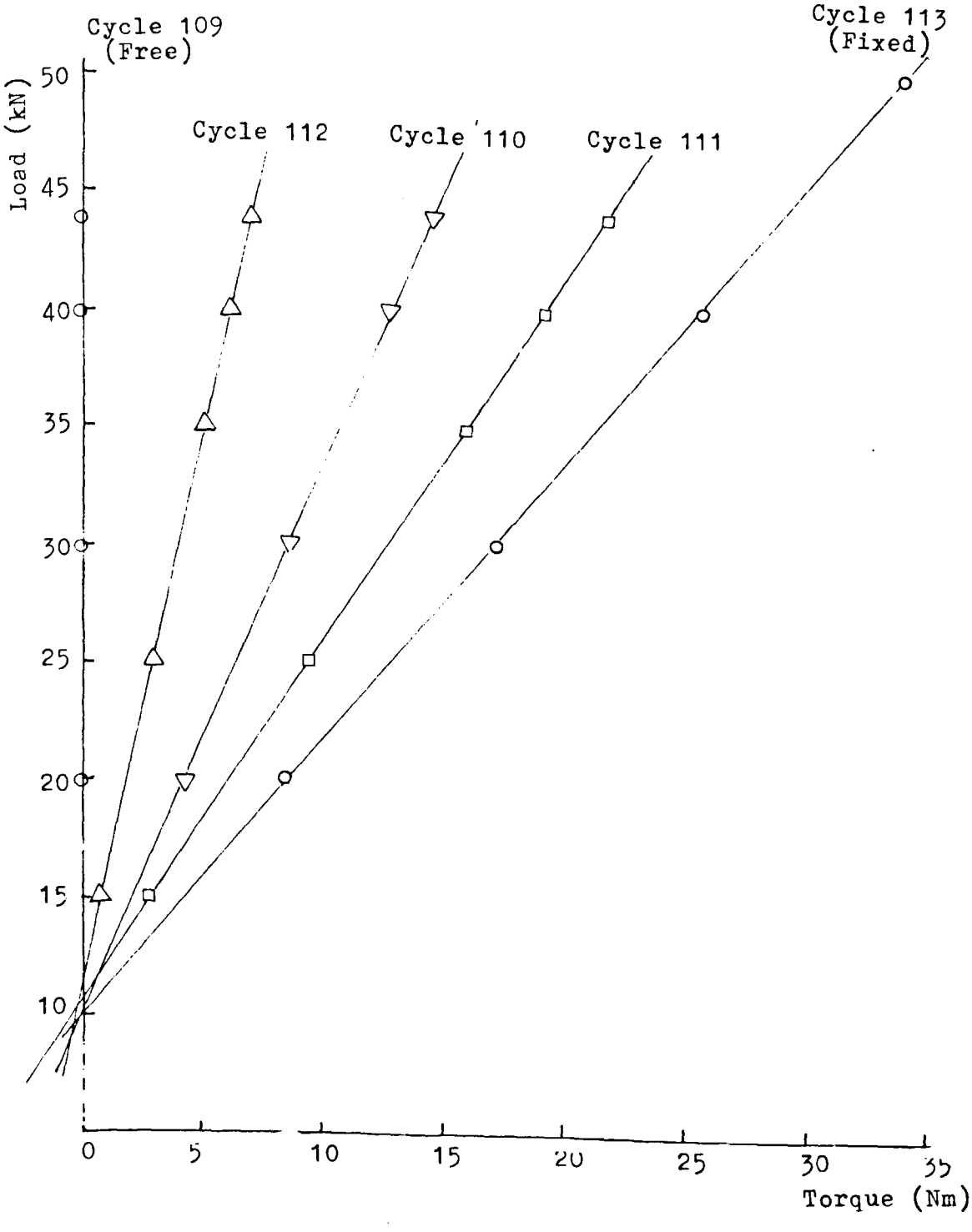

Figure 5.25. Load/Torque Generated in Strand under Load.
(Fixed,Free and Partially Restrained Ends.):Strand VI.

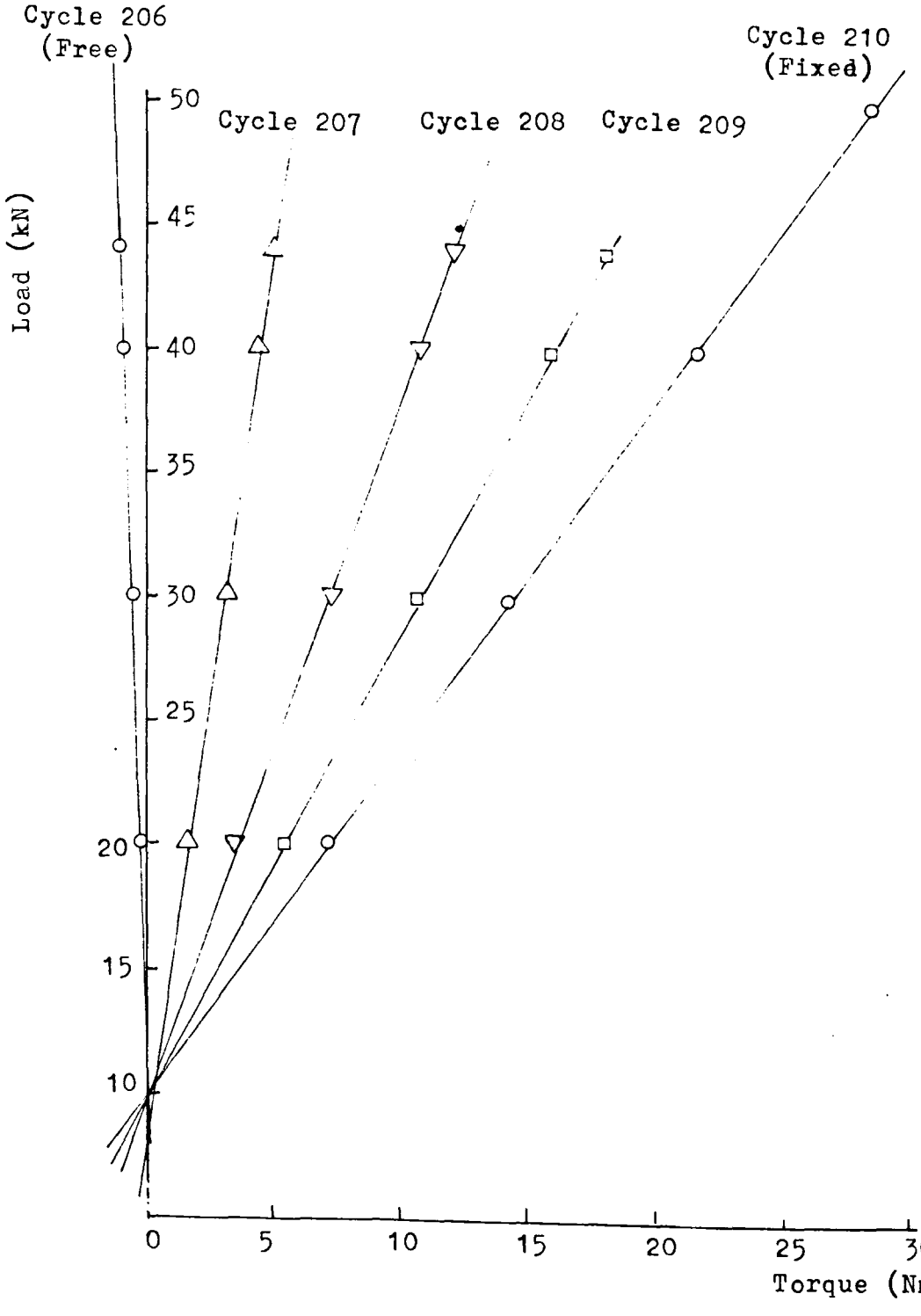

Figure 5.26. Load/Torque Generated in Strand under Load.
(Fixed,Free and Partially Restrained Ends.):Strand VII

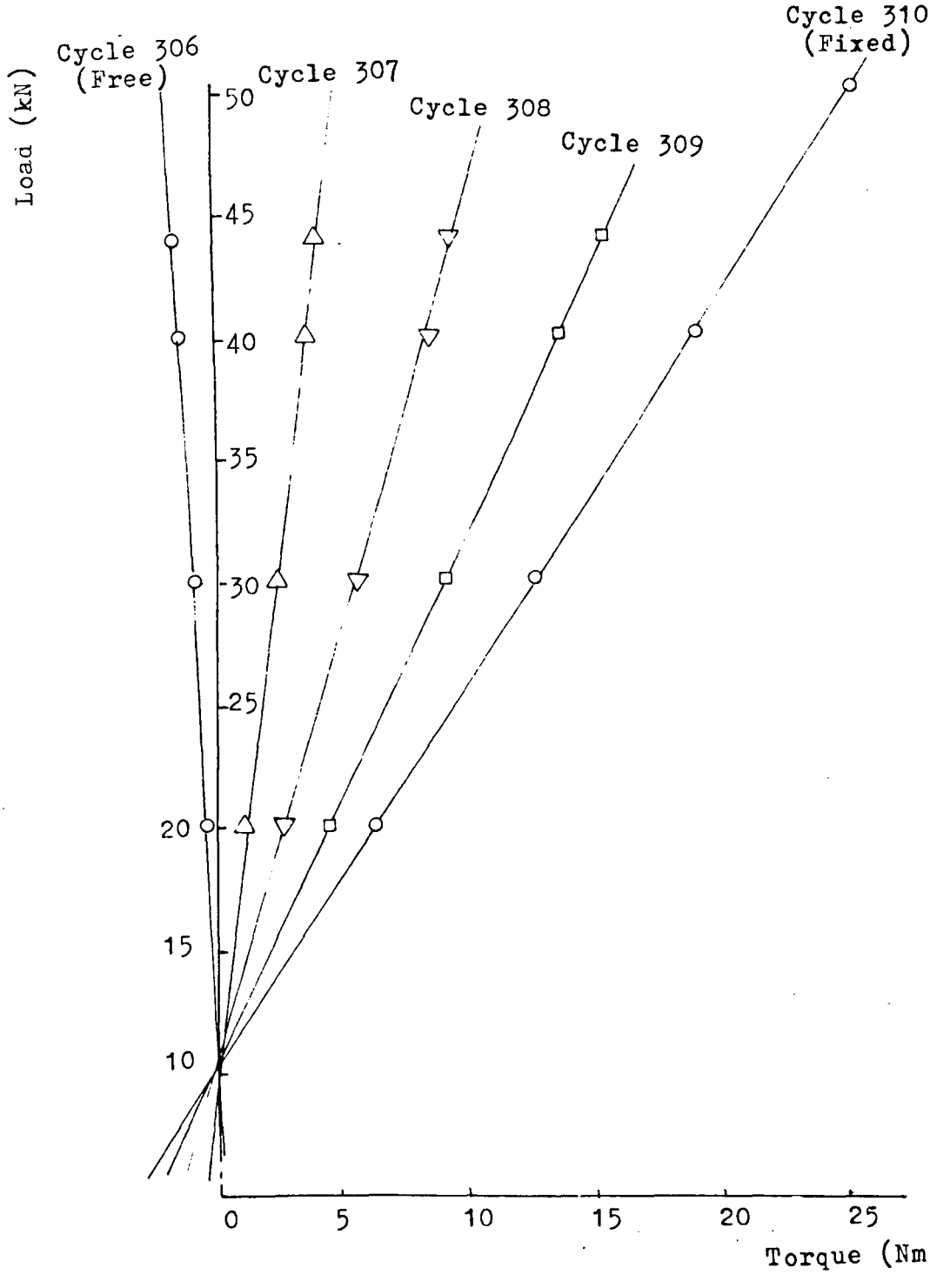

Figure 5.27. Load/Torque Generated in Strand under Load.
(Fixed,Free and Partially Restrained Ends.):Strand X.

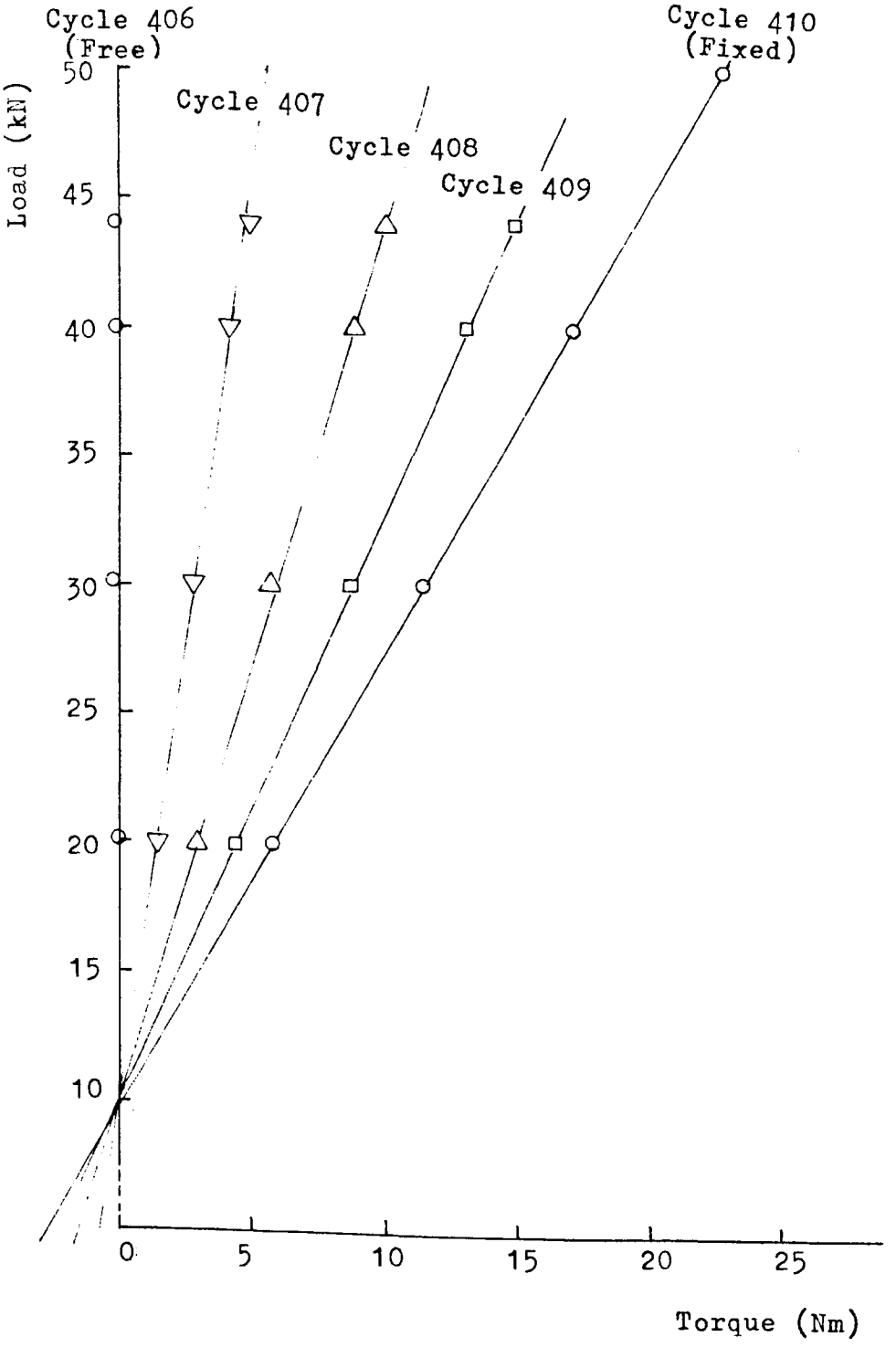

Figure 5.28. Load/Torque Generated in Strand under Load.
(Fixed,Free and Partially Restrained Ends.):Strand IX.

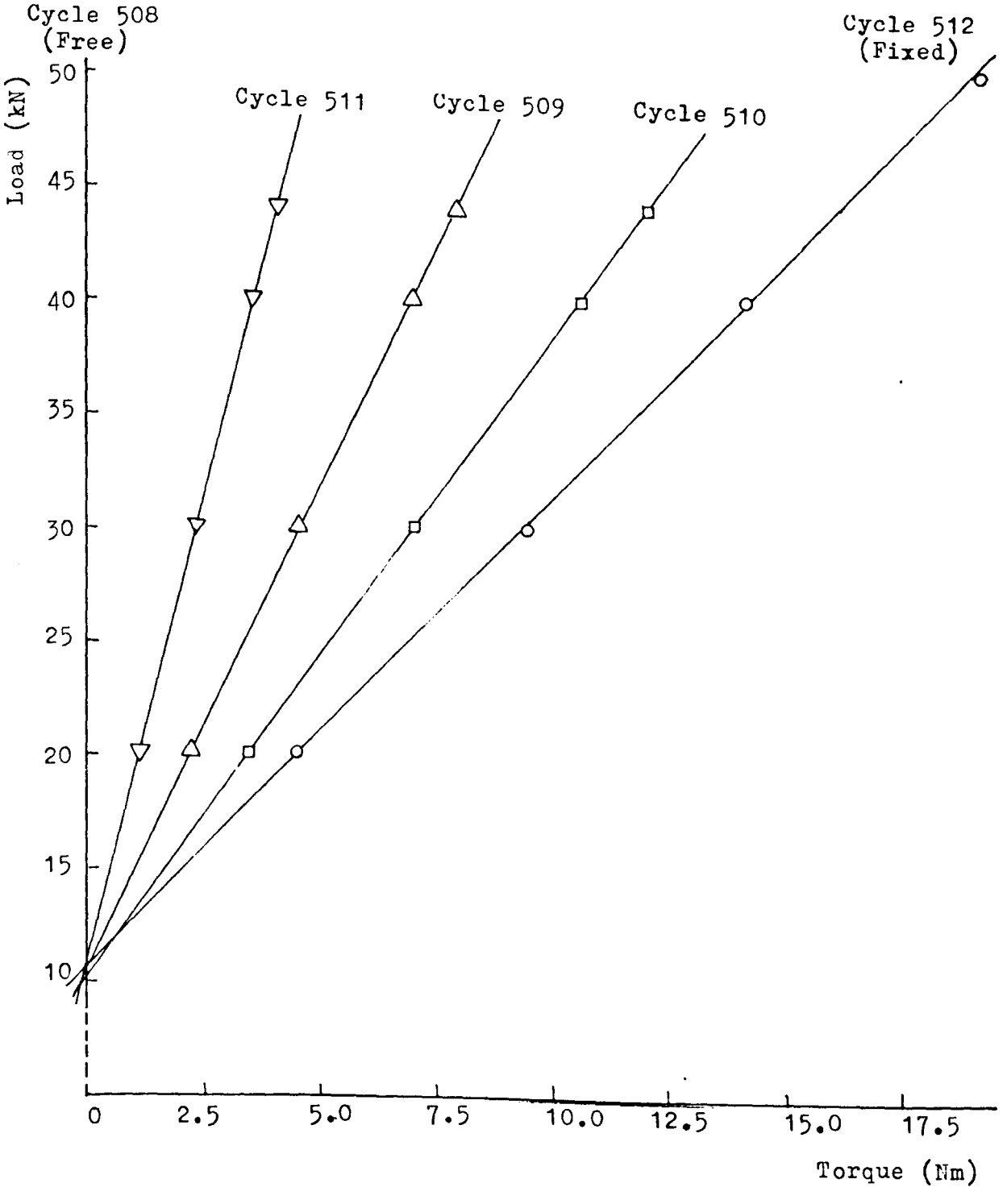

Figure 5.29. Load/Torque Generated in Strand under Load.
(Fixed,Free and Partially Restrained Ends.):Strand VII.

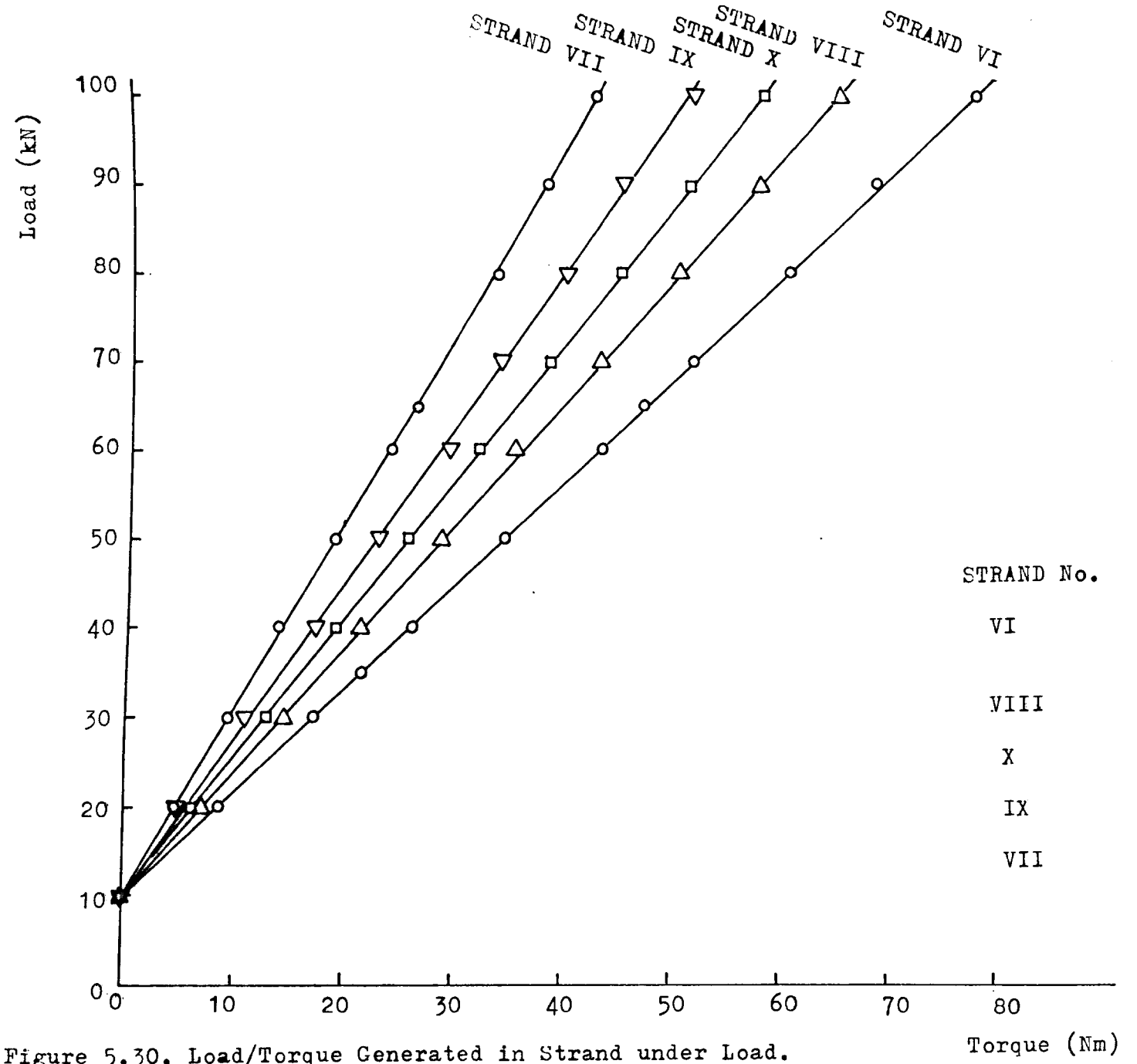

STRAND No.	Helix Angle.
VI	73.6° (nominal) 73.0° (measured)
VIII	76.2°
X	77.7°
IX	78.9°
VII	80.9°

Figure 5.30. Load/Torque Generated in Strand under Load. (Fixed End Tests.):Strands VI,VII,VIII,IX,X. Loading up to 100 kN.

Strand Load/Torque Generated

Reciprocal of slopes from Figs 5.25 to 5.29.

Table 5.13.

Nominal End Condition	Torque Generated Nm/kN				
	Strand VI (Cycle No.)	Strand VIII (Cycle No.)	Strand X (Cycle No.)	Strand IX (Cycle No.)	Strand VII (Cycle No.)
Fixed	0.86(113)	0.72(210)	0.65(310)	0.58(410)	0.47(512)
$\frac{3}{4}$ Fixed	0.59(111)	0.54(209)	0.47(309)	0.45(409)	0.36(510)
$\frac{1}{2}$ Fixed	0.43(110)	0.36(208)	0.29(308)	0.30(408)	0.24(509)
$\frac{1}{4}$ Fixed	0.22(112)	0.13(207)	0.12(307)	0.14(407)	0.13(511)
Free	0 (109)	-0.03(206)	-0.05(306)	0 (406)	0 (508)

NOTE: See Table 5.3. (Loading programmes) for an explanation of the cycle numbers.

end conditions, Fig. 5.30 shows load/torque plots from loading in the fixed end condition, for all strands, taken up to 100 kN. This is 10 kN below the load at which the extrometer was disconnected. The testing to loads above 100 kN had to be performed at a speed which did not permit accurate written recording from the digital display output of the FYLDE bridge/amplifier unit, and torque results from higher loads are therefore not plotted.

5.5.8 Surface Strain Ranges (Manual Plotting)

Tabulated results of surface strains at each axial load for all loading cycles have been obtained in printouts of the type given in Tables 5.7 to 5.10. A measure of the variation in load sharing between wires can be obtained by consideration of the strain range per unit load (kN) of the strain parallel to wire axis at a particular load, defined as the difference between the maximum and minimum strains recorded in columns 2 to 7 (wires 1 to 6) divided by the load recorded in column 1. For fixed end tests, these strain ranges are given in Table 5.14 and plotted in Fig. 5.31, at loads of 20 kN to 100 kN in 20 kN increments, for both mid-strand and end positions. Strain ranges for the current loading cycle (e.g. Tables 5.7 and 5.8) are given as well as for the overall strain (e.g. Table 5.10). Distinction is also made between strain ranges at the first and second occasion on which a particular load is attained during the test programme on a particular strand.

Strain Ranges on Helical Wire Surface. (Strain/kN: Fixed End Tests)

Table 5.14.

MID STRAND POSITION

Strand Load kN	Strand VI		Strand VIII		Strand X		Strand IX		Strand VII	
	Current Cycle $\mu\varepsilon$/kN	Overall $\mu\varepsilon$/kN	Current Cycle $\mu\varepsilon$/kN	Overall $\mu\varepsilon$/kN	Current Cycle $\mu\varepsilon$/kN	Overall $\mu\varepsilon$/kN	Current Cycle $\mu\varepsilon$/kN	Overall $\mu\varepsilon$/kN	Current Cycle $\mu\varepsilon$/kN	Overall $\mu\varepsilon$/kN
20 1st	37.5	-	24.9	-	26.8	-	22.3	-	37.7	-
20 2nd	29.6	23.7	22.7	27.3	28.6	30.5	22.3	22.3	35.0	37.9
40 1st	35.7	36.3	18.7	21.2	30.6	31.5	23.4	36.1	26.8	28.0
40 2nd	12.2	20.7	18.2	23.2	6.6	10.8	20.8	32.0	20.8	28.8
40 1st	15.4	13.8	16.9	22.9	32.8	42.0	31.1	36.7	12.5	31.2
40 2nd	9.5	8.8	17.9	23.3	33.6	43.2	31.9	37.8	21.1	31.9
60 1st	8.5	11.3	12.7	16.1	25.6	31.3	32.4	33.7	18.1	25.4
60 2nd	12.3	10.1	11.2	16.8	21.3	32.6	29.6	38.0	17.0	26.5
80 1st	10.2	13.9	10.3	11.5	23.0	25.9	30.9	31.8	16.3	27.8
80 2nd	7.4	16.0	8.0	13.1	16.7	26.4	25.9	32.2	13.8	30.1
100 1st	6.4	10.0	7.2	13.5	10.6	21.8	18.8	24.5	12.5	30.2
100 2nd	4.5	16.2	5.3	15.2	7.0	21.9	14.9	26.4	12.1	31.4

Strain Ranges on Helical Wire Surface. (Strain/kN: Fixed End Tests)

Table 5.14. (Continued)

END OF STRAND

Strand Load kN	Strand VI		Strand VIII		Strand X		Strand IX		Strand VII	
	Current Cycle $\mu\varepsilon$/kN	Overall $\mu\varepsilon$/kN	Current Cycle $\mu\varepsilon$/kN	Overall $\mu\varepsilon$/kN	Current Cycle $\mu\varepsilon$/kN	Overall $\mu\varepsilon$/kN	Current Cycle $\mu\varepsilon$/kN	Overall $\mu\varepsilon$/kN	Current Cycle $\mu\varepsilon$/kN	Overall $\mu\varepsilon$/kN
20 1st	121.6	-	38.8	-	106.3	-	80.0	-	78.3	-
20 2nd	110.1	122.7	37.1	39.4	103.3	106.3	79.4	80.6	77.3	60.2
40 1st	74.7	78.8	28.3	29.7	65.8	68.7	43.5	45.8	36.8	42.0
40 2nd	63.8	83.8	22.7	33.4	51.2	77.4	41.3	52.9	40.2	36.8
40 1st	54.5	84.4	21.8	34.8	47.8	79.3	36.7	55.9	34.5	41.0
40 2nd	53.9	85.5	21.6	35.1	47.3	80.5	36.1	56.2	30.4	34.9
60 1st	57.8	85.1	33.7	48.3	35.7	57.0	40.2	43.2	24.8	29.1
60 2nd	47.5	94.3	26.5	59.9	28.3	63.2	36.3	45.3	23.9	29.6
80 1st	54.8	75.1	23.7	30.3	32.3	48.4	29.3	31.4	15.5	20.3
80 2nd	42.3	77.2	16.0	31.8	23.3	48.9	26.9	32.8	15.0	20.9
100 1st	31.2	72.1	18.7	35.6	13.9	40.7	22.5*	27.2*	10.2	18.8
100 2nd	26.1	73.5	13.8	37.7	11.9	40.5	22.0*	27.5*	9.6	19.1

Notes: - Overall strain range is same as for current cycle on first loading.

* Range at 90 kN. (Logger not triggered at 100 kN).

Figure 5.31(a).Wire Surface Strain Range/Strand Load;Fixed End Tests. Strand VI.

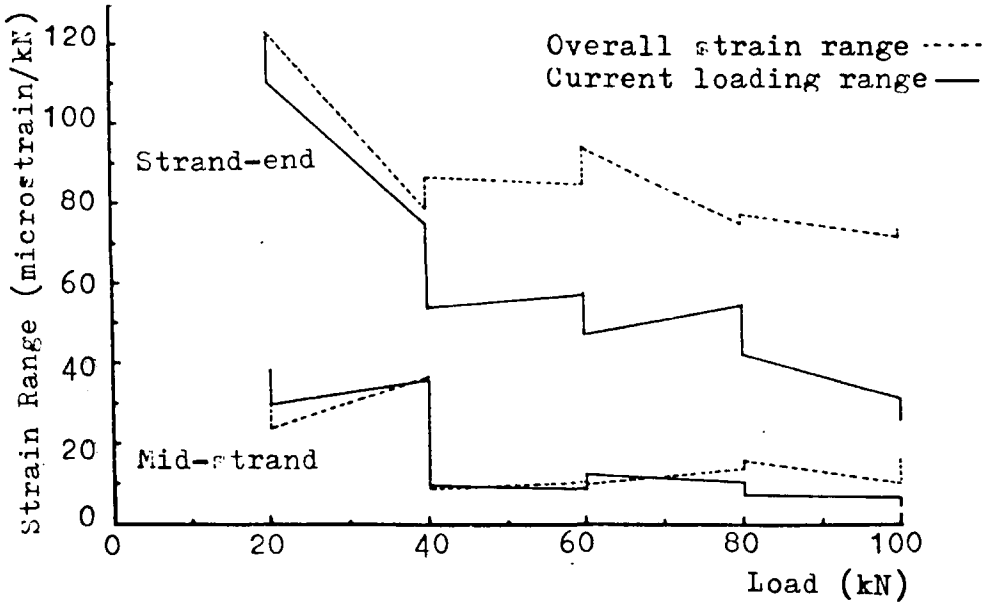

Figure 5.31(b).Wire Surface Strain Range/Strand Load;Fixed End Tests. Strand VIII.

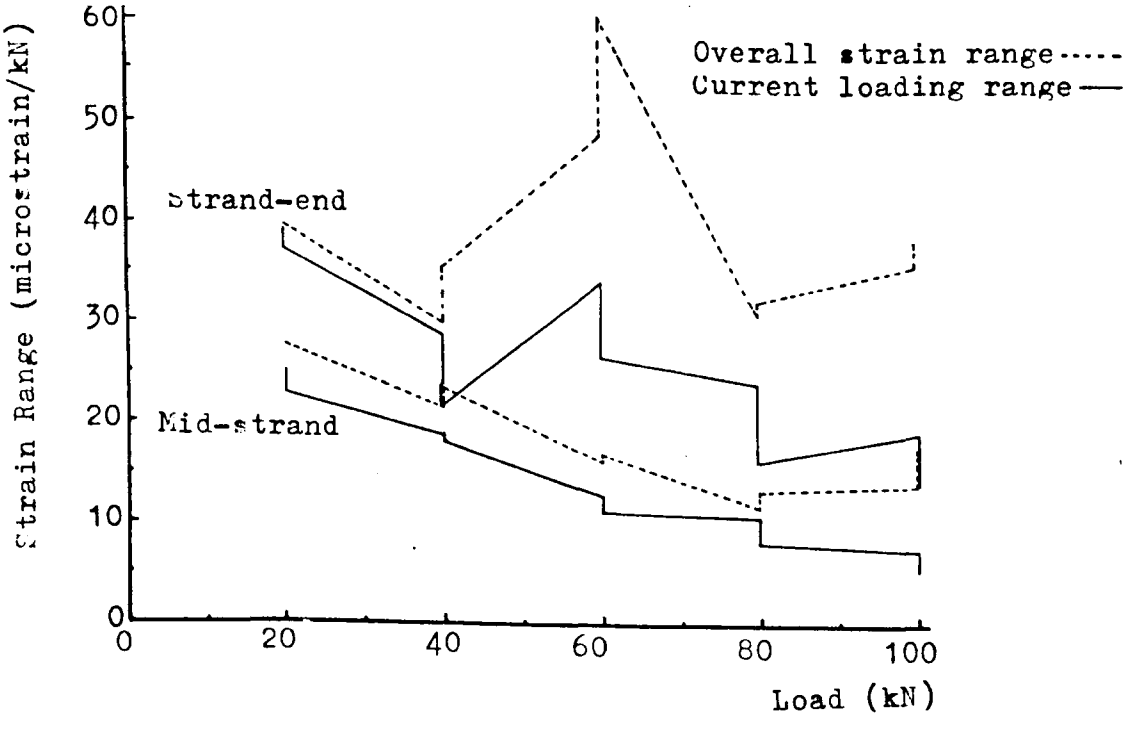

Figure 5.31(c).Wire Surface Strain Range/Strand Load;Fixed End Tests.
Strand X.

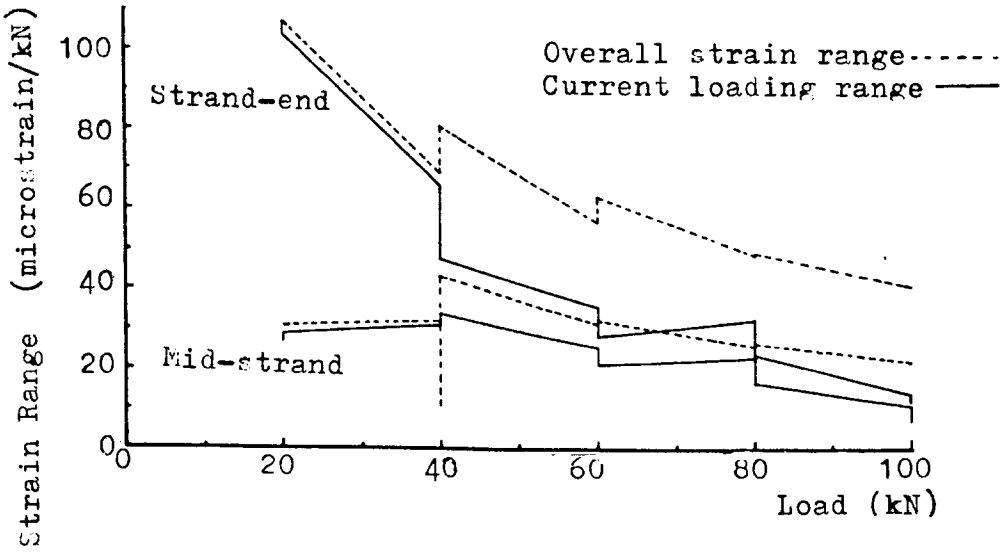

Figure 5.31(d).Wire Surface Strain Range/Strand Load;Fixed End Tests.
Strand IX.

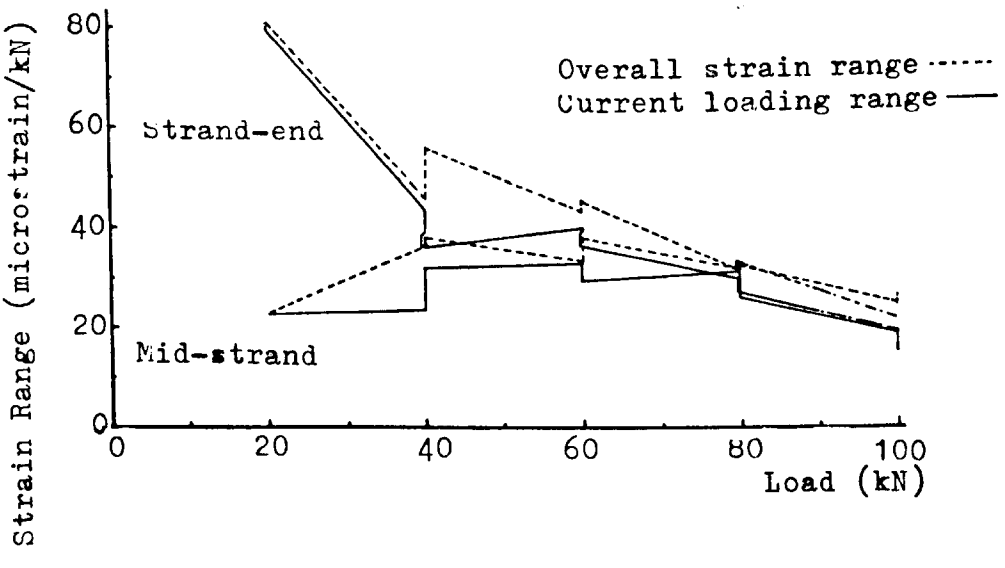

Figure 5.31(e).Wire Surface Strain Range/Strand Load;Fixed End Tests.
Strand VII.

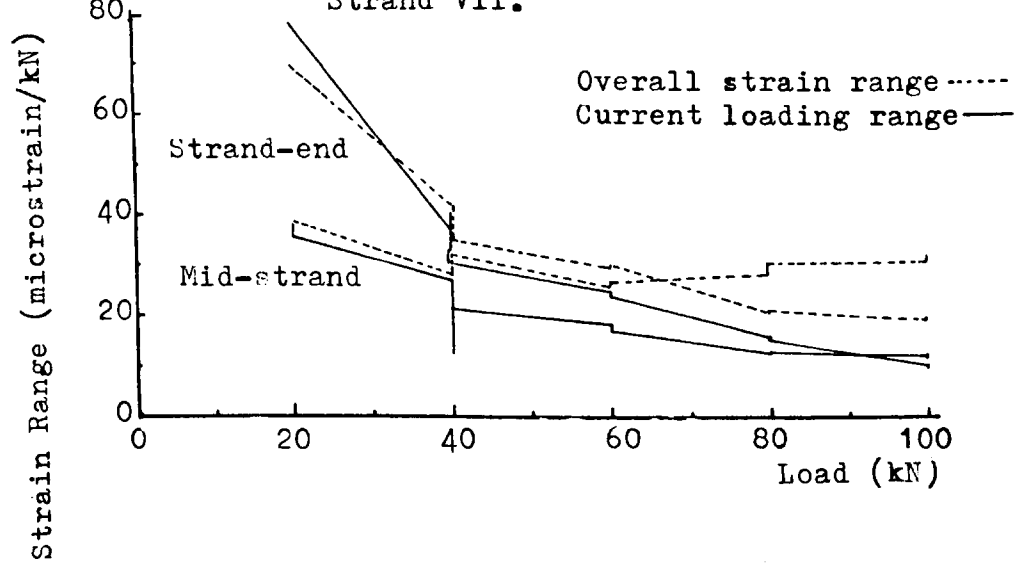

For free and partially restrained ends, strain ranges at 40 kN load against torsional restraint, as determined from Table 5.13 are given in Table 5.15 and plotted in Fig. 5.32. As with the fixed end loading, strain ranges are plotted for mid-length and end positions, distinguishing between ranges for the current cycle and the overall strain range.

Strain Ranges on Helical Wire Surface. (Strain/kN at 40 kN for All End Conditions)

Table 5.15.

MID STRAND POSITION

Nominal End Condition	Strand VI		Strand VIII		Strand X		Strand IX		Strand VII	
	Current Cycle $\mu\varepsilon$/kN	Overall $\mu\varepsilon$/kN	Current Cycle $\mu\varepsilon$/kN	Overall $\mu\varepsilon$/kN	Current Cycle $\mu\varepsilon$/kN	Overall $\mu\varepsilon$/kN	Current Cycle $\mu\varepsilon$/kN	Overall $\mu\varepsilon$/kN	Current Cycle $\mu\varepsilon$/kN	Overall $\mu\varepsilon$/kN
Fixed	15.4	13.8	16.9	22.9	32.8	42.0	31.1	36.6	22.2	31.2
$\frac{3}{4}$ Fx.	11.0	9.2	17.5	24.7	32.3	41.7	33.6	39.7	21.1	30.9
$\frac{1}{2}$ Fx.	13.4	10.8	19.2	25.5	30.3	42.2	33.6	38.6	20.7	30.4
$\frac{1}{4}$ Fx.	11.2	10.1	19.7	26.0	31.2	40.8	35.3	39.7	20.7	31.7
Free	16.6	15.5	20.4	26.7	31.7	39.8	35.8	40.8	20.6	30.8

END OF STRAND

Fixed	72.6	112.5	21.7	34.8	47.8	79.3	36.1	55.9	34.5	41.0
$\frac{3}{4}$ Fx.	69.5	108.6	20.2	35.3	47.2	79.5	34.4	58.1	35.9	44.9
$\frac{1}{2}$ Fx.	64.9	102.9	21.0	34.9	44.1	81.1	35.0	62.5	36.0	46.6
$\frac{1}{4}$ Fx.	58.6	99.2	22.0	34.2	46.2	79.8	35.3	74.1	34.4	48.9
Free	58.6	94.5	25.9	33.4	48.0	79.7	33.9	69.4	33.2	49.3

Figure 5.32(a).Wire Surface Strain Range/Strand End Condition.
Strand VI. (Free,partially restrained and fixed ends).
40kN Load.

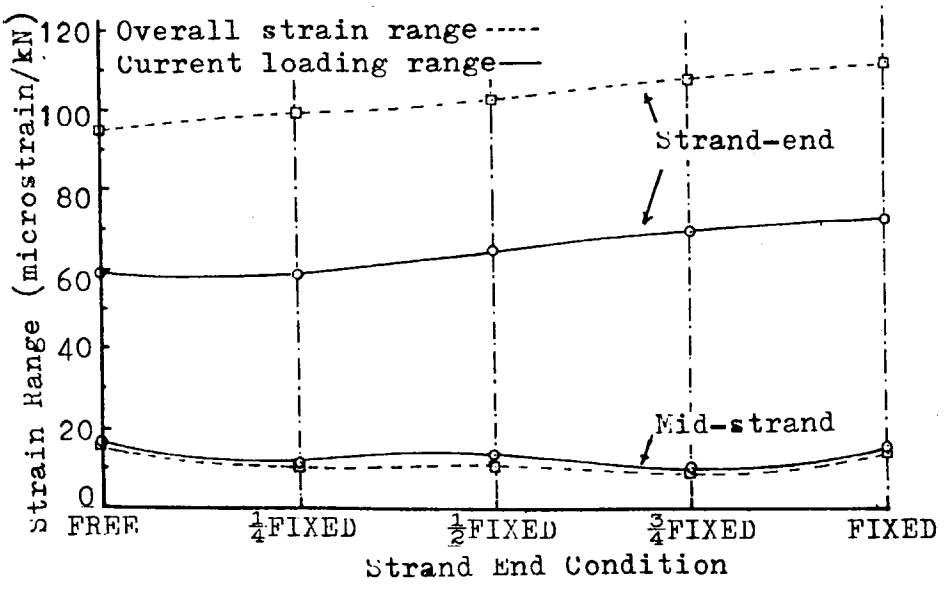

Figure 5.32(b).Wire Surface Strain Range/Strand End Condition.
Strand VIII. (Free,partially restrained and fixed ends).
40kN Load.

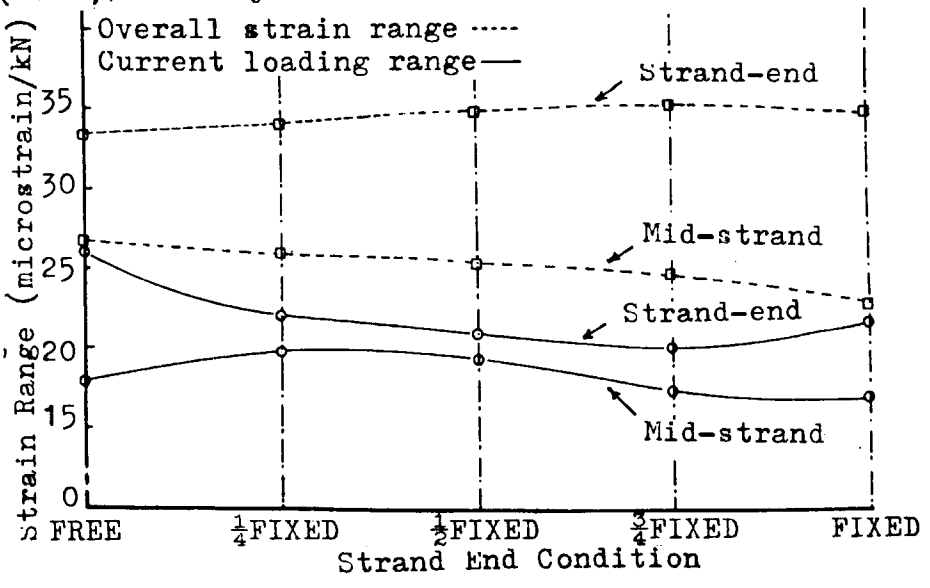

Figure 5.32(c).Wire Surface Strain Range/Strand End Condition.
Strand X. (Free,partially restrained and fixed ends).
40kN Load.

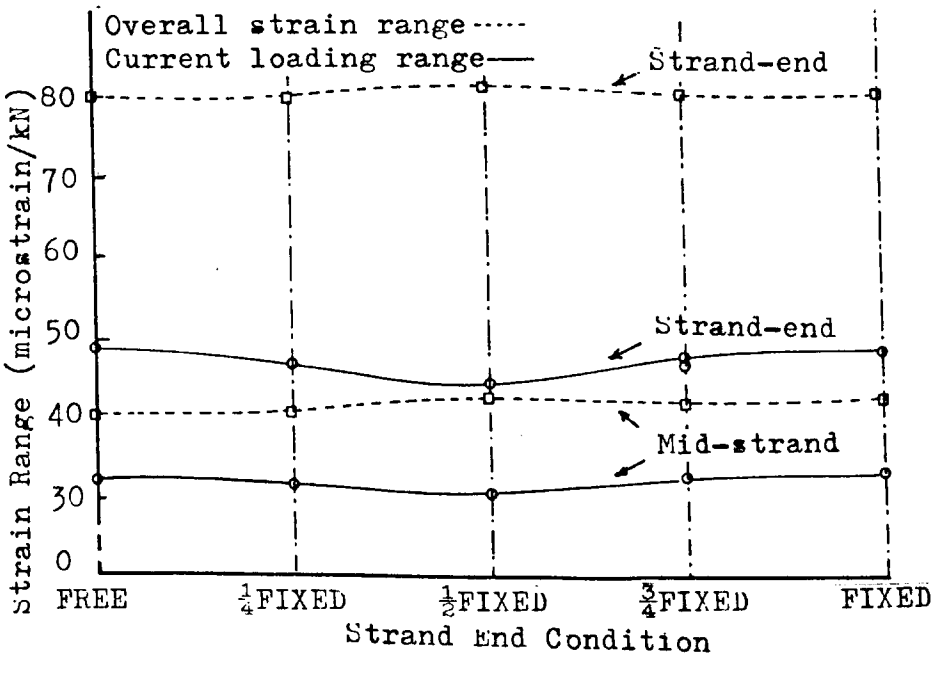

Figure 5.32(d).Wire Surface Strain Range/Strand End Condition.
Strand IX. (Free, partially restrained and fixed ends).
40kN Load.

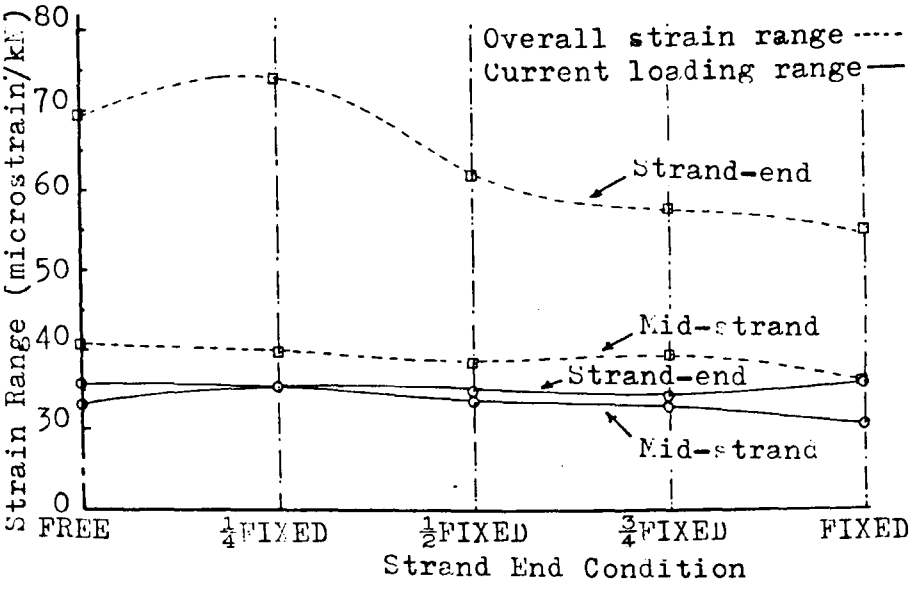

Figure 5.32(e).Wire Surface Strain Range/Strand End Condition.
Strand VII. (Free, partially restrained and fixed ends).
40kN Load.

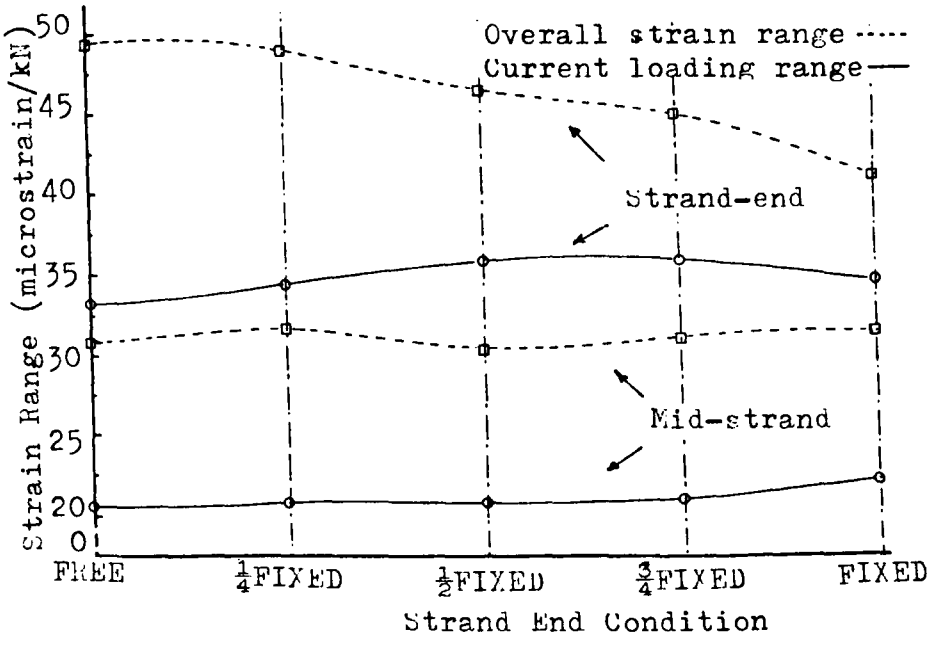

5.6 Discussion of Results

5.6.1 Summary

The next chapter is concerned with mathematical modelling and the chapter following that is concerned with comparison between experimental results and the theoretical predictions on strand response. (Chapters 6 and 7). This section is therefore confined to discussion of the results which reveal information on strand behaviour with which it is not appropriate to compare theoretical predictions. Among these are the performance of end terminations, strain gauges and the load sharing between wires.

5.6.2 Terminations

The performance of the strand terminations was satisfactory throughout the test programme. The problems encountered in preliminary tests, in which wires straightened from 180° hooks and then pulled out of the resin, or pulled straight out (in the case of unhooked wires), appear to have been completely overcome by the expedient of using wires bent through 360°. The Fig. 5.3.b, shows the resin cones from strand X, after strand fracture, and the general condition of these cones is typical of those from the other strands. The cones of strand VI (helix angle 73.6°) however, did exhibit more powdering and cracking at the throat, just before the point where the strand emerges from the grip body. At least some of this may have been due to the fact that greater torque is generated in strands with lower helix angles. This torque must be restrained in fixed end tests by the termination

which is thus subjecting the resin to a complex stress pattern with higher stress levels at higher torques.

5.6.3 Strain Gauges

Strain gauge performance was greatly improved for this programme of tests when compared with that in the preliminary tests. Only three gauges failed at the start of the loading programme (E51P on strand X and gauges E2Aa and c on strand VI) and one other became partly detached at the start of loading under free end conditions, (M12Aa on strand X). (See Table 5.2). The use of gauges with leads attached by the manufacturer was probably the major reason for the improvement.

A total of five other gauges failed at loads between 120 kN and 130 kN. None of the others failed until strand fracture and it must be assumed that the shock wave transmitted along each wire shakes loose the adhesive in most cases. However, some of the gauges at mid-strand position did survive strand fracture.

The loss of the gauge mounted perpendicular to strand axis was less significant than the loss of the axially mounted gauges. Stacked gauges of the right configuration, in which grids at different angular positions are mounted on top of each other, were not available for this type of application. The distance between gauges mounted axial with and perpendicular to wire axis, particularly near the end of the strand, where changes in tension, bending and twist make it impossible to relate axial

and perpendicular strain values on the same wire. See Figs. 5.22 and 5.23. The maximum and minimum strain values in the six wires for axial strains, 4, 3, 6, 1, 5, 2 were not mirrored in the perpendicular strains, but were in order 1, 5, 6, 2, 4, 3. Nor did the ratio of perpendicular to axial strains give a consistent value.

The failure of axial strain gauge (M12Aa) on strand X, after cycle 304 prevented estimation of wire tension during all loading under free and partially restrained ends, and for fixed end loading above 50 kN.

Outputs from gauges mounted at 45° to strand axis and parallel to strand axis were not examined as useful analysis and comparison with other outputs is not possible in regions of rapid change in wire loading along its length.

It is certain that more information on tension in helical wires would have been useful in this study. The use of the 'three in parallel' gauge configuration and stacked gauges, if available, would greatly improve the quality of information obtained from strand testing and this is among the recommendations for further work in this field.

5.6.4 Breaking Loads and Types of Fracture

The magnitudes of the breaking loads recorded in Table 5.4 are of no particular significance in this study. However, the fact that there was some consistency about the nature of the

fracture reinforces the view that testing procedure, particularly strand termination technique was also consistent.

5.6.5 High Speed Photography at Strand Fracture

Fortunately, the position of either of the extrometer bosses, seen in Figs 5.4 at about one quarter and three quarters of strand length from the strand end, did not coincide with the position of strand break, seen at about one fifth strand length from right termination. These bosses cannot be removed after the extrometer is disconnected and it can only be a matter for conjecture as to whether they restrict the movement of strand wires after break.

Considering first the left hand and longer end of the strand after break, there is evidence of wire movement radially outwards from about mid-strand and increasing up to the left hand termination from print 2 onwards. By print 6, the 'birdcage' adjacent to the left hand grip appears to have attained its maximum diameter and the remainder of the strand length, to the right of the birdcage, has returned to its original position. The diameter of the 'birdcage' then reduces until print 12 and thereafter remains at constant diameter. This final configuration is seen more clearly in the still photograph given in Fig. 5.2. The protruding core wire seen in the right hand side of still photograph, Fig. 5.3.a, is in evidence immediately after fracture in print 2 of Fig. 5.4.

In the shorter length of broken strand radial outward

movement of the wires, initially at the break point and then moving towards the termination in prints 3 and 4. Thereafter, radial inward movement occurs up to print 7, followed by outward movement which seems to attain a maximum by about print 22. Inward movement occurs again and the configuration seen more clearly in the left hand side of the still photograph given in Fig. 5.3.a appears to have stabilised at about print 37.

Birdcage propagation has been of peripheral interest in this study and does not contribute to the main objectives. However, the high speed prints do reveal some features that still pictures taken after fracture do not. In particular, the transitory appearance, repeated, of a birdcage at the broken end of the shorter length of strand was not suspected hitherto and its presence could not be easily detected by any other method. Further investigations of birdcage propagation at both ends of the strand will need higher film speed and further development of this technique, including the provision of special strand testpieces for this purpose only and therefore free from extrometer bosses.

5.6.6 Extension

The load/extension plots in Fig. 5.8 show clearly the effect that end condition has on strand axial stiffness, the free end permitting largest extension and the fixed end least. Numerical values of stiffness and comparison with strand

modelling are given in Chapter 7, section 7.3.

Extension under higher loads is shown in Fig. 5.9. All strands exhibit a departure from linearity of the load/extension plots at loads higher than about 50 kN. It is not possible to distinguish a yield point as such, particularly as the effect of increasing helix angle under load also contributes to non-linearity.

Permanent extension in the strand is evident as load cycling is continued to increasing maximum loads, although strand stiffness up to about 50 kN appears sensibly constant.

5.6.7 Rotation

The load/rotation plots in Fig. 5.10 show clearly the effect that end condition has on rotation, the free end permitting largest rotation under load. Numerical values and comparison with strand modelling are given in Chapter 7, section 7.4.

5.6.8 Tension and Bending Moments in Wires

The wire tensions at 40 kN strand load for fixed end, partially restrained and free end tests, as recorded in tables of the type shown in Table 5.11, are tabulated in columns 3 to 7 of Table 5.16. These results show that for a given strand load helical wire tension is reduced as end restraint is reduced. Clearly the core wire takes a proportionately greater share of the total load on the strand as the strand is allowed

Tension in Helical Wires at Strand Load of 40 kN - Test Results

Table 5.16.

Strand Number	Gauge Posn	Wire Tension kN Nominal End Condition of Strand				
		Fixed	$\frac{3}{4}$ Fixed	$\frac{1}{2}$ Fixed	$\frac{1}{4}$ Fixed	Free
VI (73.0°) (Measured)	23mm From End	5.20	4.94	4.58	4.30	4.21
VI (73.6°) (Nominal)		(104)‡	(111)	(110)	(112)	(109)
VIII (76.2°)	Mid Strand	5.20 (203)	5.11 (209)	4.95 (208)	4.76 (207)	4.60 (206)
X (77.7°)	Mid Strand	5.46 (303)	* (309)	* (308)	* (307)	* (306)
IX (78.9°)	Mid Strand	5.45 (403)	5.20 (409)	4.93 (408)	4.69 (407)	4.54 (406)
VII (80.9°)	10 mm From End	5.15	4.69	4.41	4.16	3.94
VII (80.9°)	23 mm From End	5.58 (505)	5.41 (510)	5.36 (509)	5.34 (511)	5.33 (508)

* Strain gauge unserviceable after load cycle 304

‡ Load cycle numbers

to rotate under load.

There are insufficient strain gauges mounted in the 'three in parallel' configuration to give a more comprehensive assessment of the individual wire tensions. One problem is that it is not possible to determine whether tension in the particular wire is above or below the mean tension in the six helical wires. This cannot be ascertained from the outputs of strain gauges attached to the crowns of the six wires at the strand cross-section concerned since nett strain measured includes strain due to bending of the wire under load. This bending strain is not necessarily the same for all wires and is likely to be very different at positions near to the end grip. Unfortunately firm conclusions on bending moments cannot be drawn from the tabulated results (e.g. Table 5.11) since an analysis of the possible errors in Appendix A.7, sections A.7.2 and A.7.3 shows that large errors can occur due to gauge misalignment and if there is a change in the position of neutral axes of bending.

Comparison with theoretical predictions of wire tensions and bending moments is clearly not worthwhile. However, the following conclusions can be drawn from examination of test results.

(i) Helical wires take a lower proportion of the total load as torsional restraint on the strand is reduced.

(ii) Helical wires take a lower proportion of the total load near to strand end grips.

5.6.9 Torque Generated

The load/torque plots in Figs. 5.25 to 5.29 and the tabulated results from them (Table 5.13) show that a consistent degree of torsional restraint was applied throughout each loading cycle. The comparison of other parameters obtained under these quantified degrees of end restraint are compared in Chapter 7 with strand response predictions from mathematical modelling in Chapter 6.

The load/torque plots shown in Fig. 5.30 do not reveal the same departure from linearity at higher strand loads exhibited in load/extension and load/strain plots. This is to be expected since strand load and torque generated are linked; they both relate to the equilibrium of the strand. The changes in strand geometry under load, notably helix angle increase and helix radius reduction, are clearly too small to make a significant difference to the moment of the tangential component of wire tensions about strand axis, which constitutes the largest contribution to the total torque generated.

5.6.10 Strains and Strain Variations; Load Sharing

Axial strains on the outside surface of a helical wire are less than the strain on the wire axis, since bending (G') of the wire about a diametral axis (helix binormal) occurs under

loading which increases strain at the inside surface and decreases it on the outside surface. (See Fig. A.8.1). If it is assumed that the change in helix geometry is about the same for each of the six wires, differences in straining rate with load on the outside surfaces of the wires are due to differences in tension only. More rigorous analysis, including predictions on surface strain, is given in Chapter 6 and comparison with the experimental results are made in Chapter 7. However, some assessment of differences in load sharing between wires is possible from the results described in sections 5.5.5,6 and 8 above.

Mean strains in loading cycles under different end conditions are shown for strand X ($\alpha = 77.7^{o}$) in Figs 5.11 to 5.13 and for strand VI ($\alpha = 73.6^{o}$) in Figs 5.18 to 5.20. Strains are seen to be less for a given strand load as torsional restraint is reduced. For the lower helix angles these strains are negative (compressive stress) in the free end case. Reduction in strain is an indication of increase in bending moment or decrease in tension or both.

Figs 5.14 to 5.17 show that the range of strains, from maximum to minimum, between wires, is greater near the end grip than at mid-strand for these fixed end tests, up to maximum loads of 50 kN (cycle 304) and 110 kN (cycle 316), strand X. In Figs 5.21 to 5.23 strain ranges are again shown to be larger for the position near the end of the strand than in mid-strand for a free end test, on strand VI. A fixed end

load cycle on the same strand, see Fig. 5.24, shows that at mid-strand, the strain range is about the same as that in the free end test, see Fig. 5.21.;both about 700$\mu\varepsilon$ at 44kN.

A more complete picture of strain ranges is given for fixed end tests in Fig. 5.31. The range is greater near the end grip than at mid-strand throughout the loading programme for all strands. The range reduces when a particular load is applied for the second time, when the current loading cycle only is considered. However, the overall strain range is increased, when the total strain history from the start of the first loading cycle is considered. Strain ranges are generally higher for the strands with lower helix angles. Insofar as the pattern of strain ranges is similar to the pattern of tension variations between helical wires it is clear that load sharing between wires is less even near end grips than at mid-strand.

Table 5.1/ has been compiled from the strain printouts of fixed end tests, samples of which are given in Tables 5.7 and 8. It shows that the effect of load cycling to ever increasing maximum load has only a small effect on the redistribution of load between helical wires. The difference in load sharing between the wires with maximum and minimum load is completely unchanged at strand end for strands with the two lowest helix angles. The 'bedding down' effect of repeated loading appears therefore to have less to do with the migration of wires to positions giving more stability in subsequent loading than with the increased stretching of wires that are in any event taking

Changes in Wire Carrying Maximum and Minimum Strains. Fixed End Tests - Axial Strains

Table 5.17

	Load kN	VI α_o =73.6°		VIII α_o =76.2°		X α_o =77.7°		IX α_o =78.9°		VII α_o =80.9°	
		This Cycle	Overall	This Cycle	Overall	This Cycle	Overall	This Cycle	Overall	This Cycle	Overall
MID STRAND	20										
	30					O	O				
	40							C	O		
	50					O -		△	△		
	40	-	O							O	
	50	-									
	60	△ - ×				O -				-	O
	70	-								-	
	80	O								-	O
	90	△ ×		-	O					O -	
	100	- ×		-							O
	110	△ ×	O	O △	O	O	O				
	110+							×	△	O	

Continued on next page

Changes in Wire Carrying Maximum and Minimum Strains. Fixed End Tests - Axial Strains

Table 5.17 (Continued)

	Load kN	VI α_o =73.6°		VIII α_o =76.2°		X α_o =77.7°		IX α_o =78.9°		VII α_o =80.9°	
		This Cycle	Overall	This Cycle	Overall	This Cycle	Overall	This Cycle	Overall	This Cycle	Overall
END - NEAR GRIP	20									×	
	30									△	△
	40					△	△	○			
	50										
	40					△ ×		×̲	△		○
	50					△		×̲		-	
	60					△ ×			○ △	-	
	70					×				-	
	80					△		-		-	○
	90					△ ×		○ -		-	
	100					×				-	
	110					○ ×̲				-	
	110+					△ ×				-	

KEY: ○ Minimum strain - wire change] i.e. Since max. load of previous cycle, a different wire now bears
△ Maximum strain - wire change] min.(or max.) strain.

× A different wire bears max. strain for current cycle than for overall strain.

\- A different wire bears min. strain for current cycle than for overall strain.

Note: For strand X, the changes in wire bearing maximum strain at strand end for loads 40 kN, 50 kN, 60 kN, 80 kN and 90kN involves two wires only, (Nos 1 and 5), whose strain values differ by less than 40$\mu\varepsilon$.

the higher loads throughout the loading programme.

For free end tests and those with partially restrained ends, Fig. 5.32 gives an overall picture of strain ranges. Although the pattern is less clear than for fixed end tests, it can be seen that the ranges are greater near strand end than at mid-strand. The overall strain range is, again, generally greater than that when the current cycle only is considered. Conclusions on the relation between load sharing and torsional restraint are not easy to draw from Fig. 5.32 above. In fact, load sharing is less even with reduced torsional restraint for all strands since, as shown in Chapter 7, section 7.5 (Table 7.4), strains are reduced considerably, as torsional restraint is reduced, and ranges thus become a very much higher proportion of the mean.

Reports of relevance from other workers includes the uneven load sharing between wires found by Wiek (47, 48, 49, 50) in his work on stranded ropes. This is not surprising in the light of the findings of this current study reported above; it seems that this phenomenon cannot be eliminated in even the simplest strand and uneven load sharing between wires is also reported by Durelli et al. (28), Hansom (34) and Paolini and Bazzaro (43). Sharp (8) reported different load/ extension characteristics in the second and subsequent loadings of a wire rope. In strand testing, by contrast, it has been found that whereas surface strains on individual wires are different in the second loading of the strand, the overall load/

extension characteristics vary little. The 'bedding in' of ropes, reported by Sharp (8) would appear to be a physical migration of individual wires to a more stable configuration, whereas repeated loading of strands only stretches further the wires which are already bearing maximum load.

The quantitative assessment of surface strains and comparison with theoretical predictions is dealt with in Chapter 7, sections 7.5 and 7.6.

CHAPTER 6

MATHEMATICAL MODELLING OF STRAND RESPONSE TO LOAD

6.1 Introduction

Costello et al. (16, 17. 18) have considered the six wire strand and by treating the individual wires of the strand as thin rods subjected to tension, bending, twisting and bearing loads (where they have line contact with each other), after Love (26), expressions have been obtained for extension, rotation and torque generated in the strand under axial tensile load. Costello and Phillips (18) take account of wire extension in the compatibility equations and the treatment from this particular paper is given in Appendix 8. Machida and Durelli (27) have developed approximate expressions for the response to load of seven wire strand. The basis of their treatment is given in Appendix 9.

The work of Costello and Phillips (18) and Machida and Durelli (27) has been extended to take account of the relative movement between core and helicals under load in the case of 100% interwire slip, under frictionless conditions, in section 6.2. Interwire friction is considered in section 6.3 and expressions obtained for the friction force bending in helical wires and torsion in core and helicals, in conditions of no slip between core and helicals. Slip is introduced in section 6.4 and modified expressions obtained for bending and torsion in wires.

Section 6.5 considers the Poisson effect in wires of tension and the flattening effect due to pressure between helicals and core. The Costello and Phillips (18) treatment of six wire strand is modified to take account of the presence of the core under these conditions.

End effects are considered in section 6.6. A method for mathematical modelling of wire behaviour is outlined for the transition lengths of strand near the end grips.

Computing method for obtaining predicted strand response is described in section 6.7. The predictions on strand response from the approximate expressions of Machida and Durelli (27) are used in the computation as the first approximation for each of the strand geometries tested in the main experimental programme, described in Chapter 5.

Reference is made throughout sections 6.2, 6.3 and 6.4 to the Figures 6.1, 6.2, 6.3, 6.4 and 6.5, which illustrate different aspects of the forces acting on and displacement of core and helical wires.

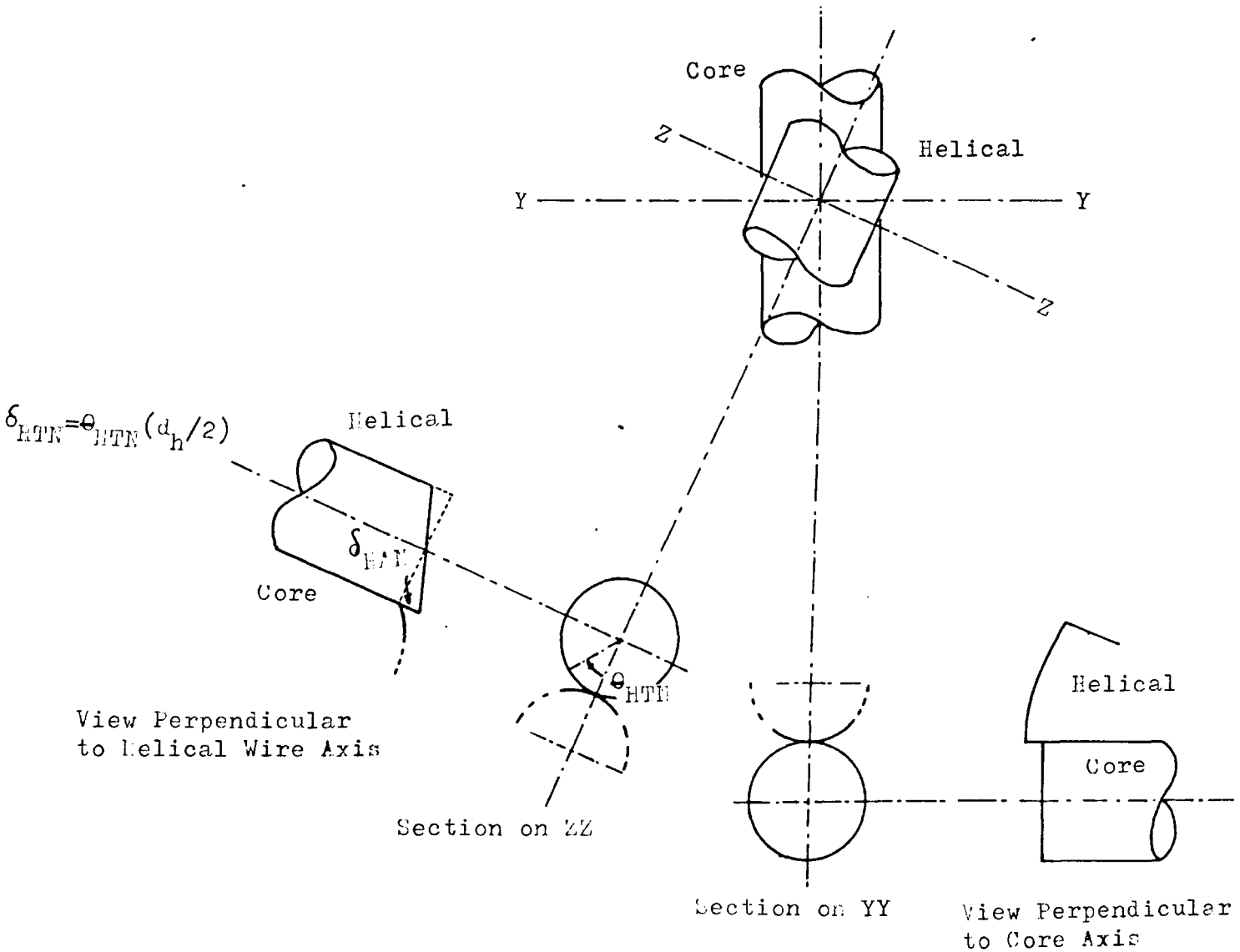

Figure 6.1.Relative Motion of Core and Helical Wires:No Friction (100% Slip).

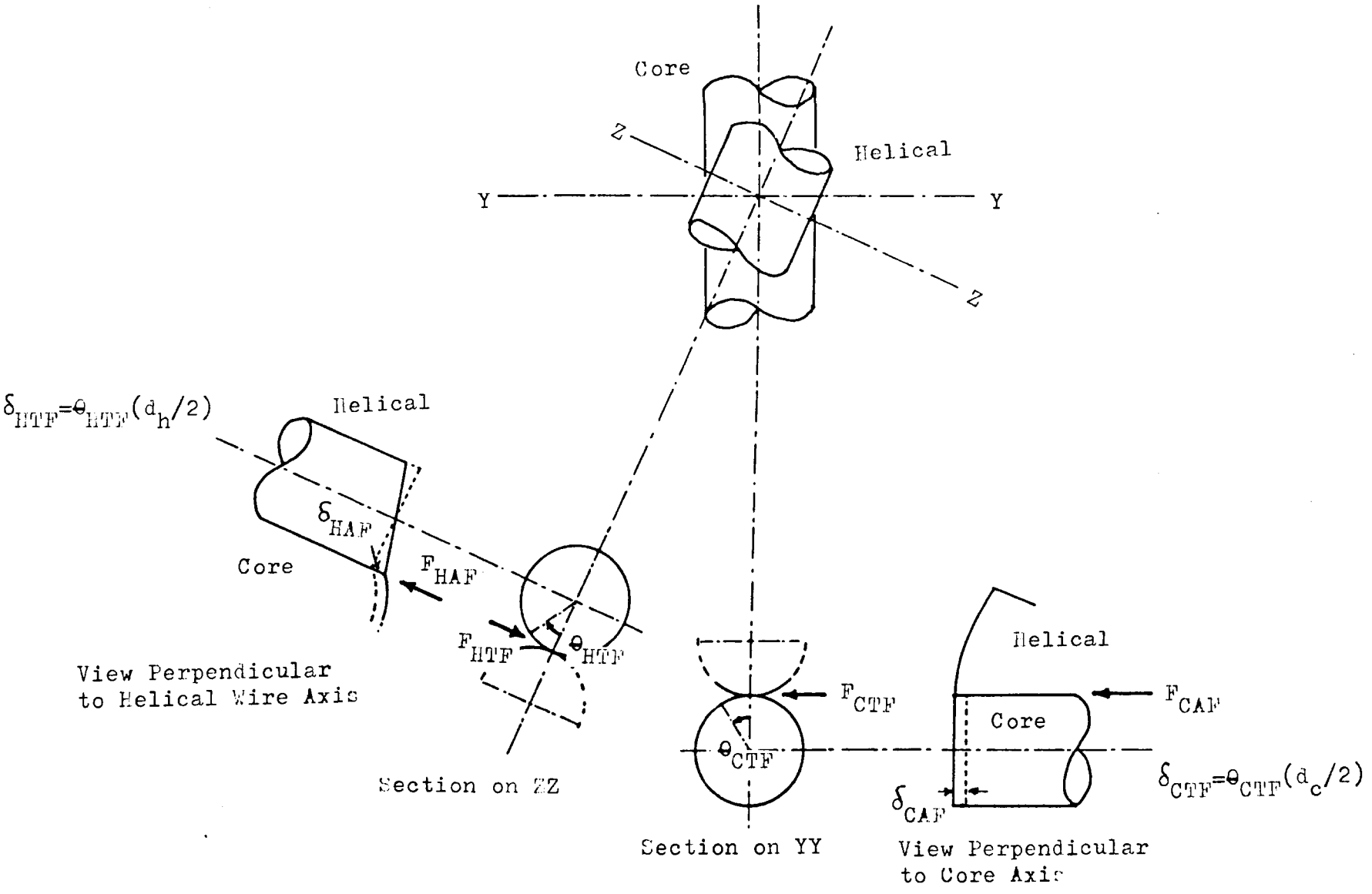

Figure 6.2.Relative Motion of Core and Helical Wires:No Slip.

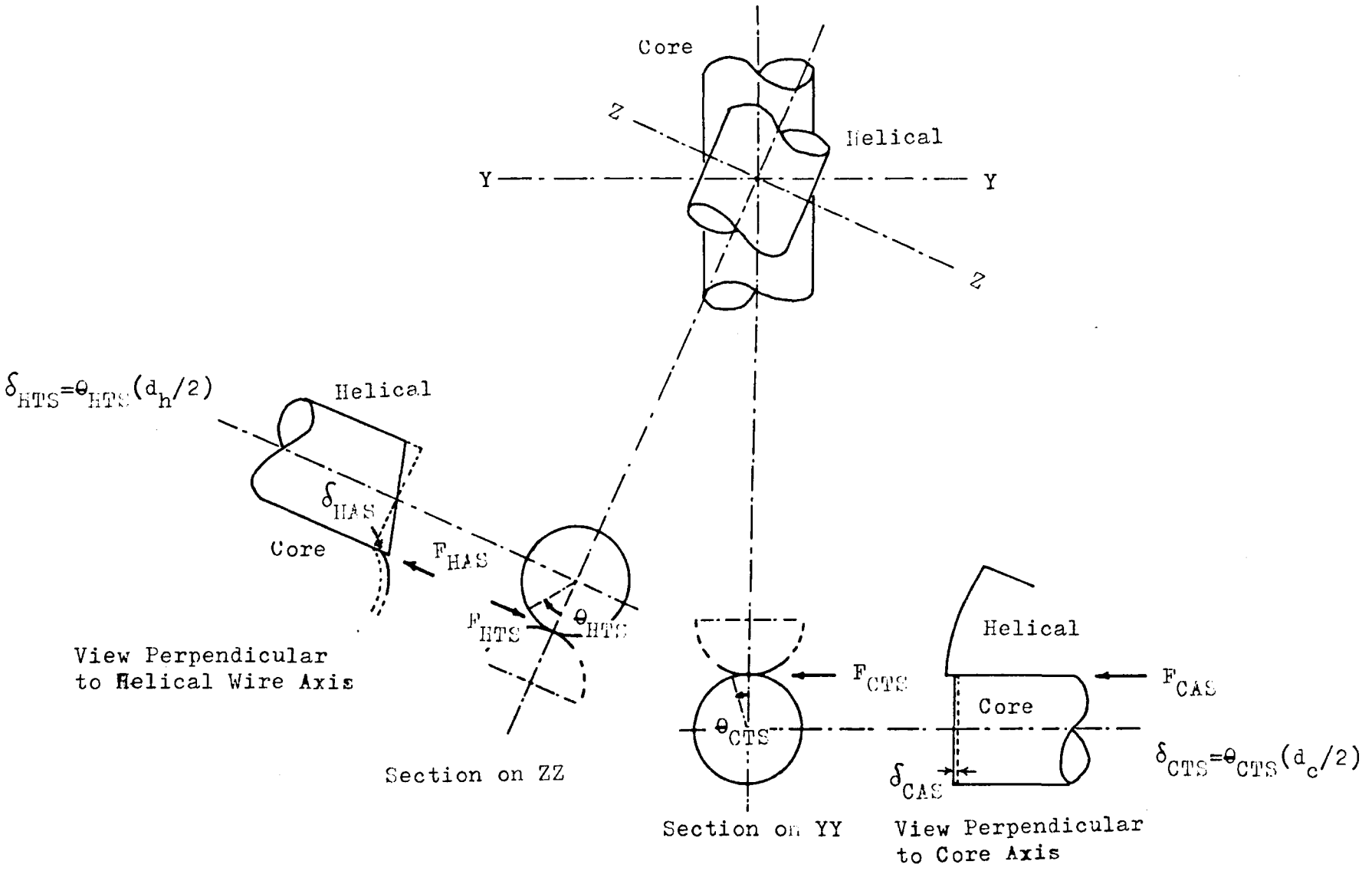

Figure 6.3.Relative Motion of Core and Helical Wires:Friction and Slip present.

Figure 6.4. Interwire Friction:Effects on Wires along the Strand.

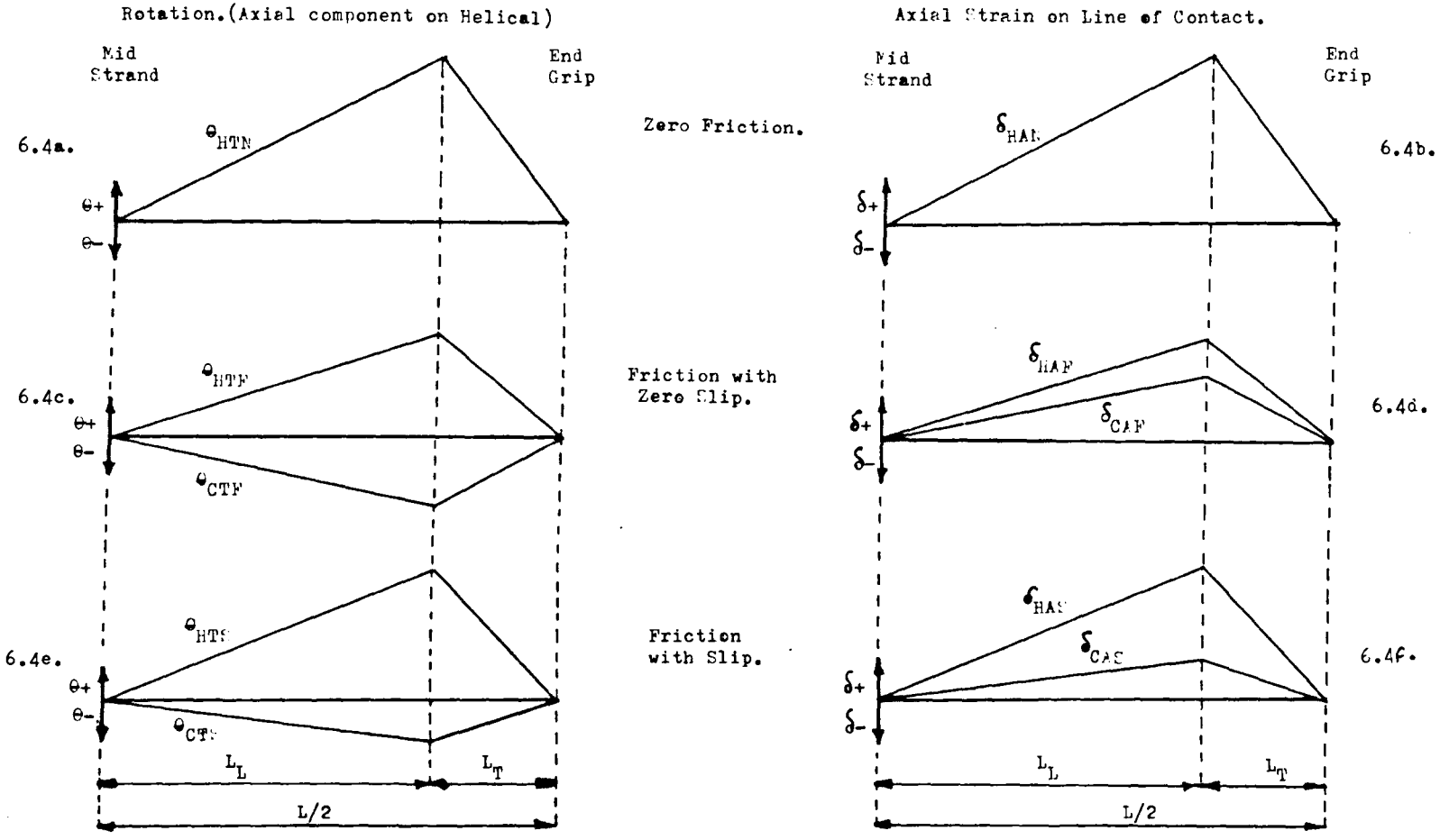

No Friction.

No Slip.

Friction and Slip present.

6.5.(a)

6.5.(c)

6.5.(e)

$\delta'_{\ } = \delta'_{HS} - \delta'_{CS}$

Displacements.

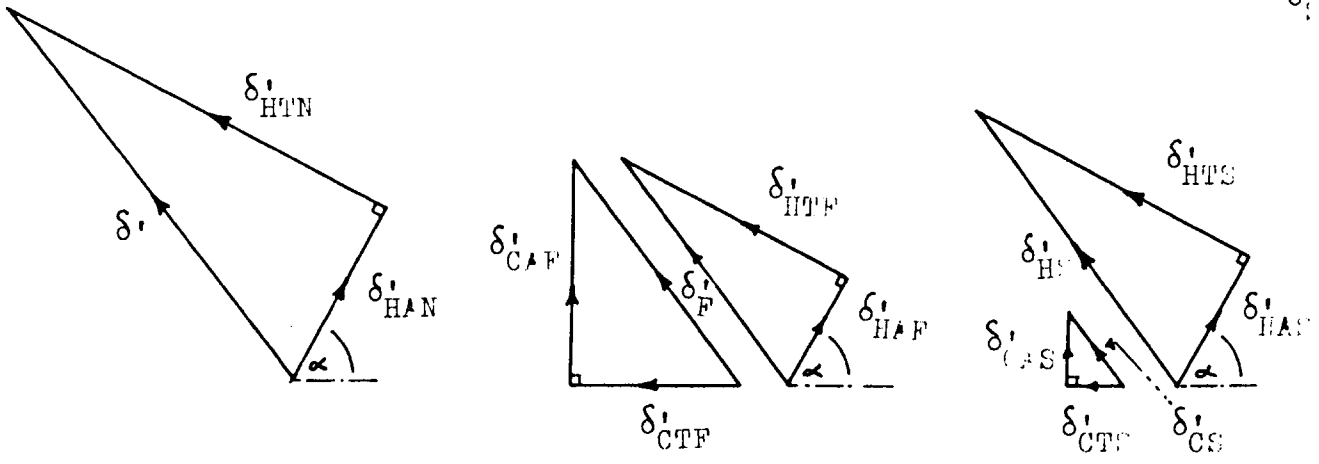

6.5.(b)

No Forces.

6.5.(d)

6.5.(f)

Forces.

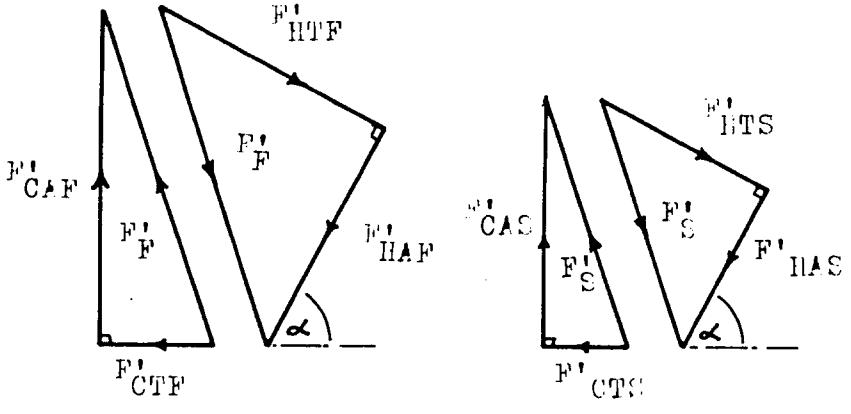

Figure 6.5.Friction between Wires:Forces and Displacements.

6.2 Zero Friction Between Wires

One assumption made by both Costello et al. (16, 17, 18) and Machida and Durelli (27) is that friction effects between wires in a strand are small enough to be neglected. As axial loading on the strand is increased, the helicals are free to rotate about their own axes, due to torque H, and to bend about their neutral axes of cross-section, (the binormal of the helix) due to bending moment G', as shown in Fig. 6.1.
Neither Costello et al. (16, 17, 18) nor Machida and Durelli (27) take account of end effects. Their analysis implies that there must be an instantaneous change from the geometry of the loaded strand (with helix angle α_1 and helix radius r_1) to that of the unloaded strand (with helix angle α_o and radius r_o) at the point where the strand enters the grip or termination. The reaction in the grip thus balances torsion H and bending moment G' in each helical and the expressions for torque generated in the strand contains a contribution from H and G'. (See second and third terms of expression A.8.19 in Appendix A.8).

Another way of regarding the end effect is to assume that changes in strand geometry occur over transitional lengths at the ends of the strand, adjacent to the grips. These changes in geometry, which must involve bending in the plane of the principal normal of the helical wire centre line, thus changing helix angle from α_1 to α_o over this length, result in a reduction of relative motion between core and helicals. As the

wires enter the end grip, relative motion between them is zero. The basis of the assumption about transitional lengths from the Costello and Durelli treatments is illustrated in Fig. 6.4.a and b. Due to symmetry only half the strand is considered. The rotation of the helical about its own axis, Θ_{HTN} increases from zero at mid-strand to a maximum at distance L_T from the strand grip, and then reduces to zero at the grip itself. Core rotation is zero throughout. A similar pattern is seen for the increase in dimension of the line of contact on the helical wire, which increases from zero at mid-strand to a maximum at distance L_T from the strand grip, and then reduces to zero at the grip itself. Core extension is unchanged. Over the strand length L_L (where $L_L = L/2 - L_T$), rotation of a helical wire is given by

$$\Theta_{HTN} = \delta_{HTN}/(d_h/2) \qquad 6.1$$

From simple torsion theory, the tangential component of linear displacement is given by

$$\delta_{HTN} = \frac{d_h H(1+\nu)L_L}{2I_h E} \qquad \text{and}$$

displacement per unit length is given by

$$\delta'_{HTN} = \frac{d_h H(1+\nu)}{2I_h E} \qquad 6.2$$

Similarly, from simple bending theory, the axial component per unit length is given by

$$\delta'_{HAN} = \frac{d_h G'}{2I_h E} \qquad 6.3$$

(see also Figure 6.5.a.)

6.3 Friction with Zero Slip

The contributions of H and G' to the overall torque generated in a strand under axial load are given in the second and third terms of expression A.8.19, (Appendix A.8), in the treatment of Costello et al. (16, 17, 18). The treatment of Durelli et al. (27) also contains a contribution to overall torque from the bending and torsion of helical wires. (See expressions A.9.25 and A.9.32 in Appendix A.9). The effect of friction is now considered over that part of the strand which is at sufficient distance from the end grips to avoid end effects. (Length L_L in Fig. 6.4). It is postulated that frictional resistance from the core wire prevents some of the rotation and bending of helical wires about their own axes which would have occurred in the absence of friction. The contribution to overall torque generated in the strand, referred to above, is therefore transmitted to the end grips partly by the helicals and partly by the core wire. Relative rotation between core and helicals thus occurs as illustrated in Fig. 6.2.

Rotation of the core is in the opposite sense to that of the helical wire. Extension of the core and increase in the dimension of the line of contact of the helical are seen to be both positive. The rotation of the helical Θ_{HTF} and core Θ_{CTF} about their own axes are shown in Fig. 6.4.c for the length from mid-strand to end grip, while Fig. 6.4.d shows the corresponding changes in dimension in the axial direction for

each wire. The components in axial and tangential directions of the rate of displacement along the strand of both wires is shown in Fig. 6.5.c. The components of friction force per unit length acting on each wire are shown in Fig. 6.5.d. It can be seen that the force acting on the helical wire is such as to reduce the displacements which occur in the absence of friction (c.f. Fig. 6.5.a) whereas the equal and opposite force acting on the core acts such as to produce the rotation and extension already shown in Figs 6.2 and 6.4.c and d.

The general equations of equilibrium of a thin rod subjected to tension, bending, twisting and bearing loads are given by Costello and Phillips (18), see Appendix A.8, equations A.8.3 to A.8.8. The effect of friction force only is now considered for each wire.

The core wire can be considered as a special case of a helix where $\alpha_o = 90^o$ and the general equilibrium equations can be simplified as follows. Due to symmetry of the loading from the six helicals,

$$X = Y = 0, \quad K = K' = 0, \quad N = N' = 0 \qquad 6.4$$

Since the core wire remains straight under loading,

$$\tau = k = k' = 0 \quad \text{and} \quad G' = G = 0 \qquad 6.5$$

From equations A.8.3 to A.8.8 and 6.4 and 6.5

$$dN/ds_C = 0, \quad dN/ds_C = 0, \quad dG/ds_C = 0, \quad dG'/ds_C = 0 \qquad 6.6$$

and $$dT/ds_C + Z = 0, \quad dH/ds_C + \Theta = 0 \qquad 6.7$$

Note that for unit length of helical wire, the corresponding length of core wire over which interwire friction acts is $1\sin\alpha$. Axial force and torque acting per unit length of core are therefore given by

$$dT/ds_C = 6(F'_{CAF})/\sin\alpha \qquad 6.8$$

and $$dH/ds_C = 6(F'_{CTF})(d_c/2)/\sin\alpha \qquad 6.9$$

Friction force acting on the core per unit length of core is given by

$$F'_C = 6(F'^2_{CAF} + F'^2_{CTF})^{0.5}/\sin\alpha \qquad 6.10$$

For the helical wires, general equilibrium equations from equations A.8.3 to A.8.8 can be simplified. The force acting along the line of contact between core and helical is regarded as applying a bending moment K' and a torque Θ per unit length of the wire, and these are the only external loads on the wire. It follows that

$$X = Y = Z = 0 \quad \text{and} \quad K = 0 \qquad 6.11$$

Strand geometry changes due to friction only are very small compared with those caused by the tensile loading of the strand overall. Terms containing curvature and twist changes (k' and τ) can therefore be omitted and the remaining equations are

$$dG'/ds + K' = 0, \quad dH/ds + \beta = 0 \qquad 6.12$$

Bending moment and torque acting per unit length of helical wire are therefore given by

$$dG'/ds = F'_{HAF}(d_h/2) \qquad 6.13$$

and

$$dH/ds = F'_{HTF}(d_h/2) \qquad 6.14$$

Friction force acting on the helical wire per unit length is given by

$$F'_F = (F'^2_{HAF} + F'^2_{HTF})^{0.5} \qquad 6.15$$

This force is equal and opposite to the force acting on the core wire per unit length of helical wire, which from 6.10 and 6.15 is given by

$$F_F' = (F'^2_{CAF} + F'^2_{CTF})^{0.5} \qquad 6.16$$

Equations of equilibrium can now be established and, with reference to Fig. 6.5.d are given by

$$F'_{CTF} = F'_{HTF}\sin\alpha - F'_{HAF}\cos\alpha \qquad 6.17$$

$$F'_{CAF} = F'_{HTF}\cos\alpha + F'_{HAF}\sin\alpha \qquad 6.18$$

Equations linking displacement of core and helical wires can also be established and, with reference to Fig. 6.5.c,are given by

$$\delta'_{CTF} = 6F'_{CTF}/S_1 \qquad 6.19$$

$$\delta'_{CAF} = 6F'_{CAF}/S_2 \qquad 6.20$$

$$\delta'_{HAF} = (F'_{HAN} - F'_{HAF})/S_3 \qquad 6.21$$

$$\delta'_{HTF} = (F'_{HTN} - F'_{HTF})/S_4 \qquad 6.22$$

Where S_1 and S_2 are the torsional and the axial tensile stiffnesses of the core wire; S_3 and S_4 are the bending and torsional stiffnesses of the helical wire. Forces F'_{HAN} and F'_{HTN} are those required to prevent any change in bending and torsion respectively of the helical wire and are given by

$$F'_{HAN} = \frac{G'/(d_h/2)}{L_L} \quad \text{and} \quad F'_{HTN} = \frac{H/(d_h/2)}{L_L} \qquad 6.23$$

Stiffnesses are given by

$$S_1 = EI_c/\ (1+\nu)\sin\alpha\,(d_c/2)^2 \qquad 6.24$$

$$S_2 = EA_c/\sin\alpha \qquad 6.25$$

$$S_3 = EI_h/\ (d_h/2)^2 \qquad 6.26$$

$$S_4 = EI_h/\ (1+\nu)(d_h/2)^2 \qquad 6.27$$

Manipulation of equations 6.17 to 6.27 yield expressions

$$F'_{HAF} = \left(\frac{H}{S_4 A_2} - \frac{G'}{S_3 A_1}\right)\left(\frac{2}{d_h}\right)/6\left(\frac{A_1}{A_2} - \frac{A_3}{A_1}\right) \qquad 6.28$$

and

$$F'_{HTF} = \left(\frac{H}{S_4 (d_h/2)} - 6F'_{HAF} A_1\right)/6A_2 \qquad 6.29$$

where

$$A_1 = \sin\alpha\cos\alpha(1/S_1 - 1/S_2) \qquad 6.30$$

$$A_2 = (\sin^2\alpha/S_1 + \cos^2\alpha/S_2 + 1/6S_4) \qquad 6.31$$

$$A_3 = (\cos^2\alpha/S_1 + \sin^2\alpha/S_2 + 1/6S_3) \qquad 6.32$$

Resultant friction force per unit length of helical is given by

$$F'_F = (F'^2_{HAF} + F'^2_{HTF})^{0.5} \qquad 6.33$$

The restraining effect of the core on the helical wires due to friction between them can be quantified in terms of restraining ratios Z_1 for bending moment and Z_2 for torsion, defined as follows

$$Z_1 = L_L F'_{HAF}(d_h/2)/G' \qquad 6.34$$

and

$$Z_2 = L_L F'_{HCF}(d_h/2)/H \qquad 6.35$$

Actual bending moment G'_A and actual torque H_A to which the helical wire is subjected under loading of the strand are therefore given by

$$G'_A = (1 - Z_1)G' \qquad 6.36$$

and

$$H_A = (1 - Z_2)H \qquad 6.37$$

Note that G'_A is less than G' and H_A is less than H, due to the restraining effect of friction from the core.

6.4 Friction with Some Slip

If the friction force is insufficient to maintain contact between points on core and helical which were in contact before loading started, then slip will occur. The helical wire is less restrained by friction force from the core and displacements are therefore greater, giving

$$\delta'_{HAS} > \delta'_{HAF} \quad \text{and} \quad \delta'_{HTS} > \delta'_{HTF} \qquad 6.38$$

The reduced friction force transmitted from helical wire to core results in smaller displacements of the core, giving

$$\delta'_{CAS} < \delta'_{CAF} \quad \text{and} \quad \delta'_{CTS} < \delta'_{CTF} \qquad 6.39$$

(See Figs 6.5.e and f)

The final distance apart of these points originally in contact is now given by

$$\delta'_{S} = \delta'_{HS} - \delta'_{CS} \qquad 6.40$$

(See Figs 6.3 and 6.5.e)

The force per unit length of helical wire, F'_S is less than F'_F as determined in section 6.3, equation 6.33 and is given by

$$F'_S = (F'^{2}_{HTS} + F'^{2}_{HAS})^{0.5} \qquad 6.41$$

where F'_S is the force acting on the helical wire per unit length of helical wire and

$$F_S' = (F'_{CTS}{}^2 + F'_{CAS}{}^2)^{0.5} \qquad 6.42$$

where F'_S, in the opposite sense, is the force acting on the core wire, per unit length of helical wire. (See Fig. 6.5.f).

Let $F_S' = C_S F'_F$ where C_S is some fraction, $C_S < 1$.

Then $$F'_S = C_S(F'_{HTF}{}^2 + F'_{HAF}{}^2)^{0.5} \qquad 6.43$$

Manipulation of expressions 6.19 to 6.35 and substitution in 6.40 yields an expression for slip distance

$$\delta_S' = \frac{2}{d_h L_L}(M_1 - M_2) \qquad 6.44$$

where $$M_1 = \left(G'^2\left(\frac{1-C_S Z_1}{S_3}\right)^2 + H^2\left(\frac{1-C_S Z_2}{S_4}\right)^2\right)^{0.5} \qquad 6.45$$

and $$M_2 = C_S\left(G'^2\left(\frac{1-Z_1}{S_3}\right)^2 + H^2\left(\frac{1-Z_2}{S_4}\right)^2\right)^{0.5} \qquad 6.46$$

Slip occurs between core and helical wire when

$$F'_S > \mu X \qquad 6.47$$

where X is the contact force per unit length of helical wire.

In the case of the 6 wire strand considered by Costello et al. (17, 18), X is the resultant of the two contact forces from the two adjacent helical wires. (See Fig. 6.6). For 7 wire strands, manufacture is such that, ideally, contact is between helicals

Figure 6.6. Contact Forces.

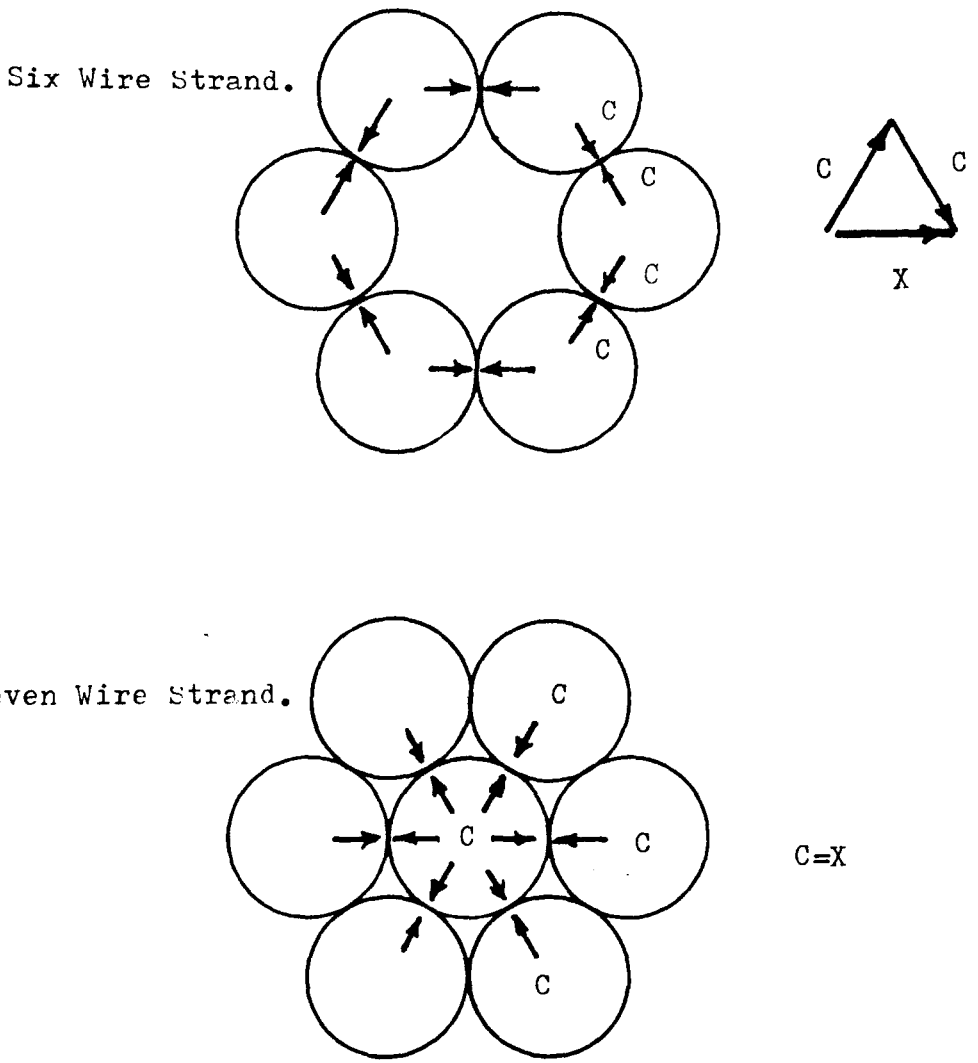

and core only, and not between helicals and other helicals. In this case C = X and X is numerically equal to X derived by Costello for the six wire strand.

The expression developed by Costello and Phillips (18) for contact force X, (Appendix A.8, expression A.8.17) must be modified to take account of the reduced bending moment and torque in the helicals, when friction between core and helicals is considered. Bending moment G'_A from 6.36 and torque H_A from 6.37 are substituted, and contact force is then given by

$$X = H_A k'_1 \gamma_1 - G'_A \gamma_1^2 + T k'_1 \qquad 6.48$$

If the coefficient of kinematic friction is known, the onset of slip for a strand of a particular geometry can be predicted. Slip distance can also be estimated. Note that these predictions ignore the effect of wire flattening at contact due to interwire pressure.

6.5 Poisson Effects and Wire Flattening

This section extends the work of Costello and Phillips (18) on six wire strand to consider a seven wire strand. In addition, account is taken of Poisson effects in the wires under tension and the flattening on wires due to interwire pressure.

Contact force per unit length on a helical wire is given in 6.48. When the six helical wires and one core wire are placed together, contact forces X (normal) and F'_F or F'_S (friction) can be regarded as internal forces in the strand. The load taken by the core is now added to that taken by the helicals and the Costello and Phillips expressions for axial load and moment, from A.8.18 and A.8.19 amended to give

$$P = 6(T\sin\alpha_1 + N'\cos\alpha_1) + T_c \qquad 6.49$$

$$M = 6(H\sin\alpha_1 + G'\cos\alpha_1 + Tr_1\cos\alpha_1 - N'r_1\sin\alpha_1) + M_c \qquad 6.50$$

where T_c and M_c are the tensile load and axial twisting moment respectively taken by the core, which are given by

$$T_c = A_c E \varepsilon_c \qquad 6.51$$

$$M_c = J_c E \phi / 2(1+\nu) \qquad 6.52$$

The expressions linking strand axial strain (equal to core strain ε) helical wire strain (ξ), strand rotation (ϕ), helix radii (r_o and r_1) and helix angles (α_o and α_1) developed by Costello and Phillips (18) for six wire strand also hold for seven wire strand.

From A.8.21 and A.8.22

$$\varepsilon = (1+\xi)\sin\alpha_1/\sin\alpha_o - 1 \qquad 6.53$$

and $$\phi = (r_o(1+\varepsilon)/r_1\tan\alpha_1 - 1/\tan\alpha_o)2\pi\tan\alpha_o \qquad 6.54$$

Poisson effect on individual wires is now taken into account.

The reduction in helical wire radius is given by

$$\delta_h = (d_h/2)\nu\xi \qquad 6.55$$

and the reduction in core wire radius by

$$\delta_c = (d_c/2)\nu\varepsilon \qquad 6.56$$

Helix radius when strand is under load is therefore given by

$$r_1 = (d_c(1-\nu\varepsilon) + d_h(1-\nu\xi))/2 \qquad 6.57$$

The helix radius is reduced further if wire flattening is taken into account. Expression 6.49 can be modified to include a flattening term.

$$r_1 = (d_c(1-\nu\varepsilon) + d_h(1-\nu\xi))/2 - \delta_x \qquad 6.58$$

where $\delta_x = f(X)$

In the computation, section 6.7, empirical relations based on the experimental work of Hamlet (76) are substituted for δ_x in evaluating the predictions for final helix radius from 6.58.

After flattening, the wires are no longer of circular cross-section and, in the case of helical wires, are also unsymmetrical. However, it is assumed that response to tension bending and torsion remain unchanged after flattening since the magnitude of these dimension changes is so small.

6.6 End Effects

6.6.1 A Descriptive Treatment

The analysis in section 6.3 considers the interaction between core and helicals, due to friction, over that part of the strand which is sufficiently distant from the end grip to be unaffected by the changes in strand geometry which occur at the ends of a strand under load. If the whole length of the strand is now considered, including those sections embedded in the socketing medium of the end grips, it is possible to postulate a mechanism in which the core undergoes changes in the rate of angular displacement along its length, even in the case of fixed end loading. Fig. 6.4 illustrates the relative motion between core and helicals that can occur. Of critical importance is the transition length (L_T) of strand adjacent to each grip. The next section outlines a mathematical model which attempts to analyse wire behaviour in this area.

6.6.2 Analytical Preliminaries to Solution by Numerical Methods

If the grip socketing medium is considered rigid, the geometry of the strand in the unloaded state is maintained within the grip length. Since the wires at the end of the strand are embedded in the socketing medium under conditions of zero axial load, there is no contact force between wires, and this condition of zero contact force then constitutes an end condition of the transition length adjacent to the end grip when the strand is now subjected to load. Over the transitional length L_T, strand

geometry changes from that of the unloaded state to that of the loaded state as determined in the analysis in section 6.3. Contact force between helicals and core therefore increases from zero at the grip end to maximum at distance L_T. Friction force from the helicals, which arises due to the change in twist and bending of the helicals, also rises from zero at grip end, where strand geometry is unchanged under load, to that established in the analysis at distance L_T. Assumptions have been made about relative motion between core and helical wires over this length (see Fig. 6.4). However, more detailed analysis of the manner in which strand geometry, load sharing between wires and stress distribution within wires changes over the transition length could start with the equations of Costello et al. (16, 17, 18), for a thin rod. See A.8.3 to A.8.8.

Contact force from the core is given by X, from 6.48.

There are no other external forces along the wire $\therefore$ Y = 0.

There are no external bending moments along the wire $\therefore$ K = K' = 0.

Over the transition length, the helix angle changes from α_0, where it is embedded in the socketing medium, to α_1, at distance L_T from the end of the grip.

Fig. 6.7 shows a helical wire over the transition length L_T of the strand as unwrapped onto a flat plane. Over an elemental wire length of δs, helix angle changes $\delta\alpha$. If curvature over this length, δs, is 1/k, then in the limit

$$k = d\alpha/ds \qquad 6.59$$

Figure 6.7. Helical Wire over Transition Length.

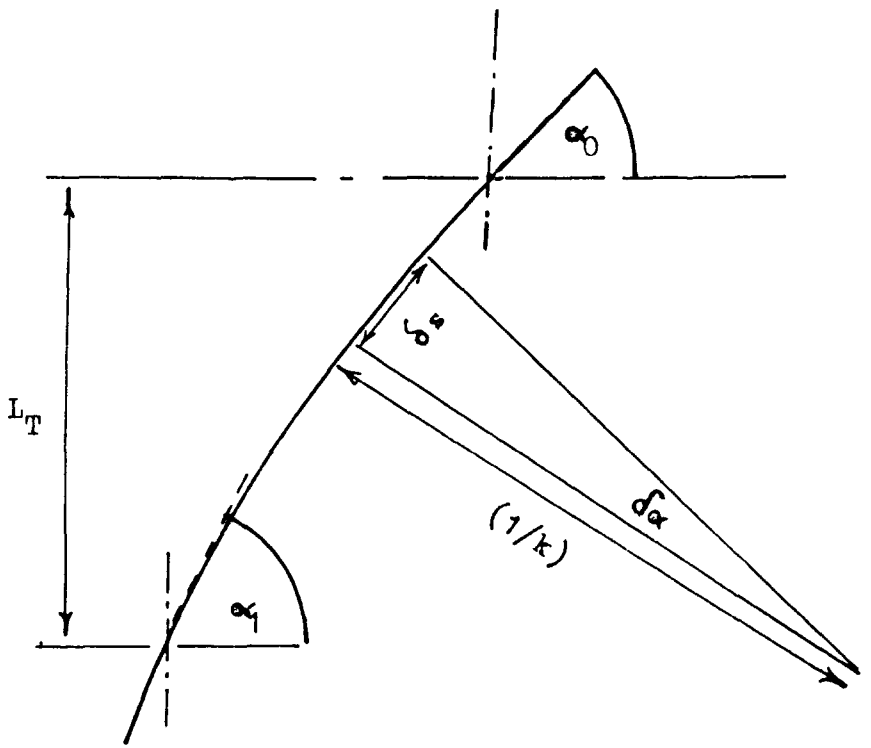

Now bending moment in this plane is given by Costello and Phillips (18) A.8.9 as

$$G = A(k - k_o) \qquad 6.60$$

where k_o is initial curvature, equal to zero inside grip, and

$$A = EI_h \qquad 6.61$$

From 6.59 and 6.60

$$G = Ad\alpha/ds \qquad 6.62$$

Differentiating $$\frac{dG}{ds} = Ad^2\alpha/ds^2 \qquad 6.63$$

If each elemental length is regarded as part of a helix, each element having a progressively different geometry from that of the adjacent element, the analysis developed in section 6.3, which considers friction force without slip, or that developed in section 6.4, which considers slip with friction, can be applied. The general equilibrium equations for a thin rod as postulated by Costello and Phillips (18), see Appendix A.8, A.8.3 to A.8.8, can be modified to apply to this transition length of strand L_T.

$$\frac{dN}{d\alpha}\frac{d\alpha}{ds} - N'\tau + Tk' + X = 0 \qquad 6.64$$

$$\frac{dN'}{d\alpha}\frac{d\alpha}{ds} - T\frac{d\alpha}{ds} + N\tau = 0 \qquad 6.65$$

$$\frac{dT}{d\alpha}\frac{d\alpha}{ds} - Nk' + N'\frac{d\alpha}{ds} + Z = 0 \qquad 6.66$$

$$A \frac{d^2\alpha}{ds^2} - G'_H + H_H k' - N' = 0 \qquad 6.67$$

$$\frac{dG'_H}{d\alpha} \frac{d\alpha}{ds} - H_H \frac{d\alpha}{ds} + A \frac{d\alpha}{ds} \tau + N = 0 \qquad 6.68$$

$$\frac{dH_H}{d\alpha} \frac{d\alpha}{ds} - A \frac{d\alpha}{ds} k' + G'_H \frac{d\alpha}{ds} + \Theta = 0 \qquad 6.69$$

The external force parallel to the wire axis, per unit length of the helical wire is given by

$$Z = F'_{HAF} (d_h/2) C_S \qquad 6.70$$

and the external torque is given by

$$\Theta = F'_{HTF} (d_h/2) C_S \qquad 6.71$$

where C_S can vary from 1, with no slip to zero with 100% slip.

F'_{HAF} and F'_{HTF} can be expressed in terms of the helix angle α and wire diameters (see expressions 6.28 to 6.37) since G'_A (G') and H_A (H) are themselves expressed in terms of final (loaded) and original (unloaded) helix angles.

Equation 6.69 can therefore be expressed in terms of three variables α, C_S and $d\alpha/ds$.

The end conditions for the transition length L_T are given at grip $\alpha = \alpha_o$, $\frac{d\alpha}{ds} = 0$, $C_S = 0$, and at distance L_T from the grip, $\alpha = \alpha_1$, $\frac{d\alpha}{ds} = 0$, $C_S > 0$.

Numerical methods are required to solve this and/or other

equations among the equilibrium equations 6.64 to 6.69, in an attempt to determine strand geometry, load sharing between wires and stress distribution over this transitional length. As indicated in the title to this section, the above constitute only the preliminaries to such an investigation. Its continuation is among those items suggested as worthy of future study.

6.7 Computation

6.7.1 Introduction

A first attempt involved programming in BASIC computing language on a Systime PDP11 computer belonging to the Mechanical Engineering Department. However, it soon became obvious that the degree of precision inherent in BASIC and the capacity of the computer were inadequate for the task. For the practical strand geometries considered - those tested in the programme described in Chapter 5 - the differences in strand response between the predictions of Durelli and the computed predictions were eventually found to be as much as 4.3% for extension, at about 35% of breaking load, (see table 6.1). But the strand geometry differences were no more than 0.02^{o} on helix angle and 0.005 mm on helix radius. For the larger helix angles and lower loads these differences were much less. For accurate execution of the iterative computing processes, discrimination of these geometry parameters had to be many orders of magnitude less than these differences. The use of FORTRAN with double precision was therefore found to be necessary. The problem of computer capacity limitation was overcome by using the University's VAX computer.

6.7.2 First Approximations

For a seven wire strand of known initial geometry and material, response under axial load can be calculated according to Machida and Durelli (27) as a first approximation. The basis of their treatment is given in Appendix A.9.

Expressions used in the computation are given below.

In the fixed end case, for the strand,

axial strain $\varepsilon = F/A$ 6.72

torque generated $M = FC/A$ 6.73

In the free end case, for the strand

axial strain $\varepsilon = FD/(AD-BC)$ 6.74

Rotation $\phi = F2\pi C/(AD-BC)$ 6.75

6.7.3 Other Expressions Required in Computation

From 6.49 and 6.50 axial load on strand is given by

$$P0 = P1 + P2 + P3 + P4 + P5 + P6 \qquad 6.76$$

where

$$\left.\begin{aligned} P1 &= T_C \\ P2 &= 6\pi A_h/\sin\alpha_1 \\ P3 &= M/r_1\tan\alpha_1 \\ P4 &= -M/r_1\tan\alpha_1 \\ P5 &= 6\sin\alpha_1 H/r_1\tan\alpha_1 \\ \text{and}\quad P6 &= 6\cos\alpha_1 G'/r_1\tan\alpha_1 \end{aligned}\right\} \qquad 6.77$$

and axial moment on strand is given by

$$M = Y1 + Y2 + Y3 + Y4 + Y5 + Y6 \qquad 6.78$$

where

$$\left.\begin{aligned} Y1 &= -Pr_1\tan\alpha_1 \\ Y2 &= T\, r_1\tan\alpha_1 \\ Y3 &= 6\xi EA_h r_1/\cos\alpha_1 \\ Y4 &= M_C \\ Y5 &= 6\sin\alpha_1 H \\ \text{and}\quad Y6 &= 6\cos\alpha_1 G' \end{aligned}\right\} \qquad 6.79$$

From 6.53, 6.54 and 6.57

$$LHS = RHS \quad \text{where}$$

$$\left.\begin{aligned} LHS &= E(\gamma(d_c+d_h\sin\alpha_o/\sin\alpha_1) + r_o\tan\alpha_o/\tan\alpha_1) \\ \text{and}\quad RHS &= r_o(1-\tan\alpha_o/\tan\alpha_1) - d_h(\sin\alpha_o/\sin\alpha_1 - 1) \end{aligned}\right\} \qquad 6.80$$

The expressions 6.53, 6.54 and 6.57 are also used individually.

6.7.4 Wire Flattening

Hamlet (76) conducted some tests in which he pressed together two solid steel cylinders of identical diameter. The axes of the cylinders were fixed for each test at an angular displacement relative to each other which varied from 90^{o} to zero (i.e. parallel axes). The last of these approximates closest to the case of a helical wire in contact with the core of a strand in that there is line contact rather than point contact before load is applied, although the line is a helix and not straight. Hamlet's results indicate an approximately bilinear relation between normal load and the flattening of the cylinder over the relevant load range, the first line, at low loads, exhibiting low stiffness and, after a short transition, the second line is much steeper as stiffness increases by almost an order of magnitude. Hamlet's work is not claimed as anything more than a preliminary study on the flattening effect of contact load and the diameter of cylinders tested was nearly twice that of the diameter of wire in the strands tested, as described in Chapter 5. (Hamlet's rods 6.35 mm; strand wire 3.94 mm core and 3.73 mm helical). However, since it seemed worthwhile making some estimate of the effect of wire flattening on strand response, the stiffness figures from Hamlet's work were inserted in the programming where appropriate. The flattening term in 6.58 can be given as

$$\delta_X = X/S_X \qquad 6.81$$

where X is the contact force per unit length (kN/mm) and δ_X is

the stiffness (kN/mm^2). The values of stiffness, from Hamlet, used in the computation were

(Separate computation on strand response was performed for each value of S_X.) $\left[\begin{array}{l} S_X = 1.25\ kN/mm^2 \\ \quad \text{or} \\ S_X = 12.5\ kN/mm^2 \end{array}\right]$ 6.82

Equation 6.58 is used in the computation, instead of 6.57 when wire flattening is taken into account.

6.7.5 Fixed End Case (See Flowchart, Fig. 6.8)

Details of strand dimensions (α, d_c and d_h), material constants (ν and E), strand loading (P) and,if required, wire flattening stiffness (S_X) and restraining factors (Z_1 and Z_2) are supplied in II. After preliminary calculations on strand geometry, first approximations on axial strain ξ, (6.72) torque generated M (6.73) and helix angle under load α_1 (6.54) are determined in III. Since helix radius under load r_1 has not been calculated at this stage, r, is assumed to equal r_o in 6.54. On entering loop IV to XV, axial strain ξ from III, first time, or from XVb, subsequently, are used to calculate α_1 (6.54), ξ (6.53) and r_1 (6.57) in IV. Lines V and VI set up the loop VII to XI in which a range of helix angles greater than α_1 from IV are examined, in increments of 10^{-9} radians with a view to satisfying strand geometry for this axial strain. In VII, ξ is determined from 6.53, r_1 from 6.57 or 6.58, depending on whether or not wire flattening is considered, and 6.80 is used in the second line (LHS = RHS etc.). Loop VIII to IX is designed

Figure 6.8.FLOWCHART:STRAND RESPONSE-FIXED END LOADING.

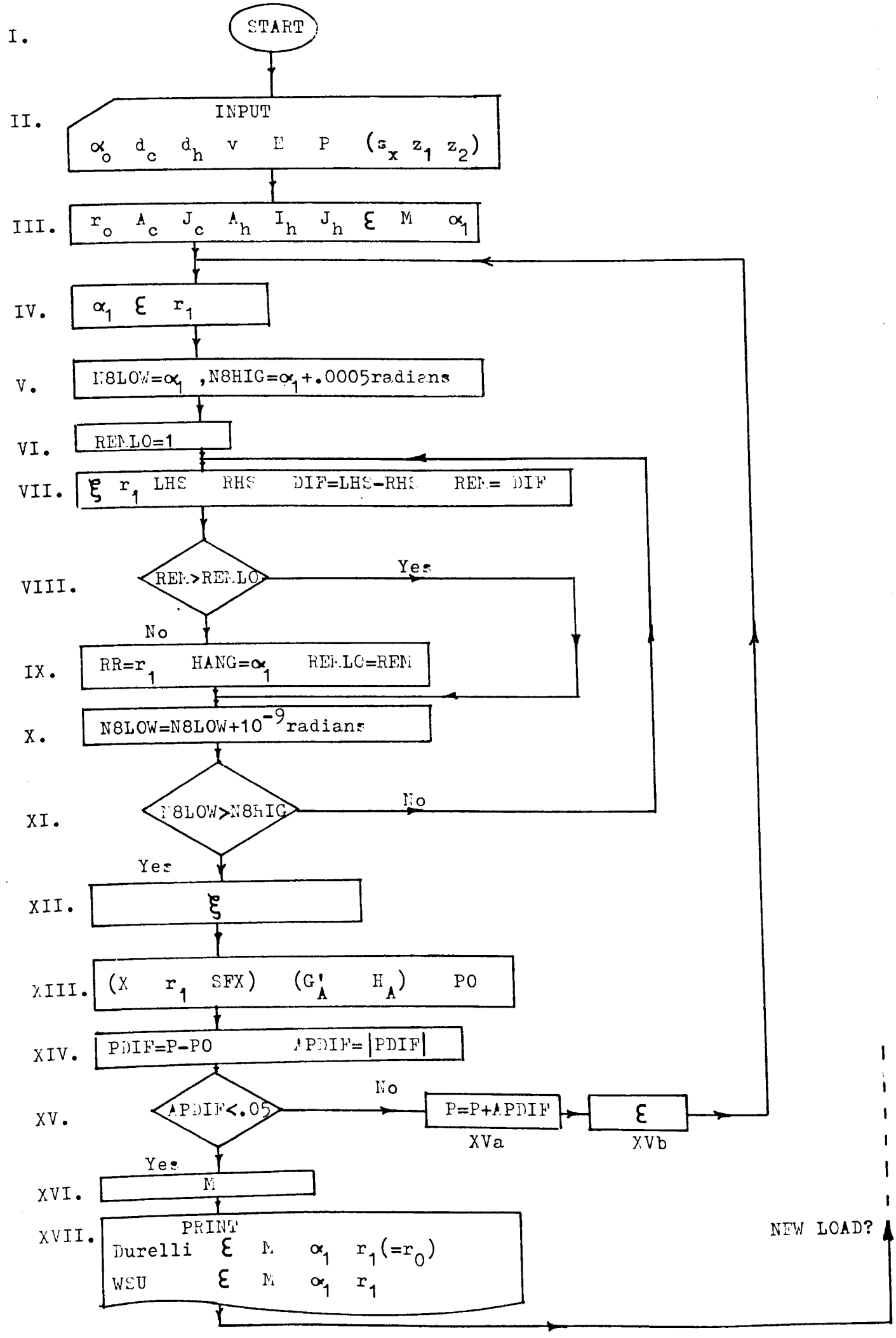

to retain the strand geometry (α_1 and r_1) which give minimum rotation - which should be zero - and this geometry is used in XII to determine ξ from 6.53. The axial load PO is calculated from 6.76, in XIII, using M from III in the fourth term of 6.76. (The use of the Durelli approximation for M at this stage is justified in the last paragraph of this section). If friction between wires is not considered, G' and H are substituted in 6.76. If friction is considered G'_A from 6.36 and H_A from 6.37 are substituted in 6.76. If flattening is considered, contact force X from A.8.17 (no friction) or from 6.48 (friction) is used in 6.81 to determine δ_X which is then used in 6.58 to determine r_1 before substitution in 6.76. Where the load calculated, PO, is different from the required load, P, by more than 0.05 kN, as determined in XIV, the Durelli approximation is used to determine extension (6.72) for a higher load and the process repeated in loop IV to XV until the strand geometry under load matches the required load.

The use of M from the Durelli and Machida approximation in the determination of axial load PO in XIII can be justified as follows. Of the parameters involved in strand response, torque generated (M) changes least when the more accurate analysis is complete since most of this torque comes from the tangential component of force in the helical wires. Helix angle difference ($.007^o$) and helix radius change (0.001 mm) under 10 kN load have an effect of less than 0.01 Nm on the restraining torque M. (Typically, restraining torque is about 8.9 Nm for a 10 kN axial

load for strand VI). The value for restraining torque is determined for the final strand geometry in XVI from (6.78). Printout gives the Durelli and Machida results as well as those computed as above, for comparison.

6.7.6 Free End Case (See Flowchart Fig. 6.9)

Details of strand dimensions, (α, d_c and d_h), material constants (ν and E), strand loading (P) and, if required, wire flattening stiffness (S_X) and restraining factors (Z_1 and Z_2) are supplied in II. After preliminary calculations on strand geometry, first approximation on strand rotation ϕ, (6.75) is calculated in III. Axial strain (6.74), helix angle under load α_1 (from 6.54 but assuming $r_1 = r_o$ at this stage), helical wire strain ξ (6.53) and helix radius r_1 (from 6.57 if flattening is not considered and 6.58 if it is considered) are determined in IV. Helix angle α_1 is then calculated again (6.54) using helix radius r_1 just calculated. Helical wire strain is calculated in V and the loop V to VI pursued until the change in $\xi < 10^{-9}$. Restraining torque M is then checked in VII, from (6.78), the fifth and sixth terms of which include H and G' respectively if interwire friction is neglected, or H_A and G'_A from (6.36) and (6.37) respectively if friction is taken into account. Restraining torque M should be zero in the free end case and helix angle α_1 is increased in VIIIa, in loop V to VIII until $M < 0.001$ Nm. Applied load PO is checked in IX from 6.76 for the strand geometry under load which has just been computed. If this differs from the original (required) load

Figure 6.9. FLOWCHART: STRAND RESPONSE-FREE END LOADING.

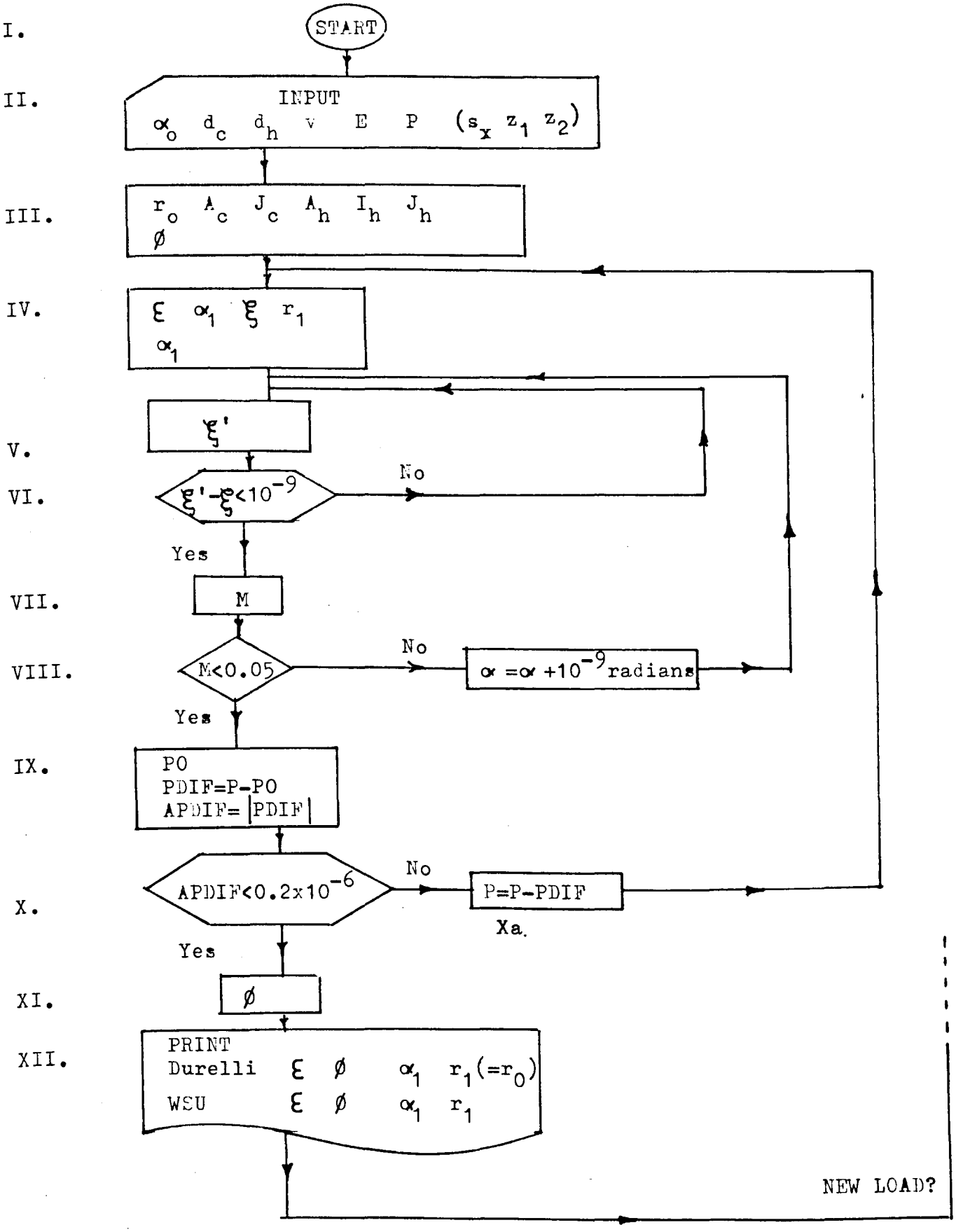

by more than 0.2×10^{-6} kN, loop IV to X is computed again with a different starting load. If applied load is within this limit, rotation from 6.54 is calculated in XI and printout given for comparison of these results with those of the Machida and Durelli predictions.

6.8 Computation: Results and Discussion

6.8.1 Results (See tables 6.1, to 6.7)

The programmes, described in sections 6.7.5 and 6.7.6 and flowcharts Figs 6.8 and 6.9, were used to predict strand response for strands having the same geometries as those of the five strands tested in the programme described in Chapter 5. For each strand both fixed and free end cases were examined and, for each end condition, both the frictionless (100% slip) and no slip condition, each with and without wire flattening, were considered. Flattening effect was examined for wire flattening stiffness values of both 12.5 kN/mm^2 and 1.25 kN/mm^2 of wire. Twelve sets of results were thus obtained for each strand geometry, as seen in the tables 6.1 and 6.2. Load increments are 10 kN up to a maximum of 40 kN, this being the maximum load applied to the strands under end conditions of partial and zero (free end) torsional restraint, in the tests described in Chapter 5.

The following sections of this chapter discuss the results from these computations. Comparison between computed predictions and experimental results is dealt with fully in Chapter 7.

As shown in Chapter 5, sections 5.1 and table 5.1, the helix angle of strand VI was found to be different from the nominal value by more than 4%. The computed predictions for a strand with helix angle 72.97°, as measured are given in tables 6.5 to 6.7.

6.8.2 Fixed End Case

(i) Extension (See table 6.1 and 6.5)

Axial stiffness is predicted to be effectively constant, increasing by no more than 0.02%. This is a decrease of 0.02% in compliance ($\mu\varepsilon$/kN) as tabulated, over the load range considered.

For the frictionless condition, predictions greater than those of Durelli range from about 1.32% at the helix angle of 80.87° to within ± 0.02 of 4.67% at the helix angle of 72.97°. If friction is taken into account excess over the Durelli predictions is reduced to about 1.30% at helix angle of 80.87° and to 4.59% at helix angle 72.97°. The effect of wire flattening on extension is predicted to be in no case greater than 0.02%. (i.e.The difference between the figure for "No flattening" and that for a flattening factor "S_x=1.25", at any given load and for either the "100% slip" or the "no slip" condition, does not exceed 0.02%.)

(ii) Restraining Torque (See table 6.3 and 6.6)

For the reasons given in section 6.7.5, predictions on the magnitude of the restraining torque can be expected to vary very little from those of Machida and Durelli. Tables 6.2.a and 6.4.a are a check that the differences are small and negative. The increased helix angle and reduced helix radius of the strand under load give a reduced tangential force component and moment arm. The maximum reduction of 0.125% is negligible when comparison is to be made with experimental results.

6.8.3 Free End Case

(i) Extension (See table 6.2 and 6.5.b)

Extension and helix angle changes under load are greater in the free end case than the fixed end case. Computed predictions on extension are in all cases less than those of Machida and Durelli (27). The difference between computed predictions and those of Machida and Durelli increases for all strands as load is increased, but in no case exceeds 1.0% for the load range considered. (Maximum is 0.98% at 40 kN load for $\alpha = 76.16^{\circ}$ in the no slip case when wire flattening is neglected). Greater differences are predicted for the non-slip case than for the frictionless (100% slip) case. The effect of wire flattening is greater in the free end case than the fixed end case, but is still not greater than 0.13% (-0.74 to -0.87 in $\alpha = 72.97^{\circ}$ for 40 kN load, see table 6.5.b).

(ii) Rotation (See table 6.4 and 6.7)

Computed predictions in all cases exceed those of Machida and Durelli (27) but never by more than 1.1% and it is only at low loads (10 kN) for the two strands with initial helix angles of 78.93° and 80.87° that the excess over the Durelli predictions is greater than 0.6%. Within the small overall differences, the effects of friction and flattening are negligible for the range of loads considered.

TABLE 6.1 COMPUTED STRAND EXTENSIONS: FIXED END CASE

Table shows percentage difference from prediction of Machida and Durelli (27)

Axial Load (kN)		10	20	30	40
$\alpha_o = 73.63^\circ$		*M. & D. $\varepsilon = 72.16 \mu\varepsilon/kN$			
100% slip	No flattening	+4.31	+4.31	+4.31	+4.30
	$S_X = 12.5$	+4.31	+4.31	+4.31	+4.30
	$S_X = 1.25$	+4.31	+4.30	+4.30	+4.29
No slip	No flattening	+4.25	+4.24	+4.24	+4.23
	$S_X = 12.5$	+4.25	+4.24	+4.24	+4.23
	$S_X = 1.25$	+4.24	+4.23	+4.22	+4.22
$\alpha_o = 76.16^\circ$		*M. & D. $\varepsilon = 70.02 \mu\varepsilon/kN$			
100% slip	No flattening	+3.06	+3.06	+3.05	+3.05
	$S_X = 12.5$	+3.06	+3.05	+3.05	+3.04
	$S_X = 1.25$	+3.04	+3.04	+3.04	+3.04
No slip	No flattening	+3.01	+3.01	+3.01	+3.00
	$S_X = 12.5$	+3.01	+3.01	+3.01	+3.00
	$S_X = 1.25$	+3.01	+3.00	+3.00	+3.00

Table 6.1 (continued)

Axial Load (kN)		10	20	30	40
$\alpha_o = 77.70^o$		*M. & D. $\xi = 68.92 \mu\xi/kN$			
100% slip	No flattening	+2.41	+2.40	+2.40	+2.40
	S_X = 12.5	+2.41	+2.40	+2.40	+2.40
	S_X = 1.25	+2.41	+2.40	+2.40	+2.39
No slip	No flattening	+2.37	+2.37	+2.36	+2.36
	S_X = 12.5	+2.37	+2.37	+2.36	+2.36
	S_X = 1.25	2.37	+2.37	+2.36	+2.36
$\alpha_o = 78.93^o$		*M. & D. $\xi = 68.15 \mu\xi/kN$			
100% slip	No flattening	+1.94	+1.94	+1.94	+1.94
	S_X = 12.5	+1.94	+1.94	+1.94	+1.94
	S_X = 1.25	+1.94	+1.94	+1.94	+1.93
No slip	No flattening	+1.91	+1.91	+1.91	+1.91
	S_X = 12.5	+1.91	+1.92	+1.91	+1.91
	S_X = 1.25	+1.91	+1.91	+1.91	+1.91
$\alpha_o = 80.87^o$		*M. & D. $\xi = 67.11 \mu\xi/kN$			
100% slip	No flattening	+1.33	+1.32	+1.32	+1.31
	S_X = 12.5	+1.33	+1.33	+1.33	+1.32
	S_X = 1.25	+1.31	+1.32	+1.32	+1.31
No slip	No flattening	+1.30	+1.30	+1.29	+1.29
	S_X = 12.5	+1.30	+1.30	+1.29	+1.29
	S_X = 1.25	+1.29	+1.29	+1.29	+1.29

* M. & D. is Machida and Durelli prediction.
Units of wire stiffness (resistance to flattening), S_X in kN/mm^2

TABLE 6.2 COMPUTED STRAND EXTENSIONS: FREE END CASE

Table shows percentage difference from prediction of Machida and Durelli (27)

Axial Load (kN)		10	20	30	40
$\alpha_o = 73.63^o$		*M. & D. $\varepsilon = 135.85 \mu\varepsilon/kN$			
100% slip	No flattening	**	**	-0.25	-0.53
	$S_X = 12.5$	**	**	-0.23	-0.52
	$S_X = 1.25$	**	**	-0.13	-0.42
No slip	No flattening	-0.07	-0.35	-0.63	-0.91
	$S_X = 12.5$	-0.05	-0.34	-0.62	-0.89
	$S_X = 1.25$	**	-0.23	-0.51	-0.79
$\alpha_o = 76.16^o$		*M. & D. $\varepsilon = 118.06 \mu\varepsilon/kN$			
100% slip	No flattening	**	-0.15	-0.40	-0.65
	$S_X = 12.5$	**	-0.14	-0.40	-0.65
	$S_X = 1.25$	**	-0.08	-0.33	-0.59
No slip	No flattening	-0.23	-0.48	-0.73	-0.98
	$S_X = 12.5$	-0.22	-0.47	-0.72	-0.96
	$S_X = 1.25$	-0.15	-0.40	-0.65	-0.90

*M. & D. is Machida and Durelli prediction.
Units of wire stiffness (resistance to flattening), S_X in kN/mm^2
**Indicates 0>%difference>-0.005

Table 6.2 (Continued)

Axial Load (kN)		10	20	30	40
$\alpha_o = 77.70^o$		*M. & D. $\xi = 107.99 \mu\xi/kN$			
100% slip	No flattening.	**	-0.22	-0.45	-0.67
	$S_X = 12.5$	**	-0.22	-0.44	-0.67
	$S_X = 1.25$	**	-0.17	-0.40	-0.62
No slip	No flattening	-0.28	-0.51	-0.73	-0.95
	$S_X = 12.5$	-0.28	-0.50	-0.72	-0.94
	$S_X = 1.25$	-0.23	-0.45	-0.68	-0.90
$\alpha_o = 78.93^o$		*M. & D. $\xi = 100.48 \mu\xi/kN$			
100% slip	No flattening	-0.04	-0.25	-0.45	-0.65
	$S_X = 12.5$	-0.04	-0.24	-0.45	-0.65
	$S_X = 1.25$	-0.04	-0.21	-0.42	-0.62
No slip	No flattening	-0.30	-0.50	-0.70	-0.90
	$S_X = 12.5$	-0.29	-0.50	-0.69	-0.89
	$S_X = 1.25$	-0.26	-0.46	-0.66	-0.86
$\alpha_o = 80.87^o$		*M. & D. $\xi = 89.77 \mu\xi/kN$			
100% slip	No flattening	-0.08	-0.25	-0.41	-0.57
	$S_X = 12.5$	-0.08	-0.25	-0.41	-0.57
	$S_X = 1.25$	-0.06	-0.23	-0.39	-0.55
No slip	No flattening	-0.28	-0.44	-0.60	-0.76
	$S_X = 12.5$	-0.28	-0.44	-0.60	-0.76
	$S_X = 1.25$	-0.26	-0.42	-0.58	-0.74

* M. & D. is Machida and Durelli prediction
Units of wire stiffness (resistance to flattening), S_X in kN/mm^2
**Indicates $0 > \%\text{difference} > -0.005$

TABLE 6.3 COMPUTED STRAND TORQUE GENERATED: FIXED END CASE

Table shows percentage difference from prediction of Machida and Durelli (27)

Axial Load (kN)		10	20	30	40
$\alpha_o = 73.63^o$		*M. & D. M = 0.887 Nm/kN			
100% slip	No flattening	-0.104	-0.104	-0.104	-0.105
	S_X = 12.5	-0.104	-0.105	-0.105	-0.105
	S_X = 1.25	-0.104	-0.104	-0.105	-0.105
No slip	No flattening	-0.106	-0.106	-0.106	-0.106
	S_X = 12.5	-0.106	-0.106	-0.106	-0.106
	S_X = 1.25	-0.106	-0.106	-0.106	-0.106
$\alpha_o = 76.16^o$		*M. & D. M = 0.749 Nm/kN			
100% slip	No flattening	-0.053	-0.053	-0.053	-0.053
	S_X = 12.5	-0.053	-0.053	-0.053	-0.053
	S_X = 1.25	-0.052	-0.053	-0.053	-0.053
No slip	No flattening	-0.053	-0.054	-0.053	-0.053
	S_X = 12.5	-0.053	-0.054	-0.053	-0.053
	S_X = 1.25	-0.053	-0.053	-0.053	-0.053

Table 6.3 (continued)

Axial Load (kN)		10	20	30	40
$\alpha_o = 77.70^o$			*M. & D. M = 0.665 Nm/kN		
100% slip	No flattening	-0.032	-0.033	-0.033	-0.033
	S_X = 12.5	-0.032	-0.033	-0.033	-0.033
	S_X = 1.25	-0.033	-0.033	-0.033	-0.033
No slip	No flattening	-0.033	-0.033	-0.033	-0.033
	S_X = 12.5	-0.033	-0.033	-0.033	-0.033
	S_X = 1.25	-0.033	-0.033	-0.033	-0.033
$\alpha_o = 78.93^o$			*M. & D. M = 0.598 Nm/kN		
100% slip	No flattening	-0.022	-0.011	-0.021	-0.021
	S_X = 12.5	-0.021	-0.021	-0.021	-0.022
	S_X = 1.25	-0.022	-0.021	-0.021	-0.021
No slip	No flattening	-0.022	-0.022	-0.022	-0.022
	S_X = 12.5	-0.021	-0.022	-0.022	-0.022
	S_X = 1.25	-0.021	-0.022	-0.022	-0.021
$\alpha_o = 80.87^o$			*M. & D. M = 0.493 Nm/kN		
100% slip	No flattening	-0.005	-0.009	-0.010	-0.010
	S_X = 12.5	-0.005	-0.009	-0.010	-0.010
	S_X = 1.25	-0.005	-0.010	-0.010	-0.010
No slip	No flattening	-0.005	-0.010	-0.005	-0.010
	S_X = 12.5	-0.005	-0.010	-0.005	-0.010
	S_X = 1.25	-0.004	-0.010	-0.010	-0.010

TABLE 6.4 COMPUTED STRAND ROTATION: FREE END CASE

Table shows percentage difference from prediction of Machida and Durelli (27)

Axial Load (kN)		10	20	30	40
$\alpha_o = 73.63^o$		*M. & D. $\phi = 68.52 \times 10^{-6}$ rads/kN/mm			
100% slip	No flattening	+0.078	+0.056	+0.125	+0.115
	$S_X = 12.5$	+0.078	+0.056	+0.112	+0.109
	$S_X = 1.25$	+0.081	+0.059	+0.133	+0.113
No slip	No flattening	+0.347	+0.208	+0.121	+0.124
	$S_X = 12.5$	+0.359	+0.196	+0.120	+0.109
	$S_X = 1.25$	+0.081	+0.224	+0.126	+0.114
$\alpha_o = 76.16^o$		*M. & D. $\phi = 61.22 \times 10^{-6}$ rads/kN/mm			
100% slip	No flattening	+0.068	+0.234	+0.129	+0.123
	$S_X = 12.5$	+0.068	+0.245	+0.131	+0.129
	$S_X = 1.25$	+0.069	+0.221	+0.140	+0.120
No slip	No flattening	+0.446	+0.221	+0.129	+0.104
	$S_X = 12.5$	+0.459	+0.227	+0.127	+0.118
	$S_X = 1.25$	+0.413	+0.215	+0.126	+0.116

Table 6.4 (continued)

Axial Load (kN)		10	20	30	40
$\alpha_o = 77.70^o$		*M. & D. $\phi = 56.07 \times 10^{-6}$ rads/kN/mm			
100% slip	No flattening	+0.065	+0.283	+0.164	+0.137
	$S_X = 12.5$	+0.065	+0.269	+0.142	+0.132
	$S_X = 1.25$	+0.066	+0.276	+0.147	+0.134
No slip	No flattening	+0.479	+0.247	+0.172	+0.136
	$S_X = 12.5$	+0.554	+0.270	+0.155	+0.116
	$S_X = 1.25$	+0.449	+0.255	+0.159	+0.150
$\alpha_o = 78.93^o$		*M. & D. $\phi = 51.59 \times 10^{-6}$ rads/kN/mm			
100% slip	No flattening	+0.606	+0.344	+0.177	+0.144
	$S_X = 12.5$	+0.562	+0.343	+0.177	+0.160
	$S_X = 1.25$	+0.560	+0.342	+0.180	+0.145
No slip	No flattening	+0.684	+0.305	+0.174	+0.135
	$S_X = 12.5$	+0.578	+0.329	+0.178	+0.161
	$S_X = 1.25$	+0.609	+0.335	+0.167	+0.146
$\alpha_o = 80.87^o$		*M. & D. $\phi = 43.87 \times 10^{-6}$ rads/kN/mm			
100% slip	No flattening	+0.983	+0.512	+0.250	+0.243
	$S_X = 12.5$	+1.038	+0.551	+0.286	+0.233
	$S_X = 1.25$	+1.071	+0.536	+0.265	+0.221
No slip	No flattening	+1.112	+0.520	+0.278	+0.256
	$S_X = 12.5$	+1.041	+0.460	+0.240	+0.190
	$S_X = 1.25$	+0.936	+0.472	+0.239	+0.217

TABLE 6.5 COMPUTED STRAND EXTENSIONS

(HELIX ANGLE = 72.97°)

(a) FIXED END

Axial Load (kN)		10	20	30	40
	M. & D. ε = 72.79 $\mu\varepsilon$/kN				
100% slip	No flattening	+4.68	+4.68	+4.67	+4.67
	S_X = 12.5	+4.68	+4.68	+4.67	+4.66
	S_X = 1.25	+4.67	+4.67	+4.66	+4.65
No slip	No flattening	+4.61	+4.60	+4.60	+4.59
	S_X = 12.5	+4.61	+4.60	+4.60	+4.59
	S_X = 1.25	+4.60	+4.59	+4.59	+4.58

(b) FREE END

M. & D. ε = 140.69 $\mu\varepsilon$/kN

100% slip	No flattening	**	**	-0.19	-0.48
	S_X = 12.5	**	**	-0.19	-0.48
	S_X = 1.25	**	**	-0.19	-0.48
No slip	No flattening	-0.01	-0.30	-0.58	-0.87
	S_X = 12.5	**	-0.28	-0.57	-0.86
	S_X = 1.25	**	-0.16	-0.45	-0.74

TABLE 6.6 COMPUTED STRAND TORQUE GENERATED (HELIX ANGLE = 72.97°)

(FIXED END)

Axial Load (kN)		10	20	30	40
M. & D. M = 0.923 Nm/kN					
100% slip	No flattening	-0.123	-0.123	-0.123	-0.123
	S_X = 12.5	-0.123	-0.123	-0.123	-0.123
	S_X = 1.25	-0.123	-0.123	-0.123	-0.123
No slip	No flattening	-0.124	-0.124	-0.124	-0.125
	S_X = 12.5	-0.124	-0.125	-0.124	-0.125
	S_X = 1.25	-0.125	-0.124	-0.125	-0.125

TABLE 6.7 COMPUTED STRAND ROTATION (HELIX ANGLE = 72.97°)

(FREE END)

Axial Load (kN)		10	20	30	40
M. & D. ϕ = 70.19 x 10^{-6} rads/kN/mm					
100% slip	No flattening	+0.081	+0.060	+0.119	+0.115
	S_X = 12.5	+0.081	+0.060	+0.121	+0.115
	S_X = 1.25	+0.081	+0.060	+0.122	+0.115
No slip	No flattening	+0.355	+0.193	+0.110	+0.111
	S_X = 12.5	+0.082	+0.205	+0.119	+0.118
	S_X = 1.25	+0.085	+0.197	+0.121	+0.112

CHAPTER 7

COMPARISON OF EXPERIMENTAL RESULTS AND MATHEMATICAL MODELLING

7.1 Introduction

In this chapter, the experimental results obtained from the main test programme, described in Chapter 5, are compared with the theoretical predictions on strand response to tensile load which are obtained from the theories described in Chapter 6. The response characteristics of torque generated, strand extension, strand rotation and wire surface strains are examined in turn. The degree of agreement with test results of the predictions of Durelli et al. (27) is compared with that computed from the theory which, starting with the basis of the theory on six wire strand, after Costello et al. (17, 18, 19), also takes account of a core wire and the effects of change in helix angle under load, interwire friction, Poisson effects and wire flattening due to contact pressure.

7.2 Torque Generated

A description is given in section 5.3.1 of how the data was acquired on torque generated in the strand, from load cell output, and the treatment of results is given in section 5.5.7. The load/torque plots from the test programme are given in Figs 5.25 to 5.30 and the load/torque characteristics for each strand are given in table 5.13.

Theory is developed in sections 6.2 to 6.5 and the computation method described in section 6.7. Fig. 6.8, gives the flowchart for the computation of predictions of strand response in the fixed end case and tables 6.3 and 6.6 give the difference between computed predictions and those of Durelli et al. (27). As explained also in section 6.8.2(ii), the difference between the predictions of Durelli and those computed is always less than 0.13% and for this reason no distinction between them is made when theoretical and experimental results are compared in table 7.1. Valid comparison of theory and the experimental results must take account of the small strand rotation resulting from elastic deformation of the resin in strand terminations, or even some breakup of the resin at the throat of the terminations. As reported in Chapter 5, section 5.5.7, this strand rotation was measured during the nominally fixed end tests. For the loading cycle which immediately followed the free and partially restrained loading cycle, the theoretical prediction for torque generated was corrected as follows:

$$M_C = M_{FX}(1 - \phi_{FX}/\phi_{FR}) \qquad 7.1$$

where M_{FX} is the torque generated in a fixed end loading over the load range considered (10 kN to 44 kN) and calculated from Chapter 6 (tables 6.3 and 6.6), $\varnothing_{FX}$ and $\varnothing_{FR}$ are the measured rotations during the period of increasing load for the nominally fixed end and completely free end cycles respectively. Table 7.1 compares experimental values of torque generated with uncorrected (fixed end) and corrected values predicted for the strand geometries concerned, including both nominal and measured configurations for strand VI. Note that no rotation was measured during cycle 310 for strand X. The comparatively large rotations recorded during the loading of strands VI and VII, cycles 113 and 512 respectively, are probably due to deterioration of the resin, particularly at the throat of the end grip, caused during the greater number of free end and partially restrained loading cycles to which these strands were subjected. (See loading programme in table 5.3).

The tabulated results show that predictions overestimate the torque generated by an amount which increases as initial strand helix angle reduces.

These and other comparisons of theory and experiment are discussed further in section 7.6.

TABLE 7.1 TORQUE GENERATED: COMPARISON OF THEORY AND EXPERIMENT

Strand Number	Torque Generated (Durelli) Nm/kN M_D	Torque Generated (Computed) Nm/kN M_{FX}	Rotation Measured Over 600mm 10kN-50kN (Cycle No.)	Corrected Torque Prediction Nm/kN M_C	Experimental Torque Nm/kN M_{EX}	Difference $(1-M_C/M_{EX})$
(i)	(ii)	(iii)	(iv)	(v)	(vi)	(vii)
VI Measured VI Nominal	0.923 0.887	0.922 0.886	2.2° (113)	0.899 0.864	0.86 0.86	-4.5% -0.5%
VIII (76.2°)	0.749	0.748	0.8° (210)	0.740	0.72	-2.8%
X (77.7°)	0.665	0.665	0 (310)	0.665	0.65	-2.3%
IX (78.9°)	0.598	0.598	0.8° (410)	0.591	0.58	-1.9%
VII (80.9°)	0.493	0.493	2.0° (512)	0.475	0.47	-1.1%

7.3 Strand Extension

The extrometer was used to measure strand extension throughout the loading programme and results tabulated, an example of which is shown in table 5.5. Computer printout on the analysis of load/extension slope, of the type shown in table 5.12 and the graph plotting facility of the computer used to obtain plots of the type shown in Figs 5.8 and 5.9.

Mathematical modelling on strand response in Chapter 6 takes account of interwire friction, Poisson effects, wire flattening and the effect of increasing helix angle under load. The differences between these predictions and those from the simpler theory of Durelli et al. (27) are given in tables 6.1 and 6.2, at a strand load of 40 kN.

Experimental results are compared with computed predictions and those of Durelli in table 7.2. The Durelli prediction is calculated in each case from equation A.8.21 and the computed predictions are explained in Chapter 6 ; an example of the best straight line analysis by least squares is shown in table 5.12. Graphs of extension against torsional restraint are plotted for each strand in Figs 7.1 to 7.6. In order to give valid comparison with the predicted extensions, which are for a load of 40 kN, the load/extension slope is taken from table 5.12 (for strand VI) at 40 kN, and from the corresponding tabulated printouts for other strands at 40 kN. In each case the slope value is taken at 40 kN in the loading cycle during which 40 kN load is exceeded for the first time. For strand VI,

TABLE 7.2 STRAND EXTENSIONS, PREDICTED AND EXPERIMENTAL

STRAND LOAD 40 kN

Strand No.	DURELLI PREDICTIONS		COMPUTED PREDICTIONS					TEST RESULTS		Nominal End Condition
	Torsional End Restr. Nm/kN	Extension $\mu\varepsilon$/kN	Torsional End Restr. Nm/kN	Extension 100% Slip N.F. $\mu\varepsilon$/kN	Extension 100% Slip F. $\mu\varepsilon$/kN	Extension No Slip N.F. $\mu\varepsilon$/kN	Extension No Slip F. $\mu\varepsilon$/kN	Torsional End Restr. Nm/kN	Extension $\mu\varepsilon$/kN	
(i)	(ii)	(iii)	(iv)	(v)	(vi)	(vii)	(viii)	(ix)	(x)	(xi)
VI 73.0° (Measured)	0.92 *(0.89)	72.8 *(72.2)	0.92 *(0.89)	76.2 *(75.3)	76.2 *(75.3)	76.1 *(75.2)	76.1 *(75.2)	0.86 0.59 0.43 0.22	80.3 103.8 108.4 119.5	Fixed ¾ Fix ½ Fix ¼ Fix
73.6°* (Nominal)	0	140.7 *(135.9)	0	140.0 *(135.1)	140.2 *(135.3)	139.4 *(134.6)	139.6 *(134.8)	0	134.6	Free
VIII 76.2°	0.75	70.0	0.75	72.2	72.1	72.1	72.1	0.72 0.54 0.35 0.13	73.9 83.7 92.7 108.2	Fixed ¾ Fix ½ Fix ¼ Fix
	0	118.1	0	117.3	117.4	116.9	117.0	-0.03	115.2	Free

Table 7.2 (Continued)

Strand No.	DURELLI PREDICTIONS		COMPUTED PREDICTIONS					TEST RESULTS		Nominal End Condition
				Extension						
				100% Slip		No Slip				
	Torsional End Restr. Nm/kN	Extension με/kN	Torsional End Restr. Nm/kN	N.F. με/kN	F. με/kN	N.F. με/kN	F. με/kN	Torsional End Restr. Nm/kN	Extension με/kN	
(i)	(ii)	(iii)	(iv)	(v)	(vi)	(vii)	(viii)	(ix)	(x)	(xi)
X 77.7°	0.66	68.9	0.66	70.6	70.6	70.5	70.5	0.65	73.0	Fixed
								0.47	82.1	$\frac{3}{4}$ Fix
								0.29	90.5	$\frac{1}{2}$ Fix
								0.12	99.0	$\frac{1}{4}$ Fix
	0	108.0	0	107.3	107.3	107.0	107.0	-0.05	107.9	Free
IX 78.9°	0.60	68.2	0.60	69.5	69.5	69.4	69.4	0.58	69.5	Fixed
								0.45	76.6	$\frac{3}{4}$ Fix
								0.30	81.8	$\frac{1}{2}$ Fix
								0.14	90.4	$\frac{1}{4}$ Fix
	0	100.5	0	99.8	99.9	99.6	99.6	0	95.8	Free
VII 80.9°	0.49	67.1	0.49	68.0	68.0	68.0	68.0	0.47	67.9	Fixed
								0.36	73.1	$\frac{3}{4}$ Fix
								0.24	77.9	$\frac{1}{2}$ Fix
								0.13	83.4	$\frac{1}{4}$ Fix
	0	89.8	0	89.3	89.3	89.1	89.1	0	88.4	Free

Note that predicted values of torque (columns (ii) and (iv)) and extension (columns (iii), (v), (vi), (vii) and (viii)) for partially restrained end conditions are pro rata between the fixed and free end values.

N.F. (columns (v) and (vii)). No flattening considered.
F. (columns (vi) and (viii)). Flattening is considered.

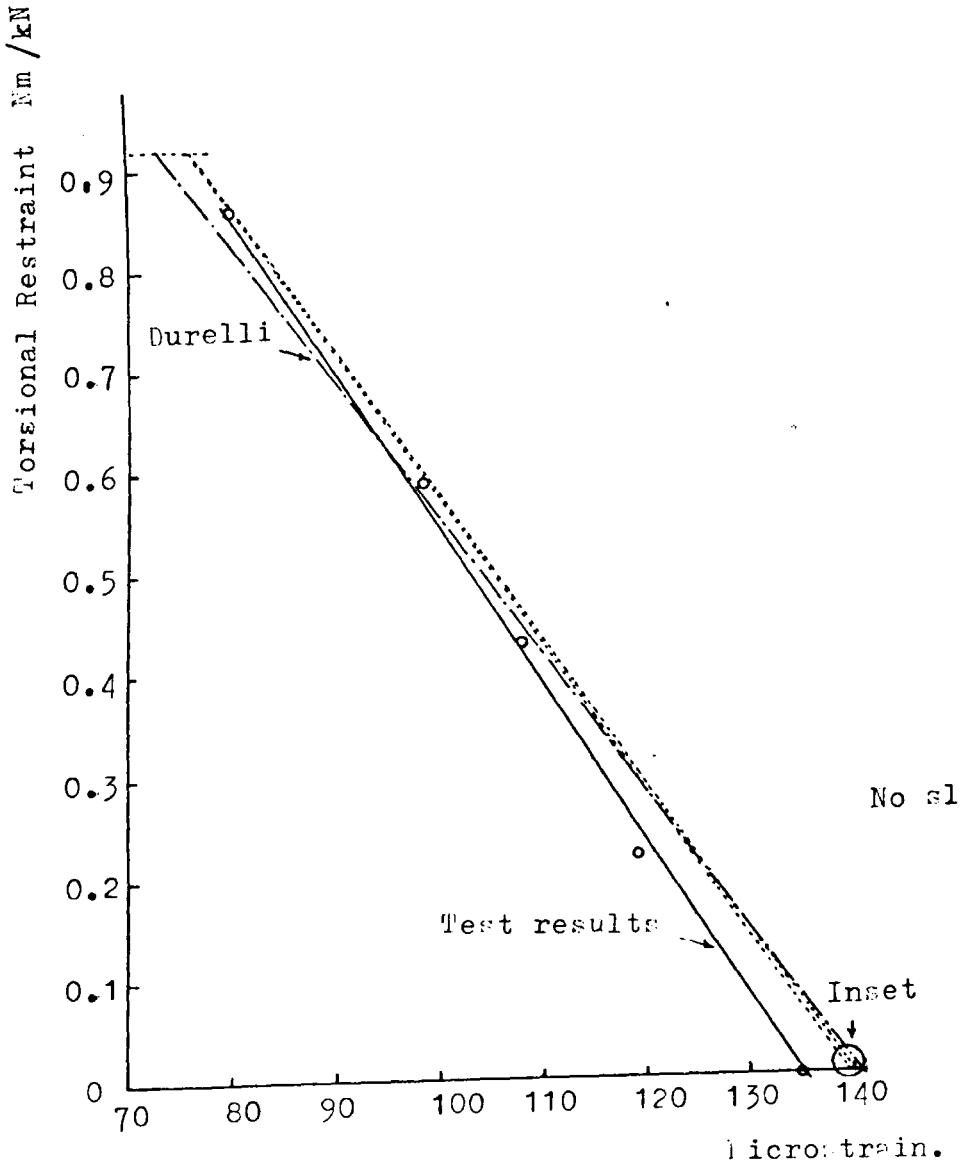

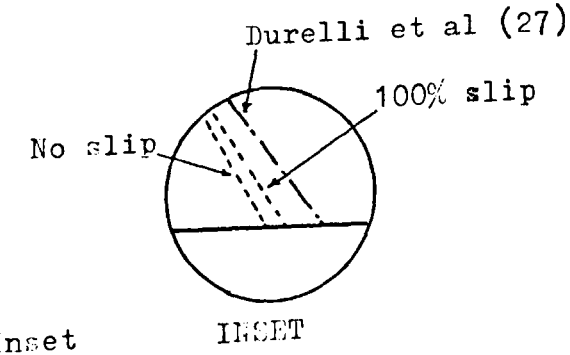

Figure 7.1. Torsional Restraint/Strand Extension.
(Strand VI. Measured Helix Angle 73.0°)

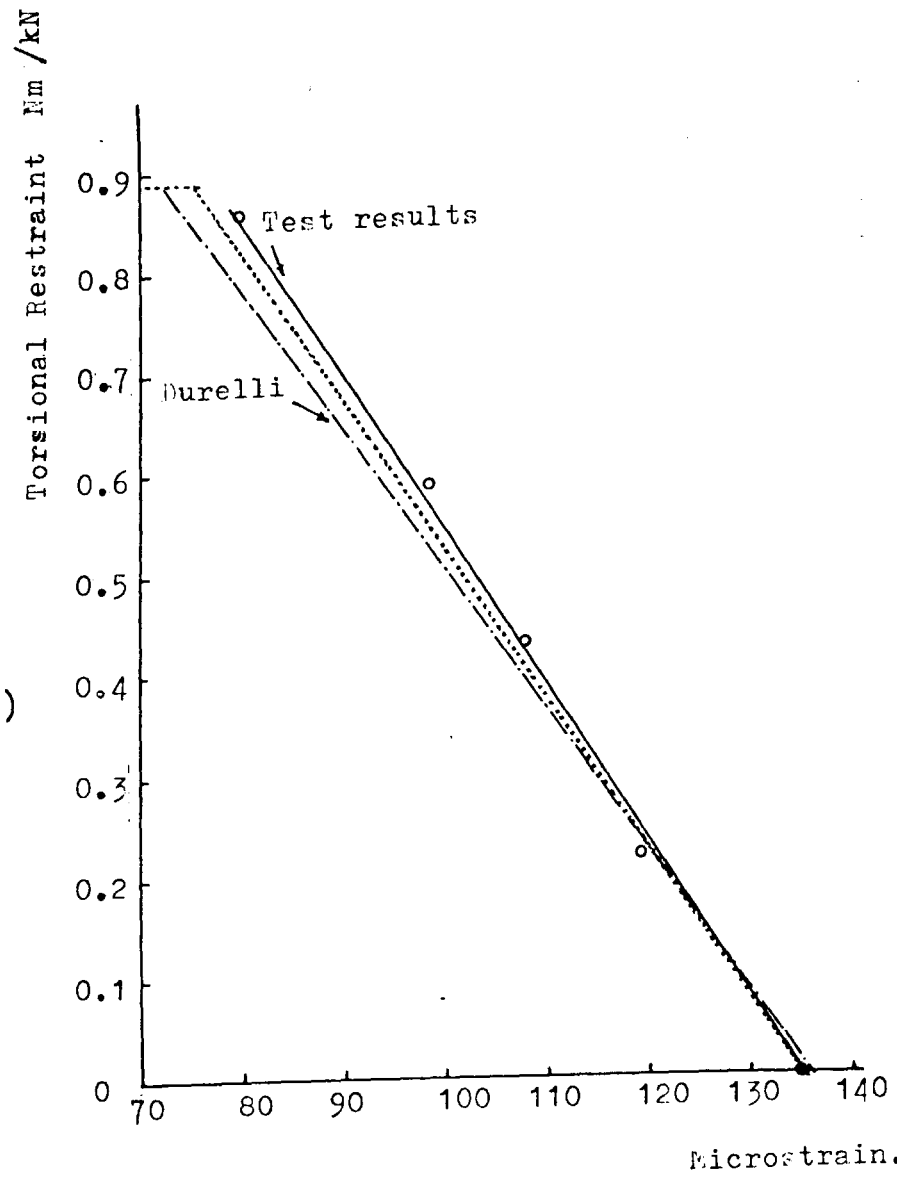

Figure 7.2. Torsional Restraint/Strand Extension.
(Strand VI. Nominal Helix Angle 73.6°)

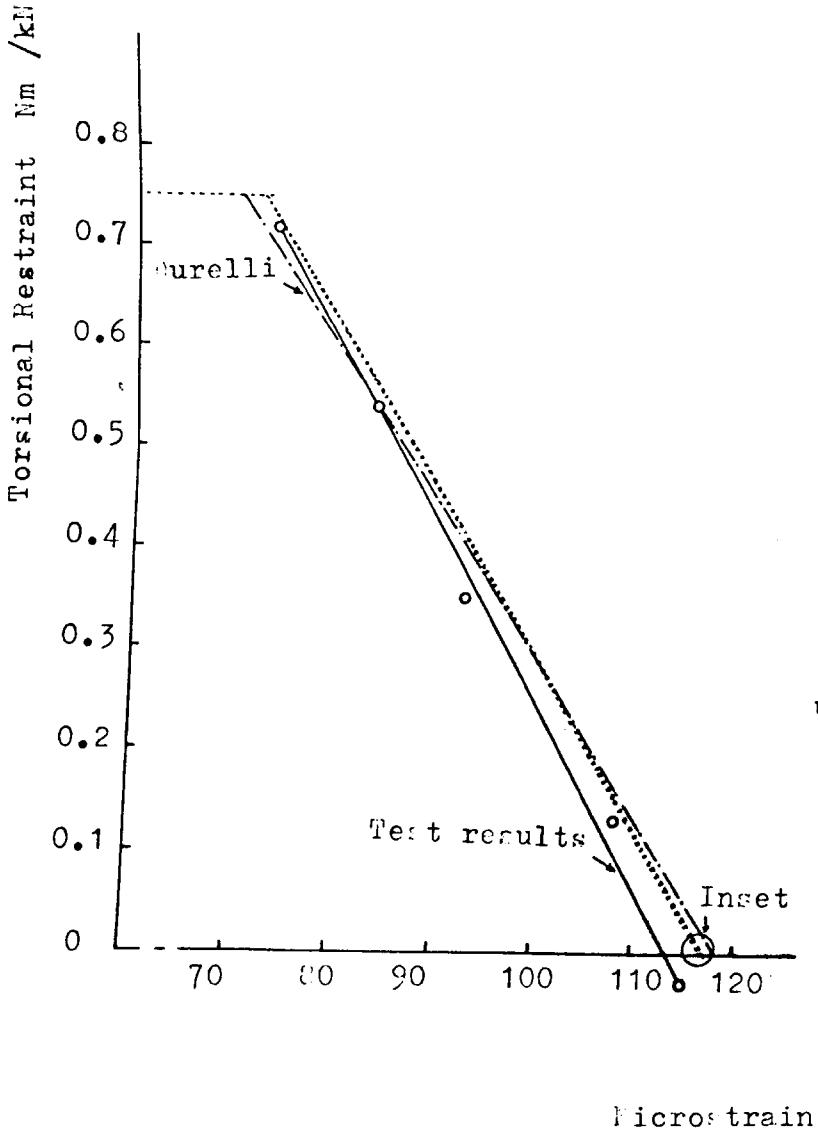

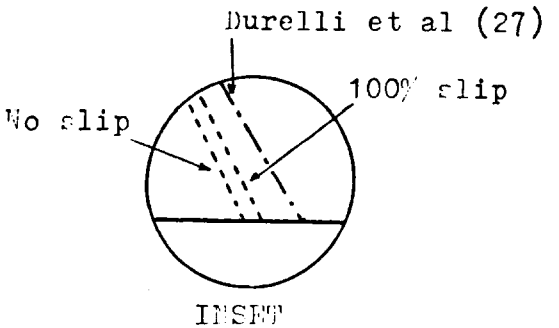

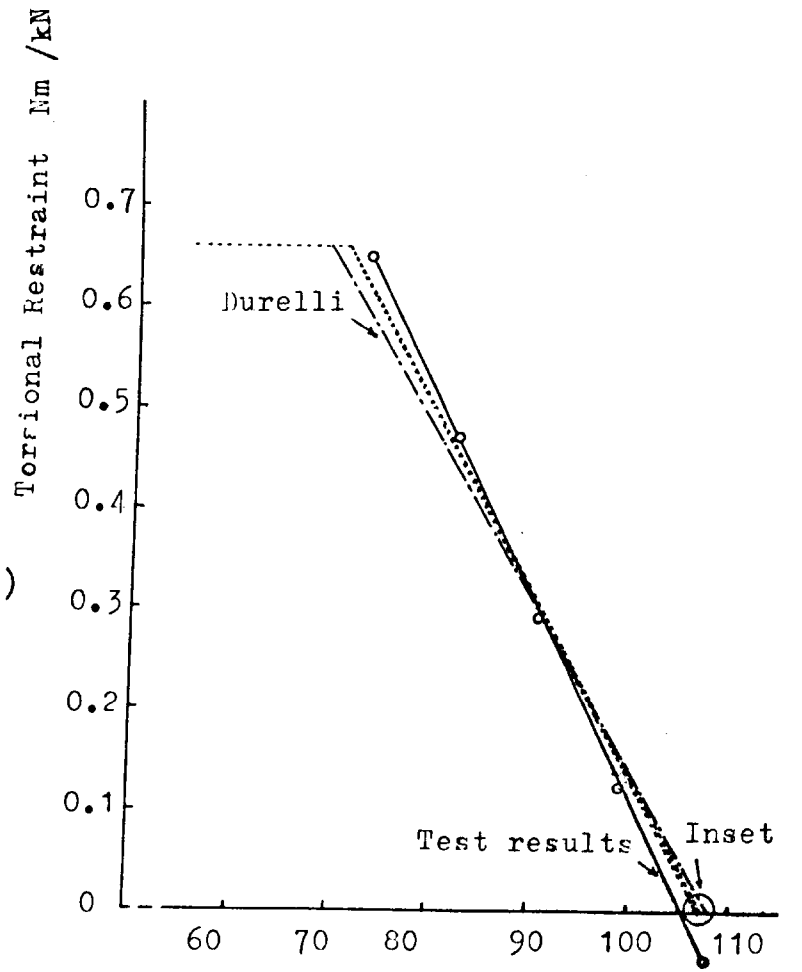

Figure 7.3.Torsional Restraint/Strand Extension.
(Strand Hill; Helix Angle 76.2°)

Figure 7.4.Torsional Restraint/Strand Extension.
(Strand X; Helix Angle 77.7°)

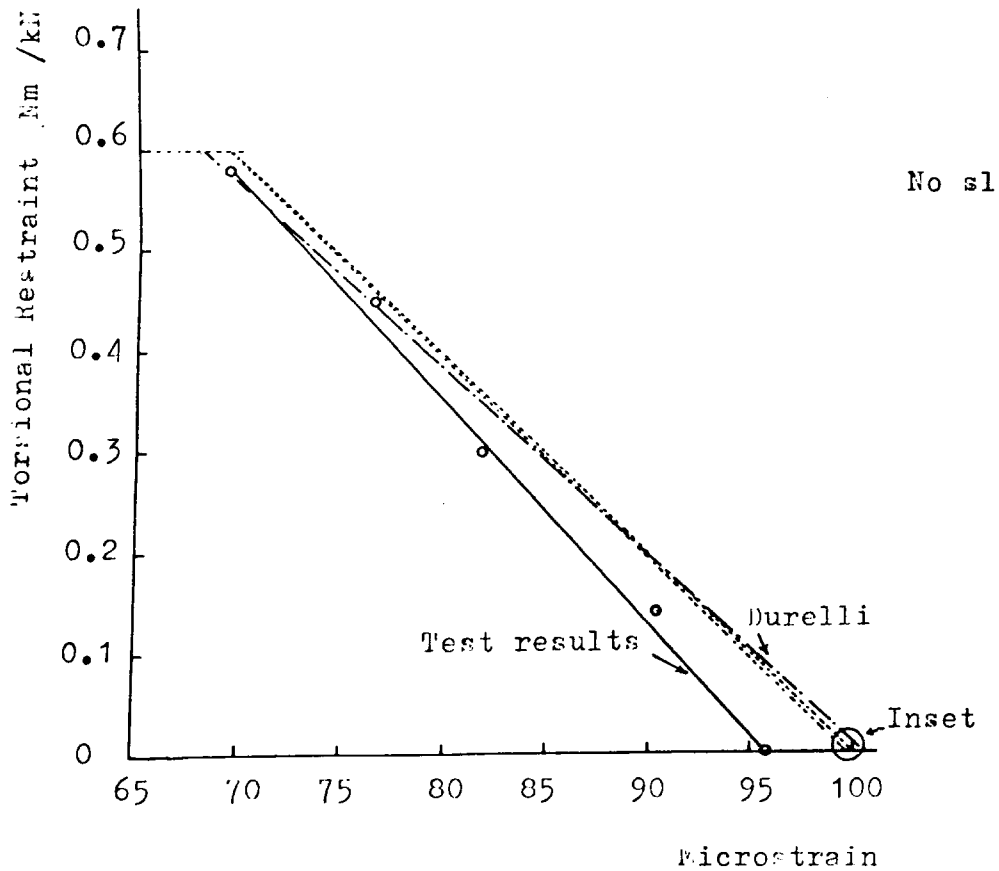

Figure 7.5.Torsional Restraint/Strand Extension.
(Strand IX; Helix Angle 78.9°)

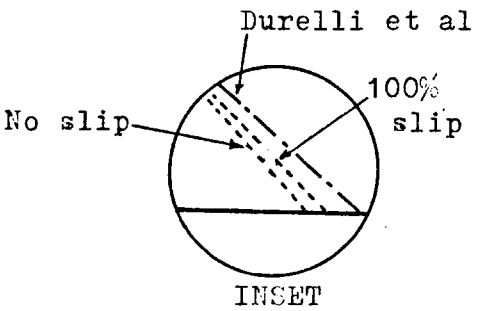

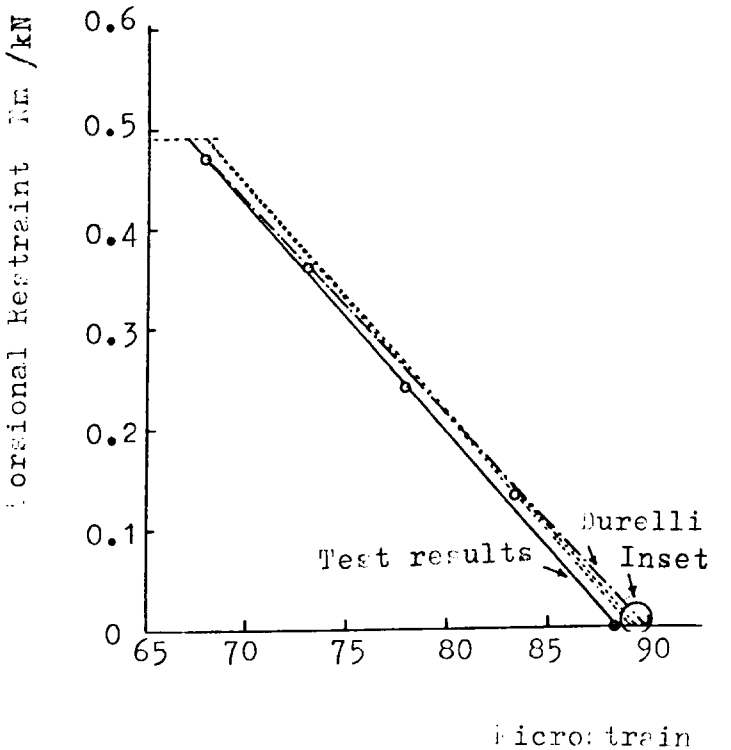

Figure 7.6.Torsional Restraint/Strand Extension.
(Strand VIII; Helix Angle 80.9°)

the experimental results are plotted against predictions for measured and nominal strand geometry. (Initial helix angles of 73.0^{o} and 73.6^{o}).

Examination of the graphs shows that a similar pattern occurs for all strands and that the predicted results for the strand VI as measured (Fig. 7.1) match the overall pattern better than do the results from the nominal strand (Fig. 7.2). Other conclusions that can be drawn from the graphs are given below.

(i) Extension is less than that predicted, under free end conditions and greater than that predicted under fixed end conditions.

(ii) The predictions of Durelli et al. (27) are less accurate than the computed predictions, as described in Chapter 6, sections 6.7 and 6.8.

(iii) Of the three theoretical predictions given, the slope of the torque/extension plot for the condition of zero interwire slip is the nearest to the slope of the test results.

(iv) Direct comparison of experimental results with the theory of Costello et al. (17, 18, 19) is not possible since they considered only 6 wire strand. However, the computed predictions of this study start with the assumption that core loading can be added to that of the six wire strand. (See Chapter 6, sections 6.1 to 6.4 and

particularly expressions 6.49 and 6.50). The 'Costello plus Core' prediction, which takes account of changing helix angle under load (which Durelli does not), but does not consider Poisson effects, interwire friction or flattening, can therefore be seen to lie between that of Durelli et al. (27) and those of this study. Costello can therefore be said to be closer to test results than Durelli but not as close as the predictions of this study.

Further discussion of strand extensions and other results is given in section 7.6.

7.4 Strand Rotation

Strand rotation in loading cycles with free and partially restrained ends was measured, using the extrometer, and results tabulated, an example of which is shown in table 5.6. Load/rotation slopes were analysed by the method of least squares and results tabulated in the same way as those for extension slopes, an example of which is shown in table 5.12.

These experimental results are compared with results from the mathematical modelling in table 7.3. They are also plotted in Figs 7.7 to 7.11. The difference between the predictions of Durelli and those which take account of friction, Poisson effects, wire flattening and the effect of helix angle change under load is very small. (See also tables 6.3 and 6.7). Discrimination between them is not possible on the graphs and a single line is therefore used in the plotted figures to show all predicted rotations.

Examination of the graphs (Figs 7.7 to 7.11) shows that a similar pattern occurs for all strands. The following conclusions can be drawn from these graphs.

(i) Rotation measured is less than that predicted by any of the theories.

(ii) The difference between measured rotation and theoretical predictions is greater, for each strand, as torsional restraint is reduced.

TABLE 7.3 STRAND ROTATIONS, PREDICTED AND EXPERIMENTAL

STRAND LOAD 40 kN

Strand No.	DURELLI PREDICTIONS		COMPUTED PREDICTIONS			TEST RESULTS		Nominal End Condition
	Torsional End Restr. Nm/kN	Rotation (rad/kN)/mm x10^6	Torsional End Restr. Nm/kN	Rotation 100% slip (rad/kN)/mm x10^6	Rotation No slip (rad/kN)/mm x10^6	Torsional End Restr. Nm/kN	Rotation (rad/kN)/mm x10^6	
(i)	(ii)	(iii)	(iv)	(v)	(vi)	(vii)	(viii)	(ix)
VI 73.0° (Measured)	0.92 *(0.89)	0 *(0)	0.92 *(0.89)	0 *(0)	0 *(0)	0.86 0.59 0.43 0.22	0 19.15 32.54 46.57	Fixed ¾ Fix ½ Fix ¼ Fix
* 73.6° (Nominal)	0	70.19 *(68.52)	0	70.27 *(68.60	70.22 *(68.55)	0	62.32	Free
VIII 76.2°	0.75	0	0.75	0	0	0.72 0.54 0.35 0.13	0 14.85 25.26 41.72	Fixed ¾ Fix ½ Fix ¼ Fix
	0	61.22	0	61.30	61.24	-0.03	55.63	Free
X 77.7°	0.66	0	0.66	0	0	0.65 0.47 0.29 0.12	0 14.39 26.69 40.67	Fixed ¾ Fix ½ Fix ¼ Fix
	0	56.07	0	56.15	56.09	-0.05	55.13	Free

Table 7.3 (Continued)

Strand No.	DURELLI PREDICTIONS		COMPUTED PREDICTIONS			TEST RESULTS		Nominal End Condition
	Torsional End Restr. Nm/kN	Rotation (rad/kN)/mm x10^6	Torsional End Restr. Nm/kN	Rotation		Torsional End Restr. Nm/kN	Rotation (rad/kN)/mm x10^6	
				100% slip (rad/kN)/mm x10^6	No slip (rad/kN)/mm x10^6			
(i)	(ii)	(iii)	(iv)	(v)	(vi)	(vii)	(viii)	(ix)
IX 78.9°	0.60	0	0.60	0	0	0.58	0	Fixed
						0.45	10.24	$\frac{3}{4}$ Fix
						0.30	22.56	$\frac{1}{2}$ Fix
						0.14	35.29	$\frac{1}{4}$ Fix
	0	51.59	0	51.66	51.65	0	47.19	Free
VII 80.9°	0.49	0	0.49	0	0	0.47	0	Fixed
						0.36	9.75	$\frac{3}{4}$ Fix
						0.24	21.03	$\frac{1}{2}$ Fix
						0.13	30.90	$\frac{1}{4}$ Fix
	0	43.87	0	43.96	43.96	0	40.52	Free

Note that predicted values of torque (columns (ii) and (iv)) and rotation (columns (iii), (v) and (vi)) for partially restrained end conditions are pro rata between the fixed and free end values.

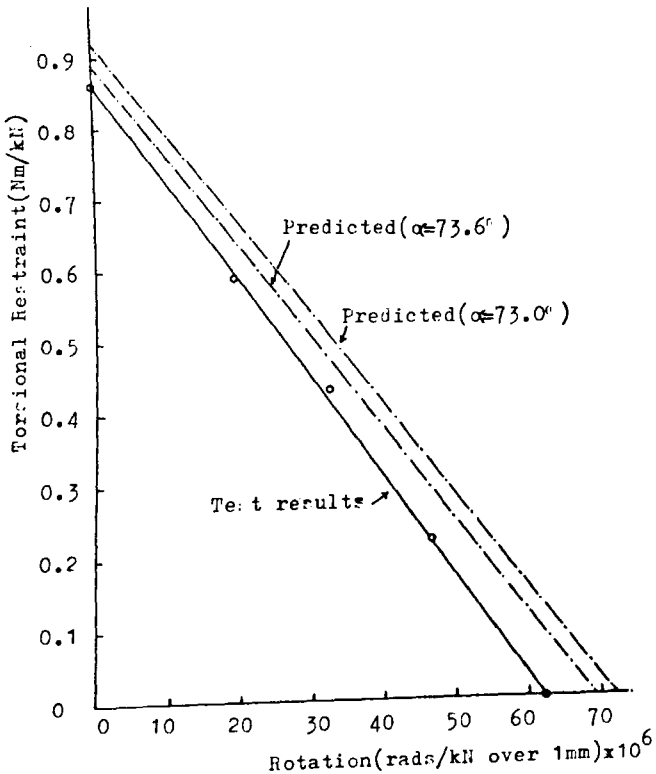

Figure 7.7.Torsional Restraint/Strand Rotation.
Strand VI.

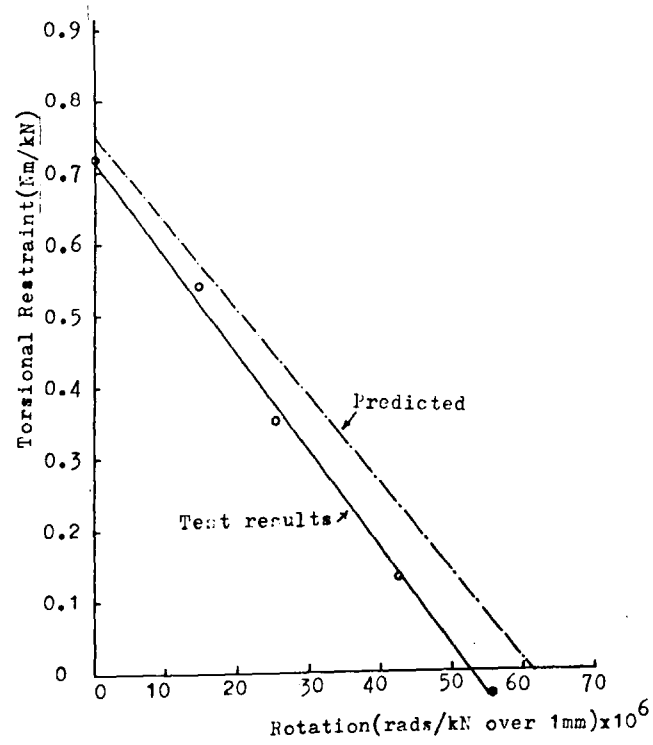

Figure 7.8.Torsional Restraint/Strand Rotation.
Strand VIII.

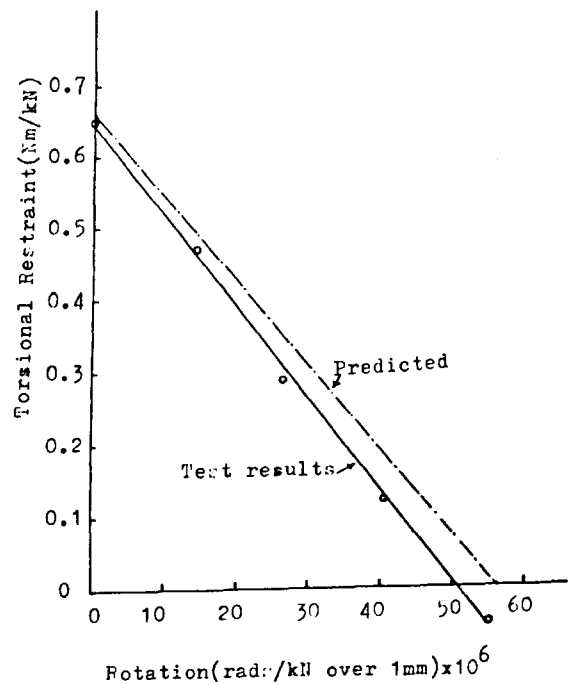

Figure 7.9.

Torsional Restraint/Strand Rotation.
Strand X.

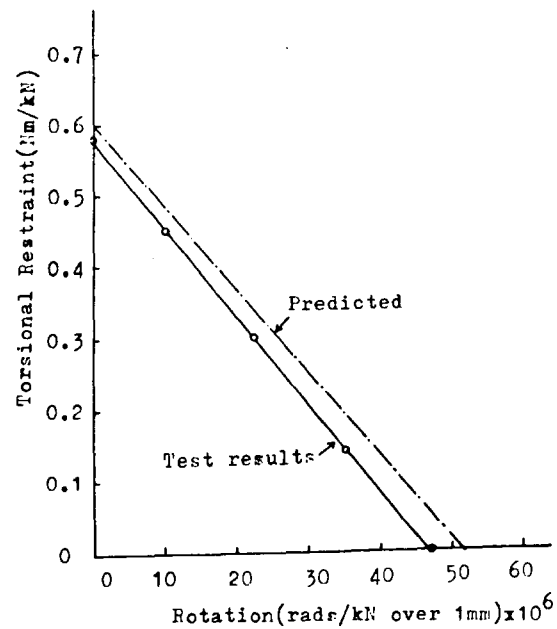

Figure 7.10.

Torsional Restraint/Strand Rotation.
Strand IX.

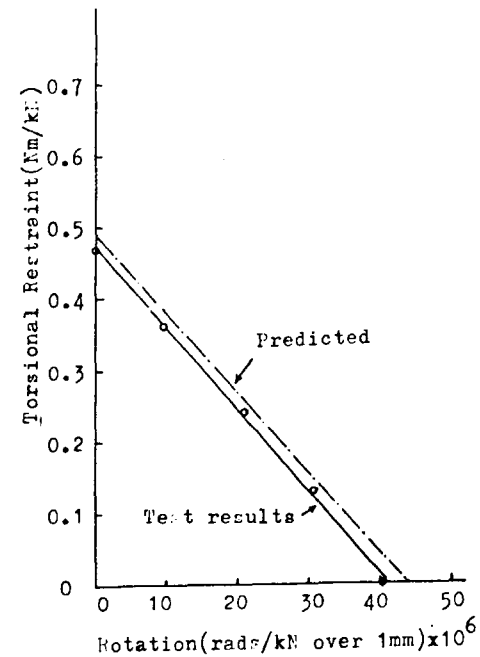

Figure 7.11.

Torsional Restraint/Strand Rotation.
Strand VII.

(iii) The difference between measured rotation and theoretical predictions is greater in strands with lower helix angles. From Fig. 7.7 it can be seen that this pattern is more consistent if the measured helix angle (73.0^{o}) is considered, rather than the nominal helix angle (73.6^{o}) for strand VI.

A mechanism which may account in part for the low values of measured rotation is shown in Fig. 7.12. Strand rotation, ϕ_S as measured by the extrometer, can be seen to be increased in the case where there is 100% slip, due to rotation of the helical wires about their own axes. (See Fig. 7.12(ii)). If there is no slip, torque transmitted from the helicals cause the core to be rotated by angle ϕ_c. (See Figs 6.2 and 6.4). Since contact is maintained between core and helicals while one rolls over the other, the configuration shown in Fig. 7.12(iii) ensues. Strand rotation, as measured by the extrometer, is now seen to be reduced. Two cases where slip does occur are shown in Figs 7.12(iv) (a) and (b). If slip is sufficiently large, measured rotation can exceed actual strand rotation.

Quantitative assessment of this effect is not attempted since the analysis depends on line contact between wires, whereas flattening of the wires results in an increasing contact area, rather than a line. The magnitude of the relative rotation between core and helicals is therefore impossible to determine. However, it can be seen that in the absence of slip between core and helicals, this reduction in the strand

Figure 7.12. Strand Rotation:Effect of Interwire Friction.

a Initial contact point (core)
b Initial contact point (helical)
c Contact with Extrometer.

ϕ_H=Component of Helical Wire Rotation on strand axis.
ϕ_C=Rotation of Core.
ϕ_s=Rotation of Extrometer.

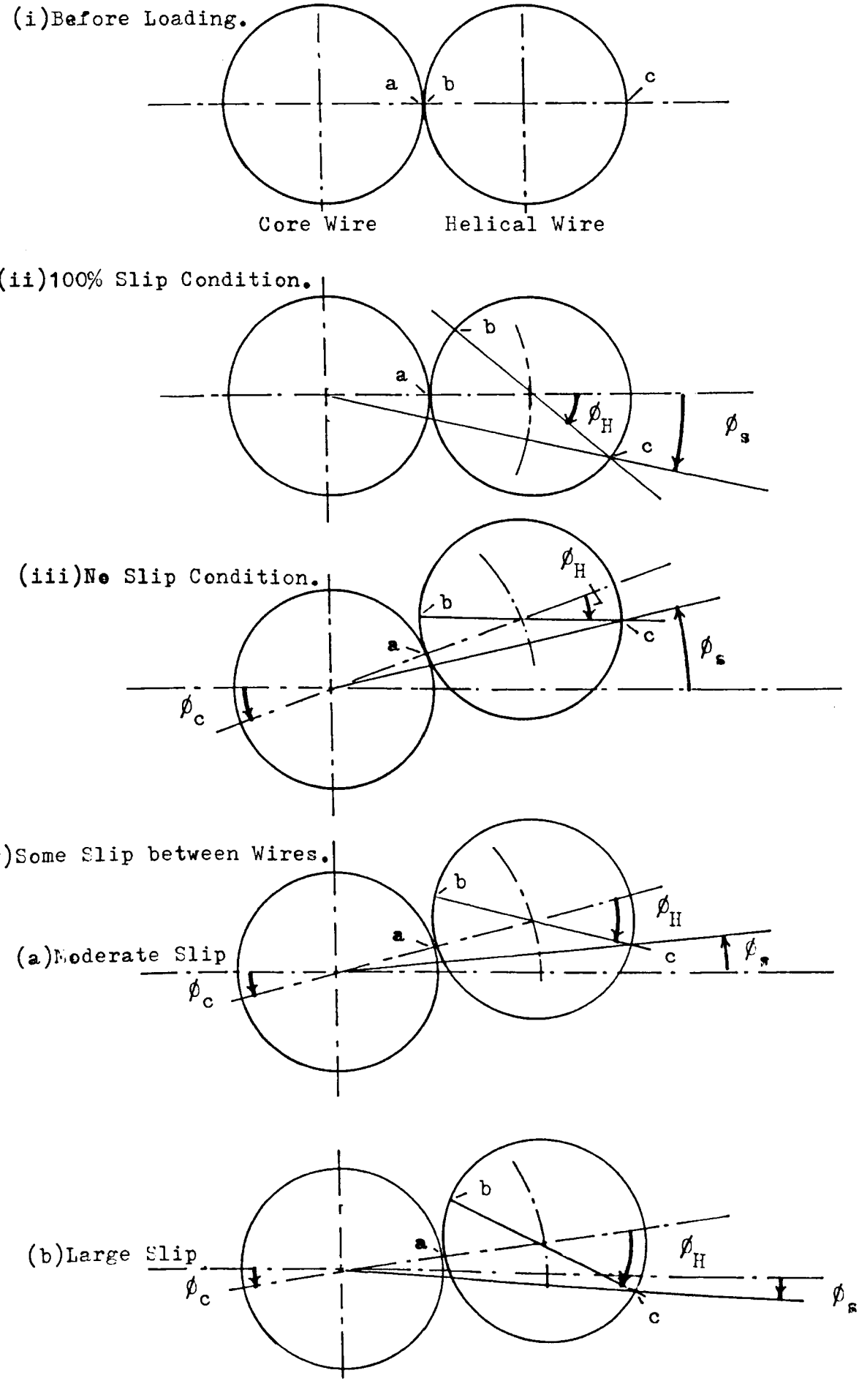

rotation is likely to be greater when the torque restrained by the core is greater, since a greater core rotation ϕ_c will occur. Results from table 7.1 show that overall torque generated in the strand is greater the lower the helix angle, for any given fraction of strand end restraint. Since this torque is generated in the helical wires, it is likely that more torque is transmitted to the core from the helicals in the strands with lower helix angles. This assumption appears valid from the results as noted in conclusion (iii) above.

7.5 Strains on Helical Wire Surface

Comparisons between theoretical predictions of surface strains parallel to helical wire axis and the strains measured in the strand tests are shown in table 7.4.

For the Durelli predictions torque is obtained from M in expression A.9.32 for the fixed end condition (see also table 7.1 column (ii) and table 7.2 column (ii)). Wire surface strain in the direction of helical wire axis (column (iii)) is given by

$$\xi_H = \xi - \xi_B \qquad 7.2$$

where ξ is strain at wire axis, obtained from strand strain in expression A.8.21 and ξ_B is strain due to wire bending under strand load given by

$$\xi_B = G' d_h / 2EI_h \qquad 7.3$$

where bending moment G' is obtained from Appendix A.8, expressions A.8.1, A.8.9 and A.8.10 and given by

$$G' = EI_h(\cos^2\alpha_1/r_1 - \cos^2\alpha_o/r_o) \qquad 7.4$$

Durelli does not consider change in helix radius and in this case

$$r_1 = r_o \qquad 7.5$$

The computed predictions on wire surface strain which take

account of Poisson effects and wire flattening due to radial interwire pressure are given in columns (v) and (vi) of table 7.4. The strand extensions at 40 kN axial load for zero interwire friction are given in table 7.2 column (vi) and strains at helical wire axis (ξ) are obtained by substituting these values in expression A.8.21. Bending strains ξ_B are given by expression 7.3. For 100% slip, G' is given by expression 7.4 and for the zero slip condition G'_A from 6.36 is substituted in 7.4 in place of G'.

Results from strain gauge outputs were tabulated for all loading cycles, examples of which are seen in tables 5.7 to 5.10 and the strand load/surface strain relations analysed by the method of least squares and tabulated in the same way as load/extension plots, an example of which is shown in table 5.12. Results from the slope plots for mean strain (six wires) at mid-strand and at strand end under conditions of fixed, partially restrained and free ends are given in table 7.4, columns (viii) and (ix), for gauges mounted parallel to the helical wire axis.

Examination of strain results in table 7.4 reveals that at mid-strand position (column (viii)), experimental values from tests in the fixed end condition lie between the predicted strains for 100% slip (column (v)) and no slip (column (vii)) conditions for only one of the five strands, (strand VI). For the free end condition, however, the experimental values of strain lie between predicted values for four of the five strands (strands VI, VIII, IX and VII). For the strand end position (column (ix)), measured

strain values are generally lower than for the mid-strand position, and for none of the strands in the free end condition does the experimental value lie between the predicted 100% slip and zero slip conditions. In an attempt to investigate whether a lower wire tension or higher bending strain at these positions affects overall strain values, strain differences from the fixed end condition were considered as follows.

In table 7.5 columns (iii) and (v) give the difference between the mean strain value for the fixed end condition and that for each other end condition in turn. The range of strain deviations from the mean are also given in columns (iv) and (vi). (The figure for range of strain deviation is the difference between strain on the wire giving maximum strain and that on the wire giving minimum strain as shown on tabulated results, examples of which are tables 5.7 and 5.8). Justification for considering that there is no interwire slip in the fixed end condition follows from the analysis given in the next section (7.7).

The Figs 7.13 to 7.22 display the information given in tables 7.4 and 7.5. For the mid-strand position strain ranges on strands VI, VIII, X, IX and VII are shown in Figs 7.13, 15, 17, 19 and 21 respectively. For the strand end position, strain ranges on strands VI, VIII, X, IX and VII are shown in Figs 7.14, 16, 18, 20 and 22 respectively.

From results and comparisons made in tables 7.4 and 7.5 and

TABLE 7.4 HELICAL WIRE SURFACE STRAIN: PREDICTED AND EXPERIMENTAL

STRAND LOAD 40 kN

Strand No.	DURELLI PREDICTIONS		COMPUTED PREDICTIONS			TEST RESULTS: MEAN STRAIN ON HELICAL WIRE (PARALLEL TO WIRE AXIS)			Nominal End Condition (Load Cycle No.)
	Torsional End Restr. Nm/kN	Wire Surface Strain με/kN	Torsional End Restr. Nm/kN	WIRE SURFACE STRAIN 100% Slip με/kN	WIRE SURFACE STRAIN No Slip με/kN	Torsional End Restr. Nm/kN	Mid Strand με/kN	End Near Grip με/kN	
(i)	(ii)	(iii)	(iv)	(v)	(vi)	(vii)	(viii)	(ix)	(x)
VI 73.0° (Measured) * 73.6° (Nominal)	0.92 *(0.89)	60.95 *(61.33)	0.92 *(0.89)	56.97 *(57.60)	59.09 *(59.74)	0.86	57.85	56.03	Fixed (104)
						0.59	38.70	41.86	¾ Fix (111)
						0.43	23.41	26.38	½ Fix (110)
						0.22	6.28	10.94	¼ Fix (112)
	0	-21.40 *(-16.31)	0	-26.75 *(-21.24)	-8.48 *(-4.49)	0	- 9.07	- 7.82	Free (109)
VIII 76.2°	0.75	62.36	0.75	59.73	61.23	0.72	63.28	57.63	Fixed (204)
						0.54	48.69	42.73	¾ Fix (209)
						0.35	36.03	28.81	½ Fix (208)
						0.13	19.92	10.68	¼ Fix (207)
	0	2.99	0	-0.58	12.11	-0.03	5.94	- 4.14	Free (206)

Table 7.4 (Continued)

Strand No.	DURELLI PREDICTIONS		COMPUTED PREDICTIONS			TEST RESULTS: MEAN STRAIN ON HELICAL WIRE (PARALLEL TO WIRE AXIS)			Nominal End Condition (Load Cycle No.)
	Torsional End Restr. Nm/kN	Wire Surface Strain $\mu\varepsilon$/kN	Torsional End Restr. Nm/kN	WIRE SURFACE STRAIN		Torsional End Restr. Nm/kN	Mid Strand $\mu\varepsilon$/kN	End Near Grip $\mu\varepsilon$/kN	
				100% Slip $\mu\varepsilon$/kN	No Slip $\mu\varepsilon$/kN				
(i)	(ii)	(iii)	(iv)	(v)	(vi)	(vii)	(viii)	(ix)	(x)
X 77.7°	0.66	62.90	0.66	60.86	62.02	0.65	55.04	59.28	Fixed (304)
						0.47	44.47	47.12	$\frac{3}{4}$ Fix (309)
						0.29	32.59	33.66	$\frac{1}{2}$ Fix (308)
						0.12	22.81	22.15	$\frac{1}{4}$ Fix (307)
	0	14.28	0	11.44	21.62	-0.05	10.34	9.18	Free (306)
IX 78.9°	0.60	63.30	0.60	61.64	62.57	0.58	63.25	55.54	Fixed (404)
						0.45	54.38	45.07	$\frac{3}{4}$ Fix (409)
						0.30	45.78	35.32	$\frac{1}{2}$ Fix (408)
						0.14	35.87	24.35	$\frac{1}{4}$ Fix (407)
	0	22.86	0	20.53	28.98	0	27.00	14.82	Free (406)
VII 80.9°	0.49	63.83	0.49	62.71	63.34	0.47	64.34	50.43	Fixed (505)
						0.36	58.33	45.34	$\frac{3}{4}$ Fix (510)
						0.24	51.65	38.09	$\frac{1}{2}$ Fix (509)
						0.13	45.59	32.23	$\frac{1}{4}$ Fix (511)
	0	35.31	0	33.66	39.61	0	39.09	25.46	Free (508)

Note that predicted values of torque and surface strain for partially restrained end conditions are pro rata between the fixed and free end values.

TABLE 7.5 HELICAL WIRE SURFACE STRAIN: DIFFERENCES AND RANGES/TORSIONAL RESTRAINT

Strand No.	Torsional End Restraint Nm/kN	STRAIN ON HELICAL WIRE SURFACE PARALLEL TO WIRE AXIS				Nominal End Condition (Load Cycle No.)
		MID-STRAND		END NEAR GRIP		
		Mean Strain Difference $\mu\varepsilon$/kN	Range Over Six Wires $\mu\varepsilon$/kN	Mean Strain Difference $\mu\varepsilon$/kN	Range Over Six Wires $\mu\varepsilon$/kN	
(i)	(ii)	(iii)	(iv)	(v)	(vi)	(vii)
VI	0.86	0	0	0	0	Fixed (104)
73.0°	0.59	19.2	4.0	14.1	23.5	$\frac{3}{4}$ Fix (111)
(73.6°)	0.43	34.5	7.6	29.6	20.6	$\frac{1}{2}$ Fix (110)
	0.22	51.6	13.5	45.1	29.8	$\frac{1}{4}$ Fix (112)
	0	67.0	12.8	63.8	24.2	Free (109)
VIII	0.72	0	0	0	0	Fixed (204)
76.2°	0.54	14.6	2.1	14.9	15.7	$\frac{3}{4}$ Fix (209)
	0.35	27.3	3.2	28.8	6.8	$\frac{1}{2}$ Fix (208)
	0.13	43.4	4.9	46.9	10.8	$\frac{1}{4}$ Fix (207)
	-0.03	57.4	6.0	61.7	13.3	Free (206)

Table 7.5 (Continued)

Strand No.	Torsional End Restraint Nm/kN	STRAIN ON HELICAL WIRE SURFACE PARALLEL TO WIRE AXIS				Nominal End Condition (Load Cycle No.)
		MID-STRAND		END NEAR GRIP		
		Mean Strain Difference $\mu\varepsilon$/kN	Range Over Six Wires $\mu\varepsilon$/kN	Mean Strain Difference $\mu\varepsilon$/kN	Range Over Six Wires $\mu\varepsilon$/kN	
(i)	(ii)	(iii)	(iv)	(v)	(vi)	(vii)
X 77.7°	0.65	0	0	0	0	Fixed (304)
	0.47	10.5	5.2	12.2	8.9	$\frac{3}{4}$ Fix (309)
	0.29	22.4	4.3	25.6	13.7	$\frac{1}{2}$ Fix (308)
	0.12	33.0	3.6	37.1	9.9	$\frac{1}{4}$ Fix (307)
	-0.05	44.7	3.0	50.1	6.5	Free (306)
IX 78.9°	0.58	0	0	0	0	Fixed (404)
	0.45	8.9	6.3	10.4	6.6	$\frac{3}{4}$ Fix (409)
	0.30	17.5	5.0	20.2	8.6	$\frac{1}{2}$ Fix (408)
	0.14	27.4	6.9	31.1	11.2	$\frac{1}{4}$ Fix (407)
	0	36.3	9.3	40.7	15.2	Free (406)
VII 80.9°	0.47	0	0	0	0	Fixed (505)
	0.36	6.0	6.0	5.1	5.9	$\frac{3}{4}$ Fix (510)
	0.24	12.6	6.9	12.3	6.7	$\frac{1}{2}$ Fix (509)
	0.13	18.7	9.0	18.2	9.4	$\frac{1}{4}$ Fix (511)
	0	25.2	9.5	24.9	11.8	Free (508)

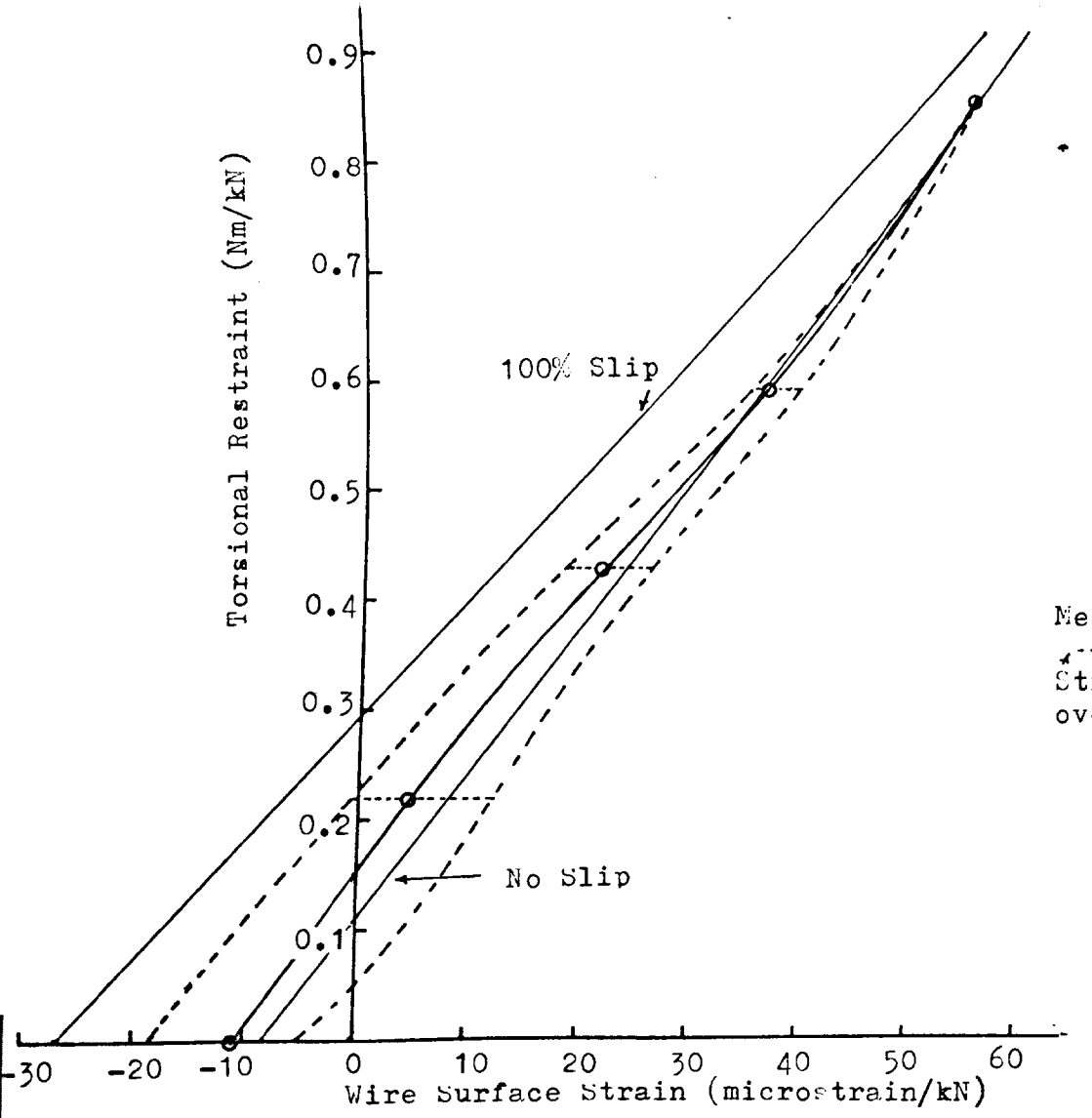

Figure 7.13.Torsional Restraint/Wire Surface Strain.
Strand VI:Mid-Length.

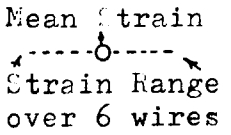

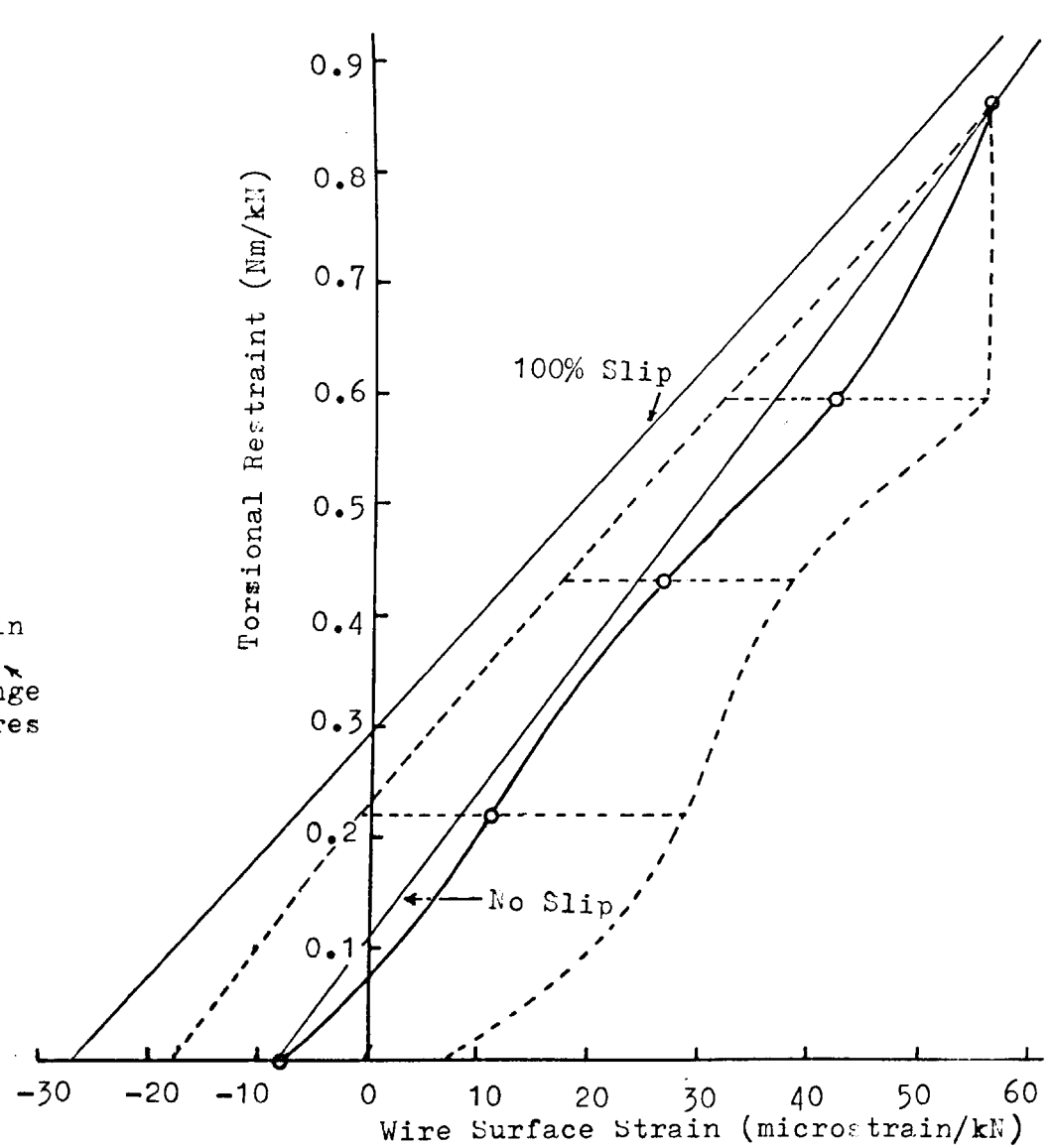

Figure 7.14.Torsional Restraint/Wire Surface Strain.
Strand VI:Strand-End.

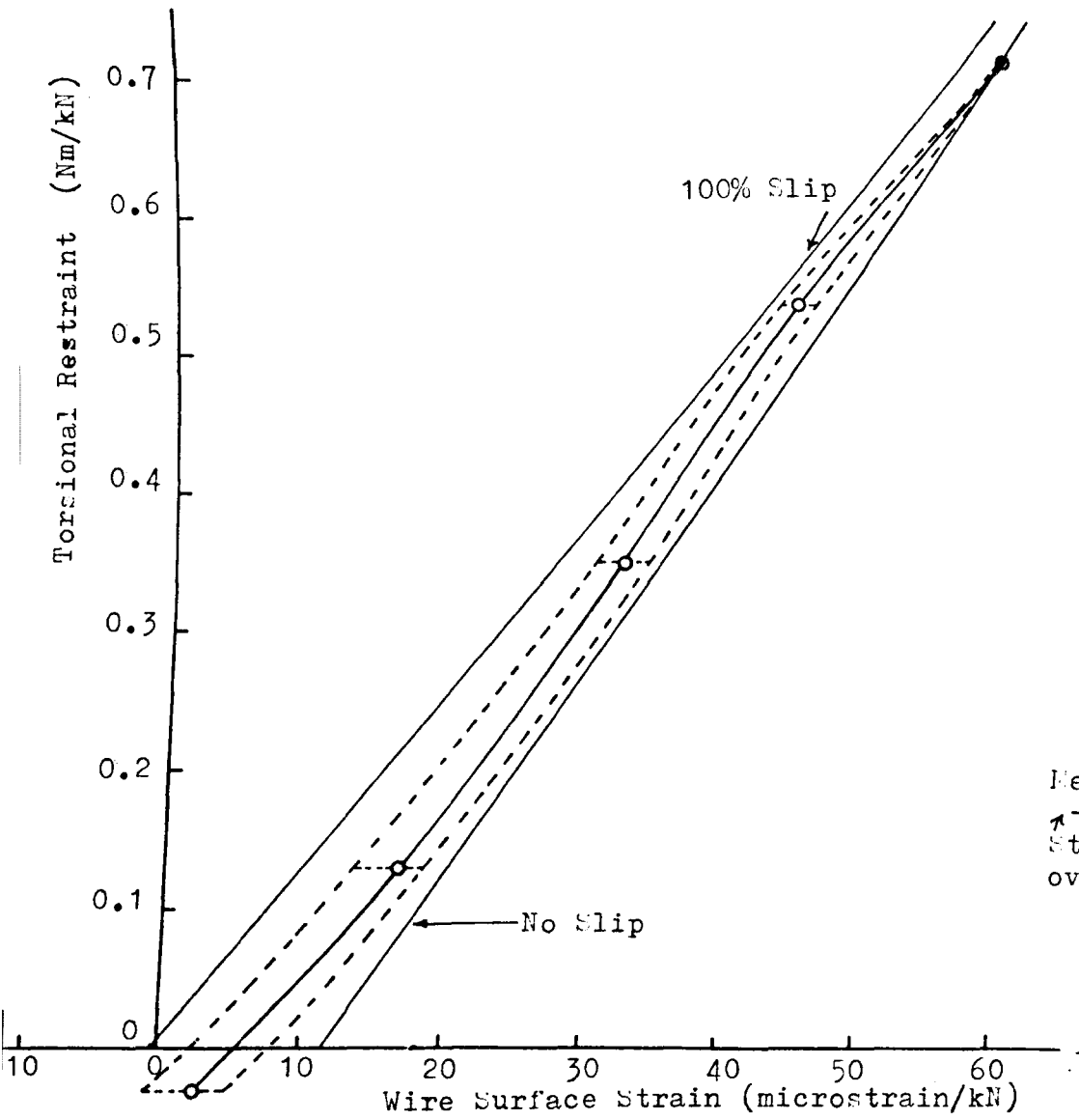

Figure 7.15.Torsional Restraint/Wire Surface Strain.
Strand VIII:Mid-Length.

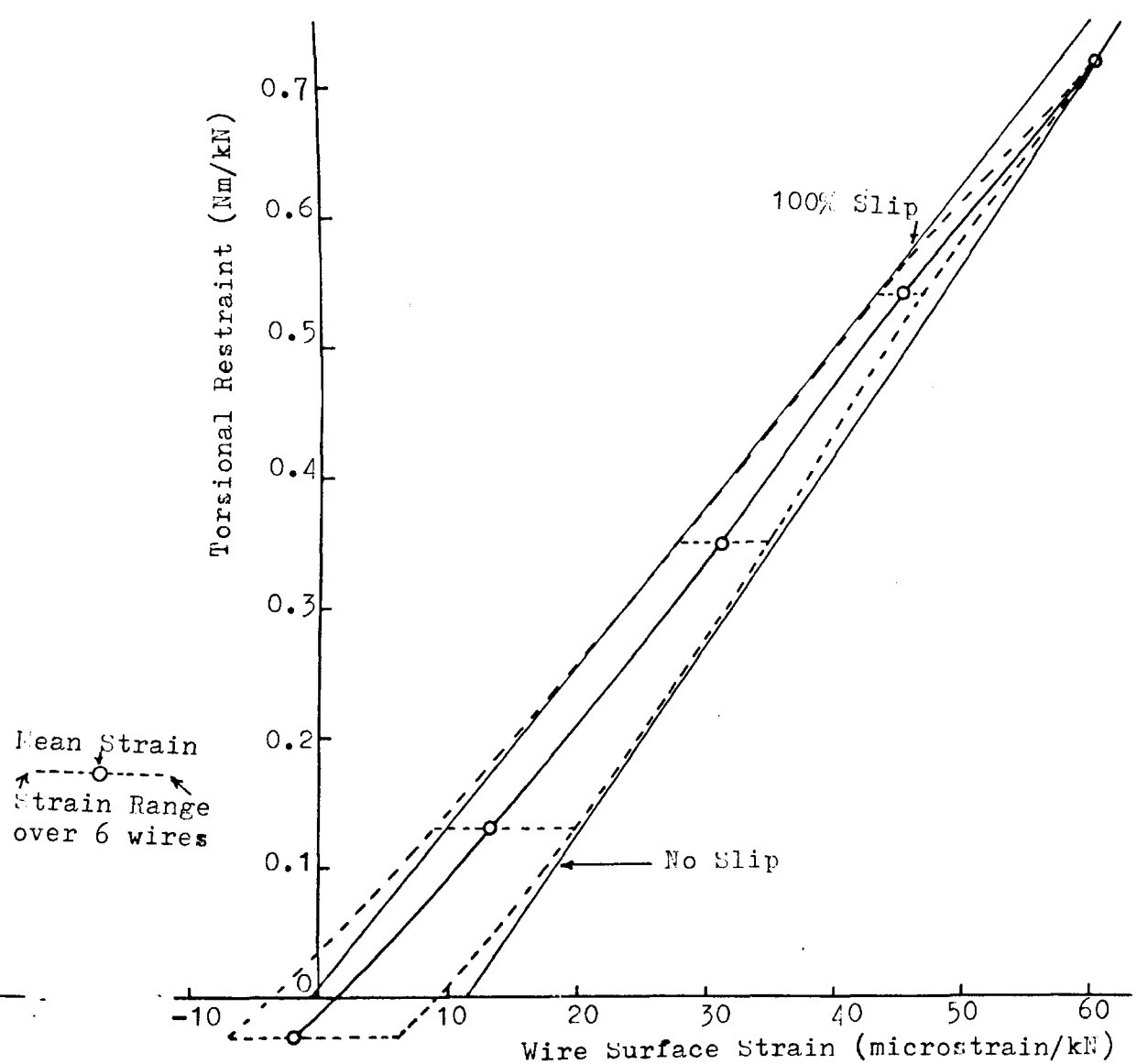

Figure 7.16.Torsional Restraint/Wire Surface Strain
Strand VIII:Strand-End.

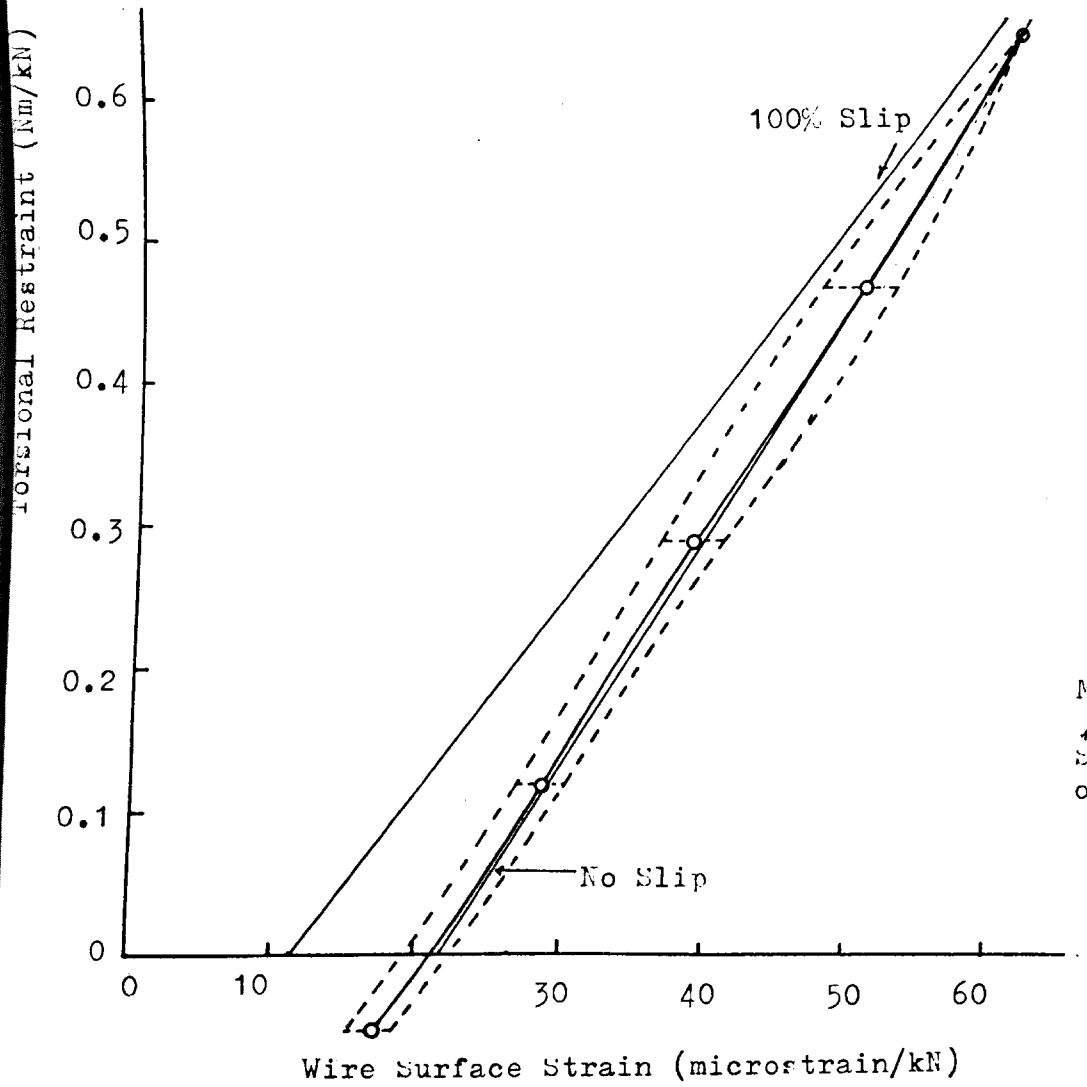

Figure 7.17.Torsional Restraint/Wire Surface Strain.
Strand X:Mid-Length.

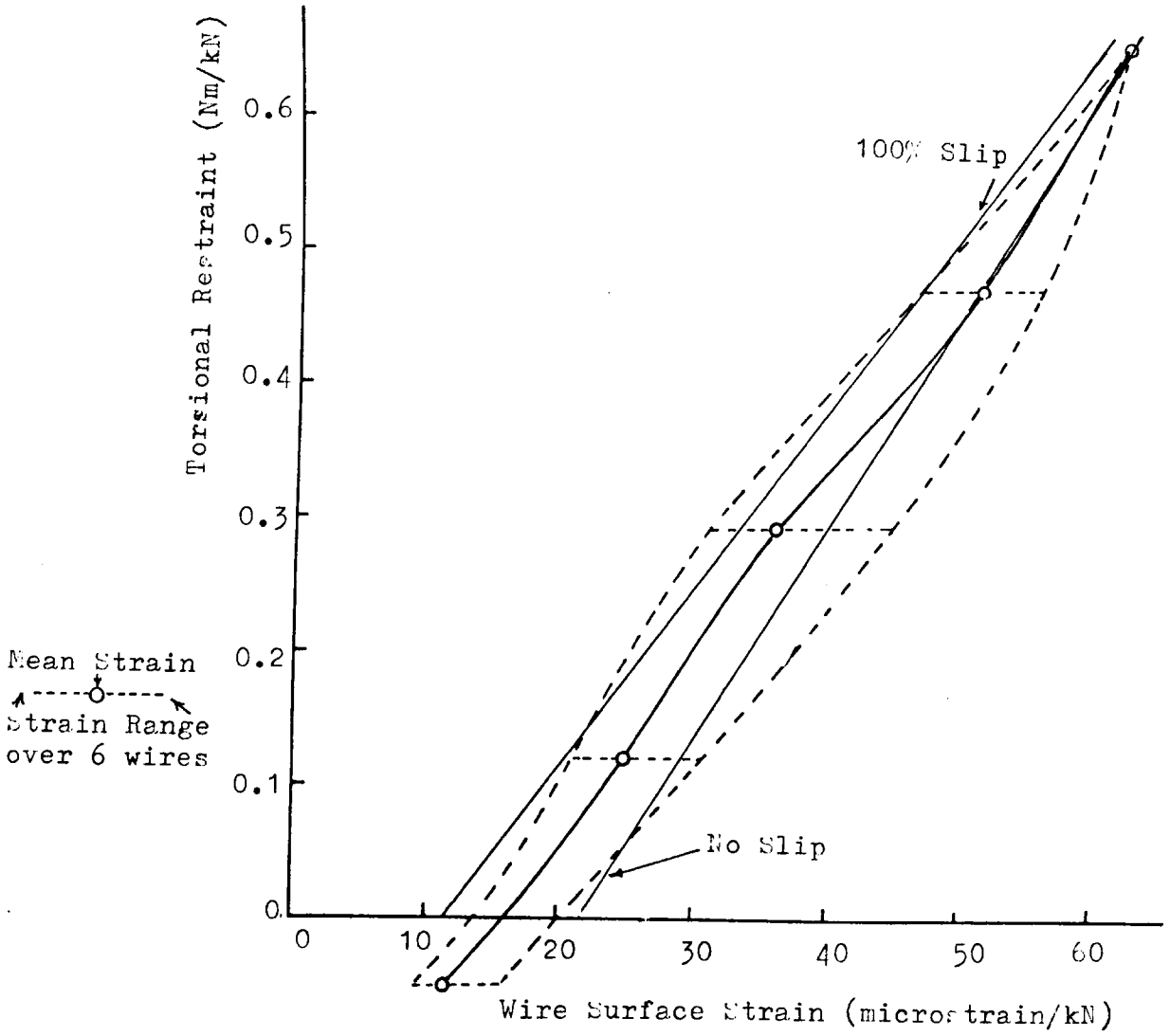

Figure 7.18.Torsional Restraint/Wire Surface Strain.
Strand X:Strand-End.

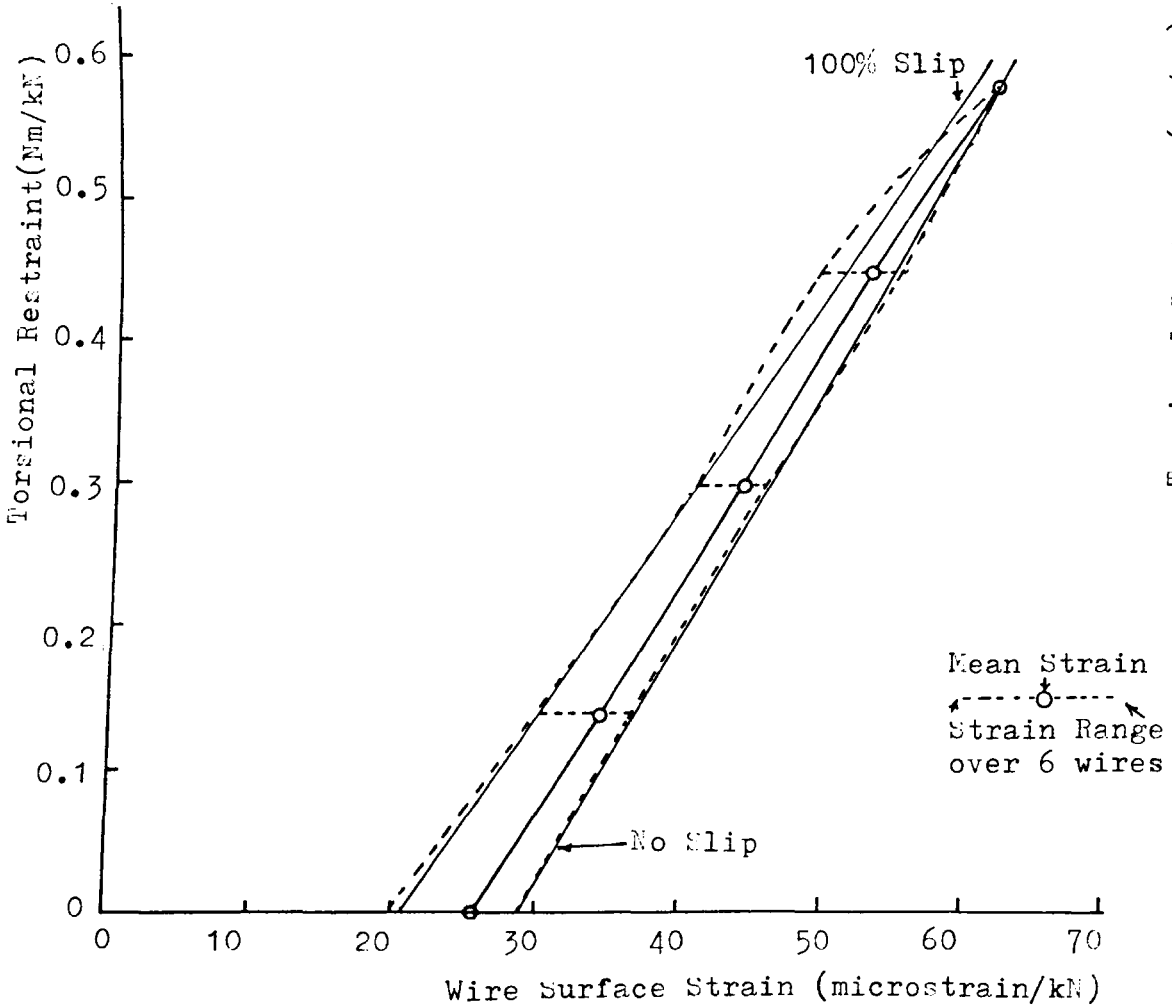

Figure 7.19.Torsional Restraint/Wire Surface Strain.
Strand IX:Mid-Strand.

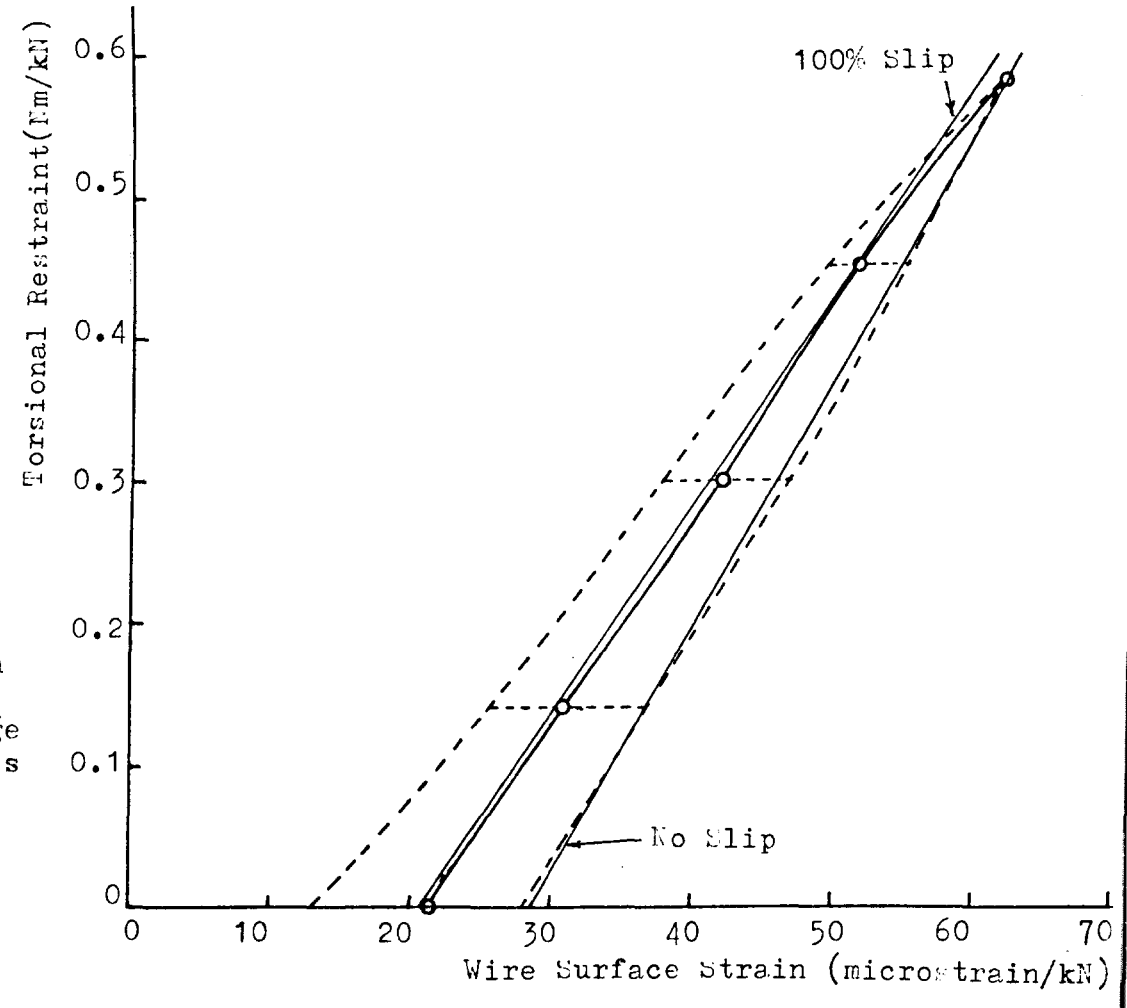

Figure 7.20.Torsional Restraint/Wire Surface Strain.
Strand IX:Strand-End.

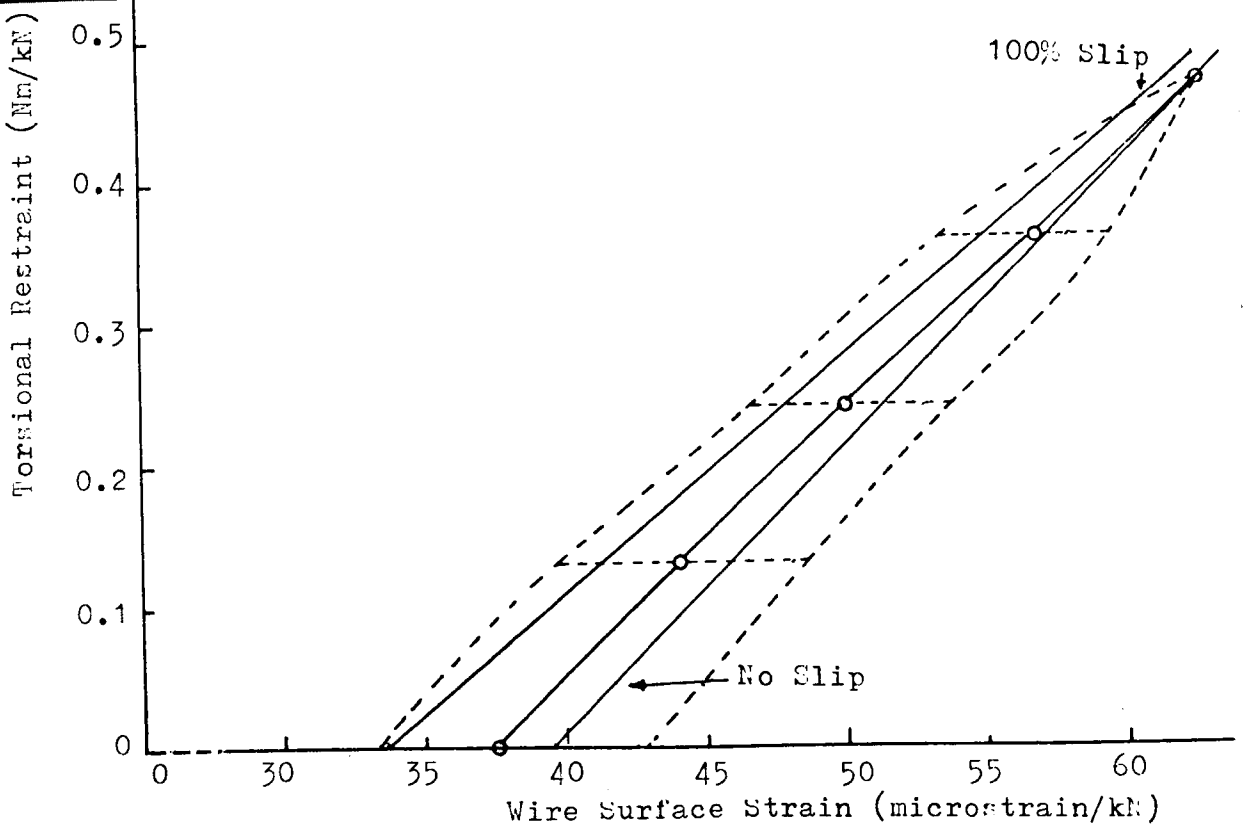

Figure 7.21.Torsional Restraint/Wire Surface Strain.
Strand VII:Mid-Strand.

Mean Strain
Strain Range over 6 wires

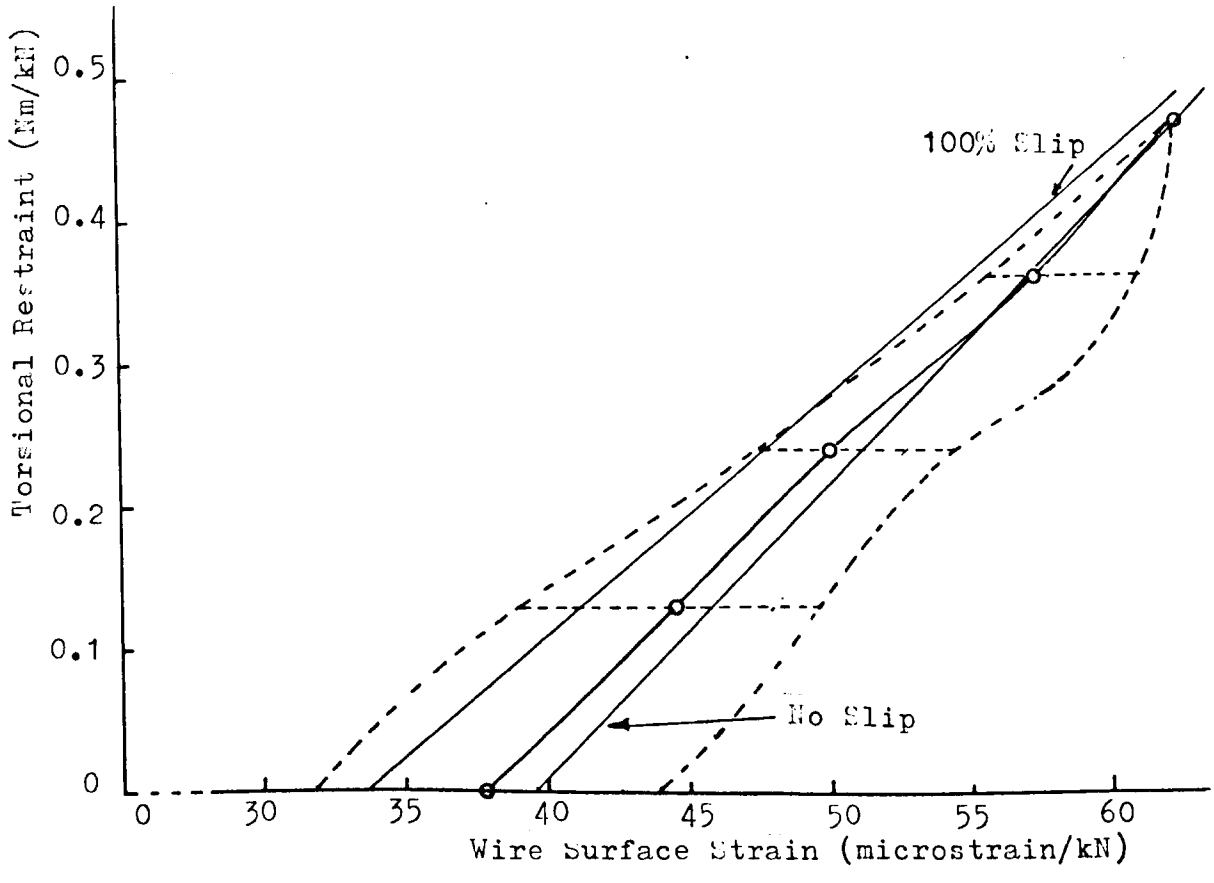

Figure 7.22.Torsional Restraint/Wire Surface Strain.
Strand VII:Strand-End.

the evidence of Figs 7.12 to 7.22 it is possible to draw the following conclusions.

(i) Deviations from the mean strain are greater near the strand end grip than at mid-strand. (See also the results shown in Chapter 5, sub-sections 5.5.8 and 5.6.10). This indicates less even load sharing between wires near strand end grip.

(ii) The lower mean strains at strand end positions indicate lower tensions or higher bending moments (or both) in the wires at this position. Evidence from Chapter 5, sub-section 5.6.8 also suggests that there is reduced tension near strand ends. The fact that strain differences, as calculated from results tabulated in table 7.5 and plotted in Figs 7.13 to 7.22 exhibit the same pattern, would also suggest that differences in wire tensions have a major influence on the wire strain measured. The low strain values at mid-strand which are peculiar to strand X may be put down to uneven stranding of the helicals in this strand only. There is some evidence for this in the greater degree of wire migration at lower loads (see table 5.17).

(iii) For the mid-length position in all strands but number VI, the mean strain values always lie between the lines showing the 100% slip and zero slip conditions. As torsional restraint reduces, the mean strain value is

further from the zero slip line. This departure from the zero slip condition and the fact that the envelope of strain difference values spreads over both the predicted 100% slip and zero slip lines, even for the mid-strand position, would appear to indicate that a mechanism other than a simple stick or slip phenomenon is present. This is discussed further in the next section.

7.6 Interwire Friction

7.6.1 The Onset of Slip

Theory developed in Chapter 6 predicts strand response which is seen to be different depending on the presence or otherwise of interwire slip. Comparison of these predictions with test results obtained for strand extension, rotation and surface strain have highlighted the desirability of being able to predict whether or not slip is present under a given loading condition for strand of a particular geometry. Normal force between core and helical wires is determined from expression 6.48. Tangential friction force F' is determined from expression 6.33 in terms of strand length L_L. Table 7.6 gives restraining factors (columns (iv) and (v)), Normal Contact Force (column (vi)) and nett Tangential frictional force over strand length L_L (column (vii)). Margetts and Spikes (79) have quoted a figure of 0.115 for coefficient of friction, in tests which simulate the motion between wires in wire ropes. This figure is used to determine the maximum strand length L_L over which slip can be expected (column (viii)). For the five strands in the test programme at loads of 10 kN and 40 kN, the information given in table 7.6 is also plotted on figures 7.23, 7.24 and 7.25.

Total strand lengths exceeded 1200 mm in all the tests so that even if transition lengths L_T are subtracted from the total length, the relevant strand length L_L is still likely to exceed 500 mm (see also Fig. 6.4). It is therefore evident from column (viii) of table 7.6 and from Fig. 7.25 that interwire slip is unlikely, even in the tests with strands free to rotate. Slip

TABLE 7.6 FRICTION BETWEEN CORE AND HELICAL WIRES: RESTRAINING FACTORS AND FRICTION FORCES

Strand No. (Helix Angle)	Fixed or Free Ends	Load kN	RESTRAINT OF CORE ON HELICAL WIRES		Normal Contact Force X kN/mm	Tangential Friction Force $F'.L_L$ (kN/mm).mm	Strand Length if slip occurs (μ=0.115) L_L mm
			Bending Factor Z_1	Torsion Factor Z_2			
(i)	(ii)	(iii)	(iv)	(v)	(vi)	(vii)	(viii)
VI (73.0°)	Fixed	10	.274	.129	.032	.019	5.22
	"	40	.275	.129	.125	.106	7.35
	Free	10	.253	.138	.023	.175	66.31
	"	40	.250	.139	.087	.686	68.54
VIII (76.2°)	Fixed	10	.270	.140	.021	.013	5.47
	"	40	.269	.141	.084	.053	5.45
	Free	10	.248	.146	.017	.136	69.77
	"	40	.245	.146	.064	.535	72.73

Table 7.6 (Continued)

Strand No. (Helix Angle)	Fixed or Free Ends	Load kN	RESTRAINT OF CORE ON HELICAL WIRES		Normal Contact Force X kN/mm	Tangential Friction Force $F'.L_L$ (kN/mm).mm	Strand Length if slip occurs (μ=0.115) L_L mm
			Bending Factor Z_1	Torsion Factor Z_2			
(i)	(ii)	(iii)	(iv)	(v)	(vi)	(vii)	(viii)
X (77.7°)	Fixed	10	.268	.144	.017	.011	5.52
	"	40	.266	.145	.066	.043	5.72
	Free	10	.246	.149	.014	.119	73.73
	"	40	.243	.149	.053	.467	76.56
IX (78.9°)	Fixed	10	.264	.147	.014	.009	5.77
	"	40	.264	.147	.054	.037	5.94
	Free	10	.245	.150	.012	.106	76.45
	"	40	.241	.151	.044	.413	81.70
VII (80.9°)	Fixed	10	.255	.151	.009	.007	
	"	40	.262	.151	.037	.028	6.56
	Free	10	.242	.153	.008	.085	92.50
	"	40	.239	.153	.031	.333	93.52

Interwire Forces.
Figure 7.23.
Torsional Restraint/Normal Force.
Strand Loads of 10kN & 40kN

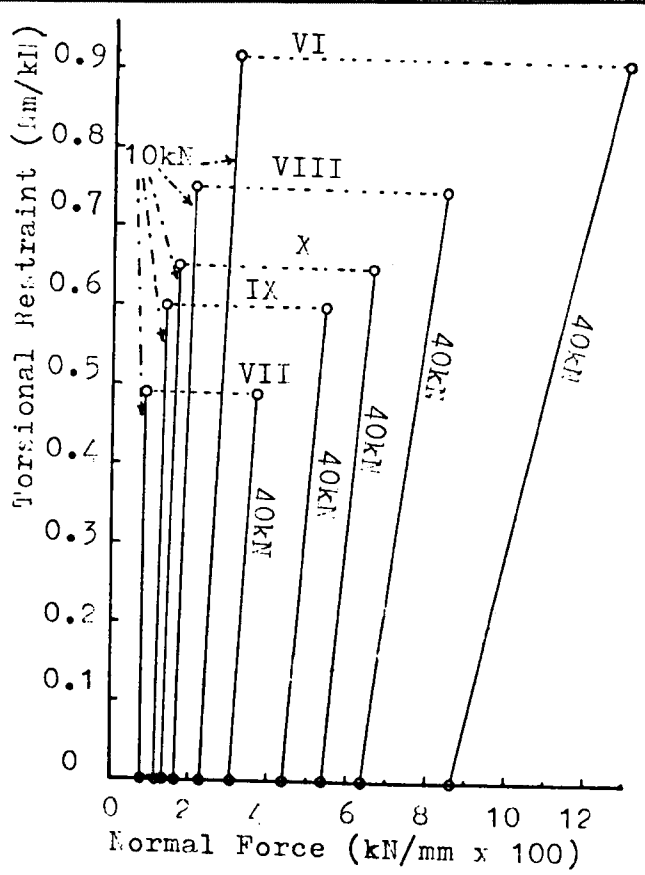

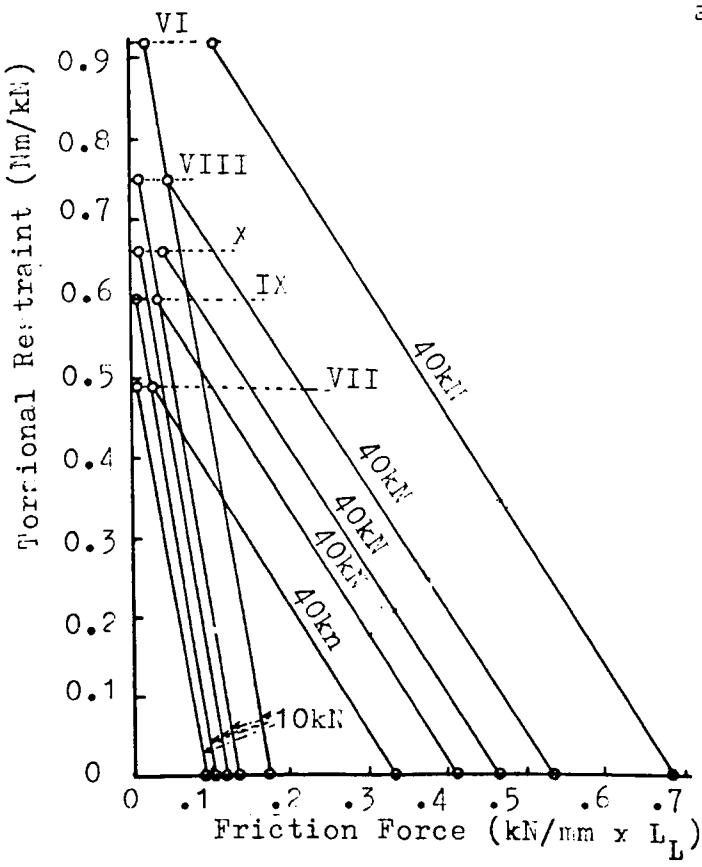

Interwire Forces.
Figure 7.24.
Torsional Restraint/Friction Force.
Strand Loads of 10kN & 40kN

Interwire Forces.
Figure 7.25.
Torsional Restraint against Minimum Strand Length over which slip can be expected.
(u=0.115)
Strand Loads of 10kN & 40kN

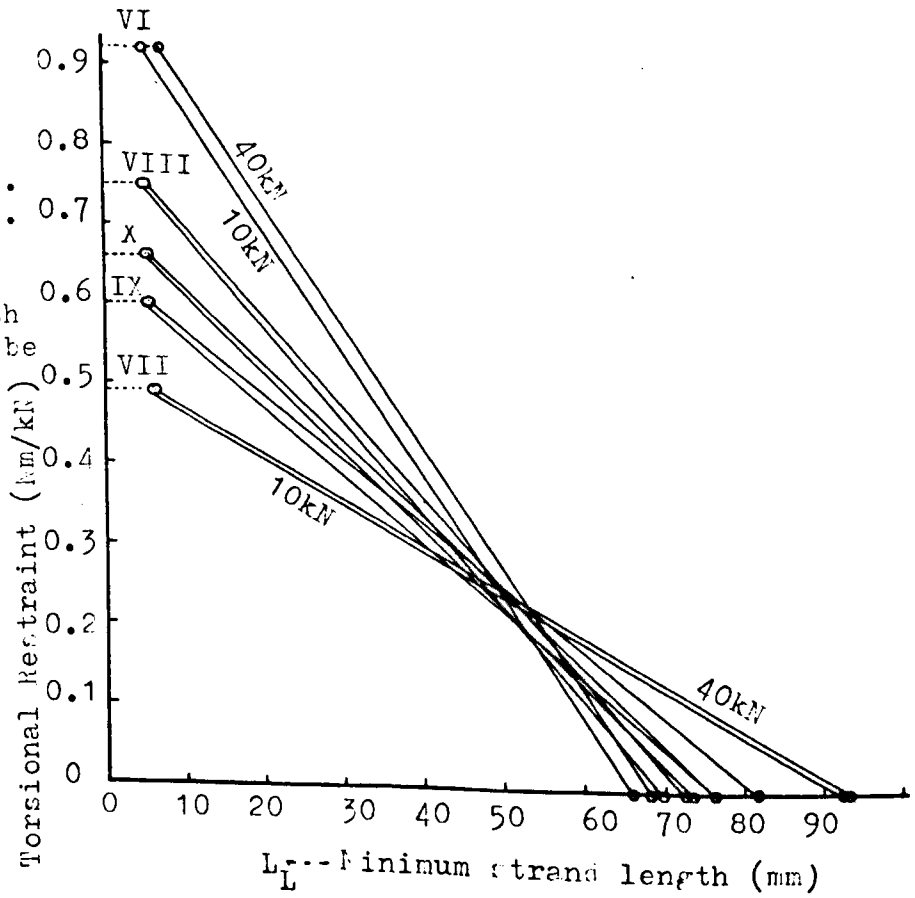

is seen to be least likely in the fixed end tests and this is the justification for placing the mean strain point from fixed end experimental results on the zero slip line from theoretical predictions in the Figs 7.13 to 7.22.

The test results, particularly the surface strain measurements (see section 7.5) cannot be entirely explained in terms of a stick/slip mechanism. In attempting to assess the validity of this analysis on the onset of slip, elements of strand response to load are therefore again examined in turn.

7.6.2 Torque Generated

The difference between predicted torque with and without interwire friction is in no case greater than 0.1% (see tables 6.3 and 6.6). In any event these predictions were found to be higher than the test results by up to 4.5% (see table 7.1). This is probably due to low tension values in helical wires, resulting in a lower moment about strand axis of the tangential component of these tensions, which constitute the largest proportion of the torque generated in the strand. Interwire slip is not of direct significance therefore in considering torque generated in the strand.

7.6.3 Wire Tension

It was shown from test results, in Chapter 5, section 5.6.8, that helical wire tension is less nearer the end grip than at mid-strand of the strand under load. Since tension contributes most

in expression 6.48 to the magnitude of predicted contact normal force (X), and a reduction in this force is more likely to result in slip between wires, it follows that slip is more likely to occur near strand ends. Evidence from the plots of torsional restraint against axial strain on wire surface is inconclusive. For strands VII, IX and X, mean strain difference at strand end is nearer to the '100% slip' line than the 'no slip' line (see Figs 7.15 and 7.16, 7.17 and 7.18, 7.19 and 7.20) but for strand VII the strand difference lines for mid-strand and strand end are very close to each other (see Figs 7.21 and 7.22). For strand VI the mid-strand line for mean strain difference lies nearer the '100% slip' line than does the strand end line (see Figs 7.13 and 7.14). Clearly, there is evidence that other factor or factors have an influence on strand response.

7.6.4 Strand Extension

The conclusions given at the end of section 7.3 do not indicate that wire slip has a direct effect on strand extension. The fact that the slopes of the graphs in Figs 7.1 to 7.6 (showing torsional restraint against extension), are closer to the computed predictions than those of Durelli indicates the significance of Poisson effects and the change of helix angle as loading increases. However, the slope from experimental results is steeper than either of the predicted slopes (for 100% slip and no slip) and it is evident that some other factor or factors must be influencing strand extension.

7.6.5 Strand Rotation

Strand rotation, as measured by the extrometer, is seen to be lower in all cases than that predicted from any of the theories. A possible mechanism which may account in part for the low values of rotation measured is described in section 7.4 (Fig. 7.12). It also follows that from a strand exhibiting lower strand rotation in the free and partially restrained tests, a lower torque generated can be expected in fixed and partially restrained tests (see 7.6.2 above). However, no direct connection with the presence or absence of interwire slip is evident.

7.6.6 Strains on Helical Wire Surface

The plots of torsional restraint against strain difference in Figs 7.13 to 7.22 are constructed such that for every wire in every strand it is assumed that there is no interwire slip under the condition of fixed end strand loading. The plot for both mean strain and the envelope enclosing strain deviations on all six wires are thus seen to start at a point on the predicted 'no slip' line, in every case. Under the classic conditions of a sharp transition from static to dynamic friction it might be expected that the strain deviation values would move away from the 'no slip' line in these plots at a value of torsional restraint that corresponds to the point where the dynamic coefficient of friction is reached. Although table 7.6 and Figs 7.23, 24 and 25 show that the analysis predicts zero slip, even in the free end case, for that part of the strand away from

transition lengths at strand ends, it might be expected that from strain plots for positions near strand end (within length L_T, Fig. 6.12), slip conditions would be revealed. However for both mid-strand plots (Figs 7.13, 15, 17, 19 and 21) and strand end plots (Figs 7.14, 16, 18, 20 and 22), no such sudden departure from the zero slip line is in evidence. The plots all show the experimental points of mean strain giving a line, in no case greatly deviant from straight, which moves closer to the 100% slip line as torsional restraint is reduced. There is plainly a mechanism other than pure stick/slip affecting stress distribution in and deformation of the wires in these conditions of axial loading of a strand. The absence of a sharp transition may be due to the fact that flattening at contact surfaces results in migration of the effective contact point of both wires without slip. Fig. 7.26 illustrates a possible mechanism by which this occurs. This movement of the initial contact point in a wire will result from distortion of the initially straight radius joining wire centre line and contact point, as the contact point now moves relative to this line in the direction of the tangential friction force acting on that wire (see Fig. 7.26.e and Figs 6.1 to 6.4). It will be evident from Figs 7.23 and 7.24 that, whereas normal force X reduces by no more than 30% as torsional restraint is reduced from the fixed end condition to zero (free end), the tangential force F'_F can increase by up to sevenfold. This suggests that the effect of tangential friction force is dominant since yield occurs and the material in the contact area has attained the plastic condition

Figure 7.26. Relative Motion between Core and Helical Wires. Flattening with no Slip.

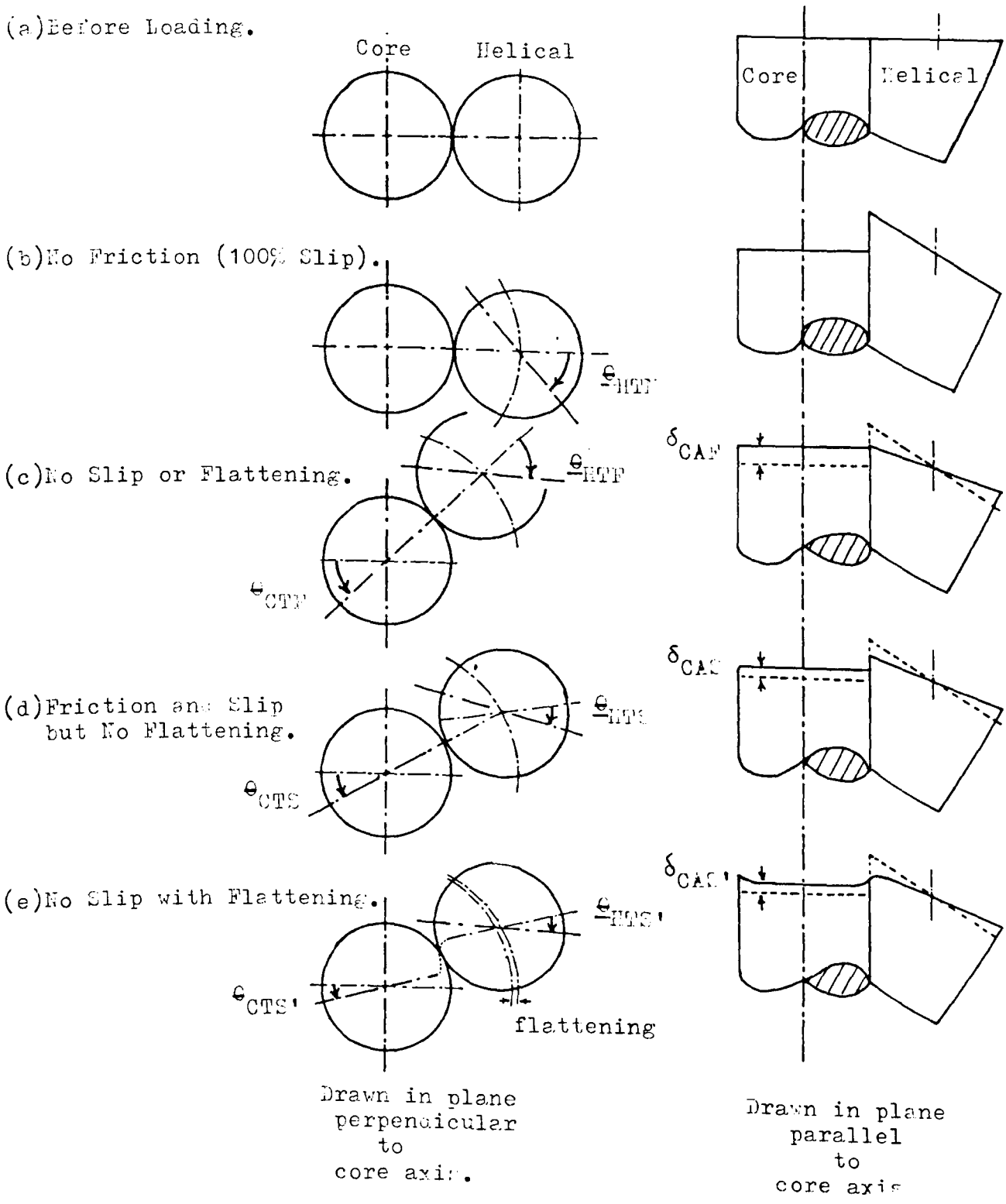

Note: θ_{HTF}, θ_{HTF}, θ_{HTS} & $\theta_{HTS'}$ are components of helical wire rotation in the plane perpendicular to strand axis.

even at the lower normal contact forces present in the free end condition of loading. The mechanism of contact point migration postulated above is thus shown to have the same effect as inter-wire slip, but without the sudden stick/slip transition, on stress distribution in helical wire cross-section and thus on surface strain measured on the outside of the wire.

Evidence of wire flattening and yielding where core and helical wire come in contact was present when strands were purposely unwrapped after fracture (strand I) and for the purpose of testing wires (see Appendix A.5). In the case of the fractured strand, distinctly flattened areas forming helices on the core corresponding to matching areas on the helical wires were observed. Even in the case of strands that had not been subject to tensile load, markings indicating small permanent deformation on core and helical wires were found to be present. Clearly, yield occurs along the line of contact even under the low contact loading imposed during the stranding process.

CHAPTER 8

CONCLUSIONS AND SUGGESTIONS FOR FUTURE WORK

8.1 Summary

This final chapter collates the conclusions from this study in terms of the objectives laid down in Chapter 2, section 2.3. Experimental results are given and are compared with both the predictions of Durelli et al. (27), and those from mathematical modelling of strand response to axial load, which takes account of Poisson effects on wires, the increase of helix angle with load, interwire friction and wire flattening under contact pressure. Direct comparison between experimental results and the predictions of Costello et al. (16, 17, 18) is not possible since these workers only considered strands without a core; mainly three and six wire strands. However, they do take account of increase in helix angle under load and the starting point of the computed predictions in this study was to superimpose the loading taken by a wire core on the loading taken by helical wires. The 'Costello + core' predictions are thus seen to be between those of Durelli and the computed predictions of this study. It is evident that further experimental work is required to improve understanding of the loading in individual wires, particularly at strand ends, near the terminations. The chapter ends by suggesting suitable future study in this field that is both experimental and theoretical.

8.2 Wire Modulus

A necessary prerequisite to valid comparison of experimental results and the mathematical modelling of strand response was an estimate of the elastic modulus of the individual wires comprising the test strands. The preliminary study described in Appendix A.5 revealed that effective modulus depends on the loading range, and was determined as 197.9 kN/mm^2 for the strand loading in this programme. This is the value used in the computations on strand response in Chapter 6.

8.3 Individual Elements of Strand Response

It is first convenient to describe the main features of the individual elements of strand response in turn. Differences between experimental results and predictions are summarized in table 8.1. Whereas it is convenient to tabulate differences of extension and restraining torque in the fixed end case, and of extension and rotation in the free end case, surface strain differences cannot be so tabulated. However, conclusions may be drawn from strain results and from wire tensions and these are discussed in later sections.

8.3.1 Strand Extension

Extension under a given load was found to be greater with reduced torsional restraint on the end terminations and in the case of the strand with lowest helix angle, extension under the free end condition is about 70% greater than that under the fixed end condition. Load/extension plots do not reveal a distinctive yield point, but departure from a sensibly linear relation occurs at a lower tensile strand load in the free end case than in the fixed end case. Test loads in which the effect of torsional restraint were compared did not exceed 50 kN, which was below the point at which this departure from linearity occurred in all strands. The slope of plots showing torsional restraint against axial compliance (extension per unit load) lie nearest to the slope of computed predictions for conditions of zero interwire slip, though experimental results were found to be greater than predictions in the fixed end case and less than

TABLE 8.1 SUMMARY OF STRAND RESPONSE

COMPARISON BETWEEN TEST RESULTS AND MATHEMATICAL MODELLING

Tabulated values in each case are given by
(Theoretical Prediction/Experimental Result -1) x 100%

FIXED END LOADING				
Strands	Extensions (Table 7.2)		Restraining Torque (Table 7.1)	
	Durelli Prediction	*Computed Prediction	Durelli Prediction	Computed Prediction
(i)	(ii)	(iii)	(iv)	(v)
VI (73.0°)	-9.3%	-5.2%	4.5%	4.5%
to				
VII (80.9°)	-1.2%	-0.1%	1.1%	1.1%

FREE END LOADING				
Strands	Extensions (Table 7.2)		Rotation (Table 7.3)	
	Durelli Prediction	*Computed Prediction	Durelli Prediction	*Computed Prediction
(i)	(ii)	(iii)	(iv)	(v)
VI (73.0°)	+4.5%	+3.7%	+12.6%	+12.7%
to				
VII (80.9°)	+1.6%	+0.8%	+8.3%	+ 8.5%

*Note: Computed prediction is that which takes account of Poisson effects, changing helix angle with load, interwire friction and flattening, (i.e. column (viii) in table 7.2 and column (vi) in table 7.3).

predictions in the free end case. Results from fixed, free and partially restrained ends are all closer to computed predictions than to those of Durelli et al. (27). The computed predictions which take account of Poisson effect on wires, helix angle increase under load and wire flattening are greater than those of Durelli et al. (27) by between 1.33% ($\alpha = 80.9^{\circ}$) and 4.31% ($\alpha = 73.6^{\circ}$) for the fixed end condition if interwire friction is neglected, reducing to 1.30% ($\alpha = 80.9^{\circ}$) and 4.24% ($\alpha = 73.6^{\circ}$) if interwire friction is considered large enough to prevent slip. In the free end case computed predictions are less than those of Durelli by between 0.76% ($\alpha = 80.9^{\circ}$) and 0.91% ($\alpha = 73.6^{\circ}$). If flattening of the wires is considered, predicted extensions are increased by no more than 0.02% in the fixed end case and by no more than 0.14% in the free end case.

8.3.2 Strand Rotation

Rotation under a given load was found to be greater with reduced torsional restraint on the end terminations. The rotation is greater for strands with a lower helix angle. Computed predictions on rotation are greater than those of Durelli by up to 1.11% but the effect of taking into account interwire friction and flattening reduces this difference by not more than 0.27% However, test results were found to be less than all predictions by more than 12% for strands with the lowest helix angle. This surprisingly large difference between measured and predicted rotation can be accounted for, at least in part, by the fact that in the event there is no slip between core and helical wires,

they roll over each other and the nett rotation of the extrometer is reduced by an amount equal to the rotation of the helical wires about their own axes. Quantitative assessment of this reduced rotation is not possible because of the modifying effect of wire flattening, due to contact pressure, on the rolling process.

8.3.3 Torque Generated

Torque generated under axial load on the strand was found to be greater in strands with lower helix angles. The load/torque relation was found to be sensibly linear in fixed end tests on all strands to loads above 80% of strand breaking load. Computed predictions on torque are in no case more than 0.13% less than those of Durelli. However, experimental results are between 1.1% ($\alpha = 80.9^{\circ}$) and 4.5% ($\alpha = 73.0^{\circ}$) less than predicted results.

8.3.4 Tension in Helical Wires

Helical wire tension for a given strand load was found to be less as torsional restraint on strand ends was reduced. It follows that the core wire takes a greater share of the overall strand load as helical wire tension reduces. Helical wire tension was also found to be less nearer strand termination, in the one strand on which wire tension was measured at two axial positions.

8.3.5 Strains on the Surface of Helical Wires

Preliminary tests (on strand V) showed that strain variations along a wire were less than variations between individual wires at any cross-section, along the strand, except at the end of the strand within one lay length of the termination. Wire strains measured during the main test programme showed that load sharing between helical wires was less even at strand ends than at mid-strand for all strands and under all conditions of end restraint. The unevenness of load sharing between wires increases with reduced torsional restraint on strand ends. Lower mean strains measured at strand ends than at mid-strand indicate lower tensions in helical wires at strand ends, an observation which is confirmed by tension measurements on the single wire of one strand (see section 8.3.4 above).

Analysis of strain ranges between the maximum and minimum strains on helical wires at a given cross-section showed that whereas these ranges, when calculated for the current cycle only, reduced when a particular strand load was applied a second time, the overall strain range increased, even up to a strand load of 100 kN, which is about 75% of breaking load. It can be concluded that repeated loading does not cause migration of wires to positions of greater stability in subsequent loading but increases the stretching of the wire or wires that are taking higher loads throughout the loading programme.

8.4 Overall Conclusions on Strand Response

The conclusions on individual elements of strand response, as considered separately in the previous section, 8.3, are now considered together and, from their mutual interaction, general conclusions drawn as to strand response under axial load and the validity of the assumptions made in the mathematical modelling.

8.4.1 Wire Tensions

Tests showed that under fixed end conditions, strand extensions were greater and torques generated were less than those predicted. From this it can be concluded that tensions in helical wires are less than those predicted since a lower share of total load taken by helicals results in a greater share being taken by the core which therefore extends further, as does therefore the whole strand. The major share of generated torque is contributed by the moment about strand axis of the tangential components of helical wire tensions. A reduction in these tensions results in a reduction in the torque.

Further evidence on wire tensions is found in results from free end tests. Strand rotation is less than predicted, as is strand extension. It follows that lower tensions in helical wires result in a lower torsional moment which in the free end case is balanced by torsional resistance in the core wire. This lower torsion results in lower core rotation and therefore strand rotation. Rotation measurements which were more than

12% less than predicted values in the case of lower helix angles, differed more from predictions than did any of the other measured strand responses to load. It seems likely, therefore, that in addition to the explanation that involves helical wire tensions being less than those predicted in the mathematical modelling, this reduction is due also to the rolling of helical wires over the core, as described in sub-section 8.3.2.

A further consequence of reduced rotation is that the unwrapping action of the helical wires is reduced. Since this is a major contribution to overall extension, a reduction in strand extension would be expected for free and partially restrained ends. This is borne out by test results. (See sub-section 8.3.1).

8.4.2 Contact Forces, Flattening of Wires and Slip

Computed predictions on strand response have taken account of interwire friction. The results from surface strain measurements on helical wires are in closer agreement with these predictions than those of Durelli et al. (27), which assume 100% interwire slip. The computed predictions also take account of the effect on helix angle and helix radius of wire flattening due to interwire pressure, which affects these predictions by no more than 0.4%. However, predictions do not take account of the fact that wire flattening results in interwire contact which is no longer line contact. Furthermore, the mathematical modelling predicts that, except possibly in the transitional lengths near strand ends, slip does not occur between wires in strand under

load. Even though mean values of surface strain on helical wires show a departure from the zero slip condition (see Figs 7.13 to 7.22) it is unrealistic to predict the onset of inter-wire slip in an assumed stick/slip mechanism as coefficient of friction reaches a certain value. The plots from test results of torsional restraint against wire surface strain ranges show clearly that another mechanism is present. It can be concluded that the initial contact points of both surfaces remain together, but due to yielding in the contact area of both wires, relative rotation about the centre lines of these wires occurs in the same direction as that which would occur if slip between wires is present. (See Fig. 7.26). It follows that whereas slip distances can be predicted under assumed conditions of line contact and a known coefficient of dynamic friction, they cannot be so predicted when there is wire flattening and movement of the line of contact in the yielded materials.

8.4.3 Strand Behaviour Near Terminations

Test results from strain measurement on the surface of helical wires indicated clearly that strand behaviour adjacent to strand termination, within about one lay length from it, is very different from that over the remainder of the strand. The mean tension in helical wires is lower and the unevenness of the load sharing between helicals is greater near the strand ends. It can be concluded that the core wire takes a greater tensile load in this region. However, it may be significant that four of the five strands broke at a position about one third of the

strand length from the strand grip and in the fifth strand, a helical wire broke first at a position just inside the resin of the grip. (See table 5.4). Even with a higher tension load in the core near strand ends, principal stress and maximum shear stress levels may be lower here than elsewhere in the strand where higher interwire contact pressures occur. The fact that the higher stress level gives rise to fracture in a tensile test at some distance from the end grip does not alter the fact that the larger stress ranges, due to uneven load sharing between wires, which occurs adjacent to the grip, makes this region most vulnerable to fatigue fracture in the repeated loading environment of normal rope usage.

8.5 Suggestions for Future Work

8.5.1 Wire Modulus

This study showed clearly the need to establish a figure for wire modulus before valid comparisons can be made between predictions from mathematical modelling and test results. The dependence of the value of modulus on the stress range used in tests makes it highly desirable that work is done on the determination of the range of such values over the working range of wires in wire ropes. The establishing of a standard test procedure for such wires would be of great benefit to manufacturers and users, as well as researchers in this field.

8.5.2 High Speed Photography at Strand Fracture

Though peripheral to the main objectives of this study, this technique demonstrated potential for acquiring information about strand breaks that cannot be acquired in any other way. It is probably worthwhile preparing a range of strand lengths specially for such tests, in which the extrometer bosses will not obscure possible fracture locations. More information is likely to be obtained if camera speed is increased above the 588 pictures/sec. reported here. (147 frames/sec. at $\frac{1}{4}$ frame).

8.5.3 Tension in Helical Wires

The differences between predictions on strand response to axial load and the experimental results obtained in this study are largely attributable to tension in the helical wires being slightly lower than expected. Any future work on strand or

rope testing, whether in tension or bending should include provision for tension measurement on all wires in selected locations. Three gauges on each wire with grids parallel to wire axis should be used, although strip gauges with three or more grids on the same backing would be preferable, if they are available. Load sharing between helical wires at mid-strand and over a range of distances up to one lay length from strand end could then be determined.

8.5.4 Testing of Rope and Strand of Complex Constructions

The experimental techniques developed in this study are suitable for use in tests on ropes of any construction. The extrometer can be adapted by using grips and, if necessary, bosses, of larger or smaller diameter to accommodate different strands or ropes. However, it would be difficult to attach strain gauges on individual wires that are very much smaller than those used in this study (i.e. 3.73 mm dia.), especially if wire tensions were to be examined. (This involves three gauges in parallel on a single wire). The first step in any future test programme could involve a spiral strand with one more layer than the seven wire strand of this study. If the same wire sizes were retained, a 12-6-1 strand construction would be suitable.

8.5.5 Bending Tests on Strand and Rope

The strands tested in this study are typical of those which are incorporated in stranded ropes of more complex constructions.

When such stranded ropes are subjected to tensile loads, the individual strands are subjected to tension, torsion and bending in the same way that the individual wires of a strand are loaded when the strand is subjected to tension. If, therefore, an individual strand is loaded in combined tension and bending, some indication may be obtained of the behaviour of such a strand when incorporated into a rope which is subjected to tensile load. That proportion of the torsional loading which occurs due to the change in tortuosity of a loaded helix is not present in the combined bending and tension test of a strand, but an additional controlled torsional loading can be introduced if required. An advantage of using strands of the same size as those used in the current study is that strain gauges are readily attached to wires of the size which make up these strands. Modifications to the existing rig are possible without the need to increase loading capacity.

8.5.6 Interwire Pressure and Slip

From the strain measurements made on the outside surface of the helical wires it was not possible to detect the onset of interwire slip or indeed to determine whether slip occurs at all. There is evidence that the flattening and yielding due to interwire pressure has an effect on the stress distribution in the wires of the strand and possibly on the sharing of strand load between them. A better understanding of the mechanism occurring at the core-helical interface would result from an extension of

the work of Hamlet (76) to determine the effect of tangential force on cylinders that have been flattened by contact pressure along their line of contact. Testing under conditions where a helix is wrapped around a cylinder would be difficult to arrange but the pressing together of two cylinders, one of which can be subjected to both torque and axial force of controlled magnitudes, approximates sufficiently to the actual conditions, particularly if the cylinders are kept short compared with their diameters.

8.5.7 Strand Behaviour Near Terminations

The foregoing paragraphs of this section have outlined a number of suggested experimental studies which can be undertaken with a view to better understanding of strand and rope behaviour. They include, as a major element, the study of the particular phenomena found near strand ends, where the geometry of the loaded strand changes from that of the initially unloaded strand, inside the resin (or other socketing medium), to one of increased helix angle and reduced helix radius at some distance from the termination. It may be profitable to pursue the mathematical modelling, started in Chapter 6, section 6.6, which attempted to set up equations for deformation and equilibrium over this transitional length of strand. Their solution for strands of particular initial geometry may provide an idealized standard, departure from which, in the experimental results on wire tensions and strains, can be used to estimate the quality of different types of socketing medium or wire preparation for termination.

REFERENCES

1. ALBERT, W.A.J. - 'On the Manufacture of Whim Ropes from Iron Wire', The Mining Journal and Commercial Gazette, Supplement XII, Feb. 25, 1837. (extracts from Foreign Scientific Works V), pp 47-48.

2. WEBER, W. - 'Development and Production of Wire Rope I and II', Wire World International, (I) Vol. 16, 1974, pp 286-291, (II) Vol. 17, 1975, pp 20-24.

3. FORESTIER-WALKER, E.R. - 'A History of the Wire Rope Industry in Great Britain', British Wire Rope Manufacturers, 1952.

4. SAYENGA, D. - 'The Birth and Evolution of the American Wire Rope Industry', Proc. of the First Annual Wire Rope Symposium, Denver, Colorado, March 1980.

5. COSTELLO, G.A. - 'Analytical Investigation of Wire Rope', Applied Mechanics Reviews, Vol. 31 (7), 1978, pp 897-900.

6. BAHKE, E. - 'Principles Defining the Strength of Wire Ropes and Chains I and II', Wire, (I) Vol. 29, No. 2, 1980, pp 54-61; (II) Vol. 30, No. 3, 1980, pp 168-176.

7. GIBSON, P.T. - 'Wire Rope Behaviour in Tension and Bending', Proc. of the First Annual Wire Rope Symposium, Denver, Colorado, March 1980.

8. SHARP, D. M. - 'Wire Rope in the Marine Environment I and II', Wire Industry, (I) Vol. 46, No. 543, 1979, pp 198-202; (II) Vol. 46, No. 544, 1979, pp 270-272.

9. BOYLE, J.A. - 'Recent Trends in the Development of Wire Rope Strands', Wire Industry, Vol. 48, No. 565, 1981, pp 37-38.

10. BABEL, H. - 'Destructive and Non-Destructive Test Methods to Determine the Life of Wire Ropes I and II', Wire, (I) 28, No. 6, 1979, pp 263-270; (II) 29, No. 1, 1980, pp 38-44.

11. ROPEMANS HANDBOOK, National Coal Board, 3rd Edition.

12. HALL, H.M. - 'Stresses in Small Wire Ropes', Wire and Wire Products, Vol. 26, 1951, pp 228 and 257-259.

13. HRUSKA, F.H. - 'Calculation of Stresses in Wire Ropes', Wire and Wire Products, Vol. 26, 1951, pp 766-767 and 799-801.

14. HRUSKA, F.H. - 'Radial Forces in Wire Ropes', Wire and Wire Products, Vol. 27, 1952, pp 459-463.

15. HRUSKA, F.H. - 'Tangential Forces in Wire Ropes', Wire and Wire Products, Vol. 28, 1953, pp 455-460.

16. PHILLIPS, J.W. and COSTELLO, G.A. - 'Contact Stresses in Twisted Wire Cables', Proc. ASCE, Jnl. Eng. Mech. Div., Vol. 99nEM2, 1973, pp 331-341.

17. COSTELLO, G.A. and PHILLIPS, J.W. - 'A More Exact Theory for Twisted Wire Cables', Proc. ASCE, Jnl. Eng. Mech. Div., Vol. 100, 1974, pp 1096-1099.

18. COSTELLO, G.A. and PHILLIPS, J.W. - 'Effective Modulus of Twisted Wire Cables', Proc. ASCE, Jnl. Eng. Mech. Div., Vol. 102nEM1, 1976, pp 171-181.

19. COSTELLO, G.A. and SINHA, S.K. - 'Torsional Stiffness of Twisted Wire Cables', Proc. ASCE, Jnl. Eng. Mech. Div., Vol. 103nEM4, 1977, pp 766-770.

20. COSTELLO, G.A. and SINHA, S.K. - 'Static Behaviour of Wire Ropes', Proc. ASCE, Jnl. Eng. Mech. Div., Vol. 103nEM6, 1977, pp1011-1022.

21. COSTELLO, G.A. and MILLER, R.E. - 'Lay Effect of Wire Rope', Proc. ASCE, Jnl. Eng. Mech. Div., Vol. 105nEM4, 1979, pp 597-608.

22. COSTELLO, G.A. and MILLER, R.E. - 'Static Response of Reduced Rotation Rope', Proc. ASCE, Jnl. Eng. Mech. Div., Vol. 106nEM4, 1980, pp 623-631.

23. PHILLIPS, J.W., MILLER, R.E. and COSTELLO, G.A. - 'Contact Stresses in Straight Cross-Lay Wire Rope', Proc. of the First Annual Wire Rope Symposium, Denver, Colorado, March 1980.

24. VELINSKY, S. and COSTELLO, G.A. - 'Axial Response of Oval Wire Ropes', ASME Paper No. 80-WA/OCE-3, Proc. ASME Ocean Eng. Div. Conference, Chicago, Ill., 1980.

25. COSTELLO, G.A. and BUTSON, G.J. - 'Simplified Bending Theory for Wire Rope', ASCE, Jnl. Eng. Mech. Div., Vol. 108nEM8, 1982, pp 219-227.

26. LOVE, A.E.H. - 'A Treatise on the Mathematical Theory of Elasticity', Dover Publications Inc., 1944.

27. MACHIDA, S. and DURELLI, A.J. - 'Response of a Strand to Axial and Torsional Displacements, Jnl. of Mech. Eng. Science, Vol. 15, No. 4, 1973, pp 241-251.

28. DURELLI, A.J., MACHIDA, S. and PARKS, V.J. - 'Strains and Displacements on a Steel Wire Strand, Naval Engineers Journal, Vol. 84, No. 6, 1972, pp 85-93.

29. DURELLI, A.J. and MACHIDA, S. - 'Response of Epoxy Oversized Models of Strands to Axial and Torsional Loads', Experimental Mechanics, Vol. 13, 1973, pp 313-321.

30. CHI, M. - 'Analysis of Operating Characteristics of Strands in Tension allowing End Rotation', ASME Paper No. 72-WA/OCT-19, Proc. ASME Oc. Tech. Div. Meeting, New York, 1972.

31. CHI, M. - 'Analysis of Multi Wire Strands in Tension and Combined Tension and Torsion', Proc. of the Seventh South Eastern Conference on Theoretical and Applied Mechanics, Vol. 7, 1974, pp 599-639.

32. HUANG, N.C. - 'Finite Extension of an Elastic Strand with a Central Core', ASME Jnl. of App. Mechs, Vol. 45, No. 4, 1978, pp 852-858.

33. MATHESON, J.A.L. - 'The Mechanics of Locked Coil Ropes', Engineering, June 18th and 25th, 1948, pp 578-581 and 601-604.

34. HANSOM, O.P. - 'Mechanics of Locked Coil Steel Wire Ropes', Ph.D. Thesis, University of Birmingham, 1948.

35. GLUSHKO, M.F. - 'Mechanical Testing of Wire Ropes', Translated from Russian, Zavodskaya Laboratoriya Vol. 28, No. 8, 1962, pp 981-983. (SMRE, Health and Safety Exec. translation).

36. KOLLROSS, W. - 'Relationship between Torque, Tensile Force and Twist in Wire Ropes', Wire, Vol. 26, No. 1, 1976, pp 19-24.

37. KNAPP, R.H. - 'Torque and Stress Balanced Design of Helically Armoured Cables', ASME Paper No. 80-WA/OCE-1, Proc. Ocean Eng. Div. Conference, Chicago, Ill., 1980.

38. KNAPP, R.H. - 'Derivation of a New Stiffness Matrix for Helically Armoured Cables considering Tension and Torsion', Intl. Journal for Numerical Methods in Engineering, Vol. 14, 1979, pp 515-529.

39. KNAPP, R.H. - 'Non-Linear Analysis of a Helically Armoured Cable with Non-Uniform Mechanical Properties in Tension and Torsion', IEEE paper No. 75CHO, 995-1, OEC, Proc. IEEE Conference on Engineering in the Ocean, Environmental and Marine Tech. Sec., 11th Annual Meeting, San Diego, Cal., 1975, pp 155-164.

40. NOWAK, C. - 'Computer Design of Electromechanical Cables for Ocean Application', Proc. of 10th Annual Conference, Marine Tech. Society, Washington D.C., 1974, pp 293-305.

41. HOBBS, R.E. and RAOOF, M. - 'Prediction of Elastic Properties of Large Strands and Cables', Int. Wire and Mach. Assoc. Conference on 'Offshore Applications', Aberdeen, 1983.

42. MARTIN, B.C. and PACKARD, T.J. - 'Stresses in Wire Strand', B.Sc. Project report, University of Bristol, Dept. of Civil Engineering, 1966.

43. PAOLINI, G. and BAZZARO, E. - 'Study on the State of Stress in the Wires of Steel Ropes under Tensile Loads', Proc. OIPEEC Round Table, Milan 1973, pp 112-122.

44. MANCINI G. and ROSSETTI U. - 'Sur l'analyse des constraintes et des deformations des cables flechis', Proc. OIPEEC Round Table, Milan 1973, pp 65-86.

45. MOLINARI, G. - 'Experimental Research on the Strains Distribution in the Wires of a Simple Spiral Strand under Tensile Loading during the Breaking of One of Them', (in Italian), Elevatori, Vol. 6, 1980, pp 30-39.

46. WIEK, L. - 'The Influence of Broken Wires on Wire Rope Strength and Discarding', Proc. OIPEEC Round Table, Luxemburg, 1977.

47. WIEK, L. - 'Facts and Figures of Stresses in Ropes, I and II', Wire, (I) Vol. 26, No. 4, pp 173-178, (II) Vol. 26, No. 5, pp 214-216.

48. WIEK, L. - 'Measured Differences between Steel Wire Ropes in Normal Lay and in Lang Lay', Report, Technische Hogeschool, Delft, 1975.

49. WIEK, L. - 'Strain Gauge Measurements at Multi Strand Non-Spinning Ropes', Publ. No. 212, Technische Hogeschool, Delft, Transportkunde, 1979.

50. WIEK, L. - 'Stress Deviations in Steel Wire Ropes', Proc. OIPEEC Round Table, Cracow, 1981.

51. NESTEROV, P.O., SHABANOV-KUSHNARENKO, YU.P. and KOZYUBERDA, N.I.- 'A New Method of Determination of Stresses in Wire Ropes', translated from Russian, Zavodskaya Laboratoriya, Vol. 27, No. 2, 1961, pp 191-194. (SMRE, Health and Safety Exec. translation).

52. HANKUS, J. - 'The Permanent and Percentage Elongation of Winding Ropes in Factory Condition', translated from Polish, Glowny Instytut Gornictwa Katowice 1977, Kommunikat No. 862, pp 3-14. (SMRE, Health and Safety Exec. translation).

53. HANKUS, J. - 'Elastic Modulus of Mine Winding Ropes in Conditions of Static Loading', (in Polish with English abstract), Glowny Instytut Gornictwa, Katowice 1978, Kommunikat No. 695.

54. HANKUS, J. - 'Spinning Moment in Winding Ropes', (in Polish with English abstract), Glowny Instytut Gornictwa, Katowice 1973, Kommunikat No. 579.

55. GIBSON, P.T., CRESS, H.A., KAUFMANN, W.J. and GALLANT, W.E. - 'Torsional Properties of Wire Rope', ASME Paper No. 69-DE-34, Proc. Design Eng. Div. Conference, N. York, 1969.

56. SLIGHT, G.C. - 'The Torsional Properties of Three and Seven Strand Wire Ropes with a View to their Use in Multiple Strand Helical Springs', M.Sc. Thesis, University of London (Woolwich Polytechnic), 1949.

57. KROLEVETS, M.S. - 'The Modulus of Elasticity in Steel Wire Ropes', Issled po voprosam ustoichovosti i prochnosti, KIEV, AN, USSR, 1956, pp 243-253. (SMRE, Health and Safety Exec. translation).

58. HANKUS, J. - 'Examination of Elastic Modulus of Mine Winding Ropes in conditions of Dynamic Loading'. (In Polish with English abstract). Katowice 1978, Glowny Instytut Gornictwa, Kom. No. 700.

59. STONESIFER, F.R. and SMITH, H.L. - 'Tensile Fatigue in Wire Rope', Proc. Offshore Technology Conference, Vol. 1 1979.

60. DRUCKER, C.C. and TACHAU, H. - 'A New Design Criterion for Wire Rope', Jnl. of Applied Mechanics, Trans. ASME Vol. 67, 1945, pp A33-A38.

61. STARKEY, W.L. and CRESS, H.A. - 'An Analysis of Critical Stresses and Mode of Failure of a Wire Rope', Jnl. of Engineering for Industry, Trans. ASME Vol 81, 1959, pp 307-316.

62. LEISSA, A.W. - 'Contact Stresses in Wire Ropes', Wire and Wire Products, Vol. 34, 1959, pp 307-314 and 372-373.

63. BERT, C.W. and STEIN, R.A. - 'Stress Analysis of Wire Rope in Tension and Torsion', Wire and Wire Products, Vol. 31, 1962.

64. DONG, R.G. and STEIDEL, R.F. - 'Contact Stress in Stranded Cable', Experimental Mechanics, May 1965, pp 142-147.

65. LAURA, P.A., VANDERVELDT, H. and CAFFNEY, P. - 'Mechanical Behaviour of Stranded Wire Rope', Marine Tech. Soc. Journal, Vol. 4(3), 1970, pp 19-32.

66. BECHTLOFF, G. - 'Longitudinal Elongation and Transverse Contraction of a Six-Stranded Wire Rope under Tensile Load', Wire World, Vol. 5, No. 6, 1963, pp 247-252.

67. MYERS, W.H. - 'Major Part of Lifting Devices; Wire Rope End Attachments', Wire Journal, March 1977, pp 67-71.

68. HILGERS, W. - 'Wire Rope Tail Cones and Alloys', Wire, Nov/Dec 1973, pp 251-263.

69. CHRISTEN, R. - 'Tail Cones: Does Doubling Back of the Wire Increase Safety', Wire, Vol. 23, E4, 1973, pp 160-164.

70. DODD, J.M. - 'Resin as a Socketing Medium', Wire Industry, Vol. 48, No. 569, 1981, pp 343-344.

71. GATHMAN, D.W. - 'Resin Socketing for Wire Rope Attachments', Wire Journal, Vol. 12, No. 6, 1979, pp 82-85.

72. MATANZO, F. Jr. and METCALF, J.T. Jr. - 'Efficiency of Wire Rope Terminations Used in the Mining Industry', Proc. OIPEEC Round Table, Luxemburg, 1977. Also Journal of Engineering Materials and Technology, trans. ASME Vol. 103, 1981, pp 164-170.

73. CHAPLIN, C.R. and SHARMAN, R.C. - 'Mechanisms of Load Transfer in Resin Socketed Terminations', Int. Wire and Mach. Assoc. Conference on 'Offshore Applications', Aberdeen, 1983.

74. POPLE, J. - 'D.I.Y. Strain Gauge Transducers, I and II', Strain, (I) Vol. 16, No. 1, 1980, pp 23-36; (II) Vol. 16, No. 2, 1980, pp 69-80.

75. VIRGOE, R.J. - 'Load Transducers - Design, Manufacture and Use', Strain, Vol. 8, No. 2, 1972.

76. MM TECHNICAL NOTE TN-138-4, 'Errors due to Misalignment of Strain Gauges', Welwyn Strain Measurement Ltd.

77. KERR, J. - 'The Effect of Trimming on Strain Gauge Accuracy', Strain, Vol. 17, No. 4, 1981, pp 147-150.

78. HAMLET, C.D. - 'Contact Stresses and Loads between Individual Wires in a Stranded Wire Rope', B.Eng. Project Report, Department of Mechanical Engineering, University of Liverpool, 1983.

79. MARGETTS, R.G. AND SPIKES, J. - 'Single Contact Testing and Lubrication of Wire Ropes', Int. Wire and Mach. Assoc. Conference on 'Offshore Applications', Aberdeen, 1983.

80. PLANT, H.B. - 'Private Communication', British Ropes Research Development.

APPENDIX A.1

LOAD CELL CIRCUITS AND CALIBRATION

A.1.1 Tension Circuit

Eight gauges are mounted as shown in Fig. A.1.1.a., four having their grid axes parallel and four having their grid axes perpendicular to that of the loading rod. When connected as shown in Fig. A.1.1.b., output from strains due to bending and torsional loading on the loading rod are balanced out and the output from tension only is recorded at G. Gauges 1, 3, 5 and 7 are subjected to axial strain ε and gauges 2, 4, 6 and 8 suffer the Poisson strain $-\nu\varepsilon$

The output from this circuit is given by

$$\delta v = \varepsilon f v n/4 \qquad \text{A.1.1}$$

where ε is the axial strain in rod surface due to tensile load,

f is the gauge factor of the strain gauges,

v is the applied voltage,

and $n = 2(1+\nu)$ for this configuration of gauges.

The gauges used were type EA-250-UW-350 from Welwyn Strain Measurement Ltd., having a grid resistance of 350Ω and a gauge factor (f) of 2.06. Assuming Poisson's ratio of 0.3 and by using a bridge voltage of 10v, output δv is given by

$$\delta v = \varepsilon .13.39 \qquad \text{A.1.2}$$

Suitable amplification in the Fylde bridge/amplifier gave convenient calibration figures. See Table A.1 and Fig. 3.3.a.

Figure A.1.1.Load Cell-Tension.

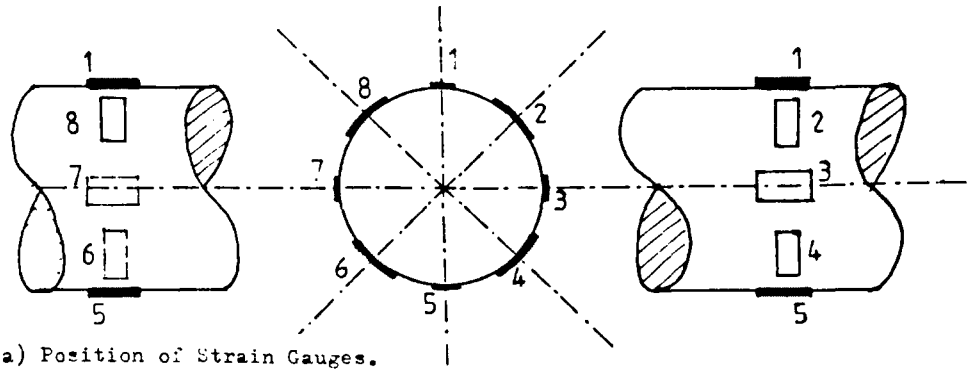

(a) Position of Strain Gauges.

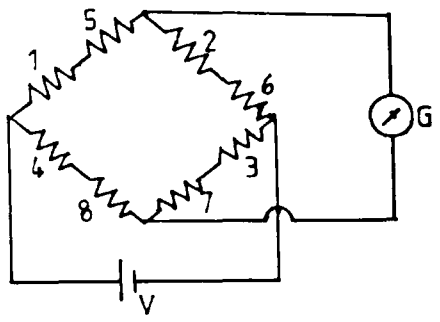

(b) Tension Circuit.

Figure A.1.2.Load Cell-Torsion.

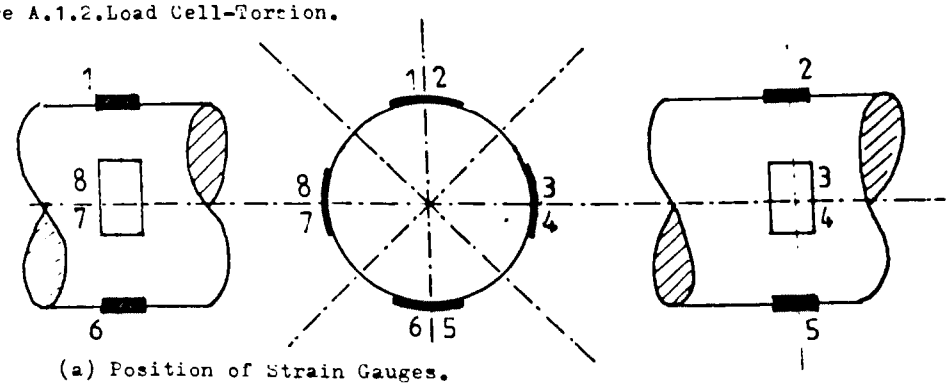

(a) Position of Strain Gauges.

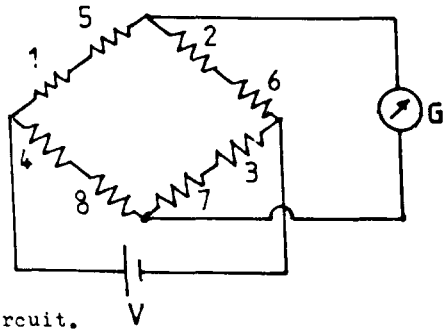

(b) Torsion Circuit.

A.1.2 Torsion Circuit

Eight gauges are mounted as shown in Fig. A.1.2.a. They are special torque gauges which are in the form of matched pairs having their grids at 90^{o} to each other and at 45^{o} to marked axes on the gauge backing material. When connected as shown in Fig. A.1.2.b., output from strains due to bending and tension loading on the loading rod are balanced out and the output from torsion only is recorded at G.

The output from this circuit is given by

$$\delta v = |\varepsilon| fvn \qquad \text{A.1.3}$$

where ε is the principal strain (in the direction of strain gauge grid axes),

f is the gauge factor of the strain gauges,

v is the applied voltage,

and $n = 1$ for this configuration of gauges.

(Note that $\varepsilon = MR_R (1 + \nu)/J.E$ where R_R = radius of loading rod).

The gauges used were type EA-250-TD-120 from Welwyn Strain Measurement Ltd., having a grid resistance of 120Ω and a gauge factor (f) of 2.055. Assuming Poisson's ratio of 0.3 and by using a bridge voltage of 5v, output δv is given by

$$\delta v = |\varepsilon| .10.28 \qquad \text{A.1.4}$$

Suitable amplification in the Fylde bridge/amplifier gave convenient calibration figures. See Table A.3 and Fig. 3.3.c.

A.1.3 Crosstalk on Load Cell Circuits

The effect of tension on the output of the torsion circuit is significant (see Fig. 3.3.b.). However, the effect of torsion on the output of the tension circuit is undetectable. The same degree of care was taken in the application of both these sets of gauges to the surface of the loading rod, so that differences in the magnitude of gauge misalignment alone cannot account for the difference in their performance.

The fact that the range of strain up to a given strand loading is very much greater due to tension than that due to torque generated is the most probable reason for this difference. The effect of nett gauge misalignment under the loading conditions of these tests is analysed below.

Output on torque circuit is given by

$$M = M' + 0.053P \qquad \text{A.1.5}$$

(from Chapter 3, section 3.3.2, expression 3.4)

where M is actual torque generated in Nm,

M' is apparent torque generated in Nm,

P is tension in strand in kN.

For an axial load of 1kN, the apparent torque on the load cell rod is therefore 0.053 Nm. Strain on the axis of one gauge at 45° to rod axis, due to a torque of 0.053 Nm is given by

$$\varepsilon_{45^o} = \frac{0.053}{J} \cdot \frac{d}{2} \; (1 + \nu)/E = 0.01351 \times 10^{-6} \qquad \text{A.1.6}$$

where $E = 197.9 \text{ kN/mm}^2$

$d = 50.8 \text{ mm}$

$J = \pi d^4/32$

$\nu = 0.3$

Strain on axis of rod due to tensile load of 1kN is given by

$$\varepsilon_A = \frac{1}{A.E}$$

$$\varepsilon_A = 0.8735 \times 10^{-6} \qquad \text{A.1.7}$$

From MM Technical Note (Welwyn Strain Measurement)TN-138-4 (76) the error due to misalignment in a strain gauge is given by

$$\eta = \frac{(\varepsilon_p - \varepsilon_q)}{2} \cdot (\cos 2 \; (\varnothing \pm \beta) - \cos 2\varnothing) \qquad \text{A.1.8}$$

where ε_p and ε_q are the maximum and minimum principal strains,

$\varnothing$ is the angle between the maximum principal strain axis and the intended axis of strain measurement,

β is the angular mounting error.

In this case, the error due to 1kN axial tension on the rod is given by

$$\eta = \varepsilon_{45^\circ} = 0.01351\,\mu\varepsilon$$

$$\phi = 45^\circ$$

$$\varepsilon_p = 0.8375\,\mu\varepsilon \qquad \text{A.1.9}$$

$$\varepsilon_q = 0.3\varepsilon_p$$

Substituting A.1.9 in A.1.8 gives

$$\sin 2\beta = 0.02482$$

$$\text{and} \qquad \beta = 0.71^\circ \qquad \text{A.1.10}$$

Since the eight gauges in the circuit are mounted in pairs, it is possible that this error may be shared between the four pairs, giving an average error of less than 0.2°. It cannot be established whether the output from the torsion circuit is due to attaching the gauge or gauges along an axis or axes at angles in error by the amount determined above, or due to the fact that the loading axis of the rod is not coincident with the geometric axis, but at some angle to it, due perhaps to the inherent inaccuracy of the screwed ends. (See Virgoe (75)). Whatever the reasons for this error, the validity of torsion results from the strand tests is not in doubt, since effective calibration of this output was carried out. See Table A.2 and Fig. 3.3.b.

Similar analysis of the effect of torsion on the tension circuits of the load cell shows that an overall error of 3.17° in gauge alignment is needed to cause a 1% error in the tension circuit. In fact no effect was detected and it must be concluded that any errors in gauge alignment were very much less than this.

A.1.4 Load Cell Outputs

Axial Tensile Load

Tension Circuit (Tensile loading in Denison 50tonf test machine)

Bridge/Amplifier Settings :

Toggle switch 10 mv F.S.D.
Dial switch 635
Bridge volts 10 v

Table A.1.1.

Load kN	Output from Amplifier			
	Output Loading		Second Loading	
	Load Increase mv	Load Decrease mv	Load Increase mv	Load Decrease mv
0	0.01	0.02	0.02	0.02
20	1.02	1.02	1.01	1.01
40	2.02	2.03	2.02	2.01
60	3.01	3.02	3.00	3.02
80	4.01	4.01	4.00	3.98
100	5.0	5.01	5.00	4.99
120	5.98	6.02	5.98	6.00
140	7.02	7.00	7.01	6.98
160	8.01	8.02	8.00	8.00
180	9.03	9.02	9.02	9.00
200	10.02	-	10.01	-

See Fig. 3.3.a. Slope = 20 kN/mv

Torsion Circuit (Tensile load in test rig)

Bridge/Amplifier Settings:

Toggle switch 10mv F.S.D.

Dial switch 24

Bridge volts 5 v

Table A.1.2

Load kN	Output from Amplifier			
	First Loading		Second Loading	
	Load Increase μv	Load Decrease μv	Load Increase μv	Load Decrease μv
0	0	50	25	45
5	-50	-25	-40	-10
10	-100	-75	-90	-70
15	-150	-130	-140	-130
20	-190	-175	-180	-170
25	-210	-210	-200	-200
30	-240	-235	-230	-230
35	-270	-265	-260	-260
40	-290	-290	-280	-280
45	-320	-315	-305	-310
50	-345	-	-335	-

See Fig. 3.3.b. Slope = -0.188 kN/μv

Torsion Load

Torsion Circuit (Torsion loading in Avery Torsion machine)

Bridge/Amplifier settings:

Toggle switch 10 mv F.S.D.

Dial switch 635

Bridge volts 5 v

Table A.1.3

Torque Nm	Output from Amplifier			
	First Loading		Second Loading	
	Load Increase μv	Load Decrease μv	Load Increase μv	Load Decrease μv
0	660	650	650	610
5	1150	1150	1130	1100
10	1660	1630	1620	1590
15	2140	2130	2120	2090
20	2630	2610	2610	2580
25	3130	3120	3120	3070
30	3630	3600	3620	3570
35	4120	4100	4110	4070
40	4620	4600	4610	4560
45	5110	5090	5110	5060
50	5620	5590	5610	5550
55	6110	6070	6100	6060
60	6610	6580	6600	6550
65	7120	7080	7090	7050
70	7620	7590	7590	7550
75	8090	8080	8090	8050
80	8600	8580	8580	8550
85	9080	9090	9060	9040
90	9580	9570	9570	9530
95	10080	10070	10060	10030
100	10570	-	10550	-

See Fig. 3.3.c. Slope = 9.9×10^{-3} Nm/μv

Note: No detectable change in output from tension circuit

APPENDIX A.2

"EXTROMETER" CIRCUITS AND CALIBRATION

A.2.1 Extension Circuit

It was possible to connect the leads from the displacement transducer direct to one channel of the bridge/amplifier unit. Selection of a suitable amplification facilitated calibration with convenient output units.

A.2.2 Rotation Circuit (See Fig. A.2.1)

The two rotary potentiometers are of 1000Ω each nominal. In order to ensure linear output with relative angular position of the potentiometers, some fine tuning was necessary. The angles over which the 1000Ω resistance of the two potentiometers (less than 360° due to the space taken by terminal connections) are different from each other. By trial and error, the variable resistor (max 500Ω) R2 was adjusted so that overall output was linear.

Bridge amplification was adjusted to give an output of about 5mv/degree of rotation.

Now bridge output is given by

$$\delta v_{XY} = I(R_A - R_B)/2 \qquad \text{A.2.1}$$

where I is current to bridge, given by

$$I = \frac{2.v}{1470} \qquad \text{A.2.2}$$

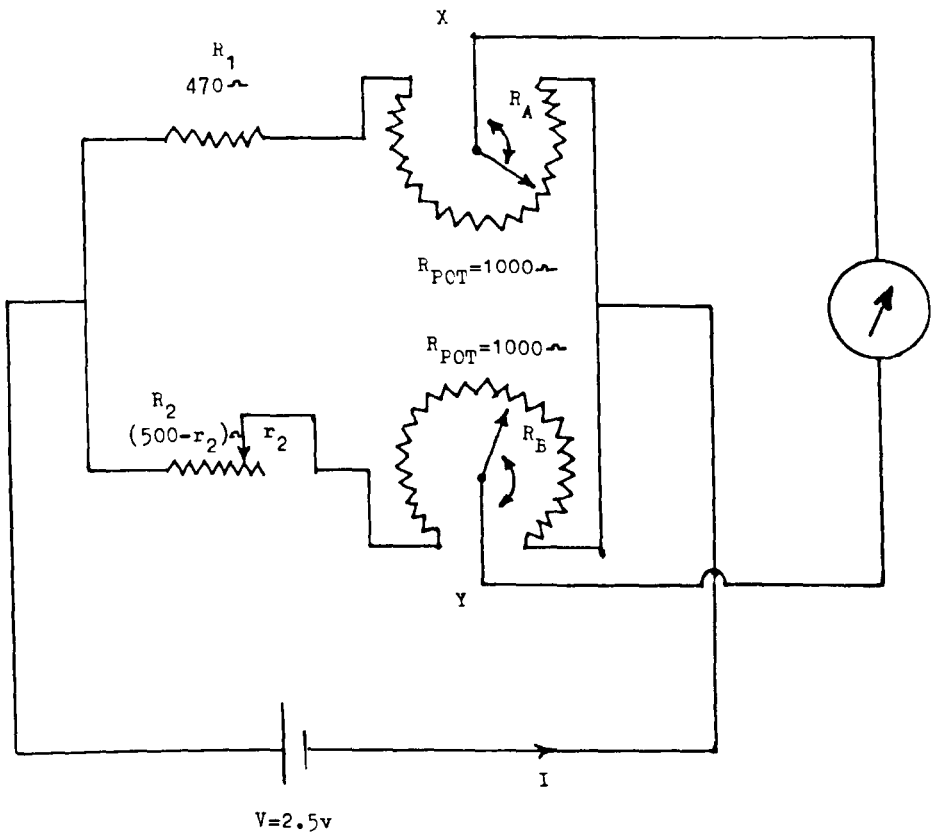

Figure A.2.1. Rotary Potentiometers Circuit.

The sprockets attached to the potentiometer axes have 25 teeth. Assuming that 1000Ω covers 24 of the 25 teeth, resistance rate is given by about 2.9Ω/degree.

If bridge voltage is 2.5 and setting $(R_A - R_B) = 2.9$, bridge output, from A.2.1, is given by

$$\delta v_{XY} \doteq 5 \times 10^{-3} v/\text{degree}$$

Calibration tables in section A.2.3 (ii) confirmed this estimate.

A.2.3 "Extrometer" Outputs

Extension

Bridge/Amplifier Settings:

Toggle switch 10 mv F.S.D.

Dial switch 30

Bridge volts 4.0 v

(Note: only readings at 90° increments are shown)

Table A.2.1

Screw Rotation Degrees	Extension mm	Output L_F	
		Increasing mv	Decreasing mv
0	0	-1035	-998
90	0.25	- 950	-902
180	0.50	- 852	-802
270	0.75	- 744	-695
360	1.00	- 641	-598
450	1.25	- 549	-500
540	1.50	- 453	-399
630	1.75	- 338	-294
720	2.00	- 241	-198
810	2.25	- 152	-106
900	2.50	- 49	- 3
990	2.75	+ 50	+ 95
1080	3.00	158	207
1170	3.25	250	300
1260	3.50	350	397
1350	3.75	460	503
1440	4.00	560	603
1530	4.25	653	696
1620	4.50	750	792
1710	4.75	864	900
1800	5.00	959	996
1890	5.25	1051	-

(Readings at 10^{o} increments at reversal)

Table A.2.1.a

Screw Rotation Degrees	Extension mm	Output L_F	
		Increasing mv	Decreasing mv
1800	5.00	959	996
1810	5.03	968	1007
1820	5.06	976	1017
1830	5.08	986	1027
1840	5.11	998	1037
1850	5.14	1008	1047
1860	5.17	1017	1053
1870	5.19	1027	1052
1880	5.22	1040	1052
1890	5.25	1051	-

By method of least squares, best straight lines were found to be

$$\delta_{INC} = 2.498 \times 10^{-3} L_F + 2.612 \text{ mm} \qquad \text{A.2.3}$$

$$\delta_{DEC} = 2.505 \times 10^{-3} L_F + 2.499 \text{ mm} \qquad \text{A.2.4}$$

This gives an output of 400 mv/mm, within 0.1%.

By difference of intercepts, backlash is 0.11 mm.

From Table A.2.1.a. it can be seen that reversal of the extrometer mechanism is completed by extension of 5.14 mm (i.e. at distance of about 0.1 mm from reversal point).

Rotation

Bridge/Amplifier Settings:

Toggle switch 1 v F.S.D.

Axial switch 1000

Bridge volts 2.5 v

(Note: Increments of 5^{o} were used, but 20^{o} increments, only, are shown below).

Table A.2.2

Rotation Degrees	Output R_F	
	Increasing mv	Decreasing mv
0	809	804
20	709	706
40	609	608
60	505	507
80	405	406
100	308	295
120	203	201
140	108	104
160	6	+ 6
180	- 93	- 92
200	-194	-189
220	-292	-294
240	-393	-401
260	-490	-496
280	-596	-598
300	-698	-700
320	-796	-

By method of least squares, best straight lines were found to be

$$\varnothing_{INC} = -199.6R_F + 161.29 \qquad \text{A.2.5}$$

$$\varnothing_{DEC} = -199.6R_F + 160.83 \qquad \text{A.2.6}$$

This gives an output of 5 mv/degree, within 0.2%, as designed in section A.2.2.

By difference of intercepts, backlash is 0.46 degrees.

It is not possible to determine the rotation over which reversal of the extrometer mechanism is completed in the same way as for output from extension circuitry except to say that it is well within the 5 degree increment.

The significance of this backlash for both extension and rotation is discussed in Chapter 5, sub-section 5.5.4. It is concluded that the slope of load/extension and load/rotation plots are not affected and none of the results used for comparison with theoretical predictions on strand response are invalidated.

APPENDIX A.3

LINE LOSS IN OUTPUT TO DATA LOGGER

A strain calibration box (Welwyn Strain Measurement Unit 61) was used to feed the resistance change resulting from a known strain into the active arm of the bridge completed by the fixed resistors of one of the 50 channels in a data logger bridge unit. The output for each resistance change was recorded, as read from the control and indicator unit of the logger, situated some 30 metres from the bridge unit. Fig. A.3.1 is a plot of nominal strain against logger reading. Since the logger unit is designed to give an output from a gauge having nominal gauge factor of 2.0, the correction factor to be applied to data logger output is given by

$$c = s.f./2 \qquad \text{A.3.1}$$

where s is the slope of nominal strain/data logger output, from Fig. A.3.1,

and f is the gauge factor of the strain gauge

From the slope of Fig. A.3.1, $s = 1.0264$.

The strain gauges used in the strand tests are detailed and f and c listed in Table A.3.1.

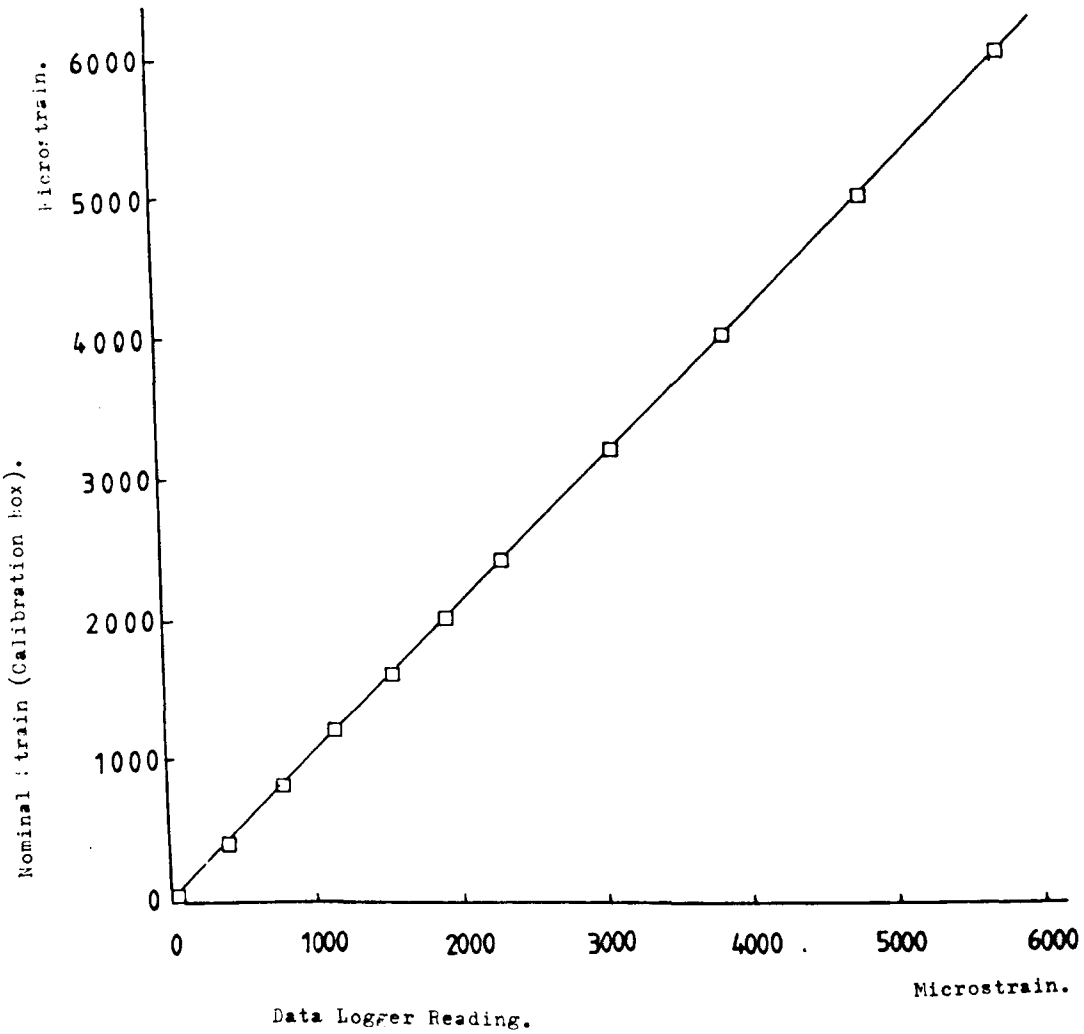

Figure A.3.1. Calibrated Nominal Strain/Data Logger Reading.

Table A.3.1

Strain Gauge Manufacturer	Gauge Type	f	c
Welwyn Strain Meas. Ltd.	Wire Axis	2.07	0.9917
Welwyn Strain Meas. Ltd.	Perp. to Wire Axis	1.90	1.0804
KYOWA	Perp. to Wire Axis	2.14	0.9593

APPENDIX A.4

STRAND TERMINATIONS

A.4.1 Conical Ends (Fig. A.4.1.a)

The end grip consists of a steel cylinder of external diameter D, having a flange of larger external diameter at one end and a conical hole of maximum diameter d_1 (47 mm), initially at the flange end and minimum diameter d_s at the other end (see Fig.A. 4.1.a). Diameter D (76 mm) was designed to fit the grips of the Denison test machine and d_s (11.4 mm) to clear the diameter of the strand to be tested. The cone angle is about 10^o to suit B.S.S. 463. After strand III had been tested, the conical hole was opened out to d_2 (65 mm) with consequent reduction in the length of the parallel throat section (ℓ_1 to ℓ_2) of diameter d_s. This greater volume was intended to reduce interference between hooked ends of the seven wires.

Figure A.4.1. Strand End Grips.

(a) Conical Ends.

(b) Pouring.

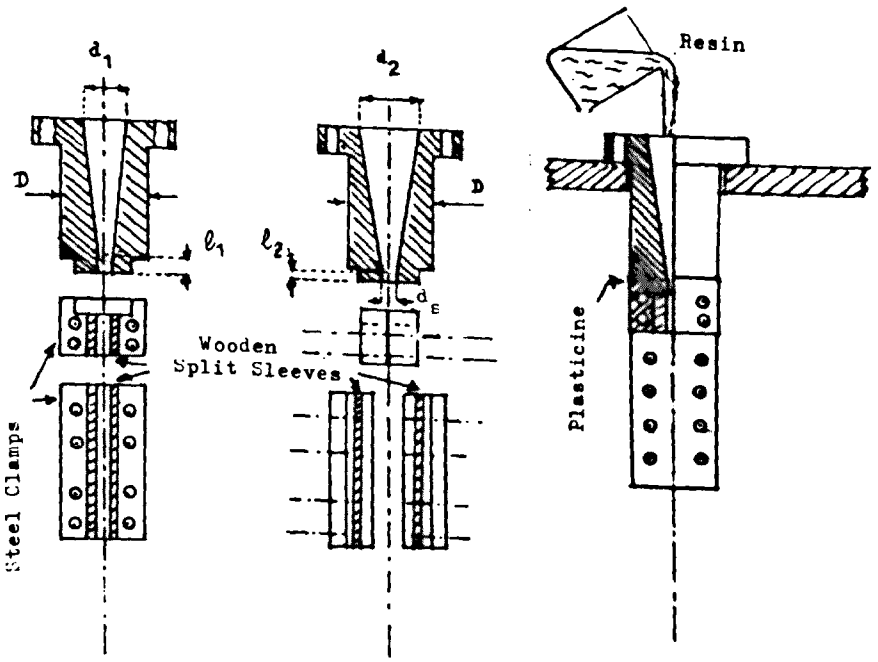

(c) Wire Ends.

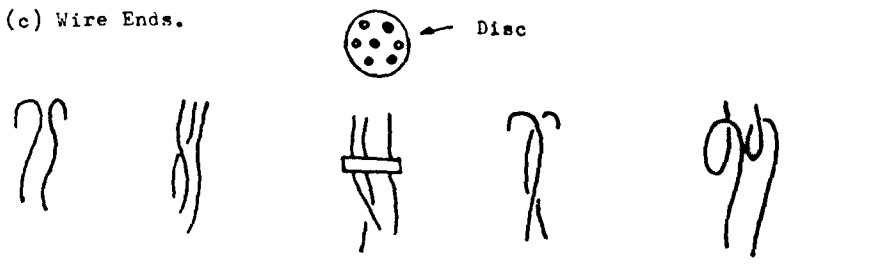

Strand I
180° Hooks

Strand II
Unbent

Strand III
Unbent
+
Disc.

Strands IV &V
180° Hooks

Strands VI to X
360° Loops

A.4.2 Socketing Medium and Procedure

Polyester based resin with silica filling, as supplied by the Wirelock Co. in a two pack kit, and described by Dodd (70), was chosen in preference to zinc based metallic socketing medium, for convenience and, as in the experience of other workers (70,71,72) grip efficiency. The socketing process is illustrated in Fig. A.4.1.b. After the strand end is threaded through the grip, from the end with the smaller diameter, the wires are unwrapped from each other and, hooked over, as in strands I, IV and V, threaded individually through the holed disc, as in strand III, or looped through 360° as in strands VI to X. The strand is then pulled firmly back into the conical hole such that no wire, hook or loop extends beyond the flanged end of the grip body. In order to ensure that no resin trickles down the outside of the strand, plasticine is wedged round the strand where it emerges from the grip body. Clamps with wooden split sleeves are then clamped over the strand, adjacent to the grip body which ensures that the strand axis is located perpendicular to the plane of the flange at the back of the grip body. The strand is then suspended with flange horizontal, checked by use of spirit level. After thoroughly mixing and stirring the liquid (resin) and solid (filler) components of the socketing medium, it is poured slowly into the conical hole until the level of the mixture is flush with the flange. Although the resin/silica mixture hardens in about 10 minutes, the strand is left for 24 hours before removing clamps and proceeding with the socketing of the other end.

A.4.3 Wire Ends

The mechanism by which axial load is transferred from the wires of the strand through the socketing medium to the grip is postulated by Chaplin and Sharman (73). The adhesive action between wire and resin first pulls the resin into the cone and the radial force transmitted from cone to resin then grips the wires. In ropes and strands of more complex construction, there are more than seven wires and the wire surface area is very much greater than in the strands of this study. The experience in strand tests II and III showed that the surface area in seven wire strands appears inadequate to institute the adhesive action, which is the necessary first step in the gripping mechanism. The wires pulled straight out as load was applied (see Figs. 4.1 and 4.2). The use of a disc with 7 holes in strand III, which was intended to ensure that wires retain equal spacing between them and thus transmit an equal share of the loading, was ineffective. In strands IV and V the hooked ends were tried again, this time with a larger conical hole. (See A.4.1. above). In strand V, even hooked ends did not solve the problem. At one end, a disc of resin beyond the hook ends cracked off the main cone, the wires straightened and pulled out again. It was therefore decided that for the main test programme, strands VI to X, wires should be bent through 360° to form a full loop within the socketing medium of the termination. This effective addition of a bollard effect of load transfer to that of the adhesive action between wire and resin, proved successful and no further termination failures occurred.

APPENDIX A.5

ELASTIC MODULUS OF WIRES

A.5.1 Background to this Study

It was necessary to obtain an estimate of the elastic modulus of the individual wires comprising the seven wire strands which have been tested in tension. Initial tests on core wire gave modulus values over 10% less than that usually quoted for steels. (These tests were performed in this Department and also, through the kindness of British Ropes (Mr. H. Plant) at the Doncaster Research Section of that company). Discussion about these results with British Ropes personnel revealed that these 'low' results were not unusual and were well within the normal range of values obtained from tests on wires over a number of years.

It was then decided to test the helical wires as well as the core from a length of the strand which had been supplied by British Ropes for the test programme on strands at Liverpool. These tests were performed at Doncaster, employing the long established techniques developed by testing staff at British Ropes. The results of the tests on helicals gave a scatter between 8% and 15% below the usually quoted modulus value for steels. The core wire result was less than 4% below this value but was 8% up on the value obtained on core wire in a previous test on the same test machine.

At this point it was decided to investigate the possibility

that modulus variations occur along the length of the core wire. Accordingly, five lengths of core wire were taken from strand lengths immediately adjacent to the five strand lengths tested in the programme on strand response to axial loading. These were tested in the Instron machine at Liverpool, using Huggenberger extensometers.

A critical re-examination of all the results from tests on core wires was then undertaken. For valid comparison of results obtained from different test machines using different instrumentation it was decided to examine modulus values from periods of increasing load only and over small load ranges. These results follow details of the test equipment and procedures, which are given below.

A.5.2 Test Equipment

A.5.2.1 Test Machines

Four machines were used in these tests; their main features are given in this section.

I J. J. Lloyd (Liverpool)

(i) Load capacity of 20 kN. (Max. load range of 20 kN used).

(ii) Vertical axis of loading. Testpiece length 1000 mm (max.) between grips.

(iii) Motor driven loading with straining rate control.

(iv) Serrated wedge grips with central groove for wire location.

(v) Easily calibrated (deadweight), used regularly.

II Instron (Liverpool)

(i) Load capacity of 5 tonne (5000 kgf). Load cell range of 2 tonne used.

(ii) Vertical axis of loading. Testpiece length 100 mm (max.) between grips mounted in universal joints.

(iii) Motor driven loading if required. Hand operation used for these tests.

(iv) Serrated wedge grips similar to those of J. J. Lloyd machine.

(v) Easily calibrated (deadweight): calibrated shortly before test on wire No. 2 - by another user. Calibrated again, just before tests on wires Nos. 4 to 8.

III Instron (British Ropes, Doncaster)

This machine is similar to the Instron machine at Liverpool. Additional features are:

(i) Increased testpiece length between grips; more than 300 mm.

(ii) Direct load/extension plotting incorporated. (Extension from output of Baldwin extensometer).

(iii) Tests performed using motor drive at slow speed.

(iv) Machine calibrated immediately before these tests.

IV Hounsfield Tensometer (Liverpool)

(i) Max. load range of 20 kN used for these tests.

(ii) Horizontal axis of loading. Testpiece length 250 mm max. between grips.

(iii) Serrated wedge grips similar to those of the Lloyd and Instron machines, but supported in horizontal position by the machines' two load bearing bars.

(iv) Load is applied manually by turning a handle on a shaft which, through a gearbox, transmits motion to the crosshead.

(v) Load is recorded when a beam of known stiffness deflects at the centre under load and displaces mercury in a cylinder. The mercury then moves along the inside of a glass tube adjacent to a scale calibrated in kN.

(vi) The manufacturers do not suggest any method of regular calibration and there is no evidence that this machine - or the four similar machines in the Department - have ever been calibrated since they were acquired more than 20 years ago.

A.5.2.2 Instrumentation

I Huggenberger Extensometers

Two of these extensometers were used, clamped diametrically opposite each other to the surface of the wire. These instruments magnify the extension over a 1 inch gauge length by means of a system of levers to a pointer which passes over a graduated scale. The magnification factors, supplied by the manufacturers for each individual instrument are 1000 (for instrument No. 442) and 1020 (for instrument No. 443).

II Baldwin Extensometer

This instrument has been developed by British Ropes for speedy and convenient testing of wires in the Instron testing machine. Extension over a 10 inch gauge length is transmitted by a knife edge lever system to the spindle of an LVDT at the lower end of the instrument. Output from the LVDT is fed to the X axis of the Instron X-Y plotter.

III Strain Gauges

These were type EA-06-031DE-120 of gauge length 0.79 mm and gauge factor 2.07, supplied by Welwyn Strain Measurement.

(This type has been used on the surface of helical wires in strands). Two gauges were attached diametrically opposite each other on the surface of the test wire with their grid axes parallel to the axis of the wire. Leads from each gauge were connected to a channel of a Welwyn Switch and Balance unit used in conjunction with a Welwyn P350A Digital Strain indicator. The P350A was calibrated before the test, using a Welwyn Type 61 Calibration unit.

A.5.3 Test Procedures

All the results quoted are from that part of each test when the load was increasing. This is for the purpose of valid comparison with results from the British Ropes Instron machine where normal practice is to load the testpiece to fracture.

I Tests with Strain Gauges

The testpiece (wire No. 1) was loaded in increments of 1 kN from 1 kN to 13 kN and strain values obtained from each gauge. The corrected mean strains (see Section A.5.2.2.III) were used to determine slopes over increments of 3 kN. A sample of the procedure is shown in Tables A.5.1.A and A.5.1.B. The results quoted in Table A.5.3 are for the J.J. Lloyd test machine and in Table A.5.4 for the Hounsfield test machine.

II Tests with Huggenberger Extensometers

Care was taken to clamp these instruments diametrically opposite each other on the surface of the wire, with the wire held under tension at or near the lower end of the load range planned for the test. The load range possible for this diameter (stiffness) of testpiece was only about 3 kN before it was necessary to reset the extensometers. Huggenberger readings were taken at increments of 40 kgf (Instron) or 0.4 kN (Hounsfield) and slopes obtained for the load range over the middle 200 kgf (2 kN) of each test. A sample of this procedure is shown in Table A.5.2. The results quoted in Table A.5.3 are for the Instron test machine (wire Nos. 2,4,5,6,7,8) and in Table A.5.4 for

the Hounsfield test machine (wire Nos. 1 and 2).

III Tests with the Baldwin Extensometer
(British Ropes Instron)

The long established procedure at British Ropes, Doncaster Laboratory is designed for quick and efficient testing of a wire to fracture. A load/extension plot is obtained as the test proceeds and for this grade of wire, two scale changes were necessary during the course of the test; the first at about half the breaking load and the second just before break. Elastic modulus is obtained by constructing a line tangential to that part of the plot having the steepest slope, for as long as that slope persists. (See Fig. A.5.1). This steepest part almost invariably starts at the holding load when the extensometer is first applied in the case of core wires. (But see later for helical wire testing - Section 5). The maximum for the range depends on where the plot is detected to deviate from the tangential construction line. For test on wire No. 3, this load range was 1.1 kN to 4.7 kN.

Figure A.5.1. Core Wire Instron Plot:Load/Extension.

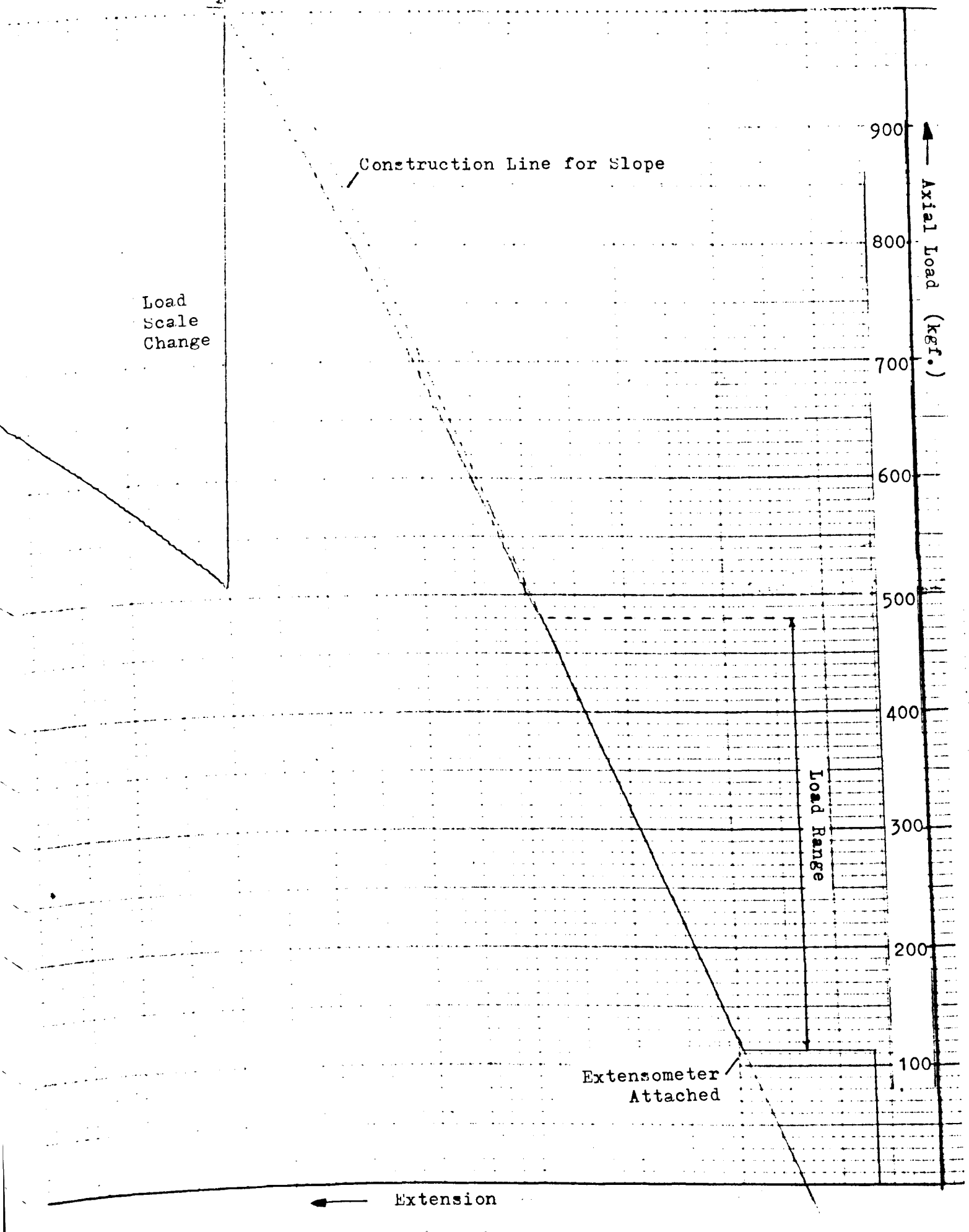

A.5.4 Summary of Results - Core Wires

Fig. A.5.2 shows elastic modulus values plotted against the mid-point of the load range for the tests performed on the J.J. Lloyd and Instron machines. Decreased modulus with increased load is a clear trend. As load approaches zero, so the points approach the generally accepted modulus value for steel of 207 kN/mm^2 (30 x 10^6 lbf/m^2).

Fig. A.5.3 shows the results for tests performed on the Hounsfield test machine. The trend for decreased modulus with increased load is similar to that seen in Fig. A.5.2, but the whole pattern of points is at lower modulus values. This difference is put down to inaccurate load recording in the Hounsfield. (See A.5.2.1.IV). The reason why the Hounsfield test results are not rejected outright is that they do show the same trend. For actual load values, the results from the three other machines, Fig. A.5.2, are considered to be more reliable.

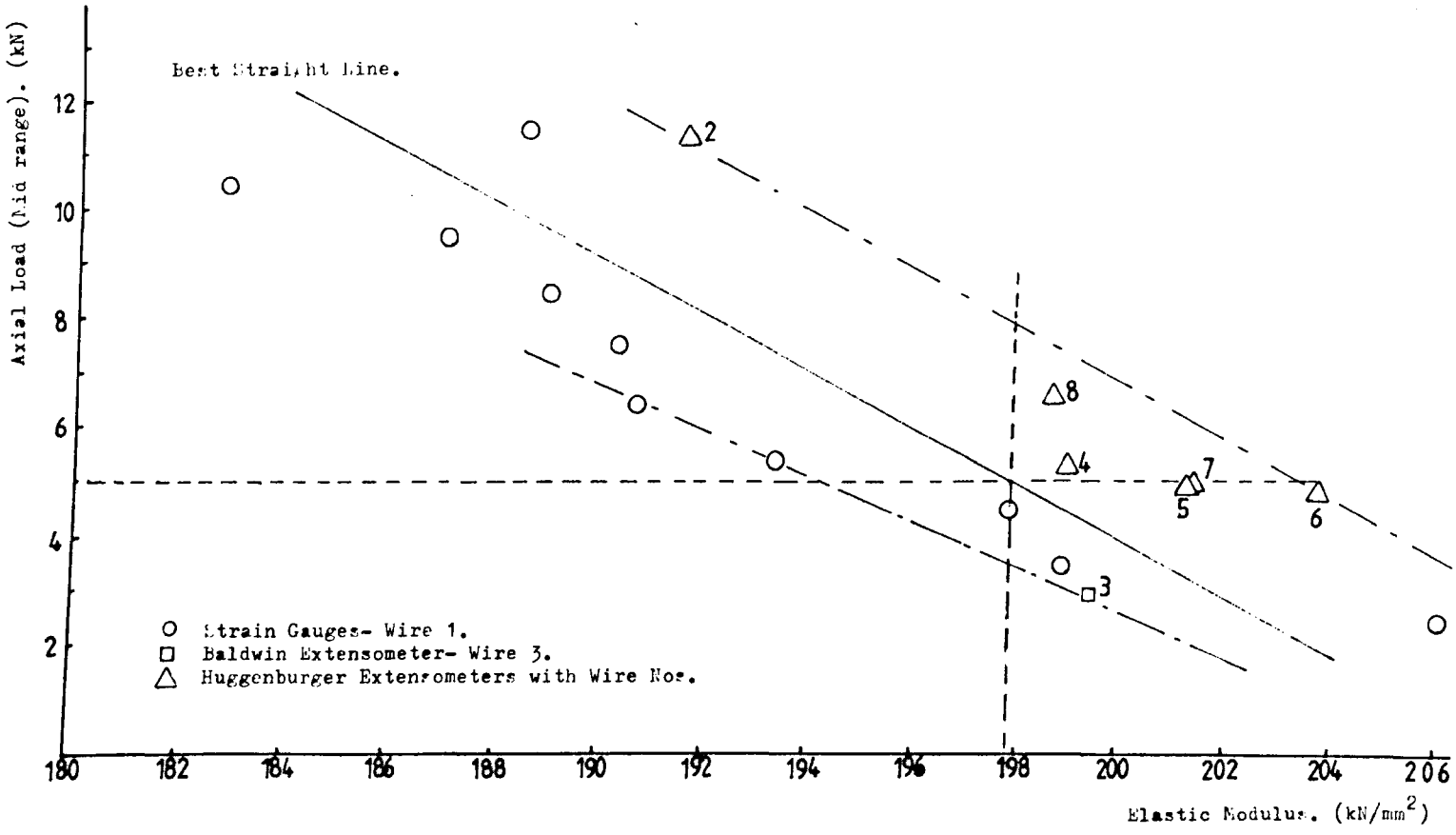

Figure A.5.2. Core Wire;Elastic Modulus/Mid-Point of Axial Load Range.

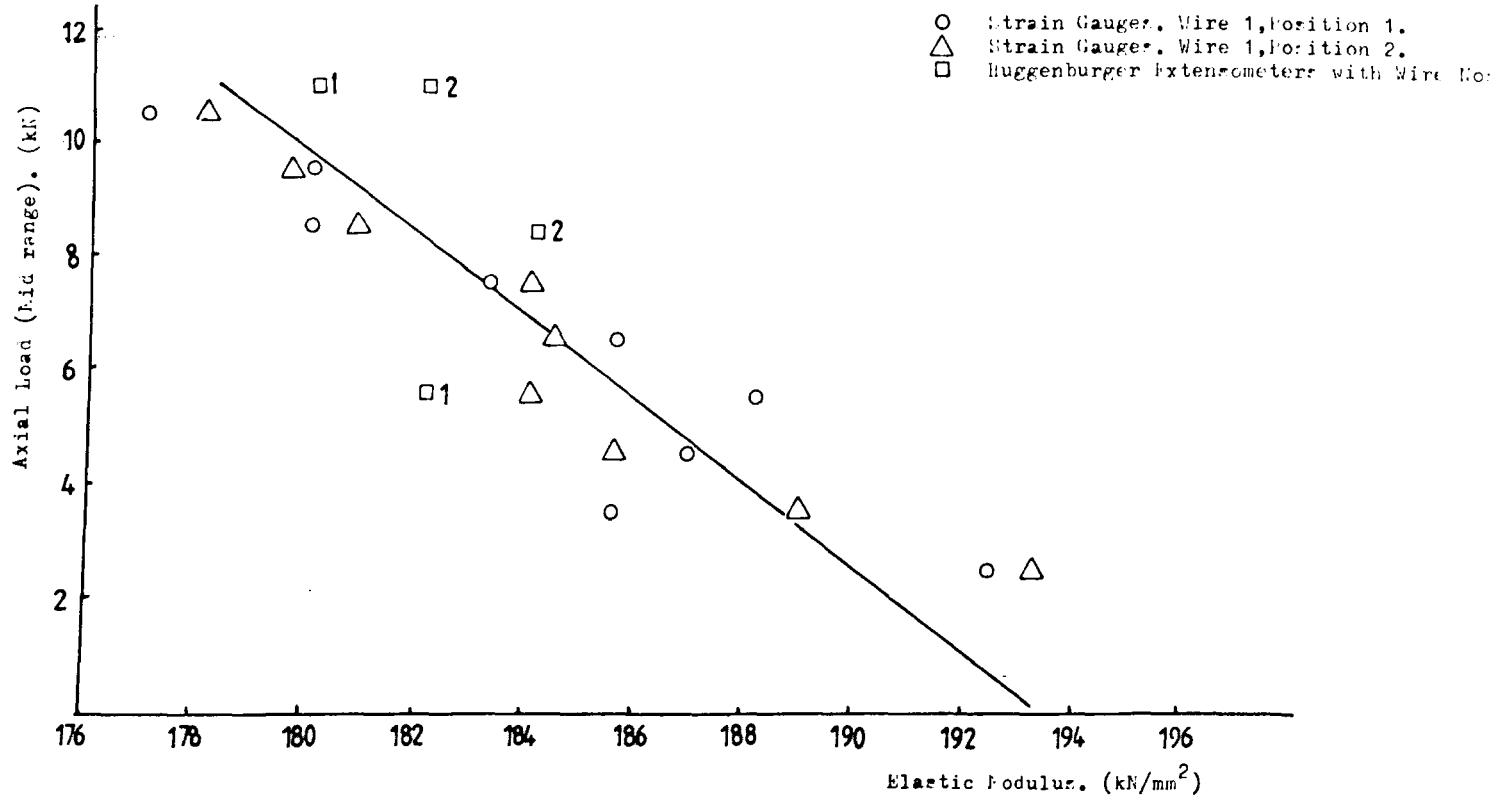

Figure A.5.3. Core Wire;Elastic Modulus/Mid-Point of Axial Load Range.
(Hounsfield Tensometer Test Machine Results.)

A.5.5 Tests on Helical Wires

The trend for decreased modulus with increased load that is evident from the results of tests on core wires is not evident from the tests on helicals. It is necessary, however, to attempt some prediction on the modulus of helicals as they constitute the major part of the load-bearing capacity of a strand. This section describes the tests performed on the helical wires but concludes by suggesting that the results cannot be used as the effective modulus of helical wires in a strand.

A.5.5.1 Test Procedure

A 500 mm length of the seven wire strand adjacent to one of the strand lengths used in the strand testing programme was taken to the testing laboratory at British Ropes, Doncaster and prepared for the testing of individual wires. This involves unwrapping the helicals from the core and from each other. (The core wire was tested as wire No. 3 - See Table A.5.3). The helicals, which are preformed during the stranding process, retain their helical form after unwrapping and have to be straightened before testing. This is effected by careful hammering, using a copper hammer and a hard wood anvil. There is one technician who does this straightening and his skill, acquired over many years of testing wires and ropes for British Ropes, ensures a degree of uniformity in wire condition at the start of each test. After inserting the wire in the Instron grips, a load of about 1 kN is applied and the load held at this

level while the Baldwin extensometer is attached. Load is then increased steadily to fracture, scale changes on the load axis of the plotter being effected, as required, by the turn of a switch, as the test proceeds. The extensometer is removed at about 85% of the estimated breaking load. After the wire breaks, the machine is switched off and the load/extension plot removed for the determination of slope and hence elastic modulus.

Figures A.5.4 to 9 show load/extension plots from the tests and include construction lines to determine slope. The decisions on slope and load range over which the slope is to be drawn are a function of the acquired skill of the technician to whom reference has already been made.

Table A.5.5 gives results of the tests on the six helical wires. The load ranges over which each slope has been constructed are also given.

A.5.5.2 Discussion of Results

The technician who performed these tests and determined the modulus values observed that these results are not untypical of the many tests he has performed on helical wires over a number of years. More specifically this means that:

(i) the shapes of the load/extension plots were not unusual,

(ii) that it was no more difficult than usual to decide that part of the plot over which the slope line

Figure A.5.4. Helical Wire No.1 Instron Plot:Load/Extension.

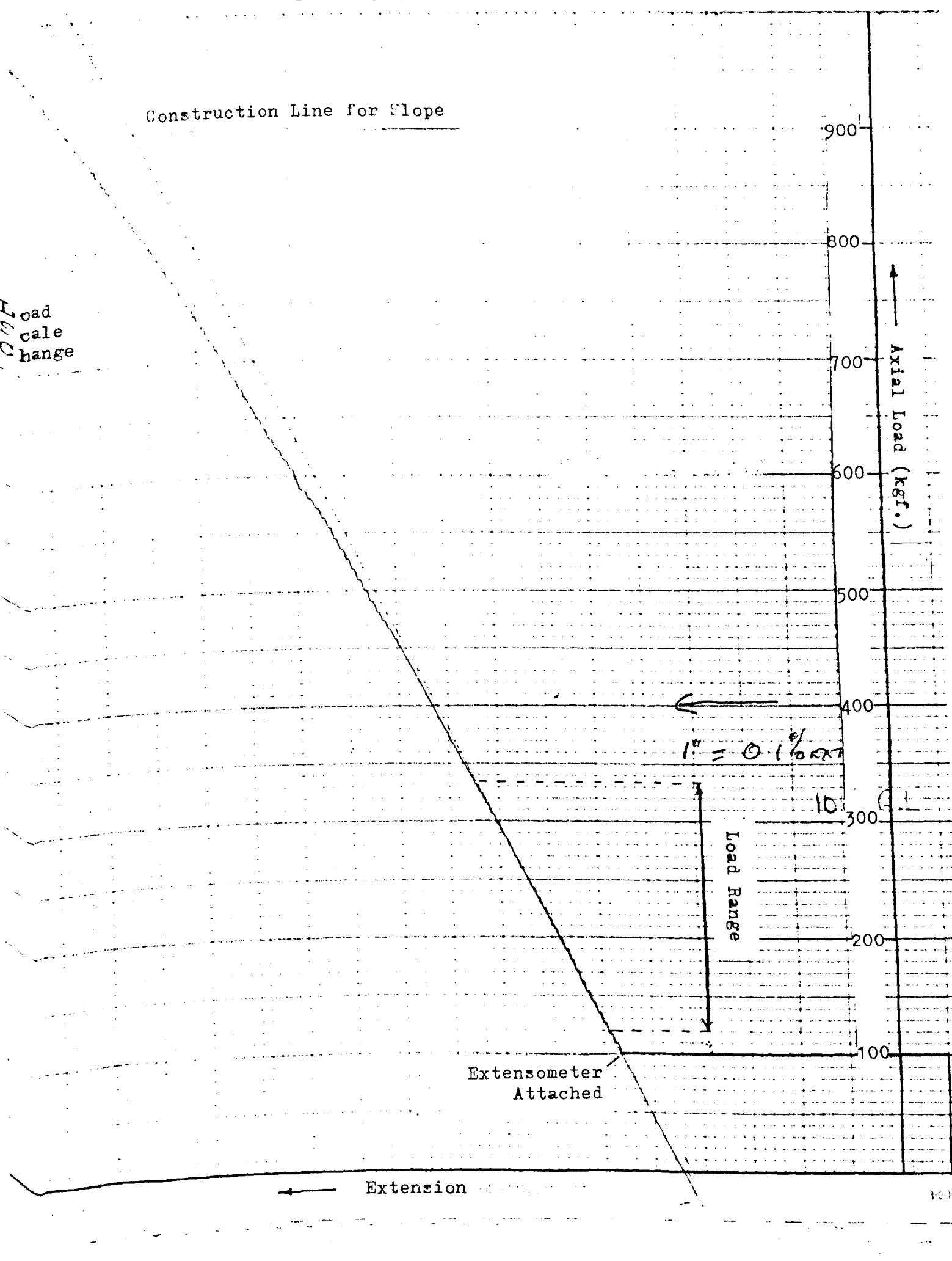

Figure A.5.4. Helical Wire No.1 Instron Plot:Load/Extension.

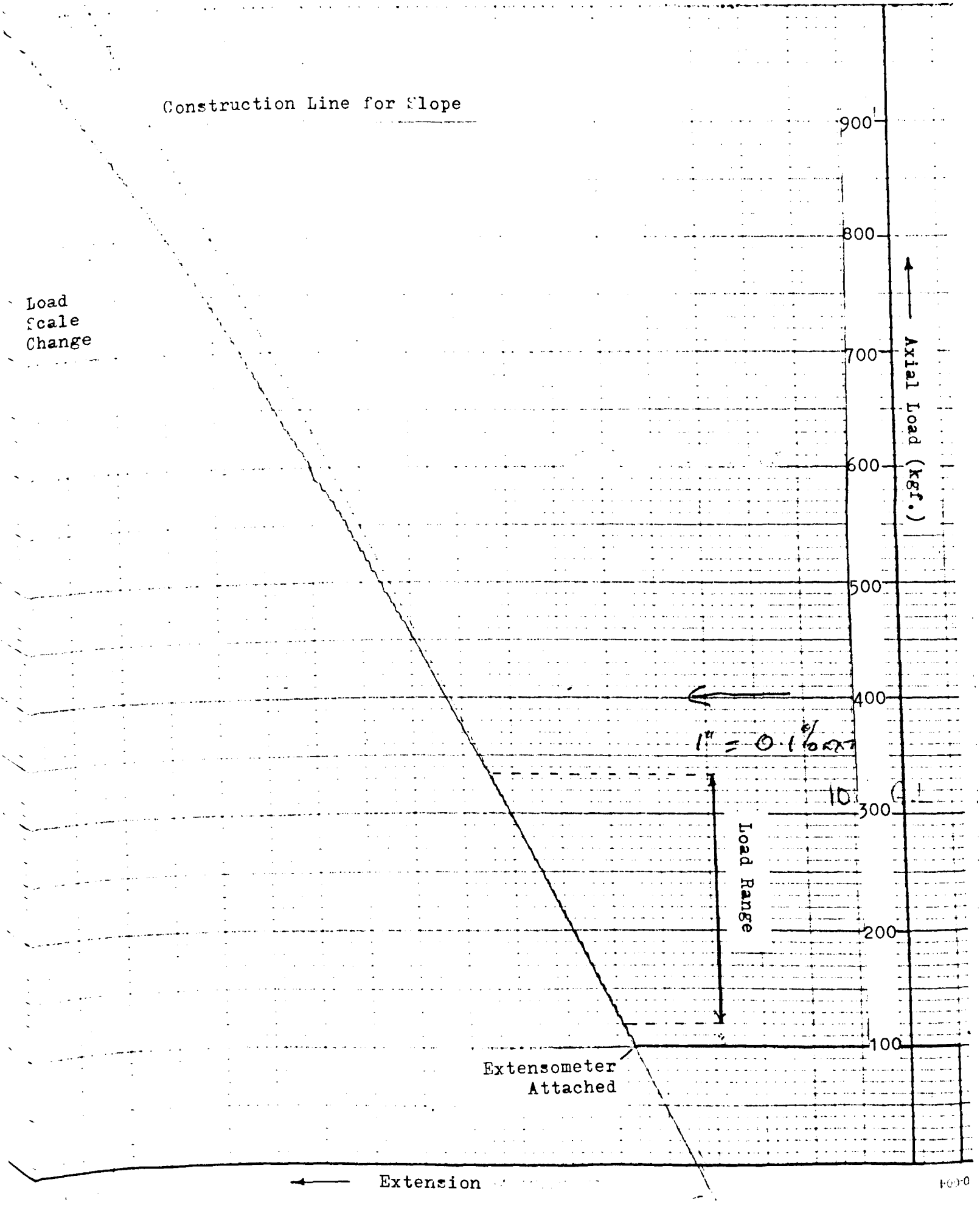

Figure A.5.5. Helical Wire No.2 Instron Plot:Load/Extension.

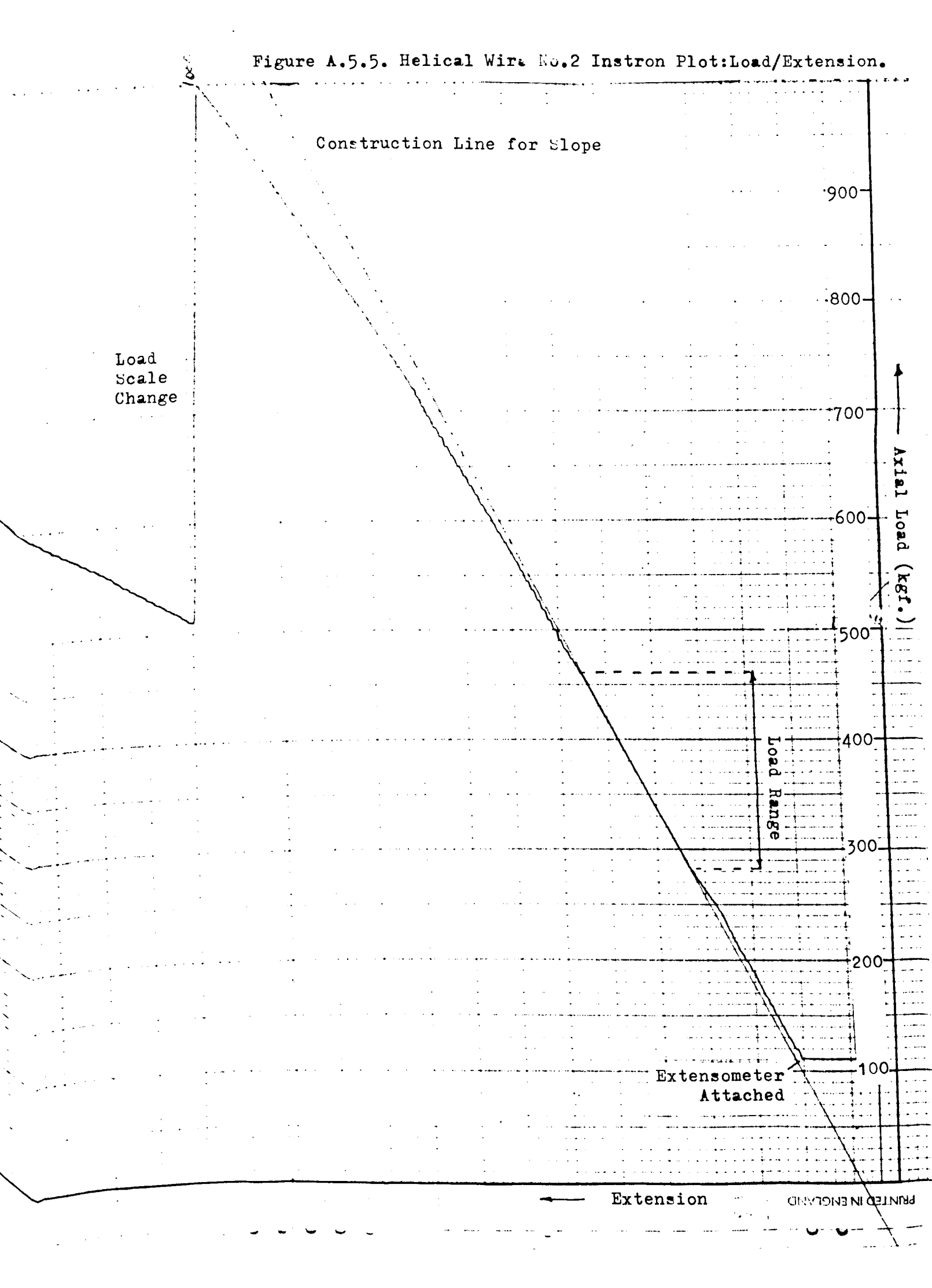

Figure A.5.6. Helical Wire No.3 Instron Plot:Load/Extension.

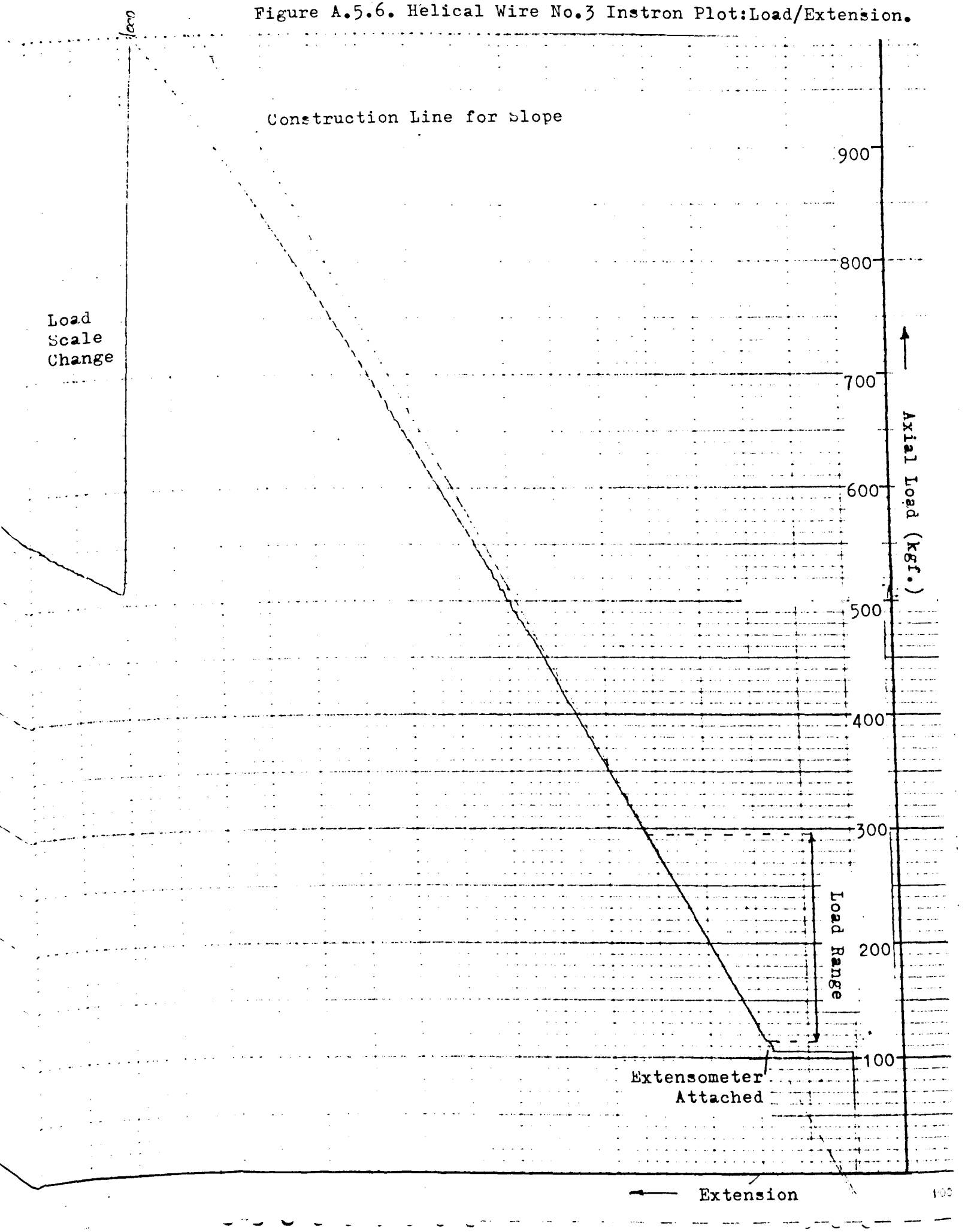

Figure A.5.7. Helical Wire No.4 Instron Plot:Load/Extension.

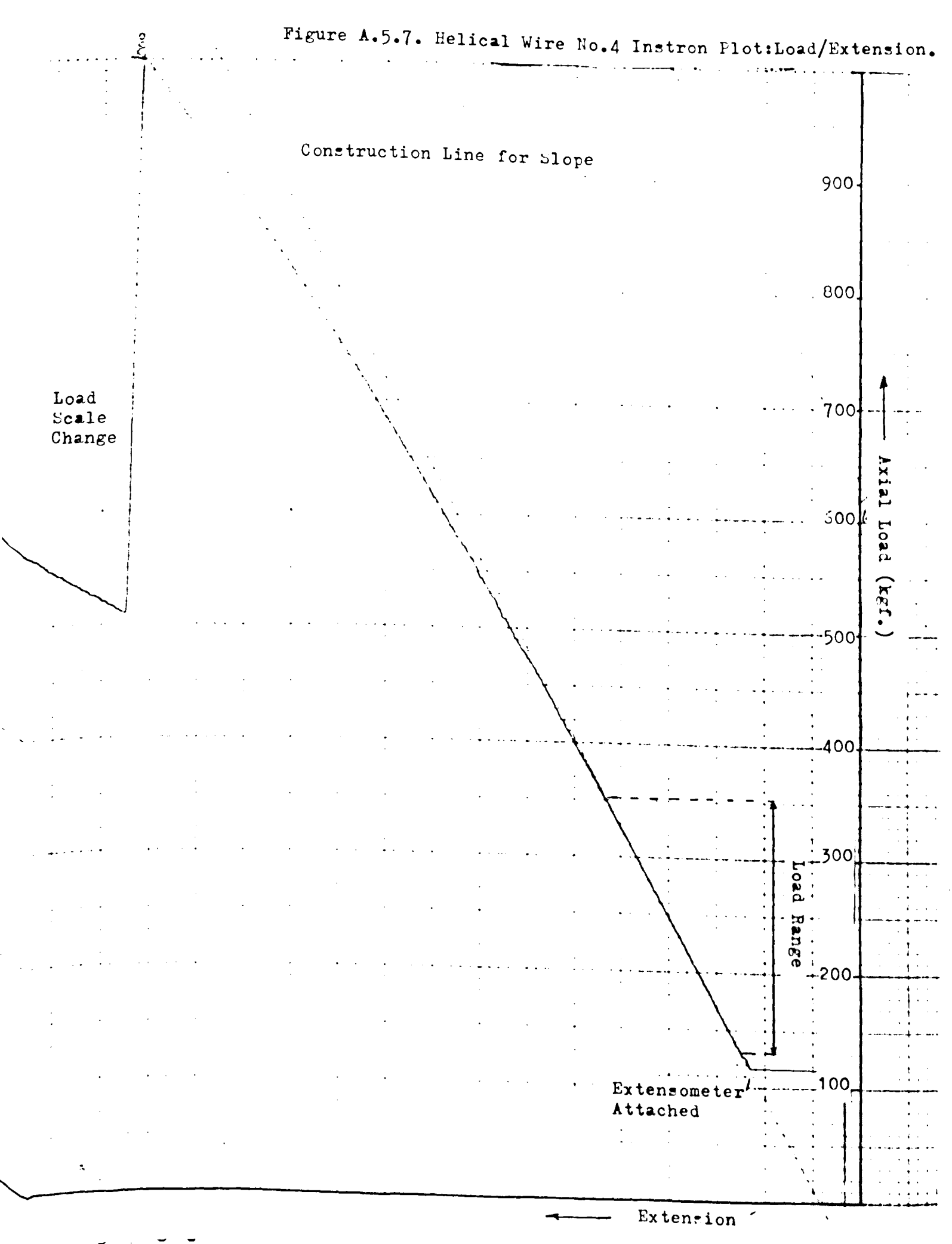

Figure A.5.8. Helical Wire No.5 Instron Plot:Load/Extension.

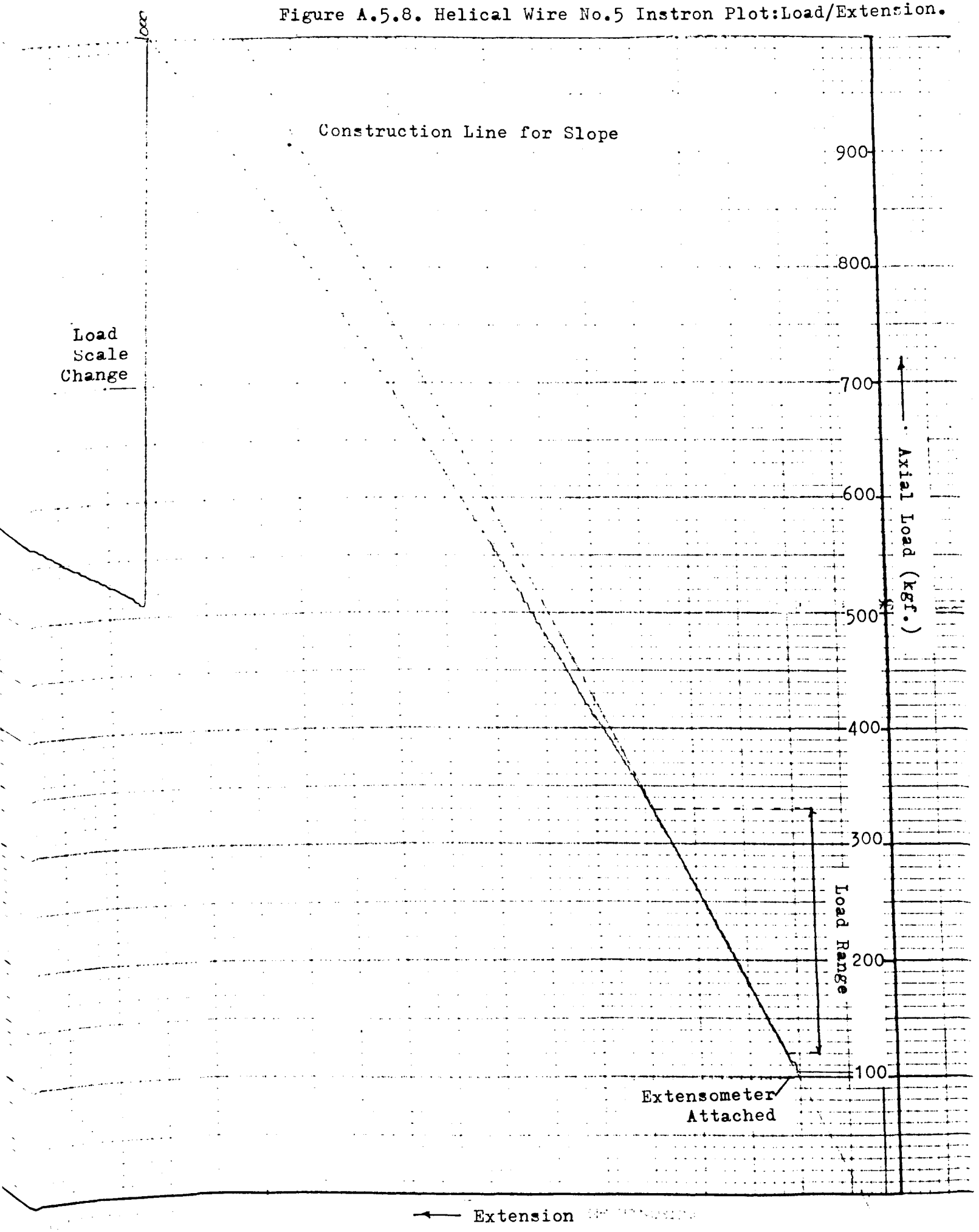

Figure A.5.9. Helical Wire No.6 Instron Plot:Load/Extension.

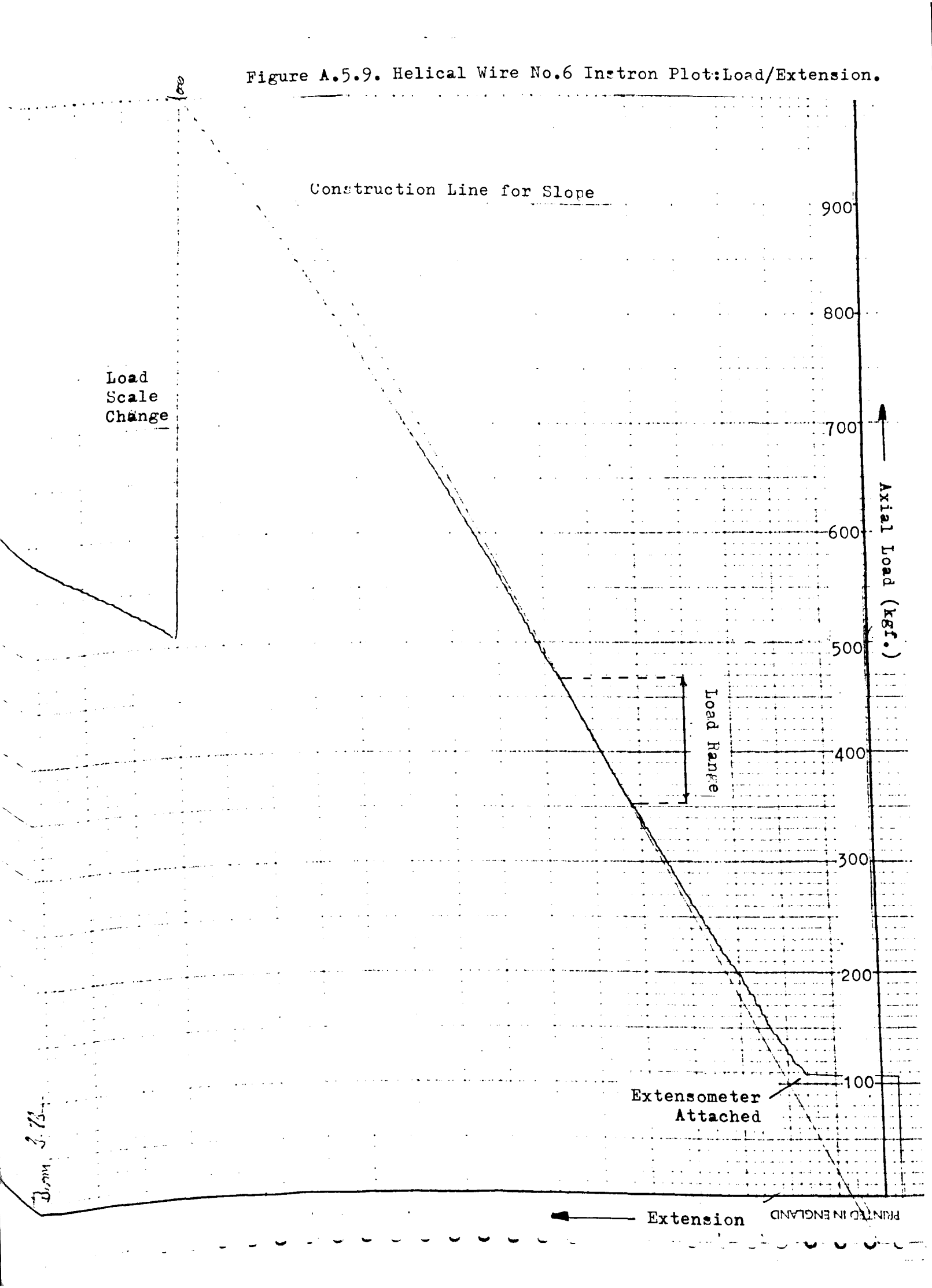

was to be drawn, and

(iii) the scatter of modulus values obtained from these helicals in the same strand was no larger than usual.

Inspection of these modulus values reveals values ranging between 8% and 15% below the generally accepted value for steel of about 207 KN/mm^2. Moreover, unlike the tests on core wires which show a trend to lower moduli with increasing load, the tests on helicals have produced a random scatter of modulus values. Two possible reasons for this scatter and for the low values of modulus are suggested.

(i) No amount of skill in the straightening of helical wires can ensure that further straightening does not occur at loads higher than the holding load at which the extensometer is attached. There is evidence for this in the plot from wire 6H (Fig. A.5.9) in which slope increases gently from the holding load of about 100 kgf up to 355 kgf, where the slope construction line starts to coincide with the plot. The plot from wire 2H (Fig. A.5.5) reveals a less regular straightening pattern between holding load and about 285 kgf, at which point the slope construction line starts to coincide with the plot.

(ii) The reduction in value of elastic modulus as load

increases, as observed in test results from the core wires, may be a function of the total work done on the wire or the strain history imposed on the wire. The straightening of helicals involves both the above but applied in a less controlled manner than in a tensile test. The effective load, as far as modulus value is concerned, is therefore likely to be higher, by an unquantifiable amount, than the load subsequently applied to a helical in a tensile test. This would result in a lower modulus for a helical than for a core wire over the same load range, due in effect to the residual stresses in the helical after straightening.

A.5.6 Conclusions

Tests on core wires show that the modulus value reduces with increasing load. It should be possible, therefore, to select from Fig. A.5.2 the appropriate modulus which will, within certain confidence limits, apply for a given load range.

Modulus values from tests on helical wires cannot be used in theoretical predictions on strand response to load. The results exhibit a random scatter as well as an unaccountably low mean value. It is necessary, however, to attempt some prediction on the modulus of helicals and the justification for using values from tests on core wire can be reasoned as follows.

(1) The chemical and metallurgical compositions of helicals and core wires are identical.

(2) All available theories on strand response predict that tension in helicals is less than tension in the core wire of a strand under axial load. If the effective load range on the helical has been raised by the bending and torsion to which it has been subjected during both the stranding process and also the axial loading, effective load range on core and helicals might attain similar values.

The elastic moduli of both core and helicals are therefore likely to be within the confidence limits determined from the tests on core wires for the relevant load range.

A more comprehensive investigation into the variations in elastic modulus of wires in a strand is beyond the scope of the current project. It can only be reported that there is a non-linear relation between load and extension; the reason why should be the subject of some more fundamental research. This brief study does however provide a method of selecting an elastic modulus, which, within certain confidence limits, can be used for the purpose of comparison between experimental results and the different theoretical models put forward.

In estimating errors likely to arise when determining wire modulus by this method, wire diameter ($\pm$ 0.005 mm in 3.73 mm dia. wire), load ($\pm$ 0.5%) and extension ($\pm$ 0.5%) give a cumulative modulus accuracy of $\pm$ 1.28%. This is very much less than the scatter of results actually obtained from the tests (see Fig. A.5.2).

For a selected mid-range load value of 5kN, the wire modulus is given as 197.9 kN/mm^2, from Fig. A.5.2. This is the value used in the computations of Chapter 6 and is appropriate for the individual wire loads in strand loadings up to about 80 kN.

Table A.5.5 gives modulus values from some other sources. There seems to be no reason to consider that the value obtained in this study is any less valid than they are.

Sample of Test with Strain Gauges on Core Wire

Wire No. 1 dia. 3.73 mm

J.J. Lloyd Test Machine

Table A.5.1.A

Load kN	Strains as Read x10^6		Mean Increment of Strain x10^6
	Gauge 1A	Gauge 2A	
1	2000	2000	-
2	2440	2344	392
3	2886	2728	415
4	3324	3118	414
5	3773	3530	431
6	4211	3933	420
7	4669	4366	445
8	5132	4799	450
9	5566	5213	423
10	6040	5650	455
11	6504	6110	462
12	6977	6546	455
13	7388	6957	411

Table A.5.1.B

Load Range kN	Strain Mean Increment per kN	Elastic Modulus	
		kN/mm^2	lbf/in^{2}x10^{-6}
1- 4	407	205.2	29.8
2- 5	420	198.9	28.8
3- 6	422	197.9	28.7
4- 7	432	193.3	28.0
5- 8	438	190.7	27.7
6- 9	439	190.3	27.6
7-10	443	188.5	27.4
8-11	447	186.9	27.1
9-12	457	182.8	26.5
10-13	443	188.5	27.4

Sample of Test with Huggenberger Extensometers on Core Wire

Wire No. 6 dia. 3.73 mm

Instron Test Machine. 1st loading

Table A.5.2

Load kgf/200	Huggenberger Reading		Mean Strain Increment x 10^3
	No. 442 (Mag.Factor = 1000)	No. 443 (Mag.Factor = 1020)	
1.6	-0.14	-0.01	-
1.8	0.04	0.14	0.164
2.0	0.20	0.30	0.158
2.2	0.36	0.45	0.154
2.4	0.55	0.61	0.170
2.6	0.71	0.78	0.167
2.8	0.90	0.95	0.178
3.0	1.05	1.10	0.145
3.2	1.20	1.26	0.154
3.4	1.37	1.43	0.171
3.6	1.54	1.60	0.166

For load range 400 kgf - 600 kgf. (3.9 kN - 5.9 kN)

Elastic Modulus = 201.5 kN/mm^2

For 2nd loading by same method as above

Elastic Modulus = 205.8 kN/mm^2

$\therefore$ Average Elastic Modulus = 203.7 kN/mm^2 (29.5 x 10^6 lbf/in^2)

See Table A.5.3. (Wire 6).

Core Wires: Results from J.J. Lloyd and Instron Machines

Table A.5.3

Wire No.	Load Range kN	Test Machine	Extensometer or Strain Gauge	Gauge Length mm	Elastic Modulus	
					kN/mm^2	$lbf/in^2 x10^{-6}$
1	1.0- 4.0	J. J. Lloyd	Strain Gauges	0.79 (0.031 in)	205.2	29.8
	2.0- 5.0	"	"	"	198.9	28.8
	3.0- 6.0	"	"	"	197.9	28.7
	4.0- 7.0	"	"	"	193.3	28.0
	5.0- 8.0	"	"	"	190.7	27.7
	6.0- 9.0	"	"	"	190.3	27.6
	7.0-10.0	"	"	"	188.5	27.3
	8.0-11.0	"	"	"	186.9	27.1
	9.0-12.0	"	"	"	182.8	26.5
	10.0-13.0	"	"	"	188.5	27.3
2	10.4-12.4	Instron	Huggenbergers	25.4 (1 in)	191.5	27.8
3	1.1- 4.7	Instron (B.Ropes)	Baldwin	254 (10 in)	199.5	28.9
4	4.3- 6.3	Instron	Huggenbergers	25.4 (1 in)	198.9	28.8
5	3.9- 5.9	"	"	"	201.2	29.2
6	3.9- 5.9	"	"	"	203.7	29.5
7	3.9- 5.9	"	"	"	201.3	29.2
8	5.7- 7.7	"	"	"	198.6	28.8
9	*	Instron (B. Ropes)	Baldwin	254 (10 in)	184.0	26.7

* This load/extension plot from the Instron testing machine at British Ropes, Doncaster, is not now available. The load range (over which the slope of the plot is determined) is therefore unknown. (See para. A.5.3.III).

Core Wires: Results from Hounsfield Testing Machine

Table A.5.4

Wire No.	Load Range kN	Test Machine	Extensometer or Strain Gauge	Gauge Length mm	Elastic Modulus	
					kN/mm^2	$lbf/in^2 x10^{-6}$
1	1.0- 4.0	Hounsfield	Strain Gauges	0.79 (0.031 in)	192.4	27.9
1	2.0- 5.0	"	"	"	185.6	26.9
1	3.0- 6.0	"	"	"	186.9	27.1
1	4.0- 7.0	"	"	"	188.1	27.3
1	5.0- 8.0	"	"	"	185.6	26.9
1	6.0- 9.0	"	"	"	183.2	26.6
1	7.0-10.0	"	"	"	180.0	26.1
1	8.0-11.0	"	"	"	180.0	26.1
1	9.0-12.0	"	"	"	177.0	25.7
1*	1.0- 4.0	"	"	"	193.3	28.0
1*	2.0- 5.0	"	"	"	189.0	27.4
1*	3.0- 6.0	"	"	"	185.6	26.9
1*	4.0- 7.0	"	"	"	184.0	26.7
1*	5.0- 8.0	"	"	"	184.4	26.7
1*	6.0- 9.0	"	"	"	184.0	26.7
1*	7.0-10.0	"	"	"	180.8	26.2
1*	8.0-11.0	"	"	"	179.6	26.1
1*	9.0-12.0	"	"	"	178.1	25.8
1	4.6- 6.6	"	Huggenbergers	25.4 (1 in)	182.1	26.4
1	10.0-12.0	"	"	"	180.1	26.1
2	7.4- 9.4	"	"	"	184.1	26.7
2	10.0-12.0	"	"	"	182.1	26.4

* Wire turned through 90° for second loading.

Tests on Helical Wires

Instron (British Ropes) Test Machine with Baldwin Extensometer

Table A.5.5

Wire No.	Elastic Modulus			Load Range	
	kgf/mm^2 x10^{-3}	kN/mm^2	lbf/in^2 x10^{-6}	kgf	kN
1H	19.39	190.2	27.6	120-340	1.18-3.33
2H	18.87	185.1	26.8	285-465	2.79-4.56
3H	17.94	175.9	25.5	115-295	1.13-2.89
4H	18.38	180.2	26.1	130-355	1.27-3.48
5H	18.99	186.2	27.0	120-330	1.18-3.24
6H	18.38	180.2	26.1	355-470	1.27-4.61

Mean value of Elastic Modulus: 183.0 kN/mm^2

Deviations: + 3.9% to - 3.8%

Wire Modulus

(Other values of Modulus)

Table A.5.6

Modulus Value kN/mm^2	Wire Size	Other Description	Source
179-193	Not specified	Normal mill coil	B.Ropes. Plant (80)
200-214	" "	Large coil	" "
197.2	3.18 mm	Spring spec.	Carlson "
196.5	15.88 mm	" "	" "
196	Not specified	Not specified	Bahke (6)

APPENDIX A.6

STRAIN GAUGES, ADHESIVES AND COATINGS

A.6.1 Load Cell

Gauge configuration on the loading rod surface and circuitry for torsion and tension circuits are shown in Appendix A.1. Figure A.6.1 shows the gauge types used.

Adhesives used were M. Bond AE, which is a 100% solids epoxy system, for tension circuit No. 1 and torsion circuit No. 1; M. Bond 200 which is a modified methyl-2-cyanoacrylate compound, for tension circuit No. 2 and torsion circuit No. 2. The gauges of tension circuit No. 2 were dislodged in the course of the tests (see section 3.3.1), due possibly to incompatibility between the KYOWA gauges and the Welwyn Strain Measurement adhesive, especially under the shock load after strand fracture. Torsion circuit No. 2 was reliable throughout and since it gave less output, when subjected to tension than torsion circuit No. 1 (see 3.3.2 and A.1.2 and 3), the results from torsion circuit No. 2 were used in comparison between experimental results and computed predictions.

A coating of silicone rubber protective 3140RTV was used for all load cell gauges.

Figure A.6.1. Load Cell Strain Gauges.

Tension Circuits.

Circuit No.1.

W.S.M. CEA-06-250UWC-350.

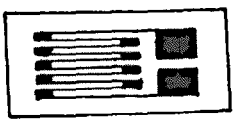

Circuit No.2.

KYOWA KFC-1-C1-11L30.

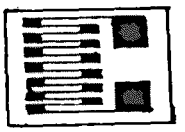

Torsion Circuits.

Circuit Nos. 1 & 2.

W.S.M. EA-06-250td-120.

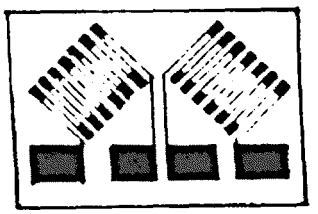

Figure A.6.2. Strain Gauges on Helical Wires.

(i) Axial.

W.S.M. EA-06-031DE-120

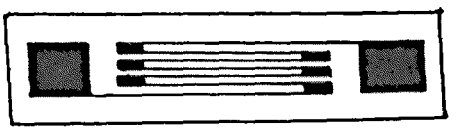

(ii) Axial (Bending & Tension)

W.S.M. EA-06-031DE-120

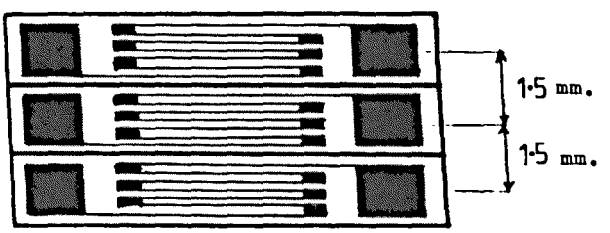

(iii) Perpendicular

W.S.M. EA-06-031CF-120
&
KYOWA KFC-1-C1-11L30.

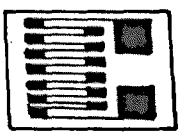

A.6.2 Helical Wire Surface

I. Gauges mounted parallel to wire axis

The grid and tab configuration used throughout was that shown in Fig. A.6.2(i). For strands I and IV, leads were soldered to the tabs after gauges were attached to wire surface. The labour involved in achieving reliable soldered joints and the failures of such joints, particularly after shocks transmitted along the strand from resin cracks in the end grips, prompted the decision to use gauges with the leads already attached (soldered and coated by the manufacturer).

In order to determine the bending moment and tension in selected locations on helical wires (see Appendix A.7) strain gauges of the type used singly on strands I and IV (described above, were mounted in threes parallel to each other, after carefully trimming the backing to size with a scalpel. The axes of the gauges were located 1.5 mm apart as shown in Fig. A.6.2(ii). Kerr (77) has shown that the effect of trimming the backing of strain gauges has an insignificant effect on the resistance change in the grid due to strain.

II. Gauges mounted perpendicular to wire axis

The grid and tab configuration used are those shown in Fig. A.6.2(iii). All these gauges had leads attached when supplied by the manufacturer.

The adhesive used was M Bond 200 for all gauges attached to the helical wires. A coating of silicone rubber protective was used on all these gauges (3140RTV).

APPENDIX A.7

TENSION AND BENDING MOMENTS IN HELICAL WIRES

A.7.1 Theoretical Expressions

Consider a section of helical wire subjected to tension T, and bending moments G' and G about axes which inclined at angle ϕ to the normal and binormal axes of the helix. (See Fig. A.7.1). The strains on axes of the three gauges are given by

$$\varepsilon_a = T/A_hE + G'(d_h/2)\cos(\theta+\phi)/I_hE - G(d_h/2)\sin(\theta+\phi)/I_hE \qquad A.7.1$$

$$\varepsilon_b = T/A_hE + G'(d_h/2)\cos\phi/I_hE - G(d_h/2)\sin\phi/I_hE \qquad A.7.2$$

$$\varepsilon_c = T/A_hE + G'(d_h/2)\cos(\theta-\phi)/I_hE + G(d_h/2)\sin(\theta-\phi)/I_hE \qquad A.7.3$$

Manipulation of these expressions gives

$$G = (2EI_h/d_h)\left[(\varepsilon_a+\varepsilon_c-2\varepsilon_b)\sin\phi/2(1-\cos\theta) - (\varepsilon_a-\varepsilon_c)\cos\phi/2\sin\theta\right] \qquad A.7.4$$

$$G' = (2EI_h/d_h)\left[(2\varepsilon_b-\varepsilon_a-\varepsilon_c)/2\cos\phi(1-\cos\theta) + Gd_h\tan\phi/2EI_h\right] \qquad A.7.5$$

$$T = A_hE(\varepsilon_b - G'd_h\cos\phi/2EI_h + Gd_h\sin\phi/2EI_h) \qquad A.7.6$$

If angle ϕ is zero

$$G = (2EI_h/d_h)(\varepsilon_c - \varepsilon_a)/2\sin\theta \qquad A.7.7$$

$$G' = (2EI_h/d_h)(2\varepsilon_b - \varepsilon_a - \varepsilon_c)/2(1 - \cos\theta) \qquad A.7.8$$

$$T = A_hE\,(\varepsilon_b - G'd_h/2EI_h) \qquad A.7.9$$

Figure A.7.1. Three Parallel Strain Gauges on Helical Wires.

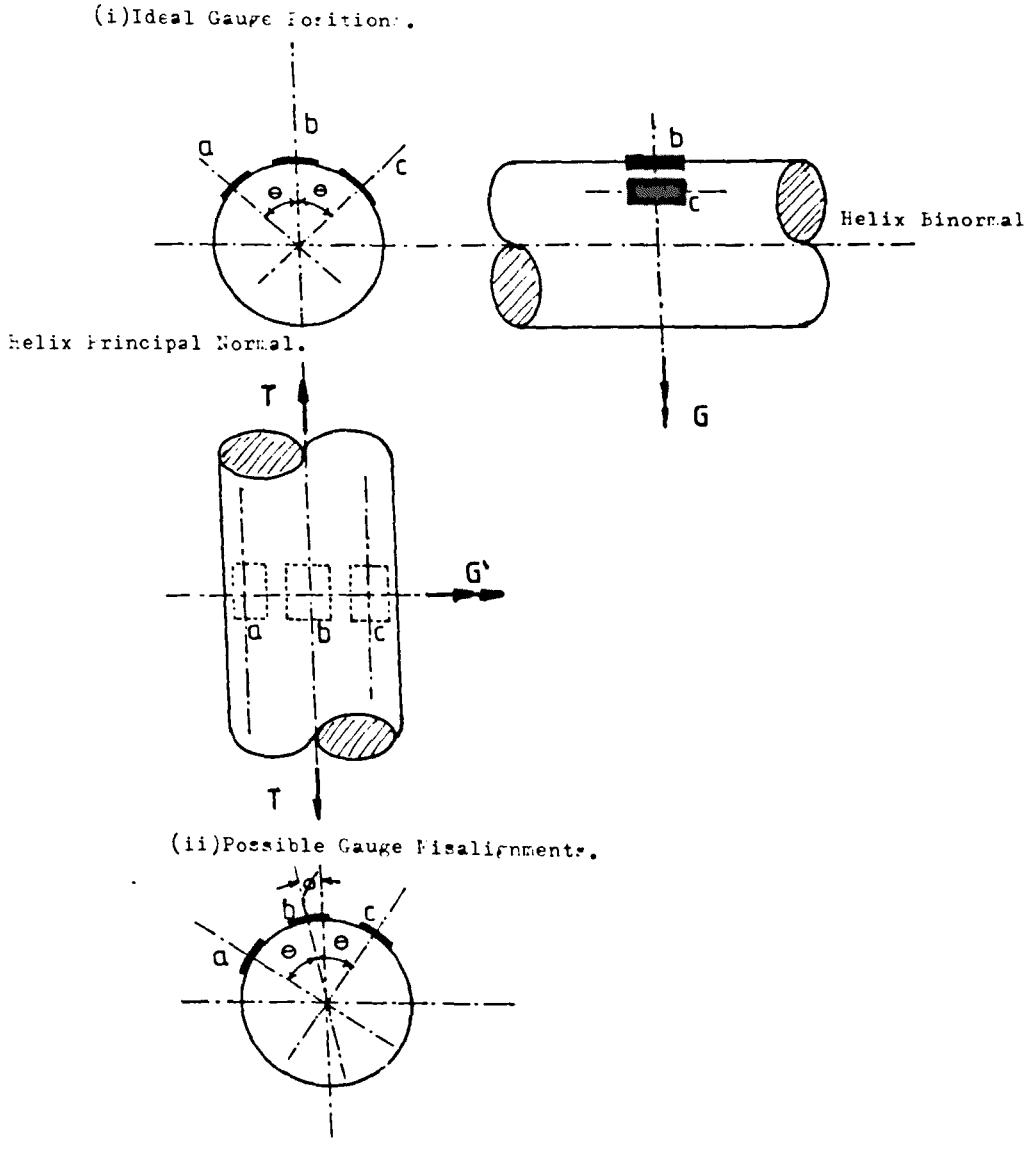

A.7.2 Errors in Relative Position of Adjacent Strain Gauges

From Appendix A.6, Fig. A.6.2(ii), the distance between strain gauge axes is designed at 1.5 mm. For a wire diameter of 3.73 mm, the angle subtended by strain gauge axes at wire centre is therefore given by $\theta = 46^{\circ}$. The error in locating the strain gauge may be up to + 0.2 mm, giving a distance between axes of 1.7 mm and in this case angle $\theta = 52.2^{\circ}$. If G_A is the apparent bending moment from gauges that have been located incorrectly, then from expression A.7.7,

$$G = G_A \sin 46^{\circ}/\sin 52.2^{\circ}$$

$$\text{i.e.} \quad G = 0.91\, G_A \qquad \text{A.7.10}$$

Similarly, if G'_A and T_A are apparent bending moment and tension values respectively, true bending moment and tension values are given, from A.7.8, by

$$G' = 0.79\, G'_A \qquad \text{A.7.11}$$

and from A.7.9 by

$$T = T_A + 0.0166\, G'/d_h \qquad \text{A.7.12}$$

$$\text{or} \quad T = T_A + 0.0131\, G'_A/d_h \qquad \text{A.7.13}$$

It is evident that possible errors in the measurement of bending moments G (9%) and G' (21%) are very much greater than errors in the measurement of tension T since $G' < T.d_h$ by at least an order of magnitude.

A.7.3 Errors Due to Assumption that Bending Axes are Helix Normal and Binormal

The values of bending moments (G and G') and tension (T) that have been computed from strain results from three parallel strain gauges (e.g. Fig. 5.10), using expressions A.7.8, 9 and 10 (i.e. that $\phi = 0$). If it is now assumed that $\phi \neq 0$, but some angle between $+5^{\circ}$ and -5°, expressions A.7.4, 5 and 6 can be used to determine the effect on calculated values of G, G' and T. Table A.7.1 shows a tabulated printout from such a range of angles in increments of 0.5°. This table is typical of those taken from a selection of load cycles and it can be seen that the errors in tension T are negligible. (Error in none of the other cycles exceeded 1%). Errors in bending moment G' go up to about 3.1% (the maximum found in other cycles was 4.3%), but errors in bending moment G go up to 27.7% (the maximum found in other cycles exceeded 120%).

Table A.7.1. Angular Error in Strain Gauge Location/Error in Bending Moment and Tension.

STRAND LOAD kN.	ANGLE ERROR Degrees.	BDG.MOM. G Nm.	G ERROR Percent.	BDG.MOM. G! Nm.	G! ERROR Percent.	TENSION T kN.	T ERROR Percent.
45	-5	.175277	27.6811	-.777422	-2.39271	5.11578	2.84280E-03
45	-4.5	.182056	24.884	-.775841	-2.18445	5.11573	3.76554E-03
45	-4	.188822	22.0926	-.774196	-1.96782	5.11567	4.88402E-03
45	-3.5	.195573	19.3072	-.772484	-1.74228	5.1156	6.36600E-03
45	-3	.202309	16.5279	-.770702	-1.50761	5.1155	8.27673E-03
45	-2.5	.209029	13.755	-.768842	-1.26267	5.11536	.0109984
45	-2	.215734	10.9886	-.766893	-1.00594	5.11516	.0150156
45	-1.5	.222422	8.22903	-.764819	-.732781	5.11481	.0218103
45	-1	.229094	5.47642	-.762525	-.430642	5.11411	.0353719
45	-.5	.235748	2.73104	-.759536	-.0369754	5.11206	.0756091
45	0	.242367	0	-.759255	0	5.11592	0
45	.5	.249001	-2.73733	-.759167	.0116186	5.12033	-.0861041
45	1	.2556	-5.4599	-.756002	.428499	5.11826	-.0457457
45	1.5	.262179	-8.17442	-.753418	.768767	5.11757	-.0321656
45	2	.268738	-10.8807	-.750941	1.09508	5.11722	-.0254081
45	2.5	.275277	-13.5785	-.748472	1.42032	5.11702	-.0214095
45	3	.281794	-16.2677	-.745977	1.74885	5.11688	-.0187345
45	3.5	.288291	-18.9481	-.743442	2.08269	5.11678	-.0167585
45	4	.294765	-21.6193	-.740864	2.42232	5.11671	-.0153045
45	4.5	.301217	-24.2813	-.738236	2.76842	5.11665	-.0141581
45	5	.307646	-26.9339	-.735558	3.12111	5.1166	-.0132726

A.7.4 Assessment of Experimental Technique

The estimate of errors in sections A.7.2 and A.7.3 indicate that for determination of bending moments this technique does not have enough control to enable errors to be limited to acceptable limits. There is little value in comparing experimentally obtained values of bending moments with the predictions from mathematical modelling.

For tension, however, even the accumulated errors due to both gauge misplacement and in the assumed inclination of bending axes appear to be within two percent. Comparison with theoretical predictions are therefore worthwhile.

APPENDIX A.8

STRAND RESPONSE AFTER COSTELLO ET AL. (16, 17, 18)

A cable (or strand) is regarded as a collection of m smooth rods whose natural or unstressed configurations are those of helices. The initial curvatures and twist for each wire are given by

$$k_o = 0; \quad k'_o = \cos^2\alpha/r; \quad \tau_o = \sin\alpha\cos\alpha/r \qquad \text{A.8.1}$$

in which

α = the original helix angle;

and r = the radius of the wire helix

When the cable is loaded, in general both α and r can change by rather large amounts and assume new values α_1 and r_1. The new configuration for each wire is then given by

$$k_1 = 0; \quad k'_1 = \cos^2\alpha_1/r_1; \quad \tau_1 = \sin\alpha_1\cos\alpha_1/r_1 \qquad \text{A.8.2}$$

The new configuration will be in equilibrium if the equations

$$dN/ds - N'\tau_1 + Tk'_1 + X = 0 \qquad \text{A.8.3}$$

$$dN'/ds - Tk_1 + N\tau_1 + Y = 0 \qquad \text{A.8.4}$$

$$dT/ds - Nk'_1 + N'k_1 + Z = 0 \qquad \text{A.8.5}$$

$$dG/ds - G'\tau_1 + Hk'_1 - N' + K = 0 \qquad \text{A.8.6}$$

$$dG'/ds - Hk_1 + G\tau_1 + N + K' = 0 \qquad \text{A.8.7}$$

$$dH/ds - Gk'_1 + G'k_1 + \text{[illegible]} = 0 \qquad \text{A.8.8}$$

are satisfied, after Love (26), in which N, N', T, X, Y, Z, G, G', H, K, K' and Θ are the external force and moment resultants acting along each wire in the normal, binormal and tangential directions (the principal torsion flexure axes), see Figs A.8.1, 2 and 3. The bending and twisting couples G, G' and H, and wire tension T are related to the curvatures k_1 and k', the twist τ_1 and the wire strain ξ by

$$G = A_c(k_1-k_o); \quad G' = A_c(k'_1-k'_o); \quad H = C_c(\tau_1-\tau_o); \quad T = D_c\xi \qquad \text{A.8.9}$$

in which the constants A_c, C_c and D_c depend on wire material and cross-section; for circular cross-section

$$A_c = EI_h; \quad C_c = EI_h/(1+\gamma); \quad D_c = EA_h \qquad \text{A.8.10}$$

The Love treatment (26) is such that equilibrium equations (A.8.3 to A.8.8) hold only if the axial strain of the wire centre line (ξ) is small.

It is now assumed that the individual wires in a cable are not subjected to external bending moments per unit length, i.e. $K = K' = 0$. It is also assumed that tension T is constant along the length of the wire. Then by virtue of Equations A.8.1, 2 and 9, equilibrium equations A.8.3 to 8 become

$$-N'\tau_1 + Tk'_1 + X = 0 \qquad \text{A.8.11}$$

$$Y = 0 \qquad \text{A.8.12}$$

$$Z = 0 \qquad \text{A.8.13}$$

$$-G'\tau_1 + Hk'_1 - N' = 0 \qquad \text{A.8.14}$$

$$N = 0 \qquad \text{A.8.15}$$

$$H = 0 \qquad \text{A.8.16}$$

The forces and moments appearing in equations A.8.11 and A.8.14 are shown in Fig. A.8.1.

The contact force per unit length, X, required for the equilibrium of a single wire is given in A.8.11. Substitution of A.8.14 into A.8.11 yields

$$X = (Hk'_1 - G'\tau_1)\tau_1 - Tk'_1 \qquad \text{A.8.17}$$

When m wires are placed together, the resultant line contact force per unit length X becomes an internal force in the cable. The total axial force and total axial twisting moment are then given by the relations

$$P = m(T\sin\alpha_1 + N'\cos\alpha_1) \qquad \text{A.8.18}$$

$$M = m(H\sin\alpha_1 + G'\cos\alpha_1 + Tr_1\cos\alpha_1 - N'r_1\sin\alpha_1) \qquad \text{A.8.19}$$

The geometrical relation between α_1 and r_1 is obtained by considering a transverse section of the cable as shown in Fig. A.8.2. Since the cross-sections are approximately elliptical it follows that

$$2r_1/d_h = (1 + \tan^2(\pi/2 - \pi/m)/\sin^2\alpha_1)^{\frac{1}{2}} \qquad \text{A.8.20}$$

This equation is also valid in the initial state when $r_1 = r$ and $\alpha_1 = \alpha$, since it is assumed that the wires are just touching each

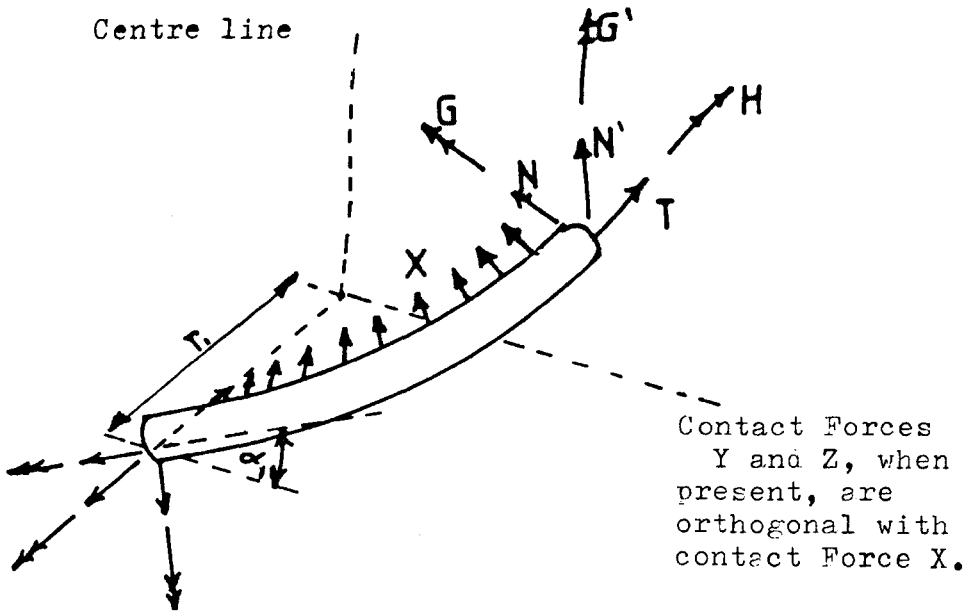

Figure A.8.1. Some Resultants that can act on a helical wire.

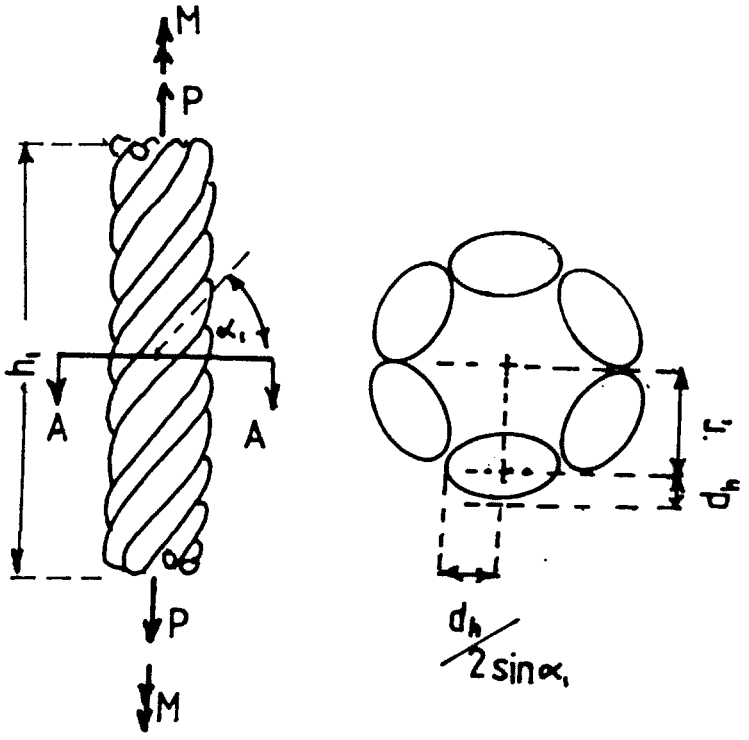

Figure A.8.2. Geometry of six-wire single -lay cable.

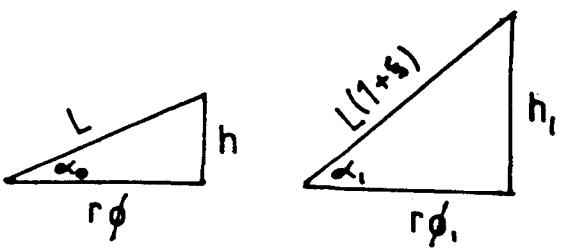

Figure A.8.3. Developed Views of Helical Wire Centre Line.

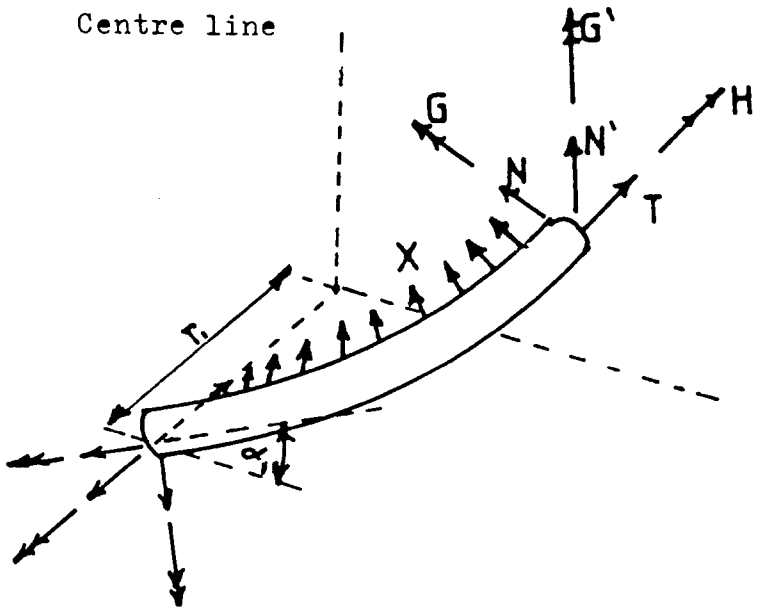

Figure A.8.1. Some Resultants that can act on a helical wire.

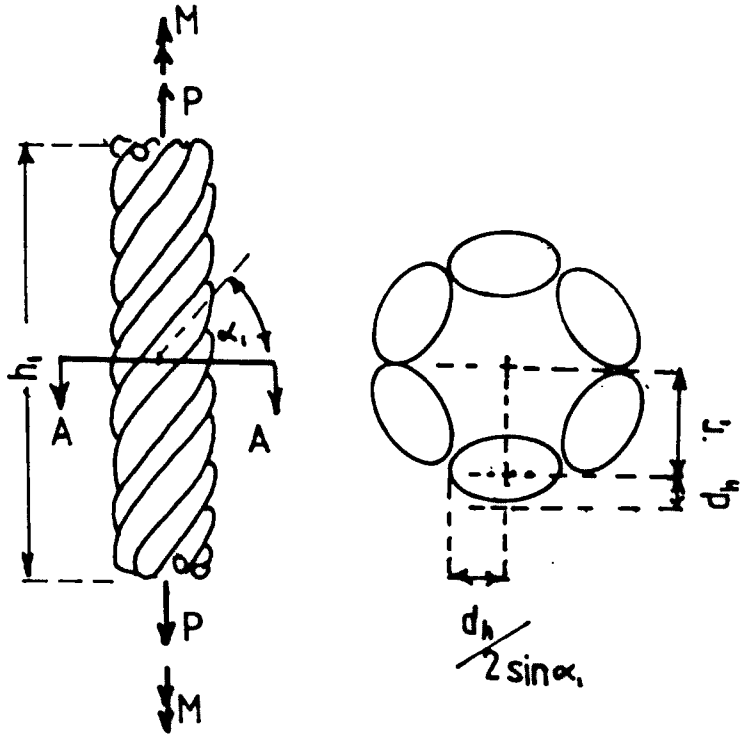

Figure A.8.2. Geometry of six-wire single -lay cable.

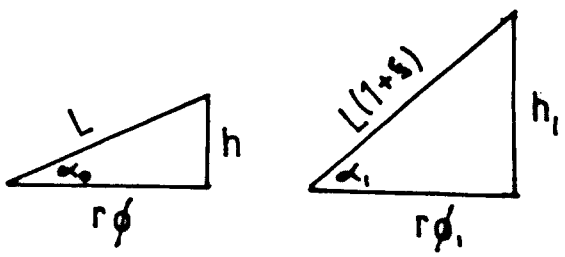

Figure A.8.3. Developed Views of Helical Wire Centre Line.

other in the unloaded configuration. It should be mentioned that A.8.20 does not account for the change in helix radius due to deformations associated with mutual contact line loads. Costello and Phillips (18) state that this is not a serious error for steel cables, but it would not be accurate for an analysis of yarn like materials.

Now the axial cable strain ξ is defined as $(h_1-h)h$, in which h = the original length of the cable, and h_1 = the final length of the cable. The rotational cable strain ϕ_c is defined as $r(\phi_1-\phi)/h$, in which ϕ = the original total angle that a given helical wire sweeps out in a plane perpendicular to the axis of the cable; and ϕ_1 = the final total angle the same wire sweeps out in a plane perpendicular to the axis of the cable. An analysis of the original and deformed configurations of a developed wire helix, shown in Fig. A.8.3, yields the following expressions for ξ and ϕ_c

$$\xi = (1 + \xi)\ \sin\alpha_1 / \sin\alpha - 1 \qquad \text{A.8.21}$$

and

$$\phi_c = \frac{r}{h}\left(\frac{h_1}{r_1 \tan\alpha_1} - \frac{h}{r\tan\alpha}\right)$$

$$= \frac{r}{r_1}(1 + \xi)/\tan\alpha_1 - 1/\tan\alpha \qquad \text{A.8.22}$$

APPENDIX A.9

STRAND RESPONSE AFTER DURELLI ET AL. (27, 28, 29)

A.9.1 Geometry and Loading

The geometry considered is that of a straight core wire wrapped around by a layer of helical wires, usually numbering six, but the theory is applicable to an arbitrary number of wires. Each helical wire is assumed to have a circular cross-section and is in contact with two adjacent wires, with the core, or with both core and adjacent wires. (See Fig. A.9.1).

Axial tension, torsion or combined torsion and tension cause elongation and rotation to the strand. Interwire contact deformation and Poisson's effect due to axial strain are neglected.

The deformation of a helical wire in a strand can be better understood with reference to Fig. A.9.2. Material line segments AB and CD are on the principal normal and binormal to the axial line (helix) at a point C respectively. After deformation, these material line segments are assumed to displace in such a way that they still are the principal normal and binormal to the deformed axial line (A'B' and C'D' in Fig. A.9.2). The forces in the helical wire associated with this deformation are (1) axial force, (2) bending in the plane containing the axial line of the helical wire and the principal normal of the helix, (3) twisting around axis of helical wire and (4) contact force, the resultant force of which lies on the plane containing the axial line of helical wire.

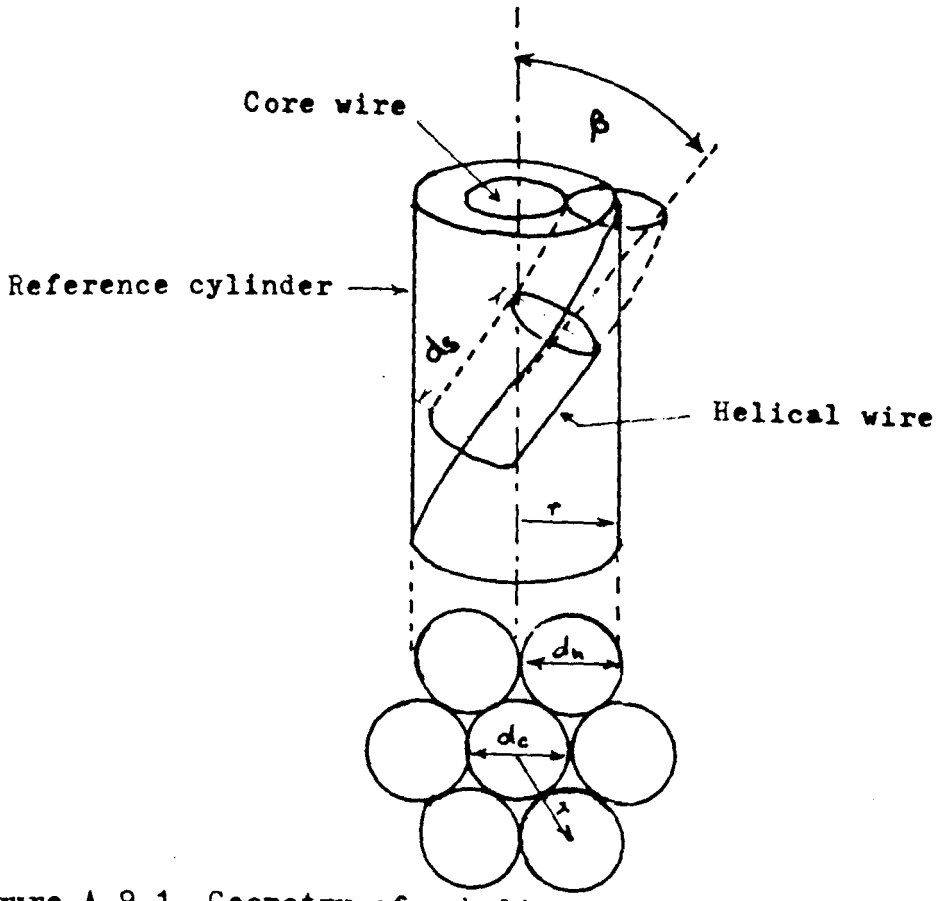

Figure A.9.1. Geometry of a helical wire wrapped around a core.

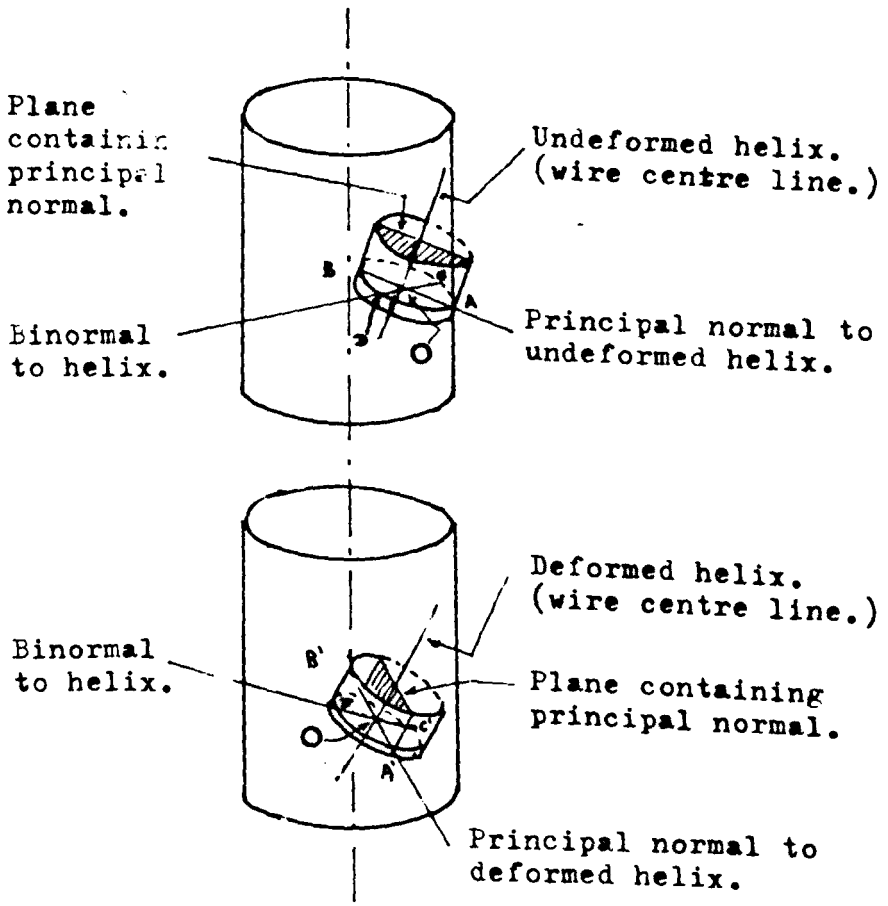

Figure A.9.2. Deformation of a cross section of a helical wire.

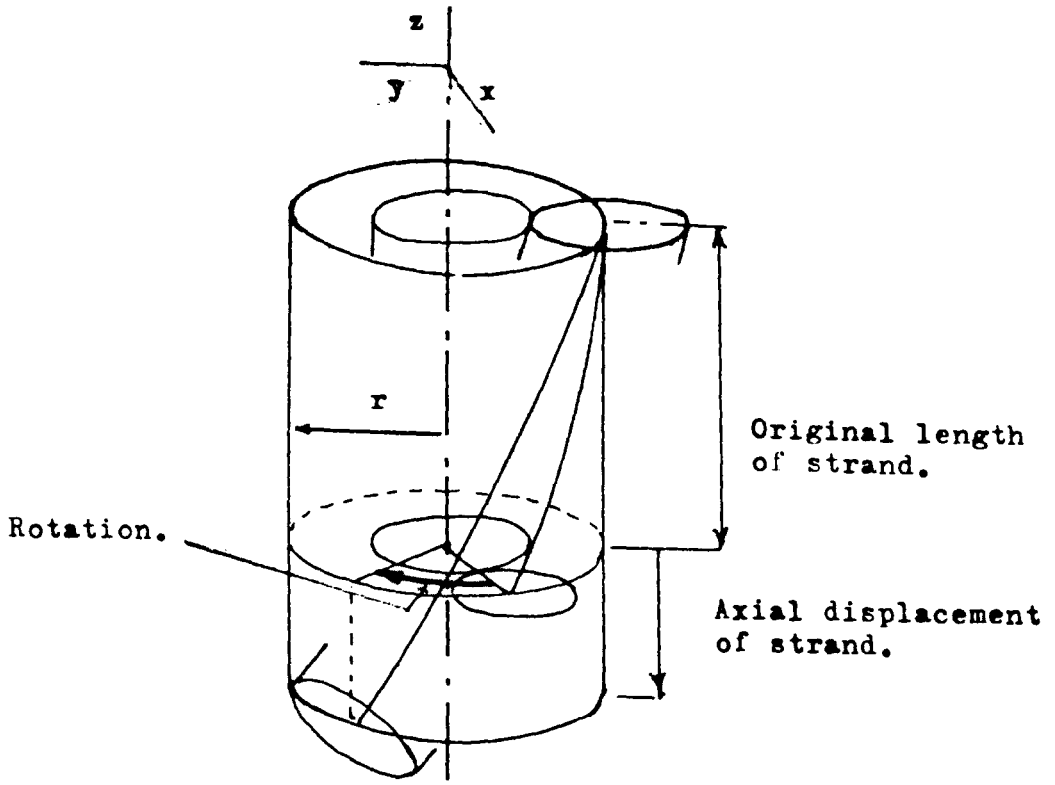

Figure A.9.3. Elongation and rotation in a helical wire.

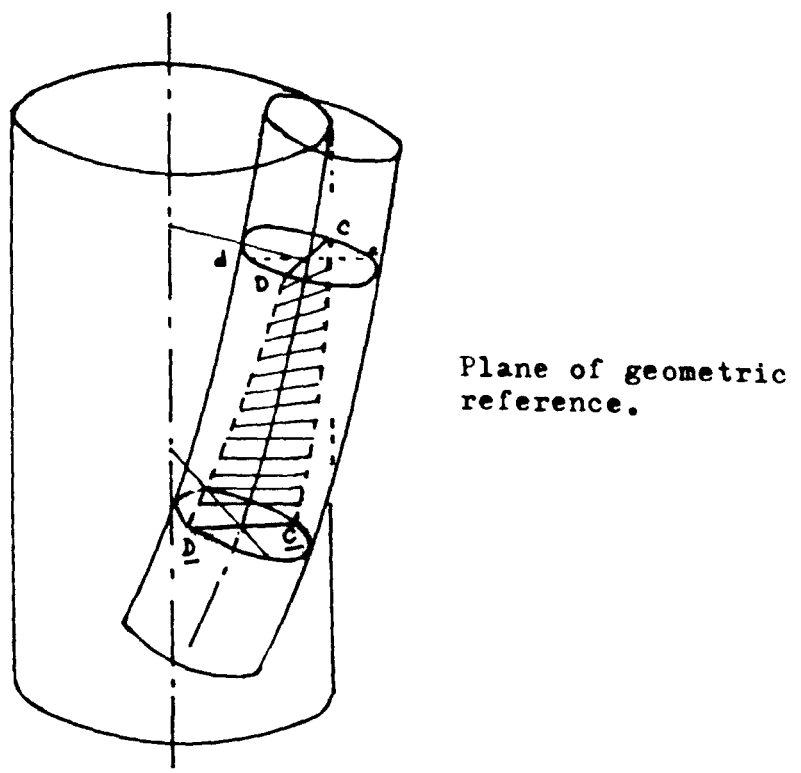

Figure A.9.4. Plane of geometric reference in helical wire for consideration of twisting deformation.

(a).Resultant contact force in the transverse cross section of helical wire.

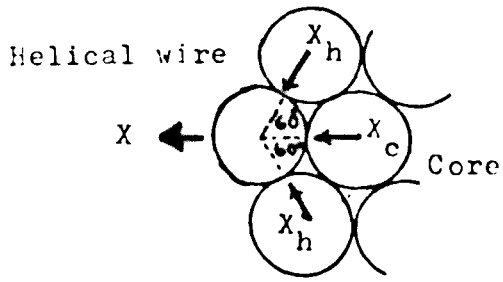

(b).Equilibrium of force in an element of a helical wire.

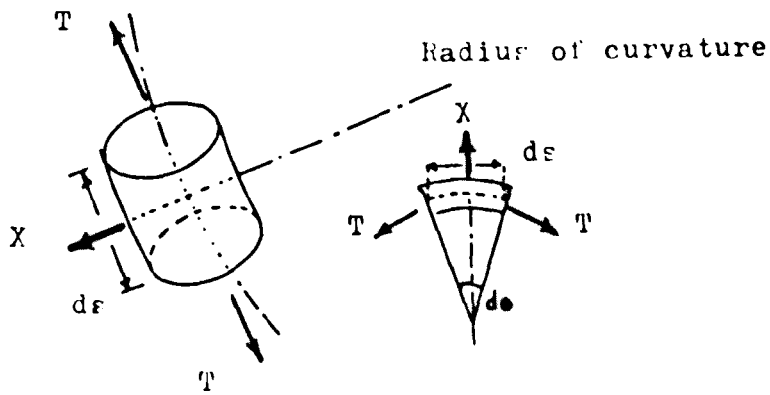

Figure A.9.5.Contact Forces.

A.9.2 Axial Force in the Wire

Axial strain can be expressed in terms of δ_D and ϕ_D. If l is length of undeformed strand and s is initial length of the axial line of a helical wire , given by

$$s = \frac{l}{p}\,(p^2 + (2\pi r)^2)^{\frac{1}{2}} \qquad \text{A.9.1}$$

Final length

$$s' = \frac{l}{p}\,((p + \delta_D)^2 + (2\pi + \phi_D)^2 . r^2)^{\frac{1}{2}} \qquad \text{A.9.2}$$

If $$\xi = (s' - s)/s \qquad \text{A.9.3}$$

$$= \cos\beta((1 + \varepsilon)^2 + (1 + \gamma)^2 \tan^2\beta)^{\frac{1}{2}} - 1 \qquad \text{A.9.4}$$

where $\varepsilon = \delta_D/p$ and $\gamma = \phi_D/2\pi$ A.9.5

assuming $\varepsilon, \gamma \ll 1$

then $\xi \simeq \varepsilon \cos^2\beta + \gamma \sin^2\beta$ A.9.6

and $T = A_h E\,(\varepsilon \cos^2\beta + \gamma \sin^2\beta)$ A.9.7

A.9.3 Bending Moment in the Wire

If ρ is the radius of curvature of the undeformed helix

$$\frac{1}{\rho^2} = \left[\left(\frac{d^2x}{d\theta^2}\right) + \left(\frac{d^2y}{d\theta^2}\right) + \left(\frac{d^2z}{d\theta^2}\right) - \frac{d^2s}{d\theta^2}\right] \Big/ \left(\frac{ds}{d\theta}\right)^4 \qquad \text{A.9.8}$$

where $x = r\cos\theta$, $y = r\sin\theta$, $z = p\theta/2\pi$, which are the cartesian co-ordinates of the helix, and where ds, line increment of the helix, is defined as

$$ds^2 = dx^2 + dy^2 + dz^2 \qquad \text{A.9.9}$$

Using equation A.9.8, radii of curvature of the undeformed and deformed helices are given by

$$\rho = r + \left(\frac{p}{2\pi}\right)^2 / r \qquad \text{A.9.10}$$

and

$$\rho' = r + \left(\frac{p'}{2\pi}\right)^2 / r' \qquad \text{A.9.11}$$

respectively. Deformed pitch p' can be expressed in terms of the original pitch p as

$$p' = (p + \delta)(2\pi/(2\pi + \phi_D)) = p\left(\frac{1+\varepsilon}{1+\gamma}\right) \qquad \text{A.9.12}$$

Considering the helical wire as an initially curved beam, the bending moment is

$$G' = EI_h(\rho' - \rho)/\rho\rho' \qquad \text{A.9.13}$$

When strains are small, $\varepsilon, \gamma \ll 1$, then $p' = p(1 + \varepsilon - \gamma)$ and equation A.9.13 becomes

$$G' = 2EI(\varepsilon - \gamma)\cos^2\beta \sin^2\beta / r \qquad \text{A.9.14}$$

Note that curvature k' from the Costello analysis (see Appendix A.8) is given by

$$k' = 1/\rho$$

A.9.4 Twisting Moment in the Wire

If ς is the radius of twist (or second radius of curvature) of the undeformed helix

$$\frac{1}{\varsigma^2} = \left(\frac{d\lambda}{ds}\right)^2 + \left(\frac{d\mu}{ds}\right)^2 + \left(\frac{d\nu}{ds}\right)^2 \qquad \text{A.9.15}$$

where λ, μ and ν are the direction cosines of the binormal at the point considered. In the case of a helix, ς is constant and are given for the undeformed and deformed helix by

$$\varsigma = (p/2\pi) + r^2/(p/2\pi) \qquad \text{A.9.16}$$

and

$$\varsigma' = (p'/2\pi) + r^2/(p'/2\pi) \qquad \text{A.9.17}$$

respectively. In the same way as the bending moment was considered for an initially curved beam in A.9.13, so torque generated in the wire is given by

$$H = \frac{EI_h}{(1+\gamma)} \; (\varsigma - \varsigma')/\varsigma\varsigma' \qquad \text{A.9.18}$$

When strains are small, $\varepsilon, \gamma \ll 1$, then $p' = p(1 + \varepsilon - \gamma)$ and equation A.9.18 becomes

$$H = \frac{EI_h}{(1+\gamma)r} \; (\gamma - \varepsilon)\sin 4\beta \qquad \text{A.9.19}$$

Note that tortuosity τ from the Costello analysis (see Appendix A.8) is given by $\tau = 1/\varsigma$

A.9.5 Contact Force Between Wires

By considering equilibrium of a unit length of helical wire, contact force resultant on a helical wire is given by

$$X = 2X_h \cos 60^\circ + X_c = X_h + X_c \qquad \text{A.9.20}$$

where X_h is the contact force between adjacent helicals

and X_c is the contact force between the core and a helical

By considering the equilibrium of a short segment of helical wire

$$2T.\sin(d\theta/2) = Xds = X\rho\, d\theta$$

As $\theta \rightarrow 0$ $\quad X = T/\rho' \triangleq T/\rho$ $\qquad$ A.9.21

(See Figure A.9.5)

A.9.6 Forces in Core

Since the core is connected with the surrounding helical wires at both ends of the strand, the core is subjected to axial strain and twist given by

$$T_c = A_c E \varepsilon \qquad \text{A.9.22}$$

and

$$M_c = E I_c 2\pi\delta/p(1+\nu) \qquad \text{A.9.23}$$

A.9.7 Forces on the Strand

Force P and moment M are given by

$$P = T_c + 6T\cos\beta' \qquad \text{A.9.24}$$

$$M = M_c + 6(H\cos\beta' - G'\sin\beta' + T_r\sin\beta') \qquad \text{A.9.25}$$

where β' is lay angle after deformation which can be expressed as

$$\beta' = \tan^{-1}\left(\frac{1+\gamma}{1+\varepsilon}\tan\beta\right) \qquad \text{A.9.26}$$

For small deformations, $\beta' \doteq \beta$ A.9.27

Equations A.24 and 25 can be expressed as

$$P = A\varepsilon + B\gamma \qquad \text{A.9.28}$$

and

$$M = C\varepsilon + D\gamma \qquad \text{A.9.29}$$

where A, B, C and D are constants

$$\left.\begin{aligned} A &= A_c E + 6A_h E\cos^3\beta \\ B &= 6A_h.E\sin^2\beta\cos\beta \\ C &= 6A_h rE\sin\beta.\cos^2\beta - \frac{3EI_h\sin4\beta\cos\beta}{2r(1+\gamma)} - \frac{12EI_h\cos^2\beta\sin^3\beta}{r} \\ D &= 6A_h rE\sin^3\beta + \frac{3EI_h\sin4\beta\cos\beta}{2r(1+\gamma)} + \frac{12EI_h.\cos^2\beta\sin^3\beta}{r} + \frac{2\pi EI_c}{p(1+\gamma)} \end{aligned}\right\} \qquad \text{A.9.30}$$

From A.28 and 29

$$\left.\begin{aligned} \varepsilon &= (D/(AD - CB))\,P - (B/(AD - CB))\,M \\ \gamma &= -(C/(AD - CB))\,P + (A/(AD - CB))\,M \end{aligned}\right\} \qquad \text{A.9.31}$$

A.9.8 Strand Response - Fixed End Case

In this case $\phi = 0$ and $\gamma = 0$. By substitution in A.9.22 to 31, strand response is given as follows

$$P = A\varepsilon$$

$$M = (C/A)P$$

$$T_c = (A_c E/A)P$$

$$M_c = 0$$

$$T = (A_h E \cos^2\beta/A)P$$

$$G' = (2EI\cos^2\beta\sin^2\beta/Ar)P$$

$$H = (EI_h \sin 4\beta/4r(1+\nu)A)P$$

A.9.32

A.9.9 Strand Response - Free End Case

In this case M = 0. By substitution in A.9.22 to 31, strand response is given

$$T_c = (A_c ED/(AD - CB))P$$

$$M_c = -(2\pi EI_h C/2(1+\nu)p(AD - CB))P$$

$$T = (A_h E(D\cos^2\beta - C\sin^2\beta)/(AD - CB))P$$

$$G' = (2EI_h \cos^2\beta \sin^2\beta(C + D)/r(AD - CB))P$$

$$H = (EI_h \sin 4\beta(C + D)/4r(1+\nu)(AD - CB))P$$

$$P = ((AD - BC)/D)\varepsilon$$

$$\phi = -(2\pi C/(AD - CB))P$$

A.9.33

APPENDIX A.10

LIST OF ENGINEERING DRAWINGS

The following are engineering drawings of the mechanical components used in the programme of testing on wire strands. These drawings are filed with the Drawing Office of the Mechanical Engineering Department and are referenced with drawing numbers.

Drawing No.	Title
ME-G-B267	End fitting for wire rope.
G-D267/1	Cutting grips.
G-D267/2	Wire rope test rig components.
G-D267/3	Components for wire rope tensile testing machine.
G-D267/4	Tensile testing machine for wire ropes - General Arrangement.
G-C267/5	Adaptor for free end tensile tests on wire rope - General Arrangement.
G-B267/6	" " " " " " " - Components.
7	" " " " " " " - Components.
8	" " " " " " " - Components.
G-B267/9	Wires guide assembly, wire strand end grip.
10	" " plate, " " " "
11	" " body, " " " "
12	Adaptor for torque calibrations: Wire rope load cell.

Drawing No.	Title
ME-G-B267/13	Adaptor for tension calibrations: Wire rope load cell.
G-E267/14	Wire rope extenso-rotatometer. ('Extrometer'). General Arrangement.
G-B267/15	Grip Components. ('Extrometer').
16	Bearing shaft components. ('Extrometer').
17	Support arms. "
18	Upper base plate "
19	Displacement Transducer Support Components. ('Extrometer').
20	Rotary Potentiometer holders. ('Extrometer').
21	Grip cradle. "
22	Gauge length rods. "
23	Grip plates. "
24	Grip body. "
25	Adjuster rods for Displacement Transducer. ('Extrometer').
26	Strand Wire bender components.
27	" " " "
28	" " " "